Monitoring Forest-Savanna Dynamics in the Guineo-Congolian Transition Area of the Centre Region of Cameroon

Le Bienfaiteur Sagang Takougoum

UNIVERSITY OF YAOUNDE I

UNIVERSITÉ DE YAOUNDÉ I

FACULTY OF SCIENCE

FACULTÉ DES SCIENCES

CENTRE FOR RESEARCH AND TRAINING IN GRADUATE STUDIES IN LIFE SCIENCE, HEALTH and ENVIRONMENTAL SCIENCES

CENTRE DE RECHERCHE ET DE FORMATION DOCTORALE EN SCIENCES DE LA VIE, SANTE ET ENVIRONNEMENT

DEPARTMENT OF PLANT BIOLOGY

DÉPARTEMENT DE BIOLOGIE ET PHYSIOLOGIE VÉGÉTALES

Monitoring Forest-Savanna Dynamics in the Guineo-Congolian Transition Area of the Centre Region of Cameroon

Thesis

Submitted in partial fulfilment of the requirements for the award of a

DOCTORAT/Ph.D. in Plant Biology

Option: Botany-Ecology

By :

SAGANG TAKOUGOUM Le Bienfaiteur

Registration : 17T4953

Master of Science in Plant Biology and Physiology

Co-Direction

BARBIER Nicolas

Scientist

Institut de Recherche pour le Développement

SONKÉ Bonaventure

Professor

COUTERON Pierre

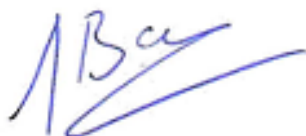Senior Scientist

Institut de Recherche pour le Développement

Year: 2022

**DEPARTEMENT DE
BIOLOGIE ET PHYSIOLOGIE VEGETALES**
DEPARTMENT OF PLANT BIOLOGY

ATTESTATION DE CORRECTION

****

Nous soussignés, membres du jury de soutenance de la thèse de Doctorat/PhD en Biologie des Organismes Végétaux option Botanique-Écologie de **Monsieur SAGANG TAKOUGOUM Le Bienfaiteur**, Matricule **17T4953**, soutenue publiquement ce mardi 11 janvier sur le sujet : « **Monitoring Forest-Savanna Dynamics in the Guineo-Congolian Transition Area of the Centre Region of Cameroon** » attestons que les corrections conformément aux remarques et recommandations du jury lors de la soutenance de ladite thèse de Doctorat/PhD ont été effectuées par le candidat.

En foi de quoi la présente attestation lui est délivrée afin de servir et valoir ce que de droit./-

Rapporteurs

BARBIER Nicolas
Chargé de Recherche
Institut de Recherche
pour le Développement

SONKÉ Bonaventure
Professeur

COUTERON Pierre
Directeur de Recherche
Institut de Recherche
pour le Développement

ZAPFACK Louis
Professeur

Membres

NDONGO Din
Professeur

NGODO Jean-Baptiste
Maître de Conférences

Président

YOUMBI Emmanuel
Professeur

DEPARTEMENT DE BIOLOGIE ET PHYSIOLOGIE VEGETALES
DEPARTMENT OF PLANT BIOLOGY

Rapport de soutenance de thèse présentée en vue de l'obtention du diplôme de Doctorat/ Ph.D par M. Le Bienfaiteur SagangTakougoum (Matricule 17T4953)

Sujet de la thèse: Monitoring Forest-Savanna Dynamics in the Guineo-Congolian Transition Area of the Centre Region of Cameroon.

Suite à l'autorisation n°2021-390/UY/VREPDTIC/DAAC/DEPE/SPD/CB du 18 novembre 2021, de Monsieur le Recteur de l'Université de Yaoundé I, Monsieur **Le Bienfaiteur SagangTakougoum** a soutenu publiquement ce 11 janvier 2022 à partir de 9 heures, dans la salle S01/02 du bloc pédagogique de la Faculté des Sciences, Université de Yaoundé I, une thèse de Doctorat/Ph.D en Biologie des Organismes Végétaux (Option Botanique-Ecologie) devant le jury composé de :

Président:	Youmbi Emmanuel, Professeur, Université de Yaoundé I ;
Rapporteurs:	Sonké Bonaventure, Professeur, Université de Yaoundé I
	Barbier Nicolas, Chargé de Recherches, Institut de Recherche pour le Développement ;
	Couteron Pierre Directeur de Recherches, Institut de Recherche pour le Développement ;
Examinateurs:	Zapfack Louis, Professeur, Université de Yaoundé I
	Ndongo Din, Professeur, Université de Douala;
	Ngodo Melingui Jean-Baptiste, Maître de Conférences, Université de Yaoundé I.

Il ressort de ces travaux que le suivi de la dynamique à long terme (45 ans) de la végétation a permis de décrire une avancée constante d'1% de la forêt sur la savane entre 1975 et 2020. Aucune fréquence de feu n'a été recensée pour les savanes ayant transité vers la forêt en 5 années de monitoring. La vitesse d'accumulation de la biomasse au-dessus du sol (AGB) est plus élevée dans les jeunes successions forestières (< 20 ans ; 4,3 Mg.ha^{-1}.year^{-1}) contrairement aux forêts plus âgées ($\geq$ 20 ans) où elle est plus basse (3,2 Mg.ha^{-1}.year^{-1}). Deux modes se distinguent nettement dans la composition spectrale de la savane correspondant à différents niveaux d'AGB. Une occurrence de feu par intervalle de 5 ans minimum est au nécessaire afin de réguler l'évolution de la savane.

Dans un exposé clair et didactique en vidéo-projection fait dans le temps imparti, M. Sagang Takougoum a présenté les principaux résultats de ses travaux. Le candidat a donné des réponses satisfaisantes aux questions à lui posées par le jury montrant ainsi la maîtrise de son sujet.

Le jury après avoir délibéré, accepte le document présenté et décerne à l'unanimité à Monsieur **Le Bienfaiteur Sagang Takougoum** le grade de Docteur/Ph.D avec la mention **Très Honorable**.

Fait à Yaoundé, le 11 janvier 2022.

Président

E YOUMBI

Rapporteurs

B. SONKE

Membres

Ngodo Melingui   ZAPFACK

NDONGO DIN

PROTOCOL LIST OF THE FACULTY OF SCIENCE

UNIVERSITÉ DE YAOUNDÉ I **Faculté des Sciences** Division de la Programmation et du Suivi des Activités Académiques		THE UNIVERSITY OF YAOUNDE I **Faculty of Science** Division of Programming and Follow-up of Academic Affaires
LISTE DES ENSEIGNANTS PERMANENTS		**LIST OF PERMANENT TEACHING STAFF**

ANNÉE ACADEMIQUE 2020/2021

(Par Département et par Grade)

DATE D'ACTUALISATION 12 Juin 2020

ADMINISTRATION

DOYEN : TCHOUANKEU Jean- Claude, *Maître de Conférences*
VICE-DOYEN / DPSAA : ATCHADE Alex de Théodore, *Maître de Conférences*
VICE-DOYEN / DSSE : AJEAGAH Gideon AGHAINDUM*, Professeur*
VICE-DOYEN / DRC : ABOSSOLO Monique, *Maître de Conférences*
Chef Division Administrative et Financière : NDOYE FOE Marie C. F., *Maître de Conférences*
Chef Division des Affaires Académiques, de la Scolarité et de la Recherche DAASR : MBAZE MEVA'A Luc Léonard, *Professeur*

1- DÉPARTEMENT DE BIOCHIMIE (BC) (38)

N°	NOMS ET PRÉNOMS	GRADE	OBSERVATIONS
1	BIGOGA DAIGA Jude	Professeur	En poste
2	FEKAM BOYOM Fabrice	Professeur	En poste
3	FOKOU Elie	Professeur	En poste
4	KANSCI Germain	Professeur	En poste
5	MBACHAM FON Wilfried	Professeur	En poste
6	MOUNDIPA FEWOU Paul	Professeur	Chef de Département
7	NINTCHOM PENLAP V. épse BENG	Professeur	En poste
8	OBEN Julius ENYONG	Professeur	En poste
9	ACHU Merci BIH	Maître de Conférences	En poste
10	ATOGHO Barbara Mma	Maître de Conférences	En poste
11	AZANTSA KINGUE GABIN BORIS	Maître de Conférences	En poste
12	BELINGA née NDOYE FOE M. C. F.	Maître de Conférences	Chef DAF / FS
13	BOUDJEKO Thaddée	Maître de Conférences	En poste
14	DJUIDJE NGOUNOUE Marcelline	Maître de Conférences	En poste
15	EFFA NNOMO Pierre	Maître de Conférences	En poste
16	NANA Louise épouse WAKAM	Maître de Conférences	En poste

17	NGONDI Judith Laure	Maître de Conférences	En poste
18	NGUEFACK Julienne	Maître de Conférences	En poste
19	NJAYOU Frédéric Nico	Maître de Conférences	En poste
20	MOFOR née TEUGWA Clotilde	Maître de Conférences	Inspecteur de Service MINESUP
21	TCHANA KOUATCHOUA Angèle	Maître de Conférences	En poste
22	AKINDEH MBUH NJI	Chargé de Cours	En poste
23	BEBOY EDJENGUELE Sara Nathalie	Chargé de Cours	En poste
24	DAKOLE DABOY Charles	Chargé de Cours	En poste
25	DJUIKWO NKONGA Ruth Viviane	Chargée de Cours	En poste
26	DONGMO LEKAGNE Joseph Blaise	Chargé de Cours	En poste
27	EWANE Cécile Anne	Chargée de Cours	En poste
28	FONKOUA Martin	Chargé de Cours	En poste
29	BEBEE Fadimatou	Chargée de Cours	En poste
30	KOTUE KAPTUE Charles	Chargé de Cours	En poste
31	LUNGA Paul KEILAH	Chargé de Cours	En poste
32	MANANGA Marlyse Joséphine	Chargée de Cours	En poste
33	MBONG ANGIE M. Mary Anne	Chargée de Cours	En poste
34	PECHANGOU NSANGOU Sylvain	Chargé de Cours	En poste
35	Palmer MASUMBE NETONGO	Chargé de Cours	En poste
36	MBOUCHE FANMOE Marceline Joëlle	Assistante	En poste
37	OWONA AYISSI Vincent Brice	Assistant	En poste
38	WILFRIED ANGIE Abia	Assistante	En poste

2- DÉPARTEMENT DE BIOLOGIE ET PHYSIOLOGIE ANIMALES (BPA) (48)

1	AJEAGAH Gideon AGHAINDUM	Professeur	*VICE-DOYEN / DSSE*
2	BILONG BILONG Charles-Félix	Professeur	Chef de Département
3	DIMO Théophile	Professeur	En Poste
4	DJIETO LORDON Champlain	Professeur	En Poste
5	ESSOMBA née NTSAMA MBALA	Professeur	*Vice Doyen/FMSB/UYI*
6	FOMENA Abraham	Professeur	En Poste
7	KAMTCHOUING Pierre	Professeur	En poste
8	NJAMEN Dieudonné	Professeur	En poste
9	NJIOKOU Flobert	Professeur	En Poste
10	NOLA Moïse	Professeur	En poste
11	TAN Paul VERNYUY	Professeur	En poste
12	TCHUEM TCHUENTE Louis Albert	Professeur	*Inspecteur de service Coord.Progr./MINSANTE*
13	ZEBAZE TOGOUET Serge Hubert	Professeur	*En poste*

14	BILANDA Danielle Claude	Maître de Conférences	En poste
15	DJIOGUE Séfirin	Maître de Conférences	En poste
16	DZEUFIET DJOMENI Paul Désiré	Maître de Conférences	En poste
17	JATSA BOUKENG Hermine épse MEGAPTCHE	Maître de Conférences	En Poste
18	KEKEUNOU Sévilor	Maître de Conférences	En poste
19	MEGNEKOU Rosette	Maître de Conférences	En poste
20	MONY Ruth épse NTONE	Maître de Conférences	En Poste
21	NGUEGUIM TSOFACK Florence	Maître de Conférences	En poste
22	TOMBI Jeannette	Maître de Conférences	En poste
23	ALENE Désirée Chantal	Chargée de Cours	En poste
26	ATSAMO Albert Donatien	Chargé de Cours	En poste
27	BELLET EDIMO Oscar Roger	Chargé de Cours	En poste
28	DONFACK Mireille	Chargée de Cours	En poste
29	ETEME ENAMA Serge	Chargé de Cours	En poste
30	GOUNOUE KAMKUMO Raceline	Chargée de Cours	En poste
31	KANDEDA KAVAYE Antoine	Chargé de Cours	En poste
32	LEKEUFACK FOLEFACK Guy B.	Chargé de Cours	En poste
33	MAHOB Raymond Joseph	Chargé de Cours	En poste
34	MBENOUN MASSE Paul Serge	Chargé de Cours	En poste
35	MOUNGANG Luciane Marlyse	Chargée de Cours	En poste
36	MVEYO NDANKEU Yves Patrick	Chargé de Cours	En poste
37	NGOUATEU KENFACK Omer Bébé	Chargé de Cours	En poste
38	NGUEMBOK	Chargé de Cours	En poste
39	NJUA Clarisse Yafi	Chargée de Cours	Chef Div. UBA
40	NOAH EWOTI Olive Vivien	Chargée de Cours	En poste
41	TADU Zephyrin	Chargé de Cours	En poste
42	TAMSA ARFAO Antoine	Chargé de Cours	En poste
43	YEDE	Chargé de Cours	En poste
44	BASSOCK BAYIHA Etienne Didier	Assistant	En poste
45	ESSAMA MBIDA Désirée Sandrine	Assistante	En poste
46	KOGA MANG DOBARA	Assistant	En poste
47	LEME BANOCK Lucie	Assistante	En poste
48	YOUNOUSSA LAME	Assistant	En poste

3- DÉPARTEMENT DE BIOLOGIE ET PHYSIOLOGIE VÉGÉTALES (BPV) (33)

1	AMBANG Zachée	Professeur	Chef Division/UYII
2	BELL Joseph Martin	Professeur	En poste
3	DJOCGOUE Pierre François	Professeur	En poste
4	MOSSEBO Dominique Claude	Professeur	En poste
5	YOUMBI Emmanuel	Professeur	Chef de Département
6	ZAPFACK Louis	Professeur	En poste

7	MBOLO Marie	Professeur	En poste
8	ANGONI Hyacinthe	Maître de Conférences	En poste
9	BIYE Elvire Hortense	Maître de Conférences	En poste
10	MALA Armand William	Maître de Conférences	En poste
11	MBARGA BINDZI Marie Alain	Maître de Conférences	CT/ MINESUP
12	NDONGO BEKOLO	Maître de Conférences	CE / MINRESI
13	NGODO MELINGUI Jean Baptiste	Maître de Conférences	En poste
14	NGONKEU MAGAPTCHE Eddy L.	Maître de Conférences	CT/ MINRESI
15	TSOATA Esaïe	Maître de Conférences	En poste
16	TONFACK Libert Brice	Maître de Conférences	En poste
17	ONANA JEAN MICHEL	Maître de Conférences	En poste
18	DJEUANI Astride Carole	Chargé de Cours	En poste
19	NSOM ZAMO Epse PIAL Annie Claude	Chargée de Cours	En poste
20	GOMANDJE Christelle	Chargée de Cours	En poste
21	MAFFO MAFFO Nicole Liliane	Chargée de Cours	En poste
22	MAHBOU SOMO TOUKAM. Gabriel	Chargé de Cours	En poste
23	NGALLE Hermine BILLE	Chargé de Cours	En poste
24	NNANGA MEBENGA Ruth Laure	Chargé de Cours	En poste
25	NOUKEU KOUAKAM Armelle	Chargé de Cours	En poste
26	GODSWILL NTSOMBAH NTSEFONG	Chargé de Cours	En poste
27	KABELONG BANAHO Louis-Paul-Roger	Chargé de Cours	En poste
28	KONO Léon Dieudonné	Chargé de Cours	En poste
29	LIBALAH Moses BAKONCK	Chargé de Cours	En poste
30	LIKENG-LI-NGUE Benoit C	Chargé de Cours	En poste
31	TAEDOUMG Evariste Hermann	Chargé de Cours	En poste
32	TEMEGNE NONO Carine	Chargée de Cours	En poste

4- DÉPARTEMENT DE CHIMIE INORGANIQUE (CI) (34)

1	AGWARA ONDOH Moïse	Professeur	*Chef de Département*
2	ELIMBI Antoine	Professeur	En poste
3	Florence UFI CHINJE épouse MELO	Professeur	*Recteur Univ.Ngaoundere*
4	GHOGOMU Paul MINGO	Professeur	*Ministre Chargé deMiss.PR*
5	NANSEU Njiki Charles Péguy	Professeur	En poste
6	NDIFON Peter TEKE	Professeur	*CT MINRESI*
7	NGOMO Horace MANGA	Professeur	*Vice Chancelor/UB*
8	NDIKONTAR Maurice KOR	Professeur	*Vice-Doyen Univ. Bamenda*
9	NENWA Justin	Professeur	En poste
10	NGAMENI Emmanuel	Professeur	*DOYEN FS UDs*

11	BABALE née DJAM DOUDOU	Maître de Conférences	*Chargée Mission P.R.*
12	DJOUFAC WOUMFO Emmanuel	Maître de Conférences	En poste
13	EMADACK Alphonse	Maître de Conférences	En poste
14	KAMGANG YOUBI Georges	Maître de Conférences	En poste
15	KEMMEGNE MBOUGUEM Jean C.	Maître de Conférences	En poste
16	KONG SAKEO	Maître de Conférences	En poste
17	NDI NSAMI Julius	Maître de Conférences	En poste
18	NJIOMOU C. épse DJANGANG	Maître de Conférences	En poste
19	NJOYA Dayirou	Maître de Conférences	En poste
20	ACAYANKA Elie	Chargé de Cours	En poste
21	BELIBI BELIBI Placide Désiré	Chargé de Cours	CS/ ENS Bertoua
22	CHEUMANI YONA Arnaud M.	Chargé de Cours	En poste
23	KENNE DEDZO GUSTAVE	Chargé de Cours	En poste
24	KOUOTOU DAOUDA	Chargé de Cours	En poste
25	MAKON Thomas Beauregard	Chargé de Cours	En poste
26	MBEY Jean Aime	Chargé de Cours	En poste
27	NCHIMI NONO KATIA	Chargé de Cours	En poste
28	NEBA nee NDOSIRI Bridget NDOYE	Chargée de Cours	CT/ MINFEM
29	NYAMEN Linda Dyorisse	Chargée de Cours	En poste
30	PABOUDAM GBAMBIE A.	Chargée de Cours	En poste
31	TCHAKOUTE KOUAMO Hervé	Chargé de Cours	En poste
32	NJANKWA NJABONG N. Eric	Assistant	En poste
33	PATOUOSSA ISSOFA	Assistant	En poste
34	SIEWE Jean Mermoz	Assistant	En Poste

5- DÉPARTEMENT DE CHIMIE ORGANIQUE (CO) (35)

1	DONGO Etienne	Professeur	Vice-Doyen
2	GHOGOMU TIH Robert Ralph	Professeur	Dir. IBAF/UDA
3	NGOUELA Silvère Augustin	Professeur	Chef de Departement UDS
4	NKENGFACK Augustin Ephrem	Professeur	Chef de Département
5	NYASSE Barthélemy	Professeur	En poste
6	PEGNYEMB Dieudonné Emmanuel	Professeur	*Directeur/ MINESUP*
7	WANDJI Jean	Professeur	En poste
8	Alex de Théodore ATCHADE	Maître de Conférences	Vice-Doyen / DPSAA
9	EYONG Kenneth OBEN	Maître de Conférences	En poste
10	FOLEFOC Gabriel NGOSONG	Maître de Conférences	En poste
11	FOTSO WABO Ghislain	Maître de Conférences	En poste
12	KEUMEDJIO Félix	Maître de Conférences	En poste
13	KEUMOGNE Marguerite	Maître de Conférences	En poste
14	KOUAM Jacques	Maître de Conférences	En poste

15	MBAZOA née DJAMA Céline	Maître de Conférences	En poste
16	MKOUNGA Pierre	Maître de Conférences	En poste
17	NOTE LOUGBOT Olivier Placide	Maître de Conférences	Chef Service/MINESUP
18	NGO MBING Joséphine	Maître de Conférences	Sous/Direct. MINERESI
19	NGONO BIKOBO Dominique Serge	Maître de Conférences	En poste
20	NOUNGOUE TCHAMO Diderot	Maître de Conférences	En poste
21	TABOPDA KUATE Turibio	Maître de Conférences	En poste
22	TCHOUANKEU Jean-Claude	Maître de Conférences	*Doyen /FS/ UYI*
23	TIH née NGO BILONG E. Anastasie	Maître de Conférences	En poste
24	YANKEP Emmanuel	Maître de Conférences	En poste
25	AMBASSA Pantaléon	Chargé de Cours	En poste
26	KAMTO Eutrophe Le Doux	Chargé de Cours	En poste
27	MVOT AKAK CARINE	Chargé de Cours	En poste
28	NGNINTEDO Dominique	Chargé de Cours	En poste
29	NGOMO Orléans	Chargée de Cours	En poste
30	OUAHOUO WACHE Blandine M.	Chargée de Cours	En poste
31	SIELINOU TEDJON Valérie	Chargé de Cours	En poste
32	TAGATSING FOTSING Maurice	Chargé de Cours	En poste
33	ZONDENDEGOUMBA Ernestine	Chargée de Cours	En poste
34	MESSI Angélique Nicolas	Assistant	En poste
35	TSEMEUGNE Joseph	Assistant	En poste

6- DÉPARTEMENT D'INFORMATIQUE (IN) (27)

1	ATSA ETOUNDI Roger	Professeur	*Chef Div.MINESUP*
2	FOUDA NDJODO Marcel Laurent	Professeur	*Chef Dpt ENS/Chef IGA.MINESUP*
3	NDOUNDAM Réné	Maître de Conférences	En poste
4	AMINOU Halidou	Chargé de Cours	*Chef de Département*
5	DJAM Xaviera YOUH - KIMBI	Chargé de Cours	En Poste
6	EBELE Serge Alain	Chargé de Cours	En poste
7	KOUOKAM KOUOKAM E. A.	Chargé de Cours	En poste
8	MELATAGIA YONTA Paulin	Chargé de Cours	En poste
9	MOTO MPONG Serge Alain	Chargé de Cours	En poste
10	TAPAMO Hyppolite	Chargé de Cours	En poste
11	ABESSOLO ALO'O Gislain	Chargé de Cours	En poste
12	MONTHE DJIADEU Valery M.	Chargé de Cours	En poste
13	OLLE OLLE Daniel Claude Delort	Chargé de Cours	C/D Enset. Ebolowa
14	TINDO Gilbert	Chargé de Cours	En poste
15	TSOPZE Norbert	Chargé de Cours	En poste
16	WAKU KOUAMOU Jules	Chargé de Cours	En poste
17	BAYEM Jacques Narcisse	Assistant	En poste
18	DOMGA KOMGUEM Rodrigue	Assistant	En poste

19	EKODECK Stéphane Gaël Raymond	Assistant	En poste
20	HAMZA Adamou	Assistant	En poste
21	JIOMEKONG AZANZI Fidel	Assistant	En poste
22	MAKEMBE. S . Oswald	Assistant	En poste
23	MESSI NGUELE Thomas	Assistant	En poste
24	MEYEMDOU Nadège Sylvianne	Assistante	En poste
25	NKONDOCK. MI. BAHANACK.N.	Assistant	En poste

7- DÉPARTEMENT DE MATHÉMATIQUES (MA) (30)

1	EMVUDU WONO Yves S.	Professeur	*Inspecteur MINESUP*
2	AYISSI Raoult Domingo	Maître de Conférences	Chef de Département
3	NKUIMI JUGNIA Célestin	Maître de Conférences	En poste
4	NOUNDJEU Pierre	Maître de Conférences	*Chef service des programmes and Diplômes*
5	MBEHOU Mohamed	Maître de Conférences	En poste
6	TCHAPNDA NJABO Sophonie B.	Maître de Conférences	Directeur/AIMS Rwanda
7	AGHOUKENG JIOFACK Jean Gérard	Chargé de Cours	Chef Cellule MINPLAMAT
8	CHENDJOU Gilbert	Chargé de Cours	En poste
9	DJIADEU NGAHA Michel	Chargé de Cours	En poste
10	DOUANLA YONTA Herman	Chargé de Cours	En poste
11	FOMEKONG Christophe	Chargé de Cours	En poste
12	KIANPI Maurice	Chargé de Cours	En poste
13	KIKI Maxime Armand	Chargé de Cours	En poste
14	MBAKOP Guy Merlin	Chargé de Cours	En poste
15	MBANG Joseph	Chargé de Cours	En poste
16	MBELE BIDIMA Martin Ledoux	Chargé de Cours	En poste
17	MENGUE MENGUE David Joe	Chargé de Cours	En poste
18	NGUEFACK Bernard	Chargé de Cours	En poste
19	NIMPA PEFOUKEU Romain	Chargée de Cours	En poste
20	POLA DOUNDOU Emmanuel	Chargé de Cours	En poste
21	TAKAM SOH Patrice	Chargé de Cours	En poste
22	TCHANGANG Roger Duclos	Chargé de Cours	En poste
23	TCHOUNDJA Edgar Landry	Chargé de Cours	En poste
24	TETSADJIO TCHILEPECK M. E.	Chargée de Cours	En poste
25	TIAYA TSAGUE N. Anne-Marie	Chargée de Cours	En poste
26	MBIAKOP Hilaire George	Assistant	En poste
27	BITYE MVONDO Esther Claudine	Assistante	En poste
28	MBATAKOU Salomon Joseph	Assistant	En poste
29	MEFENZA NOUNTU Thiery	Assistant	En poste
30	TCHEUTIA Daniel Duviol	Assistant	En poste

8- DÉPARTEMENT DE MICROBIOLOGIE (MIB) (18)

1	ESSIA NGANG Jean Justin	Professeur	*Chef de Département*
2	BOYOMO ONANA	Maître de Conférences	En poste
3	NWAGA Dieudonné M.	Maître de Conférences	En poste
4	NYEGUE Maximilienne Ascension	Maître de Conférences	En poste
5	RIWOM Sara Honorine	Maître de Conférences	En poste
6	SADO KAMDEM Sylvain Leroy	Maître de Conférences	En poste
7	ASSAM ASSAM Jean Paul	Chargé de Cours	En poste
8	BODA Maurice	Chargé de Cours	En poste
9	BOUGNOM Blaise Pascal	Chargé de Cours	En poste
10	ESSONO OBOUGOU Germain G.	Chargé de Cours	En poste
11	NJIKI BIKOÏ Jacky	Chargée de Cours	En poste
12	TCHIKOUA Roger	Chargé de Cours	En poste
13	ESSONO Damien Marie	Assistant	En poste
14	LAMYE Glory MOH	Assistant	En poste
15	MEYIN A EBONG Solange	Assistante	En poste
16	NKOUDOU ZE Nardis	Assistant	En poste
17	SAKE NGANE Carole Stéphanie	Assistante	En poste
18	TOBOLBAÏ Richard	Assistant	En poste

9. DEPARTEMENT DE PYSIQUE(PHY) (40)

1	BEN- BOLIE Germain Hubert	Professeur	En poste
2	EKOBENA FOUDA Henri Paul	Professeur	*Chef Division. UN*
3	ESSIMBI ZOBO Bernard	Professeur	En poste
4	KOFANE Timoléon Crépin	Professeur	En poste
5	NANA ENGO Serge Guy	Professeur	En poste
6	NDJAKA Jean Marie Bienvenu	Professeur	Chef de Département
7	NOUAYOU Robert	Professeur	En poste
8	NJANDJOCK NOUCK Philippe	Professeur	*Sous Directeur/ MINRESI*
9	PEMHA Elkana	Professeur	En poste
10	TABOD Charles TABOD	Professeur	Doyen Univ/Bda
11	TCHAWOUA Clément	Professeur	En poste
12	WOAFO Paul	Professeur	En poste
13	BIYA MOTTO Frédéric	Maître de Conférences	DG/HYDRO Mekin
14	BODO Bertrand	Maître de Conférences	En poste
15	DJUIDJE KENMOE épouse ALOYEM	Maître de Conférences	En poste
16	EYEBE FOUDA Jean sire	Maître de Conférences	En poste
17	FEWO Serge Ibraïd	Maître de Conférences	En poste
18	HONA Jacques	Maître de Conférences	En poste
19	MBANE BIOUELE César	Maître de Conférences	En poste

20	NANA NBENDJO Blaise	Maître de Conférences	En poste
21	NDOP Joseph	Maître de Conférences	En poste
22	SAIDOU	Maître de Conférences	MINERESI
23	SIEWE SIEWE Martin	Maître de Conférences	En poste
24	SIMO Elie	Maître de Conférences	En poste
25	VONDOU Derbetini Appolinaire	Maître de Conférences	En poste
26	WAKATA née BEYA Annie	Maître de Conférences	*Sous Directeur/ MINESUP*
27	ZEKENG Serge Sylvain	Maître de Conférences	En poste
28	ABDOURAHIMI	Chargé de Cours	En poste
29	EDONGUE HERVAIS	Chargé de Cours	En poste
30	ENYEGUE A NYAM épse BELINGA	Chargée de Cours	En poste
31	FOUEDJIO David	Chargé de Cours	Chef Cell. MINADER
32	MBINACK Clément	Chargé de Cours	En poste
33	MBONO SAMBA Yves Christian U.	Chargé de Cours	En poste
34	MELI'I Joelle Larissa	Chargée de Cours	En poste
35	MVOGO ALAIN	Chargé de Cours	En poste
36	OBOUNOU Marcel	Chargé de Cours	DA/Univ Inter Etat/Sangmalima
37	WOULACHE Rosalie Laure	Chargée de Cours	En poste
38	AYISSI EYEBE Guy François Valérie	Assistant	En poste
39	CHAMANI Roméo	Assistant	En poste
40	TEYOU NGOUPOU Ariel	Assistant	En poste

10- DÉPARTEMENT DE SCIENCES DE LA TERRE (ST) (43)

1	BITOM Dieudonné	Professeur	*Doyen / FASA / UDs*
2	FOUATEU Rose épse YONGUE	Professeur	En poste
3	KAMGANG Pierre	Professeur	En poste
4	NDJIGUI Paul Désiré	Professeur	Chef de Département
5	NDAM NGOUPAYOU Jules-Remy	Professeur	En poste
6	NGOS III Simon	Professeur	DAAC/Uma
7	NKOUMBOU Charles	Professeur	En poste
8	NZENTI Jean-Paul	Professeur	En poste
9	ABOSSOLO née ANGUE Monique	Maître de Conférences	*Vice-Doyen / DRC*
10	GHOGOMU Richard TANWI	Maître de Conférences	CD/Uma
11	MOUNDI Amidou	Maître de Conférences	*CT/ MINIMDT*
12	NGUEUTCHOUA Gabriel	Maître de Conférences	CEA/MINRESI
13	NJILAH Isaac KONFOR	Maître de Conférences	En poste
14	ONANA Vincent Laurent	Maître de Conférences	*Chef service Maintenance and du Matériel*

15	BISSO Dieudonné	Maître de Conférences	*Directeur/Projet Barrage Memve'ele*
16	EKOMANE Emile	Maître de Conférences	En poste
17	GANNO Sylvestre	Maître de Conférences	En poste
18	NYECK Bruno	Maître de Conférences	En poste
19	TCHOUANKOUE Jean-Pierre	Maître de Conférences	En poste
20	TEMDJIM Robert	Maître de Conférences	En poste
21	YENE ATANGANA Joseph Q.	Maître de Conférences	*Chef Div. /MINTP*
22	ZO'O ZAME Philémon	Maître de Conférences	*DG/ART*
23	ANABA ONANA Achille Basile	Chargé de Cours	En poste
24	BEKOA Etienne	Chargé de Cours	En poste
25	ELISE SABABA	Chargé de Cours	En poste
26	ESSONO Jean	Chargé de Cours	En poste
27	EYONG JOHN TAKEM	Chargé de Cours	En poste
28	FUH Calistus Gentry	Chargé de Cours	*Sec. D'Etat/MINMIDT*
29	LAMILEN BILLA Daniel	Chargé de Cours	En poste
30	MBESSE CECILE OLIVE	Chargée de Cours	En poste
31	MBIDA YEM	Chargé de Cours	En poste
32	METANG Victor	Chargé de Cours	En poste
33	MINYEM Dieudonné-Lucien	Chargé de Cours	*CD/Uma*
34	NGO BELNOUN Rose Noël	Chargée de Cours	En poste
35	NGO BIDJECK Louise Marie	Chargée de Cours	En poste
36	NOMO NEGUE Emmanuel	Chargé de Cours	En poste
37	NTSAMA ATANGANA Jacqueline	Chargé de Cours	En poste
38	TCHAKOUNTE J. épse NOUMBEM	Chargée de Cours	*Chef.cell / MINRESI*
39	TCHAPTCHET TCHATO De P.	Chargé de Cours	En poste
40	TEHNA Nathanaël	Chargé de Cours	En poste
41	TEMGA Jean Pierre	Chargé de Cours	En poste
42	FEUMBA Roger	Assistant	En poste
43	MBANGA NYOBE Jules	Assistant	En poste

Répartition chiffrée des Enseignants de la Faculté des Sciences de l'Université de Yaoundé I

DÉPARTEMENT	NOMBRE D'ENSEIGNANTS				
	Professeurs	**Maîtres de Conférences**	**Chargés de Cours**	**Assistants**	**Total**
BCH	9 (1)	13 (09)	14 (06)	3 (2)	**39 (18)**
BPA	13 (1)	09 (06)	19 (05)	05 (2)	**46 (14)**
BPV	07 (1)	10 (01)	15 (08)	00 (0)	**33 (10)**
CI	10 (1)	9 (02)	12 (02)	03 (0)	**34 (5)**
CO	7 (0)	17 (04)	09 (03)	02 (0)	**35(7)**
IN	2 (0)	1 (0)	13 (01)	09 (01)	**25 (2)**
MAT	1 (0)	5 (0)	19 (01)	05 (02)	**30 (3)**
MIB	1 (0)	5 (02)	06 (01)	06 (02)	**18 (5)**
PHY	12 (0)	15 (02)	10 (03)	03 (0)	**40 (5)**
ST	8 (1)	14 (01)	19 (05)	02 (0)	**43(7)**
Total	**70 (5)**	**98 (27)**	**136 (35)**	**38 (9)**	**343 (76)**

Soit un total de **344 (76)** dont :

- Professeurs **70 (5)**
- Maîtres de Conférences **98 (27)**
- Chargés de Cours **136 (35)**
- Assistants **38 (9)**

( ) = Nombre de Femmes **76**

DEDICATION

To my parents Bernard and Véronique SAGANG

I hope that this achievement will complete the dream that you had for me all those many years when you chose to give me the best education you could.

TABLE OF CONTENTS

LIST OF FIGURES

LIST OF TABLES

LIST OF APPENDICES

LIST OF ABBREVIATIONS

AGB: Aboveground biomass

AIRBUS DS: Airbus Defence and Space

ALS: Airborle Laser Scanning

BOA: Bottom Of Atmosphere

CHM: Canopy Height Model

DBH: Diameter at Breast Height (1.3m)

ETM: Enhanced Thematic Mapper

EVI: Enhanced Vegetation Index

FCS: Frequent-Cool-Small

FIL: Frequent-Intense-Large

FSE: forest-savanna ecotone

GEE: Google Earth Engine

GIMMS: Global Inventory Modelling and Mapping Studies

GNSS: Global Navigation Satellite System

ICS: Intermediate-Cool-Small

IPCC: Intergovernmental Pannel on Climate Change

IRECI: Inverted Red-Edge Chlorophyll Index

KNP: Kruger National Park

LEDAPS: Landsat Ecosystem Disturbance Adaptive Processing System

LiDAR: Light Detection and Ranging

LOO-CV: Leave-One-Out Cross-Validation

MCH: Median Canopy Height

MDNP: Mpem et Djim national park

MODIS: Moderate-Resolution Imaging Spectroradiometer

MRV: Measuring, Reporting and Verification

MSD: Mean Signed Deviation

NDVI: Normalized Difference Vegetation Index;

NHPC: Nachtigal Hydropower Company

NIR: Near Infra-Red;

NIRGR: Near Infra-Red Green Ratio;

NSCA: Non-Symmetric Correspondence Analysis

NU-REDD+: National Unit in charge of REDD +

OLI: Operational Land Imager

PCoA: Principal Coordinate Analysis

RCS: Rare-Cool-Small

REDD+: Reducing Emissions from Deforestation and Forest Degradation

RGR: Red Green Ratio

RIL: Rare-Intense-Large

RMSPE: Root Mean Square Prediction Error

RS: Remote sensing

S2REP: Sentinel 2 Red-Edge Position

SAVI: Soil-Adjusted Vegetation Index

SDG: Sustainable Development Goals

SLC: Scan Line Corrector

SR: Simple Ratio

SVH: Spectral Variation Hypothesis

SWIR: Short-wave infra-red

TM: Thematic Mapper

TOA: Top Of Atmosphere

UAV: Unmanned Aerial Vehicles

USGS: United States Geological Survey

ABSTRACT

Understanding the effects of global change (combining anthropic and climatic pressures) on biome distribution needs innovative approaches allowing to address the large spatial scales involved and the scarcity of available ground data. Characterizing vegetation dynamics at landscape to regional scale requires both a high level of spatial detail (resolution), generally obtained through precise field measurements, and a sufficient coverage of the land surface (extent) provided by satellite images. The difficulty usually lies between these two scales as both signal saturation from satellite data and ground sampling limitations contribute to inaccurate extrapolations. Airborne laser scanning (ALS) data has revolutionized the trade-off between spatial detail and landscape coverage as it gives accurate information of the vegetation's structure over large areas which can be used to calibrate satellite data. Also recent satellite data of improved spectral and spatial resolutions (Sentinel 2) allow for detailed characterizations of compositional gradients in the vegetation, notably in terms of the abundance of broad functional/optical plant types. Another major obstacle comes from the lack of a temporal perspective on dynamics and disturbances. Growing satellite imagery archives over several decades (45 years; Landsat) and available computing facilities such as Google Earth Engine (GEE) provide new possibilities to track long term successional trajectories and detect significant disturbances (i.e. fire) at a fine spatial detail (30m) and relate them to the current structure and composition of the vegetation. With these game changing tools our objective was to track long-term dynamics of forest-savanna ecotone in the Guineo-Congolian transition area of the Central Region of Cameroon with induced changes in the vegetation structure and composition within two contrasted scenarios of anthropogenic pressures: 1) the Nachtigal area which is targeted for the dam construction and subject to intense agricultural activities and 2) the Mpem et Djim National Park (MDNP) which has no management plan. The maximum likelihood classification of the Spot 6/7 image aided with the information from the canopy height derived from ALS data discriminated the vegetation types within the Nachtigal area with good accuracy (96.5%). Using field plots data in upscaling aboveground biomass (AGB) form field plots estimates to the satellite estimates with model-based approaches lead to a systematic overestimation in AGB density estimates and a root mean squared prediction error (RMSPE) of up to 65 $Mg.ha^{-1}$ (90%), whereas calibration with ALS data (AGB_{ALS}) lead to low bias and a drop of ~30% in RMSPE (down to 43 $Mg.ha^{-1}$, 58%) with little effect of the satellite sensor used. However, these results also confirm that, whatever the spectral indices used and attention paid to sensor quality and pre-processing, the signal is

not sufficient to warrant accurate pixel wise predictions, because of large relative RMSPE, especially above (200–250 Mg.ha^{-1}). The design-based approach, for which average AGB density values were attributed to mapped land cover classes, proved to be a simple and reliable alternative (for landscape to region level estimations), when trained with dense ALS samples. AGB and species diversity measured within 74 field inventory plots (distributed along a savanna to forest successional gradient) were higher for the vegetation located in the MDNP compared to their pairs in the Nachtigal area. The automated unsupervised long-term (45 years) land cover change monitoring from Landsat image archives based on GEE captured a consistent and regular pattern of forest progression into savanna at an average rate of 1% (ca. 6 km².year^{-1}). No fire occurrence was captured for savanna that transited to forest within five years of monitoring. Distinct assemblages of spectral species are apparent in forest vegetation which is consistent with the age of transition. As forest gets older AGB$_{ALS}$ recovers at a rate of 4.3 Mg.ha^{-1}.year^{-1} in young forest stands (< 20 years) compared to 3.2 Mg.ha^{-1}.year^{-1} recorded for older forest successions ($\geq$ 20 years). In savannas, two modes could be identified along the gradient of spectral species assemblage, corresponding to distinct AGB$_{ALS}$ levels, where woody savannas with low fire frequency store 50% more carbon than open grassy savannas with high fire frequency. At least two fire occurrences in five years is found to be the fire regime threshold below which woody savannas start to dominate over grassy ones. Four distinct plant communities were found distributed along a fire frequency gradient. However the presence of fire-sensitive pioneer forest species in all scenarios of fire frequencies (from low to high fire frequencies) would suggest that the limiting effect of fire on woody vegetation is not sufficient to hinder woody encroachment in the area bringing therefore sufficient humidity required for the establishment of pioneer forest saplings within open savannas. These results have implications for carbon sequestration and biodiversity conservation policies. The maintenance of the savanna ecosystem in the region would require active management actions, and contradicts reforestation goals (REDD+, Bonn challenge, etc.).

Keywords: Forest-savanna ecotone, Google earth Engine, Airborne laser scanning, aboveground biomass, fire, plant communities.

RÉSUMÉ

Comprendre les effets des changements globaux (pressions anthropiques et climatiques) sur la distribution des biomes passe par des approches innovantes qui prennent en compte la large étendue spatiale de même que la faible disponibilité des données de terrain. Caractériser la dynamique de la végétation de l'échelle locale à celle régionale nécessite à la fois un niveau de détail (résolution) élevé, acquis grâce aux mesures précises sur le terrain de même qu'une couverture suffisante de la zone (étendue) obtenue par les images satellitaires. La complexité se trouve généralement entre ces deux échelles ; avec un signal satellitaire limité par la saturation additionné aux données de terrain localisées qui impactent la précision lors des extrapolations. Les données acquises grâce au scanner laser aéroporté (Airborne laser scaning ; ALS) apportent une alternative au compromis entre la précision et la surface couverte nécessaire pour améliorer les données satellitaires. L'avènement des satellites récents (Sentinel 2) avec une meilleure résolution spatiale et spectrale permettent une caractérisation détaillée des groupes floristiques. Un autre obstacle repose sur le manque de perspective temporelle sur les dynamiques et les perturbations. La disponibilité d'archives d'images satellitaires sur plusieurs décennies (>45 ans ; Landsat) de même que l'avènement des méthodes de traitements automatiques tels que Google Earth Engine (GEE) offrent de nouvelles possibilités dans le suivi à long terme des trajectoires de succession à une fine résolution spatiale (30 m) et les relier à la structure et la composition de la végétation. À l'aide de ces outils révolutionnaires l'objectif de cette étude a été de caractériser la dynamique de la végétation dans l'écotone forêt-savane de la zone de transition Guinéo-Congolaise de la région du Centre Cameroun en lien avec des changements induits sur la structure et la composition de la végétation dans la zone de construction du barrage hydroélectrique de Nachtigal et le parc national du Mpem et Djim (PNMD). La classification supervisée avec l'algorithme de maximum de vraisemblance d'une image du satellite Spot 6/7 complété par les informations sur la hauteur de canopée dérivée des données ALS ont servi à discriminer les types de végétation dans la zone de Nachtigal avec une grande précision (96,5 %). L'utilisation des données de terrain afin d'estimer la biomasse aérienne ligneuse (AGB) pour la zone de Nachtigal à partir d'un modèle statistique (model-based approach) calibré sur les données satellitaires a conduit à une surestimation systématique des estimations d'AGB avec une erreur résiduelle moyenne des prédictions (RMSPE) allant jusqu'à 65 Mg.ha^{-1} (90 %), tandis que l'utilisation les données ALS (AGB$_{ALS}$) a conduit à un faible biais et une réduction du RMSPE d'environ 30 % (43 Mg.ha^{-1}, 58 %) avec un faible effet du type de satellite utilisé. Cependant ces résultats confirment qu'une attention particulière doit

être portée sur la qualité du capteur et le prétraitement des images pour tous les satellites. Le signal du satellite ne garantit pas une précision dans les estimations à l'échelle du pixel au-delà de 200–250 Mg.ha^{-1} à cause des valeurs élevées du RMSPE relatif. L'approche basée sur la conception (design-based approach) pour laquelle les valeurs moyennes d'AGB sont attribuées aux différents types de végétation constitue une alternative simple et fiable pour des estimations d'AGB à l'échelle du paysage pour des données ALS distribuées dans les différentes typologies. L'AGB et la diversité spécifique mesurées au sein de 74 parcelles d'inventaires (distribuées le long d'un gradient de succession de la savane vers la forêt) sont élevées pour les végétations localisées dans le PNMD comparées aux végétations semblables échantillonnées à Nachtigal. L'approche automatique non supervisée du suivi à long terme (45 ans) des changements de couvert à partir d'archives Landsat dans GEE a mesuré un avancement constant et régulier de la forêt sur la savane à une vitesse moyenne d'environ 6 km²an^{-1}. L'archive d'image Landsat est la mieux appropriée pour le suivi de la fréquence des feux dans la zone d'étude en comparaison avec les produits MODIS. Entre deux périodes de monitoring successifs (5 ans) les pixels de savane avant la transition vers la forêt n'ont enregistré aucun évènement de feu. Des assemblages distincts d'espèces spectrales (β-diversity) sont apparents en forêt et sont corrélés avec l'âge de la transition. L'accumulation de l'AGB$_{ALS}$ avec l'âge de la forêt est de of 4,3 Mg.ha^{-1}an^{-1} pour les jeunes forêts (< 20 ans) contre of 3,2 Mg.ha^{-1}an^{-1} pour les vieilles successions forestières (≥ 20 ans). En savane deux modes ont été identifiés le long du gradient de groupes spectraux correspondant aux niveaux AGB$_{ALS}$ où la savane boisée associée à une faible fréquence de feu stocke 50 % plus de carbone que les savanes ouvertes dominées par les graminées qui ont une fréquence de feu élevée. Une occurrence de feu en 5 ans est nécessaire pour limiter le boisement de la savane. Ces résultats décrivent quatre communautés végétales suivant un gradient de transition et d'historique de feu. Cependant la présence d'espèces forestières dans des parcelles avec une fréquence de feux faibles suggèrerait l'inefficacité du feu dans la limitation du boisement de la savane. Ces résultats ont des fortes implications pour la séquestration du carbone et les politiques de conservation de la biodiversité. Le maintien des écosystèmes de savane dans la région va nécessiter des méthodes de gestion appropriées et sont contradictoires aux objectifs de reforestations (REDD+, Bonn challenge, etc.).

Mots clés : Écotone forêt savane, Google Earth Engine, scanner laser aéroporté, biomasse aérienne ligneuse, feux, communautés végétales.

CHAPTER I

GENERALITIES

CHAPTER I. GENERALITIES

I.1. INTRODUCTION

I.1.1 Context and justification

A major controversy emerged after a recent study suggested large scale afforestation as the most effective solution for climate change mitigation (Bastin *et al.*, 2019). Among the issues raised, the economic cost of such a strategy is not the biggest. The actual impacts in terms of carbon storage, but also biodiversity reduction, as other ecosystems are forcibly transformed are discussed (Thomas *et al.*, 2013; Abreu *et al.*, 2017). Moreover, afforestation often implies interfering with natural succession, for clearing the land prior to planting (sometimes exotic) trees. It makes sense to improve our knowledge of the dynamics taking place naturally in absence of direct human impacts, prior to launching vast, costly, possibly damaging and ultimately uncertain national afforestation programs. In Africa, forest and savanna are the dominant biomes covering respectively 11% and 34% of the land surface of the continent (Nangendo *et al.*, 2006; Parr *et al.*, 2014) and accounting for more than 60% of terrestrial productivity (Beer *et al.*, 2010). Several studies, scattered from Guinea to the Central African Republic (Achoundong *et al.*, 1996; Youta *et al.*, 2003; Mitchard *et al.*, 2011; Mitchard and Flintrop, 2013) and central Gabon (Jeffery *et al.*, 2014; Cardoso *et al.*, 2020) have illustrated a widespread forest encroachment over savannas, while referring to time windows of variable lengths within the last six decades. While forest encroachment seems appealing for climate change mitigation policies, like the Reducing Emissions from Deforestation and Degradation (REDD+) initiative, it is at the expense of reduced species diversity especially for species-rich savannas (Abreu *et al.*, 2017). Therefore promoting forest cover (Bonn Challenge) for carbon sequestration may not always be reconcilable with a biotope conservation/restoration agenda, despite claims to the contrary (Thomas *et al.*, 2013; Abreu *et al.*, 2017; Dinerstein *et al.*, 2020).

In Central Africa, a significant challenge to predict the effect of global change on biome distributions is to bring out innovative approaches that offset the scarcity of spatially and temporally detailed landscape-scale information. Previous efforts have been either sample-based or employed coarse spatial resolution data (Youta-Happi, 1998; Youta-Happi *et al.*, 2003; Cuni-Sanchez *et al.*, 2016; Deklerck *et al.*, 2019) owing to the challenges of maintaining sampling over long periods combined with the inherent constraints of field data collection which do not consider the whole variability of the landscape. Remote sensing (RS) therefore has a great potential for use in mapping biodiversity (Broadbent *et al.*, 2008; Hill, 2013; Féret

and Boissieu, 2020), biomass (Bastin *et al.*, 2014; Kumar *et al.*, 2015; Pandit *et al.*, 2018; Forkuor *et al.*, 2019) and periodical phenomena i.e. fires (Nangendo *et al.*, 2006; Miller and Thode, 2007; Escuin *et al.*, 2008; Sunderman and Weisberg, 2011; Chen *et al.*, 2017) with continuous spatial coverage over large geographic areas. More recent satellite constellations carrying passive optical sensors (notably Sentinel 2; 10 m; Planet; 3.7 m) of improved temporal, spectral and spatial resolutions allow more detailed characterizations of compositional gradients in the vegetation, notably in terms of the abundance of broad functional/optical plant types. Féret *et al.* (2020) proposed an unsupervised method for preliminary assessment of compositional gradients, which could be crudely referred to as spectral Beta diversity (β-diversity) gradients. However the performance of such spaceborne data is known to be poor in characterising some structural properties of the vegetation (Avitabile and Camia, 2018). This is the case of aboveground biomass (AGB) where the sensitivity of currently available spaceborne data sources (prior to the launch of GEDI and Biomass sensors) is known to be poor to characterise high AGB densities (say, >200 Mg.ha-1; Avitabile and Camia, 2018; Réjou-méchain *et al.*, 2019). In areas with a high degree of cloudiness like in western Central Africa (King and Platnick, 2005), atmospheric effects are responsible for spatial artefacts observed in the surface reflectance of spaceborne optical data (Song *et al.*, 2001; Morton *et al.*, 2014) also some spaceborne sensors fail to distinguish the fine vegetation textures that are found in forest to grass transition areas. To overcome this problem, several authors (Asner, 2009; Baccini and Asner, 2013; Asner and Mascaro, 2014; Zhang *et al.*, 2017; Réjou-méchain *et al.*, 2019) recommended the integration of airborne LiDAR scanning (a.k.a. ALS) data as an intermediate level in vegetation modelling. Due to its ability to accurately characterize the vegetation's three-dimensional structure, ALS has indeed emerged as the reference technology for mapping vegetation structure at landscape scale (Asner and Mascaro, 2014; Réjou-Méchain *et al.*, 2015; Adhikari *et al.*, 2017; Jha *et al.*, 2020) leveraging on multispectral satellite imagery. It is not clear however which satellite data (between broad spectral bands and relatively high spatial resolution i.e. Spot 6-7, or narrower, more numerous spectral bands and lower spatial resolution i.e. Landsat 8 and Sentinel 2) provides the best solution for upscaling vegetation structure estimates from field data. The opening of imagery archives (i.e. Landsat and now Sentinel 2, if we focus on optical sensors) as well as common storage and computing facilities, such as the Google Earth Engine platform (Gorelick *et al.*, 2017) enable the characterization of large areas and the generation of dynamic, transparent, systematic, repeatable, and spatially exhaustive information products. Helped with these game-changing tools, it is at long last possible to have the hindsight (45 years for Landsat) and coverage allowing the study of ecosystem dynamics at

a meaningful spatiotemporal scale (Estes *et al.*, 2018; Wulder *et al.*, 2018). It is also possible to focus on phenomena involving land covers of contrasted spectral signatures. The case of forest-savanna ecotone (FSE) is a perfect study case in this respect, because the two major ecosystem states do have distinct signatures. In such conditions, transition dates can be easily assessed (Zhu and Woodcock, 2014; DeVries *et al.*, 2015; Dutrieux *et al.*, 2015; Hamunyela *et al.*, 2016). Besides, one of the main ecological drivers of the forest-savanna dynamics, fire (Sankaran *et al.*, 2005; Bond, 2008; Staver *et al.*, 2011a; Gomes *et al.*, 2020), also leaves conspicuous marks that can be successfully characterised from satellite images (Daldegan *et al.*, 2014, 2019). Thanks to the spatial resolution of Landsat image (30 m) the influence of fire on the vegetation structure can be investigated at a fine spatial details as compared to past studies that relied on burned area products derived from coarse (500 m) Moderate Resolution Imaging Spectroradiometer (MODIS) (Staver *et al.*, 2011a; Diouf *et al.*, 2012; Axelsson and Hanan, 2018; Venter *et al.*, 2018).

Emerging economies are currently experiencing a rapid expansion of built infrastructures (buildings, roads and hydroelectric dams); (Ermgassen *et al.*, 2019; Jones and Bull, 2020) for alleviating poverty and delivering economic growth (Agenor and Moreno-Dodson, 2006; Donaldson, 2018). Infrastructure can affect biodiversity in multiple ways, including direct habitat loss within the built infrastructure footprint, alteration of ecosystem properties or fragmentation (Torres *et al.*, 2016). This is even more significant with hydroelectric dam construction which generally implies the permanent flooding of naturally drylands (Jones and Bull, 2020). Implementing such long-lived infrastructures without being accompanied by strong environmental safeguards can turn out to be drivers of biodiversity and ecosystem service loss (Ranger *et al.*, 2013). This is the case in the Central region of Cameroon where the hydroelectric dam construction over the Sanaga River crossing a FSE will undoubtedly have significant impact on the vegetation. The Nachtigal Hydropower Company (NHPC) in charge of the implementation of this project therefore took the engagement to avoid/reduce carbon and biodiversity loss as regards to the Sustainable Development Goals (SDGS). Understanding the dynamics of FSE in the area and induced changes in the vegetation structure and floristic composition is essential to evaluate the negative impacts of the dam within the construction area and to guide NHPC in setting up mitigation and compensation measures which will be implemented in nearby protected areas without a management plan: the Mpem et Djim national park (MDNP) and the community forest COPAL.

I.1.2   General and specific objectives

I.1.1.1.   General objective

The general objective of this study is to characterize long-term (> 40 years) dynamics of forest-savanna ecotone (FSE) and induced changes in the vegetation structure and composition within two contrasted scenarios of anthropogenic pressures in the Guineo-Congolian transition area of the Central Region of Cameroon.

I.1.1.2.   Specific objectives

Specifically, this study aimed to:

- Describe the variation in vegetation types and aboveground biomass over a forest-savanna transitional landscape;
- Quantify the rate of forest encroachment and the induced changes on the functional properties of the vegetation;
- Examine the role of fire in shaping the vegetation structure and dynamics;
- Describe the succession pattern in the vegetation structure and floristic composition as forest encroaches over savanna.

I.1.3   Research hypothesis and questions

This work relies on four research hypotheses:

1. Airborne LiDAR data improves the precision of landscape scale description of the vegetation types and AGB variation when used as intermediate level between field inventory data and optical satellite data;
2. Satellite data with high spatial and spectral resolution and cloud computing of Landsat image archives make it possible to automate the monitoring of land cover and characterise main drivers i.e. fire, in a simple, objective and reproducible way;
3. The frequency of fire determine the fate of forest-savanna transitions by shaping the structure and composition in the woody layer;
4. Both the aboveground biomass and floristic composition follow a successional gradient corresponding to the identified landscape dynamics.

We formulated four research questions with the view of answering to our research objectives:

1- What level of accuracy can we achieve when combining ALS data and different optical satellite imageries to describe vegetation types and structure in forest-savanna transitions?

2- What is the potential of Landsat image archives and current cloud computational capacities in monitoring long-term change in vegetation structure and characterise the frequency of fire across forest-savanna transitions?

3- How do the structure and composition of the vegetation vary along a fire frequency gradient?

4- What is the rate of AGB recovery; beta-diversity structuring and compositional shifts or trends in the floristic composition along a forest successional gradient?

I.2. LITERATURE REVIEW

I.2.1. Forest-savanna ecotone in tropical areas: definitions and concepts

Transitional areas between forest and savanna are the most widespread ecotone in tropical Africa (Bouvet *et al.*, 2018) and this coexistence results into an area with evolutionary dynamism, storing genetic animal and plant diversity and acting as an important locus for the generation of new species (Smith *et al.*, 2001). At broad scales, the location of the transition is shaped by water availability, mediated strongly at local scales by disturbances such as fires, herbivory and spatial variation in soil properties. Uncertainties still remain on the relative contribution of the drivers and their interactions in determining the evolution of forest-savanna ecotones (FSE). FSE therefore constitutes a critical, yet poorly understood, component of tropical landscape dynamics. The distribution of major biomes of the world are controlled by climate, particularly the distribution of temperature and precipitation under which they are subjected (Whittaker, 1970; Olson *et al.*, 2001; Kottek *et al.*, 2006). Savannas are ecosystems characterized by the coexistence of a discontinuous tree layer with an understory that is dominated by a continuous layer of herbaceous C4 grasses (Poaceae) and sedges (Cyperaceae) (Archer, 1997; Higgins *et al.*, 2000; Bond, 2008; Ratnam *et al.*, 2011; Parr *et al.*, 2014; Oliveras and Malhi, 2016). The openness of the canopy favours the establishment of light demanding C4 grasses in the understory (Hoffmann *et al.*, 2003) which dry off during the dry season and produce sufficient biomass which promotes fires. Consequently the association with fire has led both C4 grasses and the trees that grow with them to develop fire-adaptive strategies. In

contrast, forests are characterized by closed, shaded environments with cooler and more humid micro-climatic conditions which limits the development of light demanding C4 grasses reducing thus the probability of fire occurrence (Ratnam *et al.*, 2011; Hoffmann *et al.*, 2012; Parr *et al.*, 2014). The tree species that dominate forest habitats are largely shade tolerant but very sensitive to fires (Hoffmann *et al.*, 2009a; Murphy and Bowman, 2012).

Savannas constitute the most spatially extensive biome in the world (Fig. 1) and are found along a broad range of precipitation, temperature and topo-edaphic regimes from tropical to temperate areas particularly in North America, Latin America, Africa, Australia and South East Asia (Solbrig, 1996; Archer, 1997; Marchant, 2010).
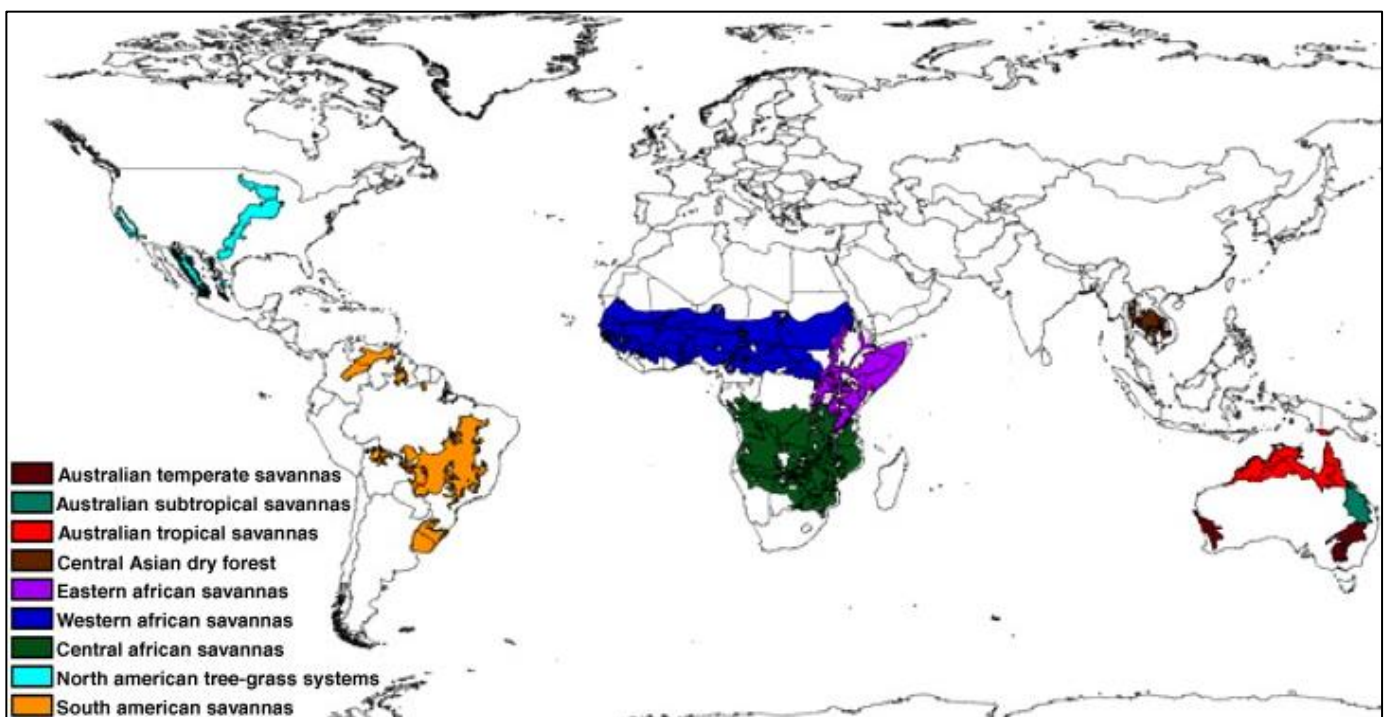
Fig. 1: Distribution of the major savanna biome across the tropics (Marchant, 2010).

In tropical humid areas like in Central Africa where mean annual rainfall varies between 1 500 and 1 800 mm moist humid forests are expected to dominate (Fig. 2; Whittaker, 1970). However, several experimental and modelling work have demonstrated that savannas can occur in areas where climate, soils, and topography suggest forest should dominate (Swaine *et al.*, 1992; Moreira, 2000; Russell-Smith *et al.*, 2003; Favier *et al.*, 2004a, 2012; Bond *et al.*, 2005; Bond, 2008). Forest-savannah transitions in tropical areas have therefore been often referred to as zones of tension between two very different biomes where the stability and distribution of each vegetation at local scales depends on the spatial and temporal variability of abiotic and biotic drivers, and ecological processes and attributes (Fig. 3; Favier *et al*., 2012; Hoffmann *et al*., 2009b; Lehmann *et al*., 2011).
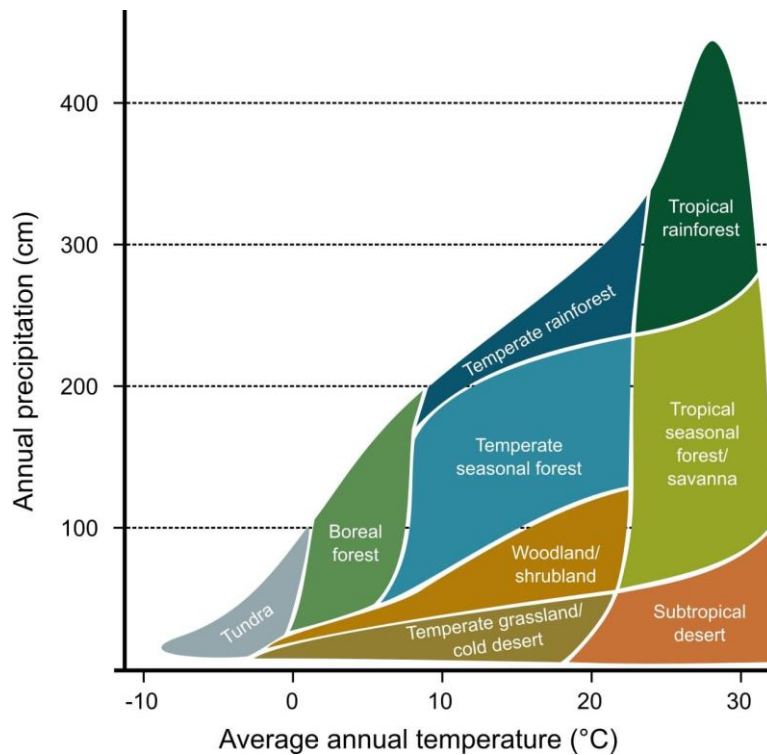
Fig. 2: Functional distribution of the main terrestrial biomes in function of the mean annual precipitation and temperature as proposed by Whittaker (1970).

Unfortunately no agreement has been reached concerning the relative importance of climate, fire, hydrology, herbivory and soil characteristics in mediating the balance between these biomes (Tinley, 1982; Hopkins, 1992; Ruggiero *et al.*, 2002; Hirota *et al.*, 2010; Good and Caylor, 2011). At the global scale, and at large time scales, climate (mean annual temperature, precipitation seasonality and dry season length), fire regimes (frequency and intensity of fires) and soil types determine distribution between forests (dark green; Fig. 3), grassy vegetation (dark purple as natural, light purple has human-modified; Fig. 3) and grassland biomes. At the community scale, fire regimes, soil properties and herbivory are the main drivers, and ecological processes are mostly reflected in tree-grass coexistence (see Fig. 3). At the local scale, many drivers and ecological processes affect the given vegetation existing at that precise point in space and time (Oliveras and Malhi, 2016)
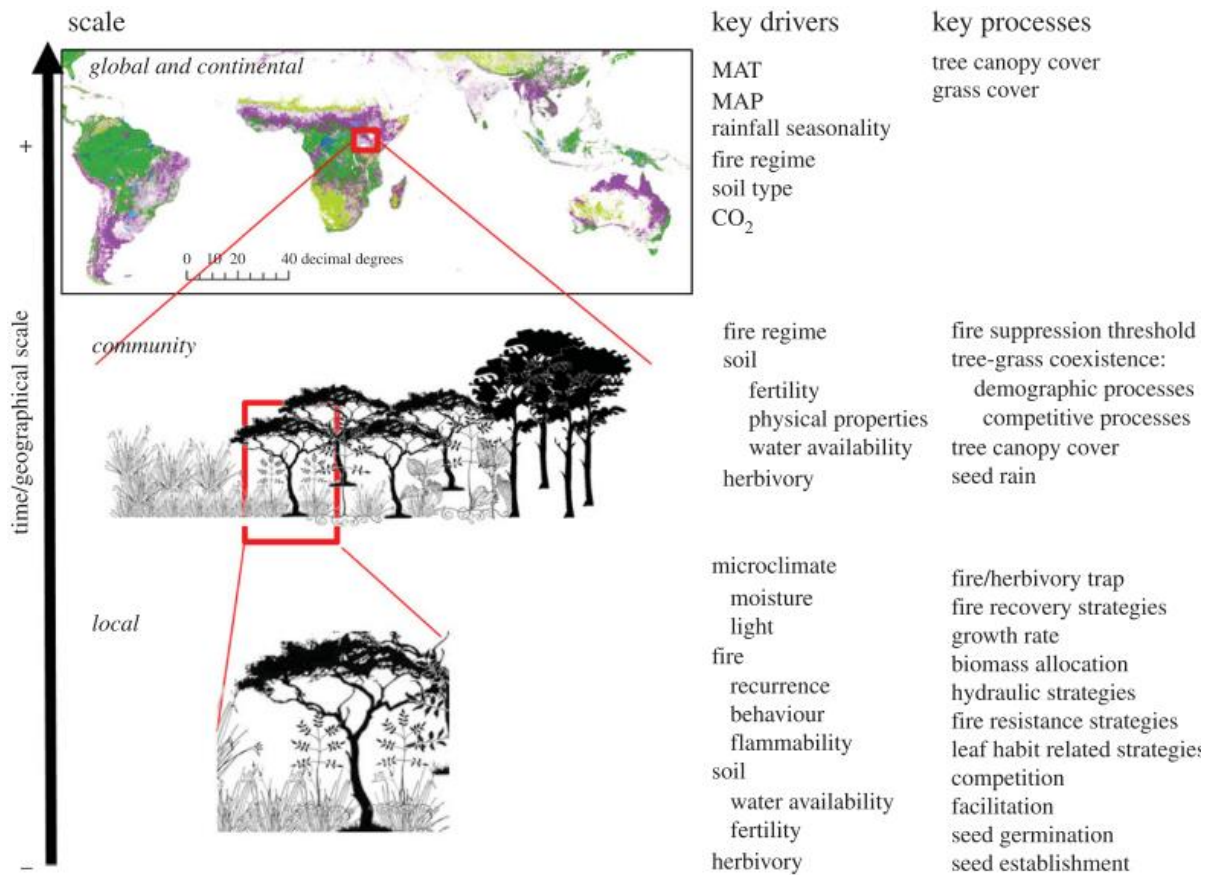
Fig. 3: Main drivers and processes operating in shaping forest–savannah transitions and their scale of operability from global scale to local scale (Oliveras and Malhi, 2016).

I.2.2. Major drivers and processes shaping the distribution of forest-savanna vegetation

I.2.2.1. Role of climate

In tropical areas where mean annual rainfall exceeds the 650-1000 mm threshold increased rainfall would have minimal effect on forest savanna boundaries, as these systems are at a disequilibrium between vegetation and climate (Bond *et al.*, 2005; Sankaran *et al.*, 2005; Bond and Midgley, 2012; Favier *et al.*, 2012). Changes in temperature could affect interactions between rainfall and woody cover as the raise in temperature increases transpiration which effectively counteract the effects of higher rainfall. Furthermore, widespread tree mortality recorded after extreme drought events offset increases in woody growth recorded during increased rainfall (Fensham *et al.*, 2009). Also empirical studies from (February *et al.*, 2013) demonstrates that increasing rainfall favours the competition between trees and grasses, ultimately suppressing tree growth. In tropical areas an increase in the CO_2 concentrations at the local scale will favour the development of trees that use the C_3 photosynthesis pathway over the dominant grasses that use more costly C_4 metabolically pathway (Higgins and Scheiter,

2012). The long-term increase in atmospheric CO_2 will thus favour trees over most abundant lowland savannah grasses (Bond and Midgley, 2012). Both woody thickening of savannahs and forest encroachment into savannahs is therefore expected at the regional scale due to increasing CO_2. The net impact may be greater in mesic than in arid savannah environments (Bond and Midgley, 2012; O'Connor *et al.*, 2014). The presence of a continuous grass layer in savanna favours frequent fires which regularly destroys the aerial biomass of woody saplings (Fig. 5; topkill Hoffmann *et al.*, 2009b). Repeated topkill results in a demographic bottleneck which limit successful tree seedling germination, establishment and/or transition to mature size classes (Higgins *et al.*, 2000, 2007; Ward *et al.*, 2014) whereas saplings that lack the ability to regenerate are eliminated under frequent fires (Fensham and Fairfax, 2003).

I.2.2.2. Role of fire

Amongst the multiple factors that limit tree cover in savanna, fire appears to be the most widespread and universal in savannas worldwide to prevent from canopy closure (Bond and Keeley, 2005; Sankaran *et al.*, 2005; Bond, 2008; Lehmann *et al.*, 2011; Staver *et al.*, 2011b; Reiche *et al.*, 2016). Grassy ecosystems in Central Africa have frequent fire occurrences (**Fig. 4**; Archibald *et al.*, 2013) therefore the distribution of savanna and forest cannot be adequately explained without explicitly considering the essential role of fire.
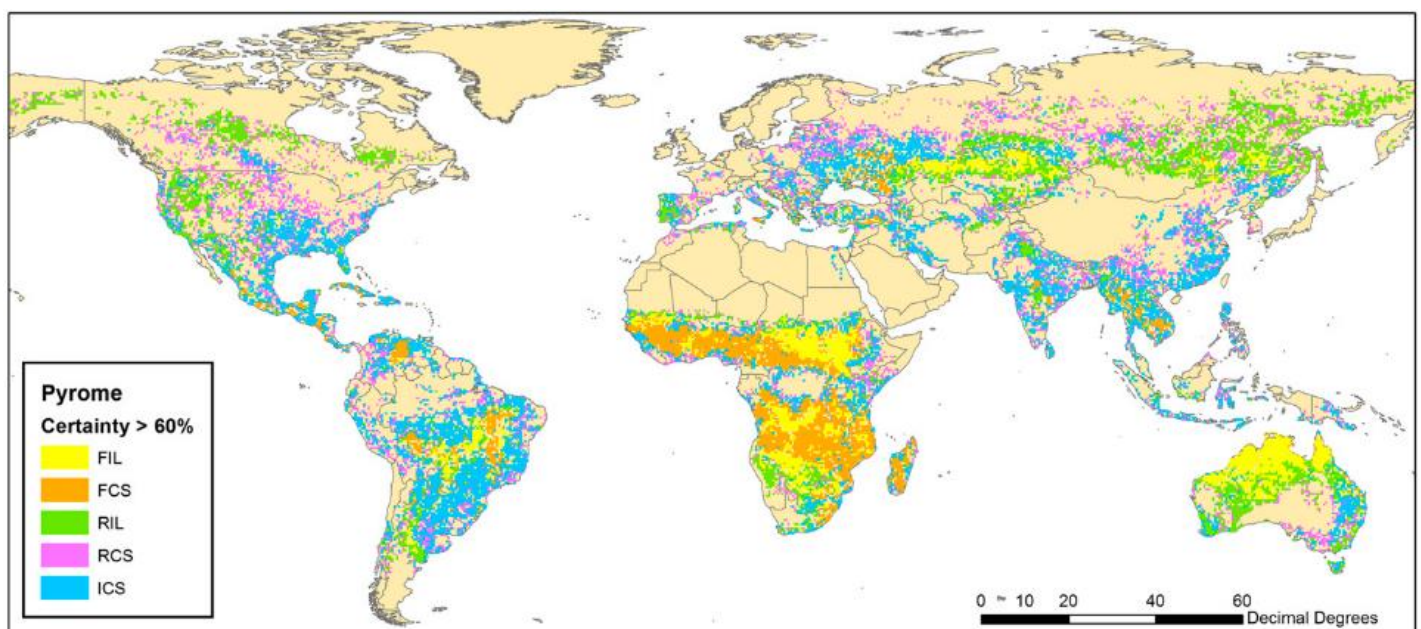
Fig. 4: Spatial distribution of pyromes (Archibald *et al.*, 2013). Pyromes represent regions of the globe that have similar fire frequencies, intensities, sizes, burned areas, and fire season lengths. Pixels with greater than 60% probability of being uniquely categorized are plotted (85% of the data). FIL = Frequent-intense-large; FCS = frequent-cool-small; RIL = rare-intense-large; RCS = rare-cool-small; and ICS = intermediate-cool-small.
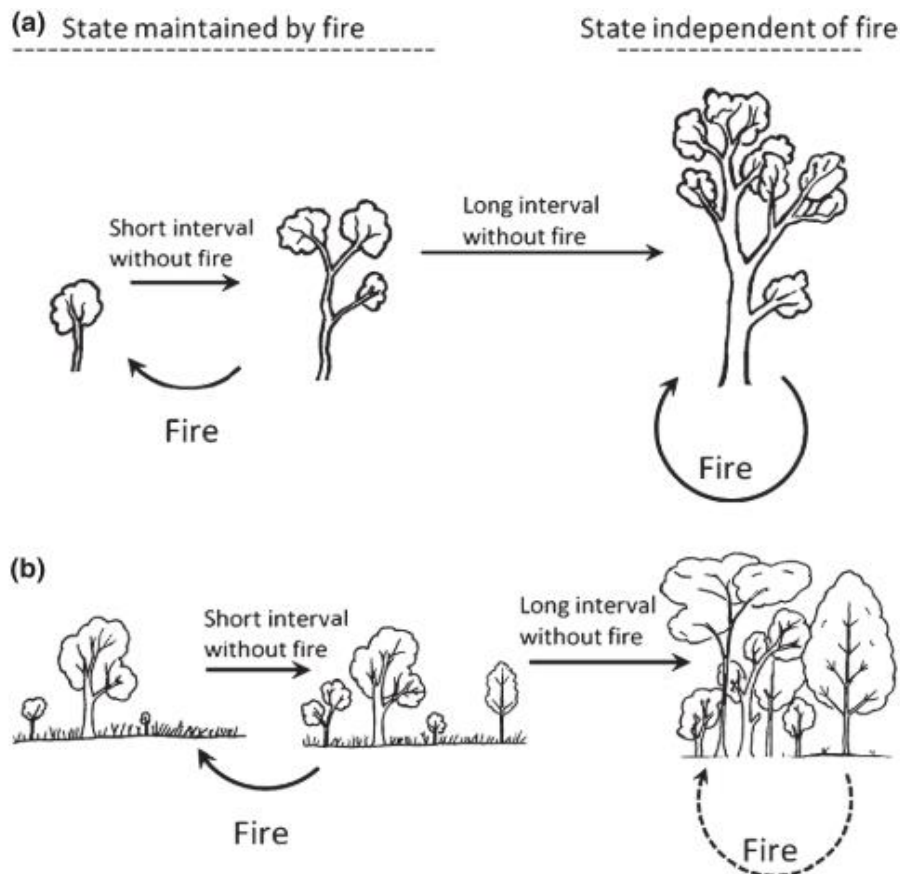
Fig. 5: The two critical thresholds that govern the response of savanna systems to fire.
(a) The fire-resistance threshold and (b) The fire-suppression threshold (Hoffmann *et al.*, 2012).

A fire-free interval of sufficient duration is therefore required to ensure woody saplings to reach an adult state with a critical size at which they are no longer susceptible to topkill (Bond and Midgley, 2000). At the individual level the point at which a tree has grown and is much less likely to be topkilled by subsequent fires can be referred to as a fire-resistance threshold and once a stem has surpassed this threshold it can continue to grow and extent his crown area leading to a gradual canopy closure (Veenendaal *et al.*, 2015, 2018). The savannah gradually reaches a fire-suppression threshold due to its canopy closure that provides moist conditions with a low-light understory environment. The light demanding grass layer which was previously dominant is gradually replaced by fire resistant grasses (*Aframomum* spp., *Chromolaena odorata*) and shrub of light-demanding forest tree species such as *Albizia* spp. (Youta and Bonvallot, 1996; Youta, 1998; Youta *et al.*, 2003; Ibanez *et al.*, 2013) which limits the occurrence of fire. Veenendaal *et al.* (2015) evidenced an increase in the proportion of forest species with an increase in canopy closure and suggested that fire suppression serves to promote the likelihood of survival of forest species. Tropical forest is much less flammable (Uhl and Kauffman, 1990; Hoffmann *et al.*, 2012) and generally burns much less frequently and less intensely, allowing it to maintain a dense canopy with distinct ecosystem properties (Eldridge

et al., 2011). Savanna and forest have been frequently regarded to represent alternate stable states maintained by the positive feedback between fire and vegetation (Hoffmann *et al.*, 2009; Hirota *et al.*, 2010; Staver *et al.*, 2011b; Dantas *et al.*, 2013). The alternative stable states theory postulates that two ecosystem states can occur under the same set of environmental conditions, and the presence of one or the other is determined by disturbance and historical pathway at the community and larger scale (Whittaker and Levin, 1977). Both fire-resistance and fire-suppression thresholds represent a switch from a state maintained by frequent fires to a state that is not strongly influenced by fire. Once either threshold is surpassed, a return to the pre-threshold state should become increasingly dependent on extreme events. Once a stem has passed the fire-resistance threshold, the probability of topkill will decline as the stem grows and accumulates more bark which protects the vessels from damages due to high temperatures generated by fires. Even so, extremely intense fires can cause some topkill of large trees that would otherwise be fire resistant (Williams *et al.*, 1999; Ryan and Williams, 2011). At the ecosystem level, once the fire-suppression threshold has been reached, subsequent fires will generally be less frequent, less intense and restricted to times of severe drought. Although low-intensity fires can be devastating in humid rainforest (Cochrane and Schulze, 1999; Barlow and Peres, 2008), forests of the seasonal tropics appear much more resilient to fire (Hoffmann *et al.*, 2009; Balch *et al.*, 2011); therefore, the return to a savanna state probably requires multiple burns to cause successive reduction in tree cover and a gradual expansion of grasses.

I.2.2.3. Role of herbivory

Several authors have explored the influence of mammalian herbivores on savanna structure (Augustine and McNaughton, 1998; Langevelde *et al.*, 2003; Augustine and Mcnaughton, 2004; Sankaran *et al.*, 2008). An increase in the level of grazing leads to reduced fuel load, which makes fire less intense and, thus, less damaging to trees and, consequently, results in an increase in woody vegetation (Fig. 6 a and b; Langevelde *et al.*, 2003).

The system then switches from a state with combined trees and grasses to a state with solely trees. This phenomenon has been observed in the region of Ilaha and Maracà in Guyana where forest species have become abundant in grazed savannas in contact with the forest (Eden *et al.*, 1990). Likewise, an increase in the woody cover was observed on the margin of savannas exploited by extensive livestock farming in the north of Côte-d'Ivoire (Buzon, 1990). In the Sudano-Guinean savannas of the Adamawa plateau in Cameroon where extensive livestock farming is traditionally practiced, overgrazing led to a reduction in the grass cover which contributes to the decrease in the intensity of fires, would have favoured the multiplication

savannah shrubs, and therefore an increase in the rate of woody cover (Hurault, 1975). In contrast large browsers (i.e. elephants) may enhance the effect of fire on trees because they reduce woody biomass, thus indirectly stimulating grass growth (Fig. 6 c and d; Accatino *et al.*, 2016; Augustine and Mcnaughton, 2004). This consequent increase in fuel load results in more intense fire and increased decline of biomass. The system then switches from a state with solely trees to a state with trees and grasses.
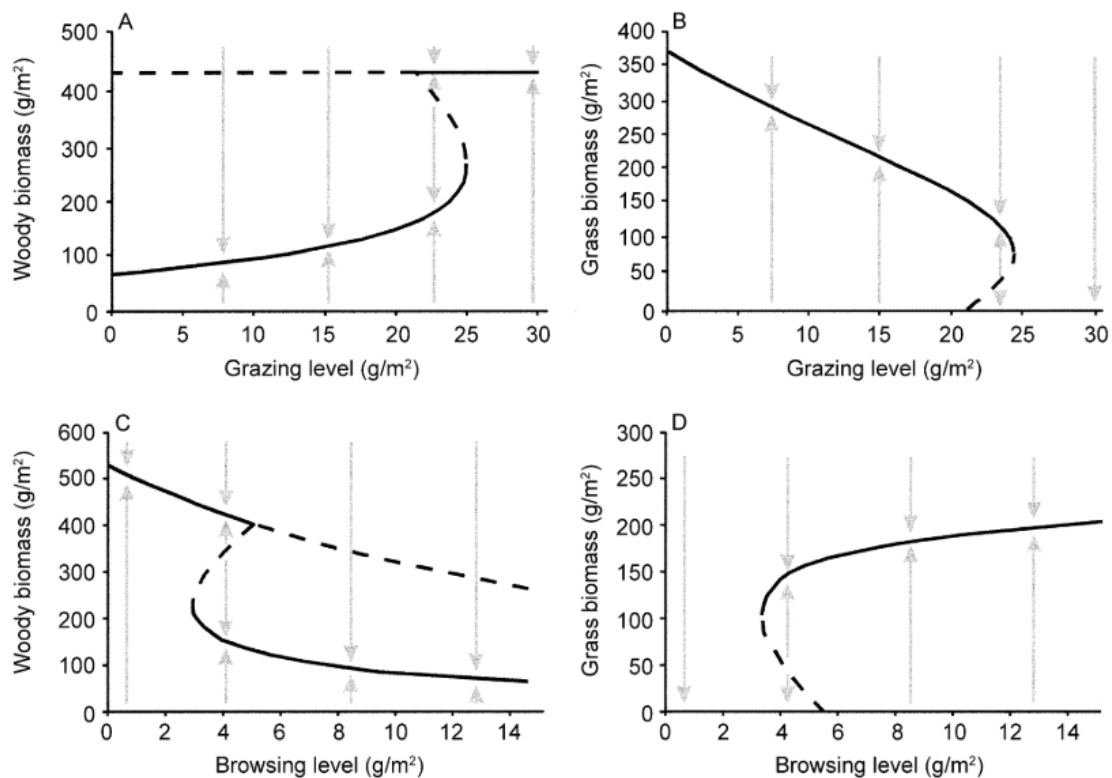
Fig. 6: Changes in the equilibrium woody and grass biomass with levels of grazing (A and B) and browsing (C and D). Sudden jumps of woody and grass biomass occur at distinct levels of grazing, and browsing. Solid lines give the stable equilibria, and dashed lines give the unstable equilibria. Arrows indicate the direction of development. (Modified from Langevelde *et al.*, 2003).

I.2.2.4.   Role of soil and topography

Locally, other edaphic factors, such as insufficient nutrient stocks, shallow, sandy or seasonally flooded soils, might prevent some sites from ever becoming forest during fire suppression. Soils can also vary spatially along the forest-savannah transition in fertility (e.g. organic matter, cation exchange capacity, macronutrients), soil physical properties (e.g. percentage of sand), and soil depth, the latter two factors combining to determine soil water availability. Soil fertility has long been recognized to be lower in savannah soils (Baillie, 1987) which is responsible for the lack of trees in savanna biomes (Bond and Parr, 2010) as low nutrient availability limits tree growth. In contrast, other studies suggest that areas of high nutrient availability are associated

with a reduction in woody cover, largely as a result of competition from grasses (Mills *et al.*, 2013). The interaction of soil fertility with water availability and soil water holding capacity can strongly influence forest-savannah boundaries (Veenendaal *et al.*, 2015). Forest patches are usually located in areas with higher soil moisture than savannah patches, but in seasonally flooded parts of the landscape the waterlogging can create anoxic conditions for roots, favouring short-lived grasses that grow in the non-flooded season. Conversely, a more regular water supply and shallower water table enables gallery forests to persist in savannah landscapes. Lehmann *et al.* (2011) show that areas of low rainfall and high nutrient availability facilitate the growth of palatable grasses, which in turn leads to increased herbivory and the maintenance of a savanna system. In contrast, high rainfall and nutrient availability facilitate rapid tree growth, resulting in a transition to a forests system. Soil nutrient availability and underlying geology may also alter vegetation communities through complex interactions with disturbance.

In tropical areas the great and very uniform depth of the ferrallitic soils which are dominant favour the growth of woody species. In fact, their water reserves are always largely sufficient to ensure a continuous plant growth, except locally when ferruginous crusts, dismantled or not, are superficial. In Kruger National Park woody cover was observed to increase in areas with nutrient-poor, granite soils and decrease in areas with nutrient-rich basalt soils over a sixty-year period, a pattern likely driven by herbivory (Eckhardt *et al.*, 2000). It is thought that grasses in nutrient-poor soils do not recover as quickly under high grazing pressure as grasses in nutrient-rich soils, resulting in decreased tree-grass competition. The findings of Levick and Rogers (2011), from a more northerly section of Kruger National Park (KNP) are similar, but point to a more ubiquitous increase. Here, woody cover increased in both nutrient-poor granite soils and nutrient-rich basalt soils but the increase was slightly more prominent in the basalt areas due to presumed higher levels of grazing and lower fire frequency, which encouraged tree growth (Levick and Rogers, 2011). Buitenwerf *et al.* (2012) also demonstrate that woody encroachment occurs rapidly on granite-based soils but is predominantly absent in basalt-based soils. Colgan *et al.* (2012) recorded lower woody aboveground biomass (AGB) levels on crests which linearly increased toward streams in the KNP. The observed pattern was different on granite substrates, where AGB was high on crests, decreased midslope, and then increased near stream channels. Overall, they observed 5-to-8-fold lower AGB on clayey, basalt-derived soil than on granites, and suggested this is due to herbivore-fire interactions rather than lower hydraulic conductivity or clay shrinkage/swelling, as previously hypothesized. Furthermore, Devine *et al.* (2015) observed much higher woody cover in a wet granite-based region than a dry granite-based area

of Kruger National park. It would appear, therefore, that though interactions between soils properties and disturbance play an important role in regulating woody cover. By mapping AGB within and outside fire and herbivore exclusion, they found that basalt-derived soils support tenfold higher AGB in the absence of fire and herbivory, suggesting high clay content alone is not a proximal limitation on AGB.

I.2.3. Dynamics of forest-savanna ecotone in Central Africa

Several authors have described a widespread woody encroachment into savannas in Central Africa (Fig. 7 and Fig. 8; Boulvert, 1990; Youta and Bonvallot, 1996; Youta, 1998; Youta *et al.*, 2003; Favier *et al.*, 2004b; Mitchard *et al.*, 2009; Mitchard and Flintrop, 2013; Cuni-Sanchez *et al.*, 2016; Aleman *et al.*, 2017; Devine *et al.*, 2017; Axelsson and Hanan, 2018; Deklerck *et al.*, 2019) with significant impacts on the global carbon budget of the continent (Poulter *et al.*, 2014).
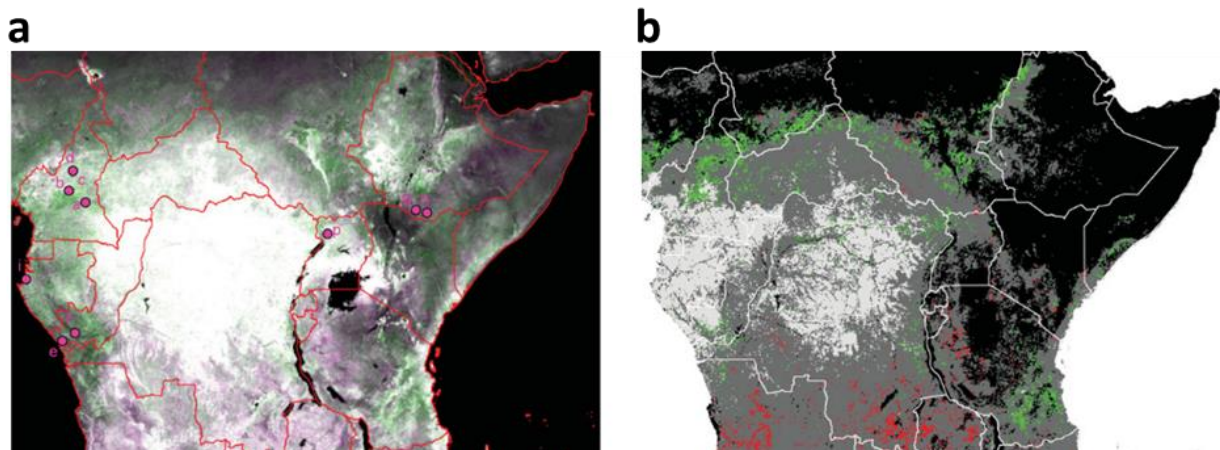
Fig. 7: Location of studies finding woody encroachment in Central Africa. (a) Overlaid on the Global Inventory Modelling and Mapping Studies (GIMMS) dataset with average three-monthly minimum NDVI from 1982 to 1986 in magenta and from 2002 to 2006. (b) Areas with significant changes in NDVI trends as increasing (green) and decreasing (red) trends (right). Modified from Mitchard and Flintrop, (2013).

Boulvert (1990) described a woody expansion occurring in the forest-savanna ecotones of Central Africa Republic and attributed it to be a consequence of the urbanization of the population. The example of the Bambari region shows that with the increase of the Fulani shepherd community and their herds, the fire regime has been totally modified. In the absence of high intensity bushfires trees took advantage over herbaceous plants, rendering pastures unsuitable and causing the migration of many herders to other areas(Gautier *et al.*, 2005) especially towards humid savannas (Boutrais and Jean, 1990). While studying the dynamics of about 3000 years old isolated savannas enclosed by forest in the eastern part of the Congolese

Mayombe, Schwartz *et al.* (1996) described an abrupt boundary between forest and savanna as a consequence of numerous savanna fires lit by hunters.
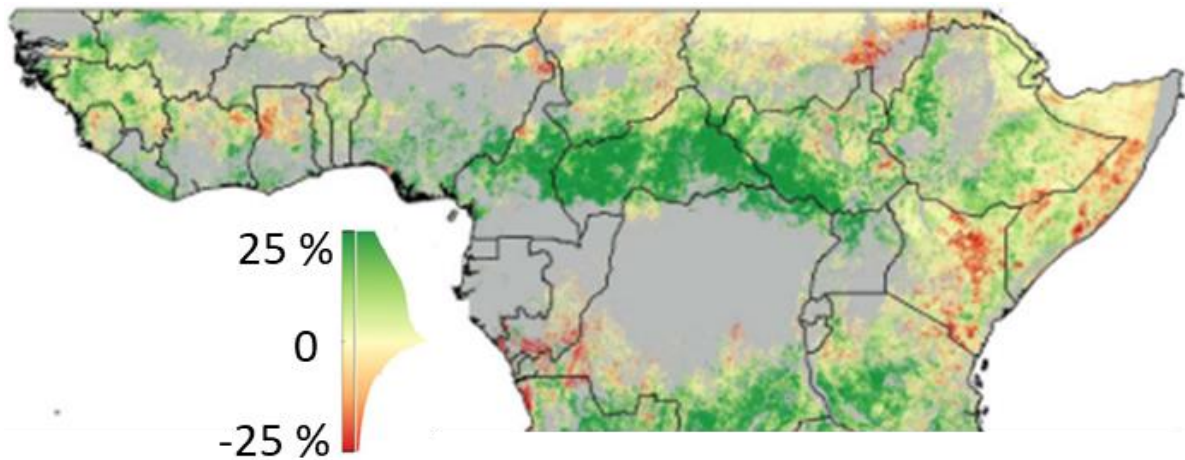
Fig. 8: Woody plant cover dynamics over sub-Saharan Africa revealing a dominant increasing trend over 30 years (1986-2016). Histogram alongside coloured scales indicate data distribution. Grey areas represent urban surfaces, wetland, cropland and forest. Modified from Venter *et al.* (2018).

They showed that forest was spreading over savanna at a rate between 14 and 75 m per century which suggested that enclosed savannas could completely disappear in the Mayombe (Democratic Republic of Congo) in about 1000-2000 years. In the same logic Favier *et al.* (2004b) described two main modes of forest progression into savanna: a linear forest edge progression which is slow (*c.* 1 m year^{-1}) and a forest clump coalescence with an increase in the man-made fire frequency that can lead to a shift from the coalescence regime to the edge progression one. Axelsson *et al.* (2018) estimated the mean annual change of woody cover across Sub-Saharan African savannas to be 0.25% per year which was negatively correlated with fire frequency.

When focusing on structural changes that occur in the vegetation structure during forest expansion after fire exclusion, Deklerck *et al.* (2019) estimated a forest species' specialist encroachment rate of 9 stems.ha^{-1}.y^{-1} and a savanna specialist disappearance rate of 16 stems stems.ha^{-1}.y^{-1} in savanna patches of the Mayombe hills. Average diameter of forest specialists did not change due to an increasing influx of recruits, while average diameter of savanna trees increased due to decreasing recruitment. Carbon stored by forest specialists increased from 3.12 to 5.60 MgC.ha^{-1}, suggesting a forest carbon recovery rate of 0.62 MgC.ha^{-1}.yr^{-1}. They estimated at least 150 years as the time required for a total forest recovery over savanna after fire exclusion. Jeffery *et al.* (2014) reported in the Lopé National Park in Gabon that savannas can sufficiently thicken up over a 15 year period to reach a structure comparable to a colonising

forest when protected from fires. Later Cardoso *et al.*, (2020) evidenced the presence of an ecotonal community in the Loppé National Park that occupies a narrow belt between savanna and forest and stabilises the forest-savanna mosaic even when the savanna is burned regularly.

In Cameroon, Youta (1998) observed the encroachment of gallery forest into the surrounding savannas at a rate of 0.6-2 m.yr^{-1} between 1950 and 1990 in the Central Region. However the encroachment rate was slower in savannas neighbouring forest established on waterlogged soils compared to savannas that were close to forest found on well-drained ferrallitic soils dominated by Malvaceae and Ulmaceae. Youta (1998) also hypothesized that human presence in Guinean savannahs reduced fire occurrence which favoured the establishment of forest species and later contributed into the formation of forest patches within savannas. Mitchard *et al.* (2011, 2009, 2013) described a rapid woody encroachment of savannas in central Cameroon (Mbam et Djerem National Park) where forest edges were dominated by young pioneer trees, with dead and dying savanna trees prevalent, which is strong evidence that this constituted young encroaching forests. They hypothesize one of the causes to be either recent reduction in fire frequency due to a reduction in human pressure caused by urbanization, as rainfall did not alter significantly over the study period. Their alternative hypothesis was that increasing atmospheric CO_2 concentrations were altering the competitive balance between grasses and trees.

In the coming decades, African biomes are predicted to experience profound changes whether through global drivers such as rainfall, temperature and atmospheric CO_2 (Malhi and Wright, 2004; Lewis *et al.*, 2005; Hély *et al.*, 2006; Lewis, 2006; Zelazowski *et al.*, 2011; Zeng *et al.*, 2013; Melissa and Ian, 2015; Western *et al.*, 2015; Vieilledent *et al.*, 2016) or through local drivers such as fire and herbivory regime (Oliveras and Malhi, 2016). Although the main lines of the vegetation history in Central Africa are known, there are few studies which actually quantify the changes in the vegetation structure. By being the zone of tension between two very different biomes close to their climatic margins, a better understanding of forest-savanna ecosystem functioning is urgently required, as well as predictions of how they may respond to changes. The growing evidence of forest encroachment into savanna in Central Africa has profound implications for biodiversity; it decreases landscape heterogeneity, reducing the diversity of invertebrates, birds and large mammals (Sirami *et al.*, 2009; Smit and Prins, 2020). Large scale vegetation change also has consequences for energy, carbon and water budgets (Woodward and Lomas, 2004; Mitchard and Flintrop, 2013).

I.2.4. Remote sensing-based modelling of vegetation structure and dynamics in forest-savanna transitional areas

Conventionally, vegetation structure have been assessed using field-based inventory plots (Jayakumar *et al.*, 2011; Higgins and Scheiter, 2012; Arellano *et al.*, 2016). Field inventories are expensive, time consuming, labour intensive and they do not integrate the spatial heterogeneity of the vegetation structure within the landscape especially for remote areas with limited access (Lu, 2006; Maniatis *et al.*, 2011; Clark and Louis, 2012; Réjou-méchain *et al.*, 2019). In Central Africa historical field inventory data of forest-savanna ecotone over several decades are especially rare (Mitchard *et al.*, 2013). Therefore it is difficult to use field plots alone in assessing natural and anthropogenic induced variation in vegetation structure and biomass over large areas. Given the extend of tropical ecosystems, access limitations and structural complexity, Remote Sensing (RS) methods have since long been used in assessing and characterize tropical ecosystems (St-Onge and Cavayas, 1997; Youta *et al.*, 2003). Moreover as new technologies emerged, RS provides a systematic and synoptic view of earth cover for changes in land cover and to reveal aspect of biological diversity directly. Satellite data are important tools in the interdisciplinary study of tropical forests that are increasingly integrated into studies that monitor changes in vegetation cover within tropical forests-savanna ecotones and also applied with other types of data (i.e. geographical, topography, hydrology) to investigate the drivers of land cover changes.

Laser scanning methods such as LiDAR (Light Detection and Ranging; Fig. 9) have also emerged as a promising technology for estimating forest height, volume and AGB in boreal, temperate and tropical forests (Drake *et al.*, 2002; Clark *et al.*, 2004). Able to provide direct descriptors of forest structure including tree height, crown size, and tree density (Heurich and Thoma, 2008; Bergen *et al.*, 2009), LiDAR sensors are of particular interest for the estimation of forest biomass and carbon stocks (Corona and Fattorini, 2008; Steinmann *et al.*, 2013). Airborne LiDAR are essential assets in the sense that they supply very high spatial and geometrical resolution (centimetre resolution) data on the tri-dimensional organization of the cover of areas that are too large or inaccessible. Recent studies proved the potentiality of very high resolution LiDAR images in accurate description of tropical forest cover, heterogeneity, cover change and biomass assessment (Vincent *et al.*, 2010).
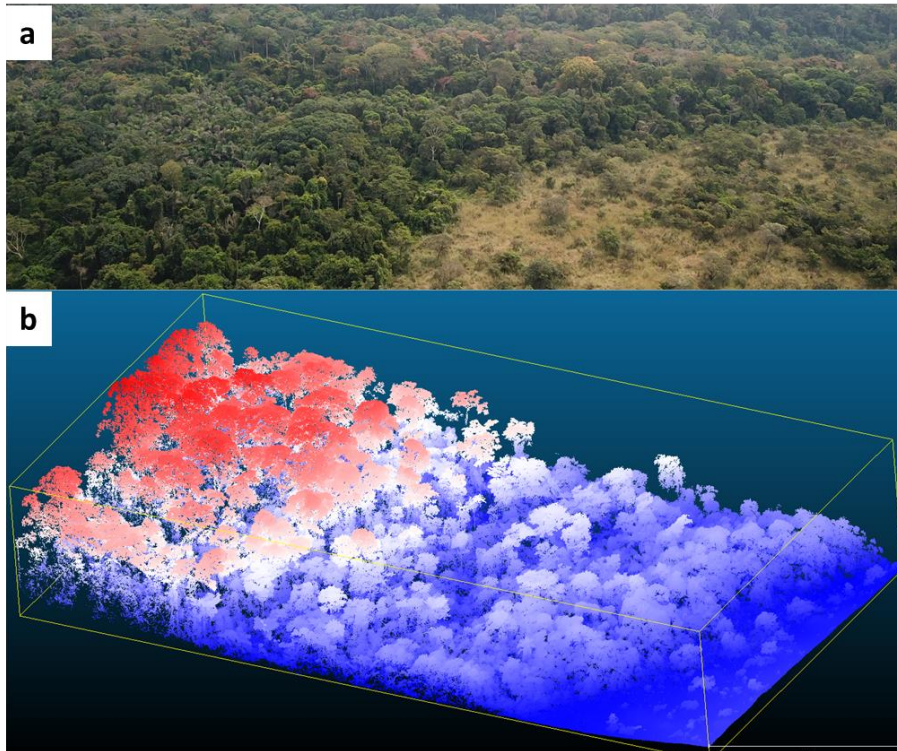
Fig. 9: Illustration of tree-dimensional data obtained from an airborne LiDAR scan over a forest-savanna transitional area. (a) Aerial view of a forest-savanna transition captured from an optical camera mounted on a Dji Mavic pro and (b) Aerial view of a forest-savanna transition captured from an airborne Laser scanner mounted on a Dji Matrice 600. The colour gradient corresponds to the variation from low (blue) to high (red) height values.

Nevertheless assessments of tree species and forest structure at regional scales are thus usually interpolated from *insitu* measurements (field inventories) which can provide accurate estimates of species richness and vegetation structure at local scales (Fig. 10).
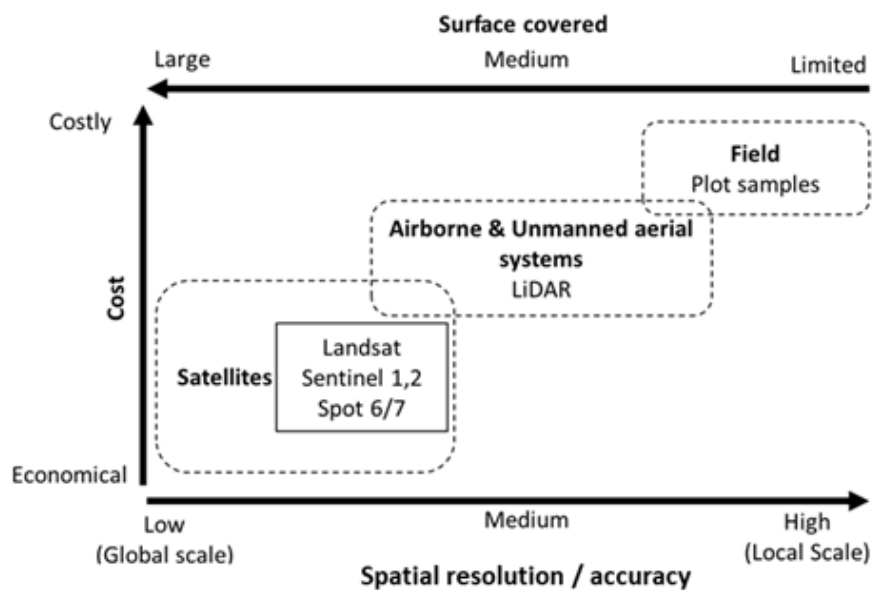
Fig. 10: Spatial resolution and cost effectiveness of field-based and remotely-sensed methods for monitoring vegetation structure (modified from Ganivet and Bloomberg, 2019).

I.2.4.1. Mapping aboveground biomass

Despite the recommendation of Ciais *et al*. (2011) to consider the contribution of savanna to the overall carbon budget, most of the studies focus only on closed forests (Saatchi *et al.*, 2011; Baccini *et al.*, 2012; Baccini and Asner, 2013; Mitchard and Flintrop, 2013) and only few studies (Mermoz *et al.*, 2014; Bouvet *et al.*, 2018) have attempted to evaluate the amount of above-ground woody biomass (AGB) stored in savannah biomes. Congo Basin countries are still in the preparatory phase of implementing REDD+ (Joseph *et al.*, 2013) which involve establishing administrative structures, determining reference levels for carbon stocks and development of credible monitoring, reporting and verification (MRV) systems, among others. Reducing the uncertainty of AGB estimates within FS transitional area is not only essential to have a better knowledge the contribution of the country to the REDD+ but is also of increasing relevance for the African and global carbon budget.

Conventionally, credible estimation of biomass stocks are achieved through a design-based approach (Kangas and Maltamo, 2006; Næsset *et al.*, 2011). The design-based approach consist in attributing to each vegetation type averaged AGB densities (referred to as Emission factors in this context) estimated from field-based inventories. Although design-based approach is still recommended in the Intergovernmental Panel on Climate Change (IPCC) guidelines for green-house gas inventories (IPCC 2019; Tier 1 and 2), precise estimation of these AGB densities require a rigorous sampling, for instance via a national forest inventory (McRoberts *et al.*, 2019), which is still lacking in many tropical countries. Such carbon inventory systems relying exclusively on ground observations alone may not be feasible for large area surveys due to expense associated with installation and re-measurement of an exhaustive ground network. In addition, regional arrays of ground plots cannot always provide accurate local estimates, for instance at sub-regional and administrative unit level, or by land-use or cover classes (Fahey *et al.*, 2010).

Recent studies indicate that forest inventories involving combination of data from field-based samples and auxiliary information from remote sensing platforms, i.e., model-based, are being preferred because they tend to reduce costs while improving precision of the estimates (Ene *et al.*, 2012; Mcroberts *et al.*, 2019). In fact auxiliary information provided by remote sensing systems has the potential to enhance the terrestrial surveys for forest carbon estimation (Ene *et al.*, 2012). However no RS technology is capable of directly measuring vegetation AGB (e.g. Asner *et al.*, 2013). Instead, indirect relationships are established between RS indices that vary

with plant's AGB and estimations of AGB in field sample plots (the 'ground truth'; Fig. 11). If we focus on multispectral optical remote sensing, the sensitivity of currently available satellite data sources (prior to the launch of GEDI and Biomass sensors) at high aboveground biomass (AGB) densities (100-200 Mg.ha^{-1}) is known to be poor (Avitabile and Camia, 2018; Réjou-méchain *et al.*, 2019) due to signal saturation (Huete *et al.*, 2002; Foody *et al.*, 2003). Also in areas with a high degree of cloudiness like in western Central Africa (King and Platnick, 2005), atmospheric effects are responsible for spatial artefacts observed in the surface reflectance of spaceborne optical data (Song *et al.*, 2001; Morton *et al.*, 2014). Another issue is that the cost of field data acquisition of sufficient quality generally leads to a poor calibration of AGB prediction models in model-based approaches. At the forest-savanna transition zone, complex mosaics of contrasted land cover and land use types exacerbate the issue making the precise quantification of AGB stocks and stock change particularly difficult. To overcome this problem, several authors (Asner, 2009; Baccini and Asner, 2013; Asner and Mascaro, 2014; Xu *et al.*, 2017; Réjou-méchain *et al.*, 2019) recommended a multi-step upscaling approach based on airborne LiDAR scanning (a.k.a. ALS). Due to its ability to penetrate the canopy down to the ground surface ALS has indeed emerged as the reference technology for mapping vegetation AGB variations at landscape scale (Asner and Mascaro, 2014; Réjou-Méchain *et al.*, 2015; Adhikari *et al.*, 2017; Jha *et al.*, 2020), although cost still prevents wall-to-wall mapping at regional or national levels.
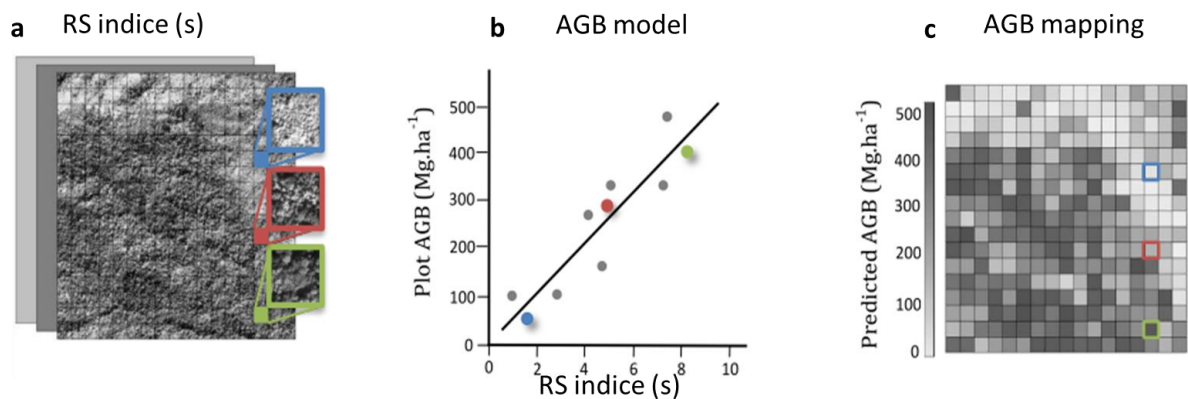
Fig. 11: General workflow of remote sensing-based AGB mapping methods.
Regardless of the remote sensing data type, remote sensing indices (s) are extracted over forest sample plots (a) and used a predictor (s) of in situ AGB estimations (b). Once calibrated, the model can be used to predict forest AGB over the entire study area (c). (modified from Ploton, 2017)

The currently held assumption seems to be that the calibration of AGB mapping models based on MS imageries (model-based approach; Fig. 12) is improved when using the larger calibration

datas*et* allowed by an ALS sampling of the territory (Réjou-méchain *et al.*, 2019; Asner and Ordway, 2020).
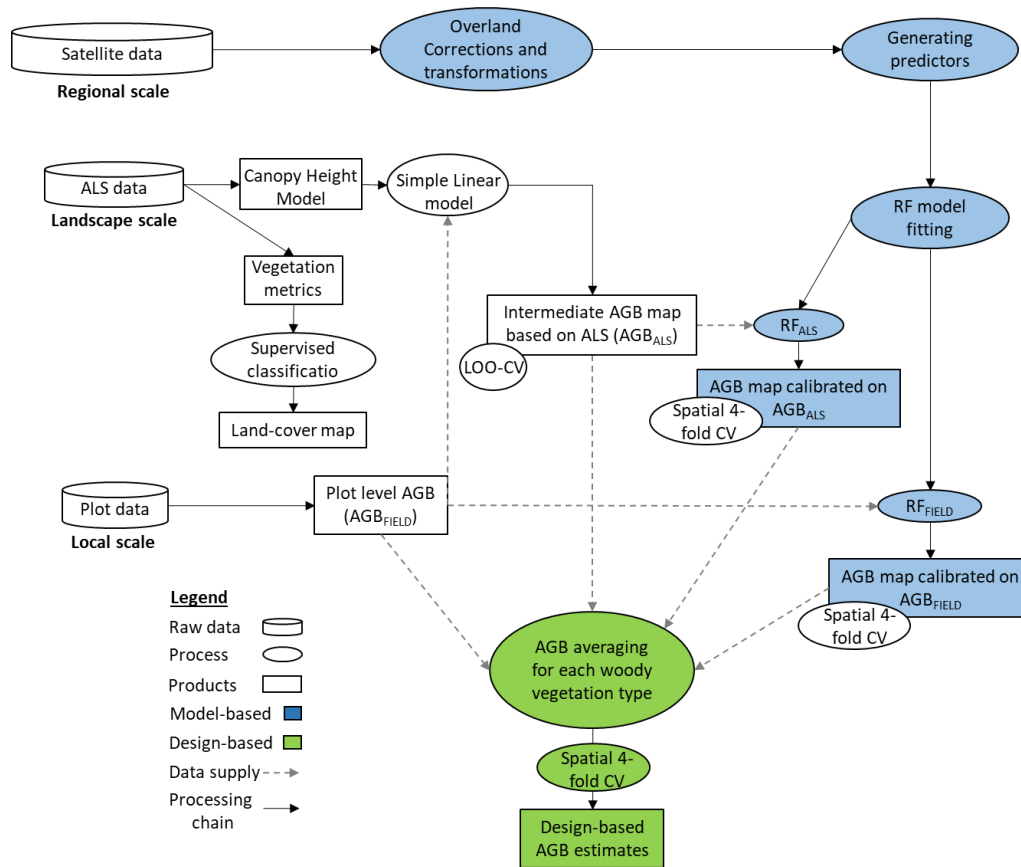
Fig. 12: General workflow of the methodology used in upscaling aboveground biomass from plot scale to satellite scale with model-based and design-based approaches from this study.

Table I presents a synthesis of a selection of previous studies that used ALS sampling to calibrate wall to wall vegetation structure (AGB, canopy height) models from MS satellite imageries and their performances. Biomass density maps derived from ALS data can be used to improve the representability of average biomass density estimates used in non-spatial methods (e.g. Langner *et al.*, 2018) or replace them altogether. The first task can be described in four detailed steps: (a) Mapping of land cover types and changes from satellite data; (b) stratified sampling of forest canopy three-dimensional (3D) structure using airborne LiDAR; (c) conversion of LiDAR structural data to aboveground carbon density estimates using new LiDAR allometrics along with a limited number of field plots; and (d) integration of the satellite map with the airborne LiDAR data to set a regional, high-resolution baseline carbon stock estimate (Fig. 12; Asner *et al.*, 2009). When spatially explicit models are sufficiently accurate and precise (which is commonly interpreted as "when estimation uncertainty is no more than 20% of the mean", Zolkos *et al.*, 2013), this approach would correspond to the highest quality tier of the IPCC (Tier 3).

Table I : Selection of studies using airborne LiDAR scanning data to parameterize model-based approaches and generate wall-to-wall AGB and tree height maps from spaceborne optical imagery.
Statistics of model predictive performance (i.e. R² and Root Mean Square Prediction Error, or RMSPE) are derived from a variety of model validation strategies, including (1) withholding of a given proportion of data for model testing, with test data selected at random (strat. 1), (2) 10-fold cross validation, with random split of data into folds (strat. 2), (3) Monte Carlo cross-validation, with random or spatial split of data into folds (strat. 3 and 4, respectively). Details of cross-validation strategies can be found in the original studies. RMSPE provided in Mg of carbon per hectare in original studies are converted to Mg of AGB per hectare with a carbon-to-AGB conversion factor of 0.5

Country	Multispectral	Spatial scale (m)	Model type	Model validation	R²	RMSPE (Mg.ha^{-1})	References
Colombia and Peru	MODIS	500	Random Forest	strat 1 (10%)	0.86	31.4-35.2	(Baccini and Asner, 2013)
China	Sentinel 2	10	Random Forest	strat 2	0.62	50.36	(Wang *et al.*, 2020)
Panama	Landsat 5,7	100	Random Forest	strat 1 (30%)	0.62	45	(Asner *et al.*, 2013)
Cambodia	QuickBird	1.5	Multiple regression	-	0.73	42.8	(Hirata *et al.*, 2018)
Democratic Republic of Congo	Landsat 8	100	Maximum Entropy	strat 3	0.76	61.29	(Xu *et al.*, 2017)
				strat 4	0.65	62.16	
Pantropical	MODIS	500	Random Forest	strat 1 (10%)	0.71-0.83	38-50	(Baccini *et al.*, 2012)
Peru	Planet Dove	100	Random Forest	strat 1 (20%)	0.7	50.76	(Csillik *et al.*, 2019)
Malaysian Borneo	Landsat 8	30	Deep learning	strat 2	0.7	83.2	(Asner *et al.*, 2018)
Panama	Landsat 7	30	Generalized Linear model	strat 1 (16%)	0.51	3.42 m	(Caughlin *et al.*, 2016)

I.2.4.2. Mapping species diversity and vegetation types

Optical sensors with a series of contiguous bands covering narrow spectral ranges allows to record information related to a range of plant properties such as the age, the water content, the leaf pigment and the chemical composition (Curran, 1989; Martin and Aber, 1997; Townsend *et al.*, 2008). Recent studies in tropical forests showed that tree species often have unique spectral signatures based on their structural and biochemical properties (Colgan *et al.*, 2012b; Rocchini *et al.*, 2016). Therefore the variability α high spatial resolution multispectral information can be used to differentiate species or group of species at a landscape scale, even in complex tropical ecosystems based on the optical traits corresponding to the reflectance of each pixel (Clark *et al.*, 2005; Ustin and Gamon, 2010; Mbobda *et al.*, 2018; Neba *et al.*, 2020). However the spectral species described from multispectral data do not directly refer to field-based species diversity but rather, the spectral species distribution within a specific area can approximate its biological species richness (Féret and Asner, 2014) according to the spectral variation hypothesis (SVH). The SVH postulates that the spectral variation of a site can be related to its ecosystem heterogeneity (Palmer *et al.*, 2002) since greater heterogeneity allows a higher number of species to coexist (Wilson, 2000; Huggett, 2002). Féret and Boissieu (2020) generated α- and β-diversity indicators from Sentinel 2 optical imagery, based on SVH (Fig. 13).
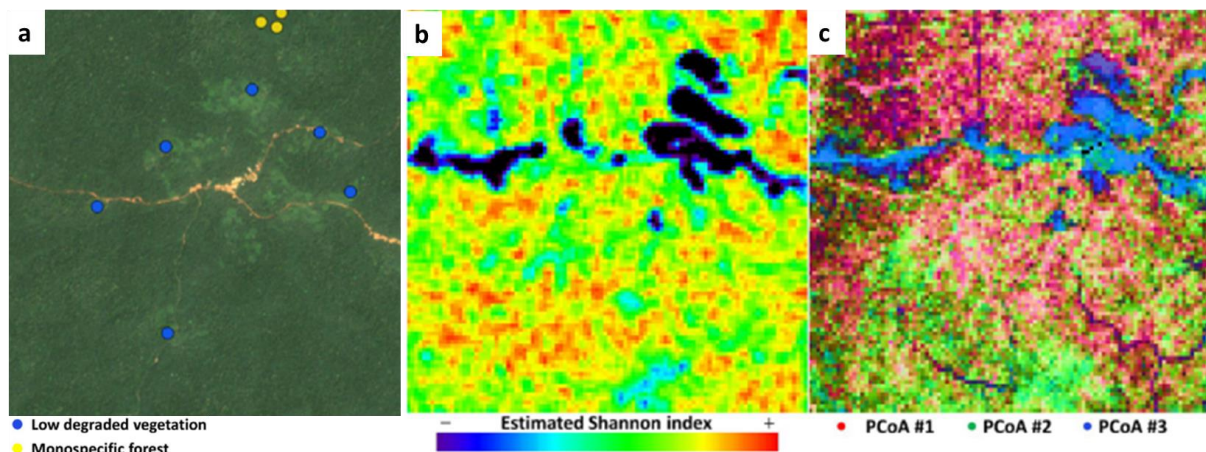
Fig. 13: Sentinel 2 satellite image (a) and derived (b) α and (c) β-diversity maps produced with biodivMapR (modified from Féret and de Boissieu (2020).

An alternative to mapping species diversity is to map habitats or vegetation types. Mapping vegetation types gives information on the spatial distribution of the land cover which is essential for planning and management activities (Chauhan and Nayak, 2005; Papastergiadou *et al.*, 2007; Lin *et al.*, 2008). An accurate and up-to-date mapping of land cover is necessary to

understand and quantify the influences of social, economic and environmental drivers over the vegetation patterns with time. However, land cover classification from satellite data remains a difficult task and it is especially challenging in heterogeneous landscapes with high degrees of cloudiness like western Central Africa. Therefore atmospheric effects needs to be corrected from the satellite images prior analysis (Song *et al.*, 2001). Another issue when generating land cover maps from passive multispectral satellite imageries (Sentinel 2; Spot 6-7; Landsat) is the confusion of spectral responses from different vegetation types which limits the accuracy of the classification result (Poursanidis *et al.*, 2015; Ustuner *et al.*, 2015). Integrating LiDAR data has clearly demonstrated the ability to accurately measure both spatial and vertical vegetation structure, even over dense tropical rainforest (Goetz *et al.*, 2007; Bergen *et al.*, 2009; Huang *et al.*, 2014). Marselis *et al.*, (2018) suggested that LiDAR-derived vegetation profiles can provide valuable information on vegetation type and successional stage in forest savanna transitional landscapes of Gabon which helped to improve vegetation classification.

I.2.4.3. Monitoring land cover changes and disturbances

A precise monitoring of forest change is a key component for the implementation of the REDD+ mechanism. Participating countries are required to establish robust Measuring, Reporting and Verification (MRV) systems with which to track activity data and land cover changes at regular timeframes (Joseph *et al.*, 2013). Remote sensing based approaches play a key role in monitoring land cover changes, as they provide the best opportunity for mapping vegetation change over large areas (Sexton *et al.*, 2013; DeVries *et al.*, 2015). With the opening of the U.S. Geological Service (USGS) data archive, large amounts of medium-resolution optical earth observation data have been made freely available to the public (Wulder *et al.*, 2016) which allowed for high temporal resolution forest change monitoring at unprecedented spatial scales (Hansen *et al.*, 2013). The Landsat program comprises the longest continuous Earth Observation mission which has been imaging the surface of the Earth for more than 40 years with consistent spatial (30 m) and temporal (16 day) resolutions since 1984 (Wulder *et al.*, 2016). Landsat time series data have been used to produce long-term reliable forest versus non-forest land-cover classifications (Hansen *et al.*, 2013; Ceccherini *et al.*, 2020; Jha *et al.*, 2020) to monitor land cover dynamics (Fig. 14).
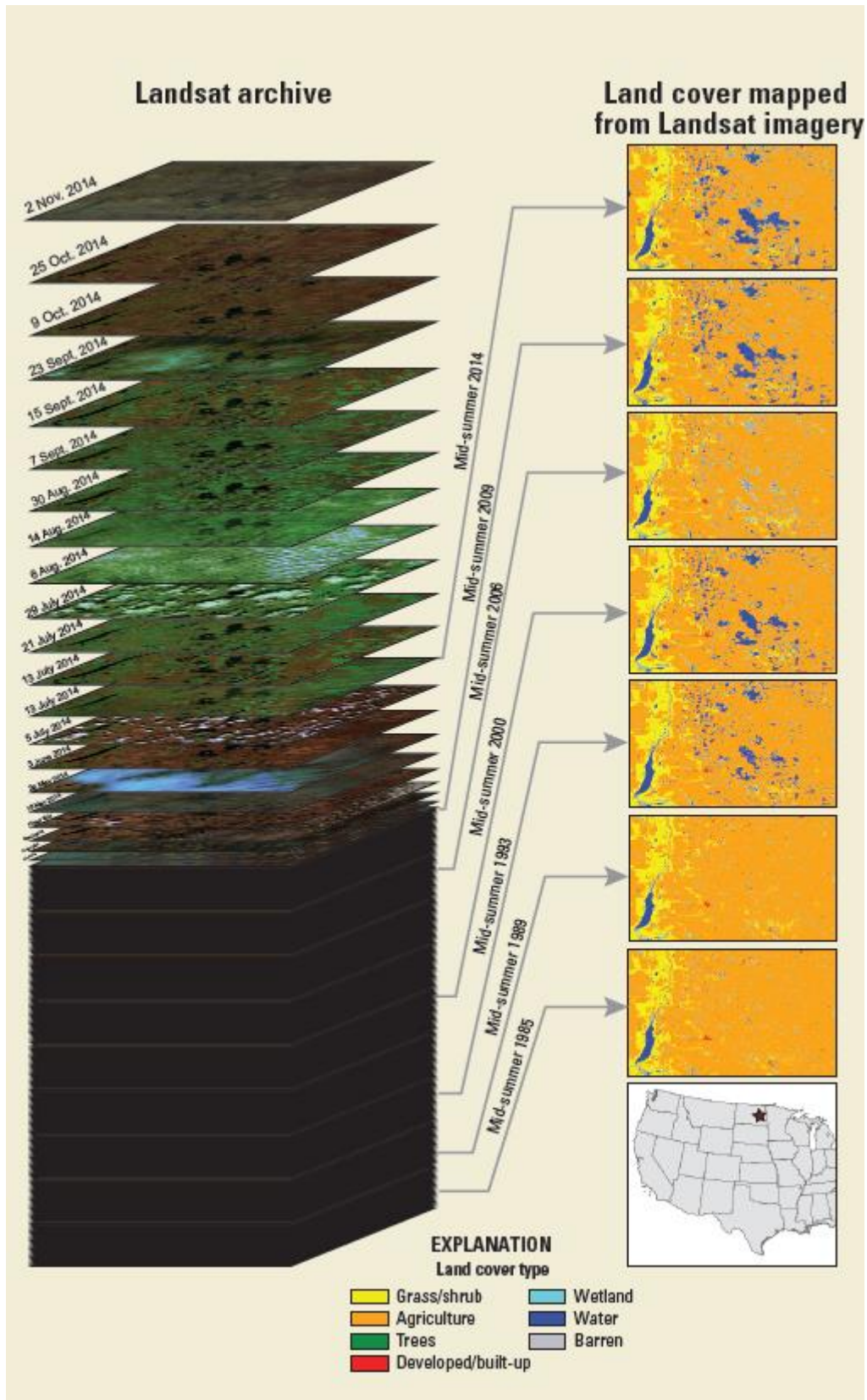
Fig. 14: Illustration of the potential offered by Landsat image archives in monitoring land cover change dynamics (modified from Young, 2017).

Also Landsat image archives have been used in mapping burned areas at a finer spatial resolution to quantify fire severity, trends and patterns in fire occurrence (Bastarrika *et al.*,

2014; Quintano *et al.*, 2017; Liu *et al.*, 2018; Daldegan *et al.*, 2019). Processing such amount of images over large extents and long-time-series has become considerably more cost-effective, given the powerful computational processing of Google Earth Engine (GEE ; Gorelick *et al*., 2017). GEE is a cloud-based platform (Fig. 15) for planetary-scale geospatial analysis that brings Google's massive computational capabilities to bear on a variety of high-impact societal issues including deforestation, drought, disaster, disease, food security, water management, climate monitoring and environmental protection. It is unique in the field as an integrated platform designed to empower not only traditional remote sensing scientists, but also a much wider audience that lacks the technical capacity needed to utilize traditional supercomputers or large-scale commodity cloud computing resources. It generates surface reflectance data from the Landsat Ecosystem Disturbance Adaptive Processing System (LEDAPS) which includes the calibration from at-sensor radiance to the top of atmosphere (TOA) reflectance and the atmospheric correction from TOA reflectance to surface reflectance (Vermote *et al.*, 1997; Masek *et al.*, 2006).
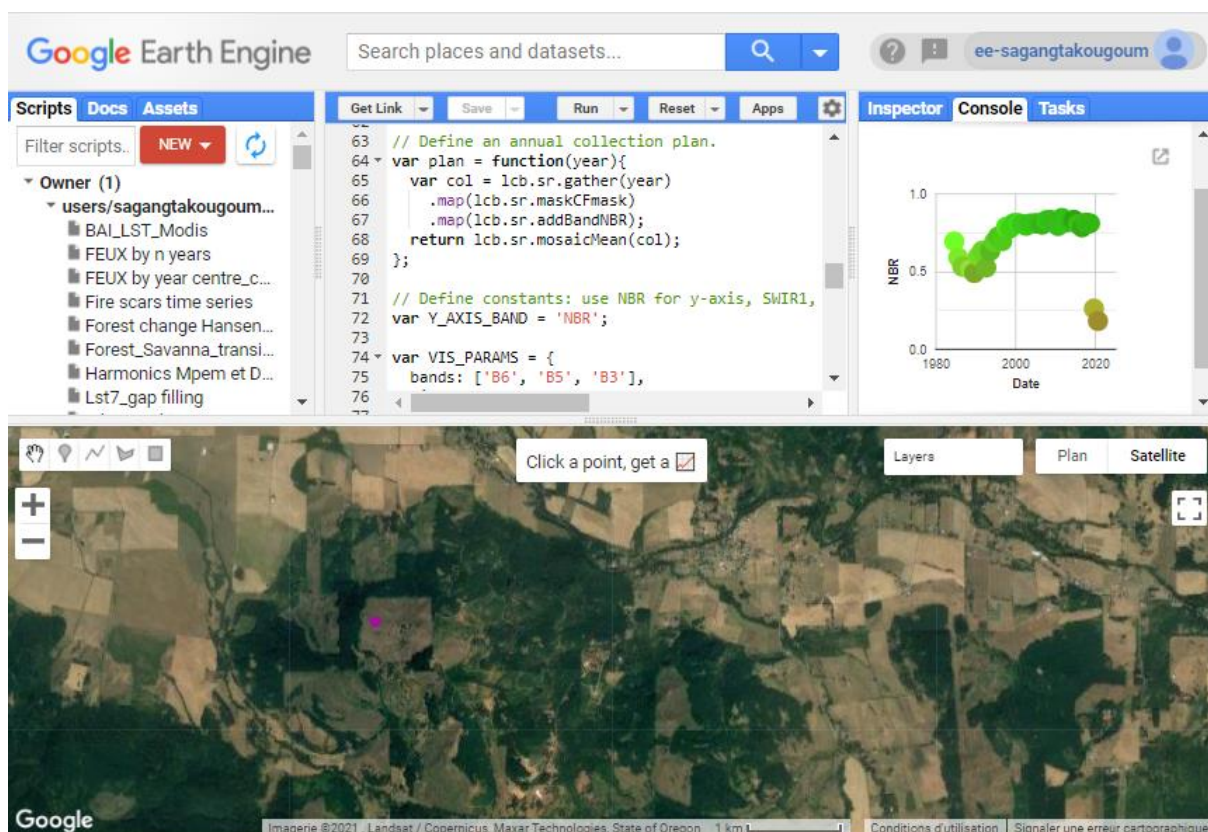
Fig. 15: Illustration of the Earth engine interactive development environment.

CHAPTER II

MATERIAL AND METHODS

CHAPTER II. MATERIAL AND METHODS

II.1.   MATERIAL

II.1.1. Study site

II.1.1.1.   Location

The study was conducted within a forest savanna mosaic of the Guineo-Congolian transitional area of the Mbam *et* Kim division in the Centre Region of Cameroon (Fig. 16). The area is under the influence of an equatorial climate of Guinean type (Djoufack, 2011), which is hot and humid with an average annual temperature of 25°C. Mean annual rainfall is 1,500 mm, with a rainfall distribution characterized by a dry season lasting over three months (December–March), during which the monthly rainfall is less than 70 mm. The soils are deep mostly ferralitic red and yellow with a complete hydrolysis of minerals from granite-gneissic basement caused by hot rains (Santoir and Bopda, 1995). Youta (1998) concluded that soils under savanna vegetation are distinguished by a sandy texture that dominates the upper horizons with lower horizons being dominated by clay. This author also reports that forest soils display a decrease in the proportion of sand in favour of clay in the upper horizons as we move from the forest edge to its core.

On the human level, the Central Region of Cameroon is witnessing a rapid population growth and recent national surveys (Anonyme, 2016) have projected that the region would hold about 20% of the country's population by 2020. The sites sampled featured two different contexts of anthropogenic influences: the construction area of the Nachtigal hydroelectric dam (a.k.a Nachtigal area) which is highly influenced by human activities in opposition to the protected area of the Mpem *et* Djim National Park (MDNP). The Nachtigal area extends over 216 km² (4°00'–4°30'N and 11°30'–12°00'E; Fig. 16) with a relief dominated by vast peneplains which slope gently towards the valleys of the Sanaga river. Topography does not pose insurmountable obstacles to human activities. As a consequence, the area has been targeted since 1950s for small and large scale agriculture such as artisanal cocoa (*Theobroma cacao* L.) and palm (*Elaeis guineensis* Jacq.) plantations (Binet, 1956; Marticou, 1962; Jagoret *et al.*, 2012) and industrial activities (e.g. hydroelectric dam construction) which result in a landscape strongly impacted by anthropogenic pressures. The MDNP was established in 2004 and covers an area of 975 km² (5°00'–5°30'N and 11°30'–12°00'E; Fig. 16).
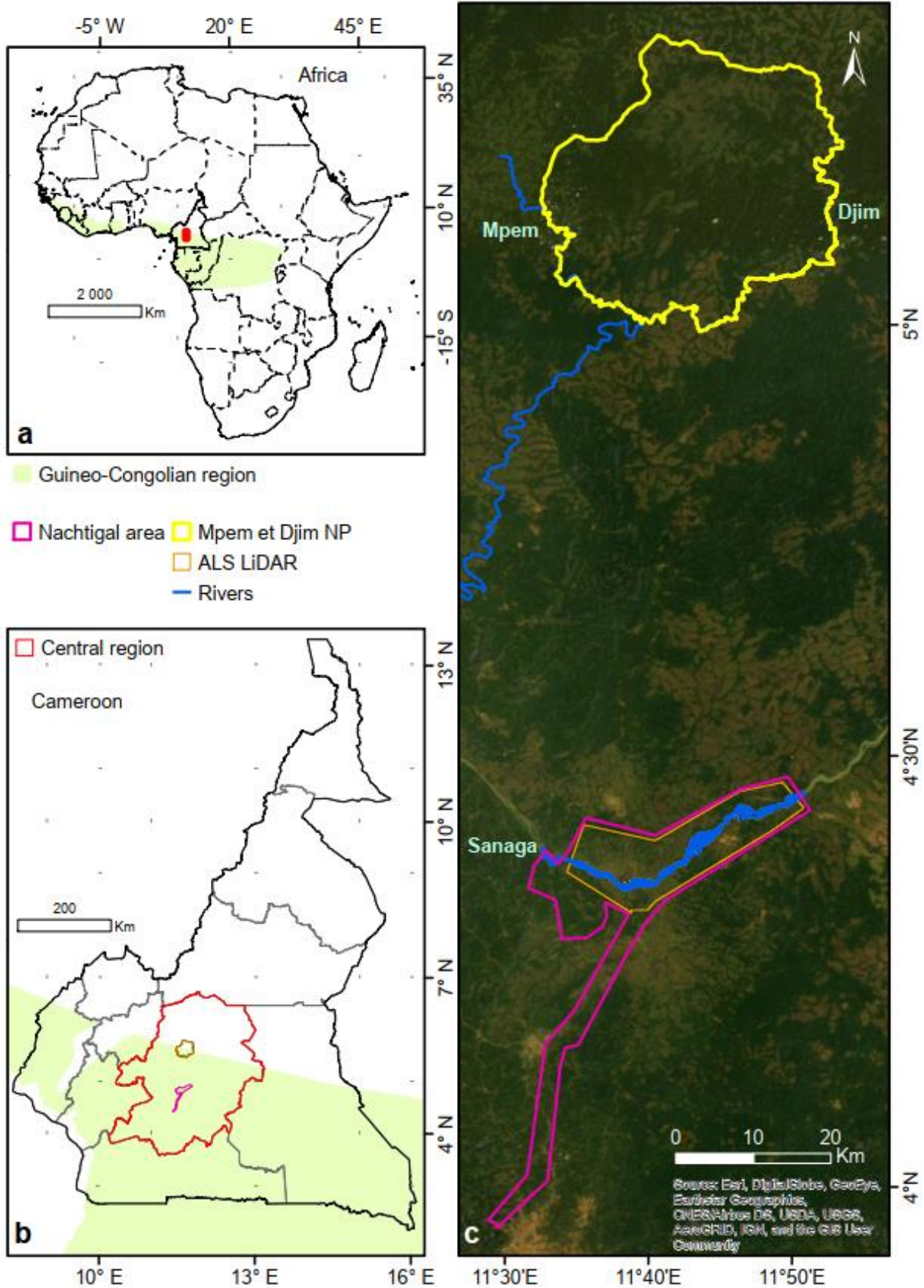
Fig. 16: Study area. (a) Location (red dot) within the Guineo-Congolian transitional area (light green) of the Mbam et Kim division in the Central region of Cameroon (b). (c) Boundaries of the Mpem et Djim National Park (yellow); the different rivers (blue); the Nachtigal area (pink) and the ALS LiDAR sampling footprint (orange).

II.1.1.2. Vegetation

Plant formations in the area belong to the Guineo-Congolian type (White, 1986; Santoir and Bopda, 1995)(Santoir and Bopda, 1995) dominated by savanna formations interspersed by semi-deciduous forests or gallery forests along watercourses (Letouzey, 1968; Youta and Bonvallot, 1996; Youta *et al.*, 2003). Young colonizing forests in direct contact with savanna are dominated by *Albizia adianthifolia* (Schumach.) W.Wight and *Albizia ferruginea* (Guill. and Perr.) Benth.), *Albizia zygia* (DC.) J.F.Macbr., *Alchornea cordifoli*a (Schumach. and Thonn.) Müll.Arg.), *Macaranga spinosa* Müll. Arg., while emergent trees species such as *Mansonia altissima* (A.Chev.) A.Chev. *Terminalia superba* Engl. and Diels and *Triplochiton scleroxylon* K. Schum dominate in older forest successions. A distinct set of mostly pyrophilous tree species characterizes the savanna, mainly: *Annona senegalensis* Pers., *Bridelia ferruginea* Benth., *Crossopterix febrifuga* (Afzel. ex G.Don) Benth., *Hymenocardia lyrata* Tul., *Lannea kerstingii* (Enql.) K. Krause., *Piliostigma thonningii* (Schumach.) Milne-Redh, *Psorospermum febrifugum* Spach. And *Terminalia glaucescens* Planch. ex Benth. Grass cover is dominated by species of the Poaceae/Andropogonae: *Andropogon* spp., *Hyparrhenia diplandra* (Hack.) Stapf., *Hyparrhenia rufa* (Nees.) Stapf. And *Pennisetum purpureum* Schumach. (Youta, 1998).

II.2. METHODS

II.2.1. Data collection

II.2.1.1. Field data collection

Field data acquisition campaigns were conducted from February 2018 to December 2020.

II.2.2.2.1. Forest sampling

Vegetation communities there were sampled within Permanent Sampling Plots (PSP) of one hectare. Permanent sampling plots refer to sampling units where trees are individually and permanently identified and tagged. The use of PSP have received much attention as a tool to assessing vegetation dynamics (radial growth; mortality, carbon accumulation, etc.) especially in tropical forests (Lewis *et al.*, 2013; Libalah, 2018; Duncanson *et al.*, 2021). PSP locations were distributed among the main types of closed-canopy vegetation's found in the area had a dimension of 100 m x 100 m (Fig. 17) following the recommendation of (Alder and Synnott, 1992).
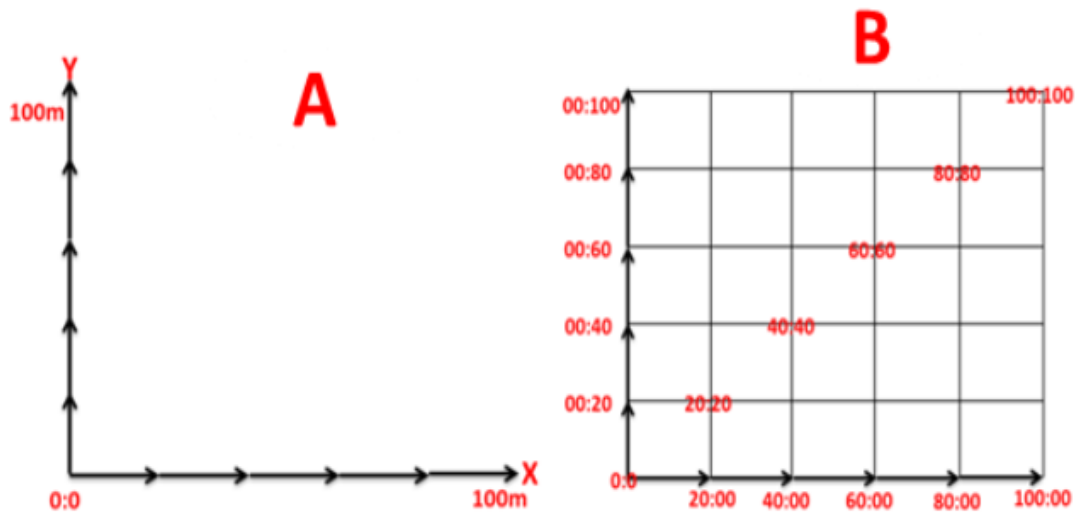
Fig. 17: Demarcation of a one ha plot for data collection. A: length and direction of first baselines; B: complete demarcation of quadrats (Libalah, 2018) displaying the cartesian coordinates of the poles of the baselines and the diagonal of the plot.

Two baselines of 100 m each are demarcated, one towards the North direction and the other towards the East direction using a compass. The two directions were named Y for the North-South axis and X for the East-West axis. A 20 m distance was measured 20 m from the origin of the marker (point 0:0) and a pole was planted at this position. The pole was marked with a ribbon depending on the location along the XY position (Fig. 18 a). Towards the X direction for example, the poles are successively numbered every 20 m thus: 0:0; 0:20; 00:40; 00:60; 00: 80 and 0: 100. Towards the direction Y, numbering was thus: 20:00; 40:00; 60:00; 80: 00 and 100: 00 as illustrated in Fig. 17 b. In each quadrat, the diameter at breast height (DBH) for all trees $\geq$ 10 cm was measured (i.e., 1.3 m or 30 cm above buttresses if present) with a diameter tape (Fig. 17 b). Tree height (H) was measured on a subsample of trees for each plot (approximately 50 sampled along the DBH range) with their crown apex visible using the laser range finder device (TruPulse 360R, Laser Technology Inc., Centennial, Colorado) (Fig. 18 c). The position of the quadrat (a quadrat measuring 20 m x 20 m) in the space was numbered according to the XY coordinates of the southwest corner of the quadrat. Each individual was assigned a tag (engraved number on a piece of metallic sheet) and was painted at the point of measurement (Fig. 18 d). Plots geolocation was recorded with a Global Navigation Satellite System (GNSS) receiver (Trimble Geo7X), by collecting a point every 20 m along each plot contour (Fig. 18 e) in order to increase geolocation accuracy (Réjou-méchain *et al.*, 2019). Measured trees were identified in the field by expert botanists, and voucher specimens were collected (Fig. 18 f) on each species for cross-identification at three herbaria including the Plant Systematic and Ecology Laboratory (Higher Teachers' Training College, University of Yaoundé I) and at two official herbaria: BRLU, YA (Thiers *et al.*, 2020).

Fig. 18: Field data collection in the forest. (a) Plot delimitation; (b and c) tree measurements; (d and e) data collection; (f) voucher specimens.

II.2.2.2.2. Savanna sampling

Savanna vegetation was sampled within non-permanent plots and were delimited following the same method as for forest plots. Given the high spatial heterogeneity of the vegetation in this ecosystem we made a compromise between the size of the plots and the number of types of vegetation sampled. Therefore following the recommendation of Ganivet and Bloomberg, (2019) savanna vegetation was sampled within smaller sampling units of 40 m × 40 m (0.16-ha as opposed to 1-ha forest plots; Fig. 19 a) which increased the number of sampling units. The DBH was measured for all trees as in forest plots (Fig. 19 b). The height was measured using a 7.5 m graduated pole for short trees (H ≤ 7 m; Fig. 19 c) and the TruPulse 360R for taller trees (> 7 m).
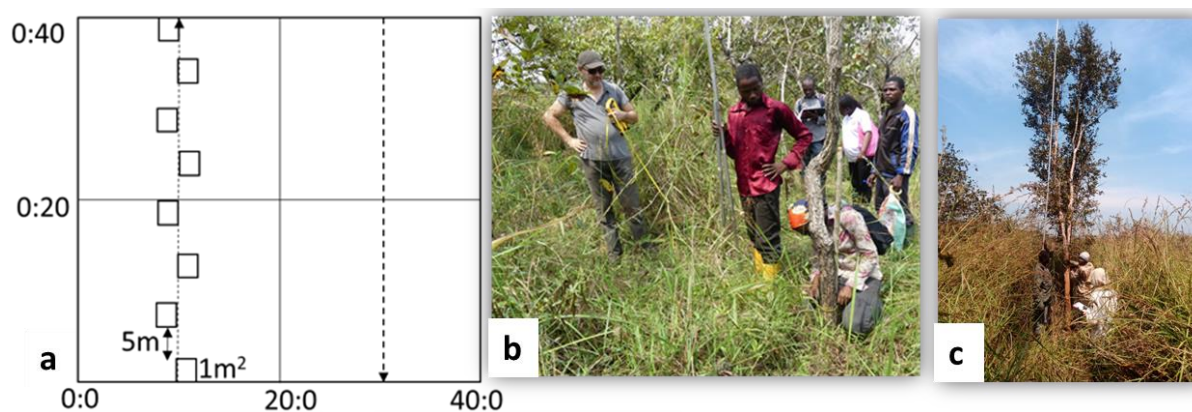
Fig. 19: Field data collection in the savanna vegetation. (a) Savanna sampling; (b and c) data collection of the woody layer.

II.2.2.2.3.   Estimating AGB from plot data

To homogenize the size of the sampling plots between forest (100 m x 100 m) and savanna (40 m x 40 m), each 1-ha forest plots was split in four subplots of 40 * 40 m selecting each time the subplots located on the external edge of the 1-ha plots (Fig. 20).
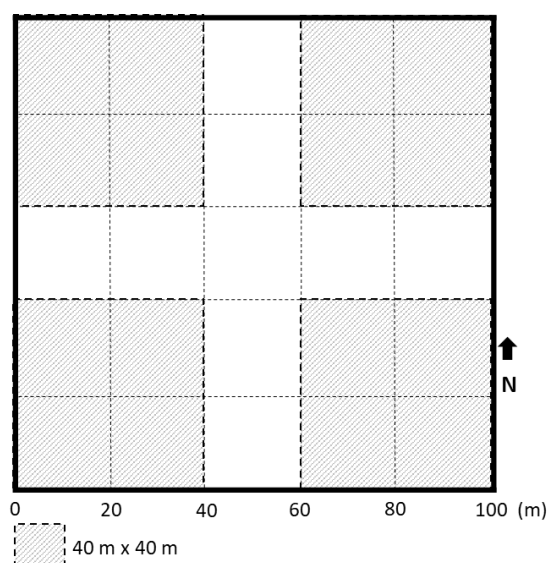
Fig. 20: Illustration of data sub-sampling within four 40 m x 40 m subplots for each 1 ha forest plot (hatched grey squares).

Subsequently the BIOMASS R package (Réjou-Méchain *et al.*, 2017) was used to fit plot-level height-diameter allometric models via a three-parameter Weibull function and predict the height of unmeasured trees in the forest whereas for savanna plots a local height-diameter linear regression model was fitted and the coefficients used to predict heights for unmeasured savanna trees. The BIOMASS R package was used to attribute a wood density (WD) value to each tree based on its taxonomy available in the Global Wood Density Database (Chave *et al.*, 2009; Zanne *et al.*, 2009). For trees identified at the species or genus level, the average WD of the respective taxonomic level was used. For trees identified at the family level, or unidentified

trees, the plot average WD was used. Tree AGB was computed using allometric models based on DBH, H and WD. For forest trees, the pantropical AGB model of Chave *et al.* (2014; Equation 1) was used. For trees from savanna plots, an AGB model developed for semi-arid savanna by Colgan *et al.* (2013; Equation 2) was used. Lastly, plot woody AGB density (AGB$_{FIELD}$) was computed as the sum of individual tree AGBs over the plot area (expressed in Mg.ha^{-1}).

Equation 1 $$AGB = 0.0673 * (WD * H * DBH^2)^{0.976}$$

Chave *et al.*, 2014

Equation 2 $$AGB = exp[-2.215 + 1.393*ln(DBH) + 0.144(ln(DBH))^2 + 0.729*ln(H) + 0.805*ln(WD)]$$

Colgan *et al.*, 2013

where DBH is the diameter at breast height (cm); H is the total height (m) and WD is the wood specific density of each individual (g.cm^{-3}).

II.2.1.2. Spatial data collection

II.2.2.2.1. Airborne LiDAR sampling

Light Detection And Ranging (LiDAR) is a remote sensing system that uses lasers to measure distances between a sensor and targets of interest (Fig. 21). LiDAR instrument consists of a high frequency laser that has the ability to emit tens of thousands of laser pulses per second, from which corresponding range measurements can be derived. Rate of laser pulse emission is quantified and referred to as the "pulse repetition frequency". Pulses are delivered by scanning, so that pulses are emitted within a set number of degrees from nadir; each laser pulse and associated returned energy has an associated "scan angle", which describes the angle from nadir of the pulse. LiDAR sensors for earth applications are frequently flown aboard fixed-wing aircraft at relatively low elevations (~1000 m above ground level when mounted on aircrafts), and unmanned aerial vehicles (UAVs) are becoming more popular as LiDAR platforms (generally flown at elevations < 150 m). Because LiDAR systems use lasers to interact with targets, LiDAR is considered a form of active remote sensing, as opposed to passive remote sensing, such as sensors aboard satellites that passively measure reflected sunlight (Klauberg, 2018).
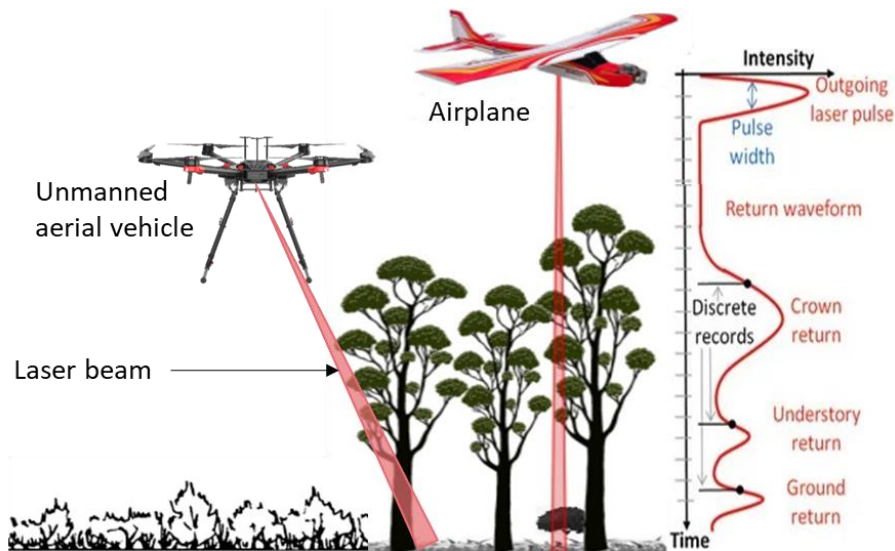
Fig. 21: Principles guiding vegetation sampling with airborne LiDAR systems.

Airborne LiDAR Scanning (ALS) data were acquired in 2012 in the Nachtigal area with a Riegl LMQ-560 sensor mounted on an airplane of type Pilatus PC6 with a flight height of 600 m above ground level and an average ground speed of 167 km.h^{-1} (Fig. 21). The scan angle was ±60° with a band swath of 690 m and 50% of overlap among adjacent flight lines which resulted in an average point density of 8.4 points.m^{-2}. The ALS point error was 10 cm vertically and 15 cm horizontally. As for the MDNP, ALS data were acquired in 2019 with a Riegl mini VUX-1UAV scanner of the YellowScan Vx-20 mounted on an unmanned aerial vehicle (UAV) Dji Matrice 600. The flight height was 70 m above ground level and an average ground speed of 8 km.h^{-1}. The scan angle was ±60° with a point accuracy was 2.5 cm vertically; a band swath of 45 m and 50% of overlap among adjacent flight lines which resulted in an average point density of 10.5 points.m^{-2}.
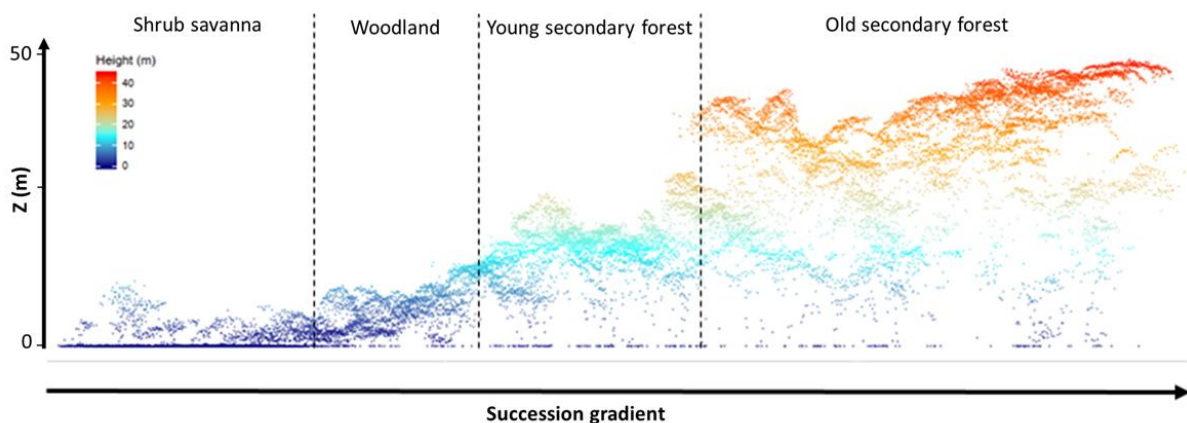
Fig. 22:Three-dimensional profile of the vegetation structure along a savanna to forest transitional gradient extracted from an UAV-LiDAR data in the study area.

Points were classified into ground and non-ground returns using the lidR R package (v2.0.2, Jean-Romain and David, 2019) for Nachtigal point clouds and Cloud Compare software (CloudCompare, 2020) for MDNP point clouds (Fig. 22). A digital elevation model (DEM) was fit to the ground returns to produce a 1-m resolution raster. The DEM was then subtracted from the elevations of all non-ground returns to produce a normalised point cloud, from which a 1-m resolution canopy height model (CHM) was constructed by averaging the first returns (Fig. 23). All further processing of the ALS data was done using the raster package in R (Hijmans, 2016; R Core Team, 2018).
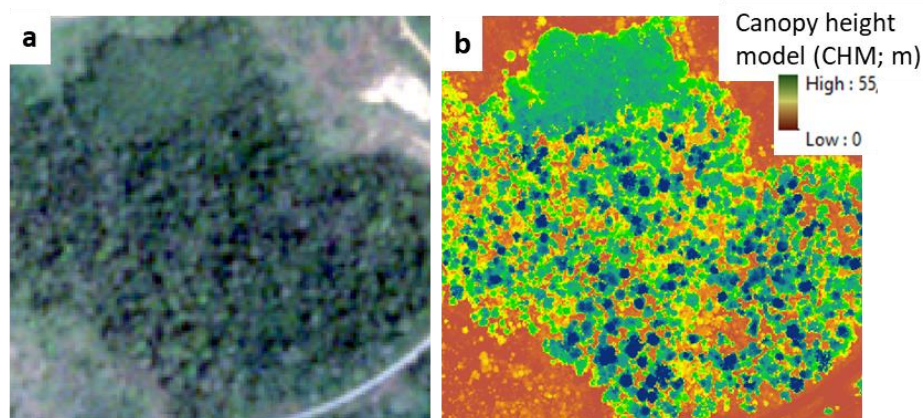
Fig. 23: Spot 6/7 image of a forest (a) with the corresponding canopy height model showing the elevation of the vegetation (b) derived from the normalized LiDAR point cloud.

II.2.2.2.2. Satellite data sampling

Products from different satellite sensors were used for specific purposes in this study as described in Table II.

Table II : Characteristics, properties and purposes of different satellite sensors used in this study. Res = sensor resolution (in m); nBands = number of spectral bands for each sensor.

Source	Acquisition period		Res(m)	nBands	Purpose
Spot 6-7	2015		3	4	- Landcover classification in the Nachtigal area - AGB modelling
Sentinel 2	2015-2020		10	10	- AGB modelling - Mapping spectral species diversity in the Mpem et Djim NP
Landsat (Lst) Collection	Lst 2	1975-1978	60	5	- AGB modelling - Land cover dynamics - Fire frequency mapping
	Lst 5	1986	30	6	
	Lst 7	1999-2013	30	6	
	Lst 8	2013-2020	30	8	
MODIS	2000-2019		500	5	- Fire frequency mapping

II.2.2. Spatial and statistical analysis

II.2.2.1. Land cover mapping

Land cover mapping remains a difficult task and it is especially challenging in heterogeneous landscapes such as forest-savanna transitions. In addition to its location within a forest-savanna transitional zone, the anthropogenic pressure over the Nachtigal area results into a complex combination of different landforms such as urban areas, agricultural fields, pasture/scrublands, bare areas, agroforest, forest and natural areas, water surfaces (Alexandre, 2013) to name but a few. One of the main issues when generating land cover maps from such complex areas is the confusion of spectral responses from different features as it can be seen in Table III. The classification accuracy from satellite images therefore depends upon both the quality of the sensor and the classification method used (Poursanidis *et al.*, 2015; Ustuner *et al.*, 2015).

In this study Spot 6/7 image was used to map land cover types over the Nachtigal area as it has already proven its potentiality in mapping heterogeneous landscapes with good accuracy (Kuzucu *et al.*, 2017). Properties of the Spot 6/7 image were given in Table II. Additional vegetation indices i.e. the Normalized Difference Vegetation Index (NDVI) and the Enhanced Vegetation index (EVI) were computed and added as additional bands to enhance the spectral information and increase the spectral separability between classes.

II.2.2.2.1. Image classification

A supervised image classification was used to distinguish between the different land cover types as it usually warrants higher quality of the final mapping product (Khatami, Mountrakis, and Stehman, 2016). Supervised classification requires labelled training data for each land cover type to establish the statistics to identify spectral classes (or clusters) in a multiband image. All classes have to be derived usually through a training stage with the use of training samples. Training samples for each land cover type was therefore manually delineated based on (i) the knowledge of the land cover type from the field; (ii) their spectral responses from Spot 6/7 satellite image and (iii) the height distribution of their canopies as obtained through the CHM (Table III). A total of approximately 2640 pixels for the different land-cover types was generated. The image was classified into 13 land cover types using the maximum likelihood algorithm from the ENVI 5.0 image classification software. Finally, a 3 x 3 majority filter was applied to each classification to recode isolated pixels classified differently than the majority class of the window.

Table III : Illustration of the relationships between the structure of the canopy of different land cover types, the height distribution from the Canopy Height Model (CHM) and the spectral reflectance from Spot 6/7 satellite image (Red-Green-Blue colour composite = NIR-Red-Green).
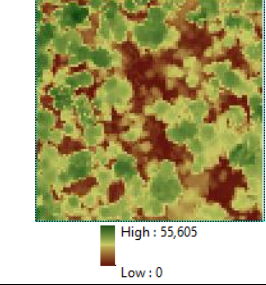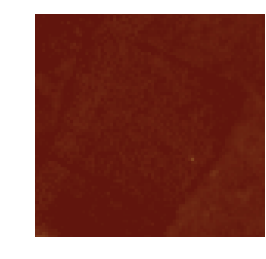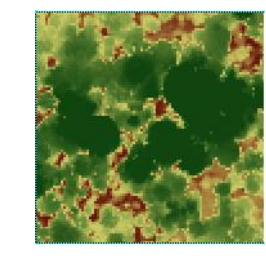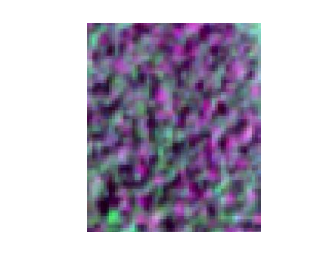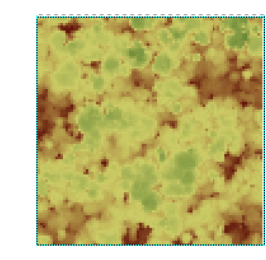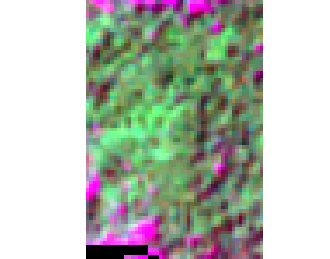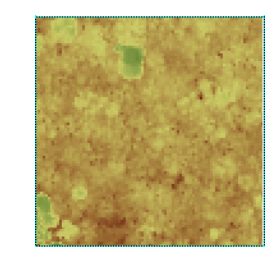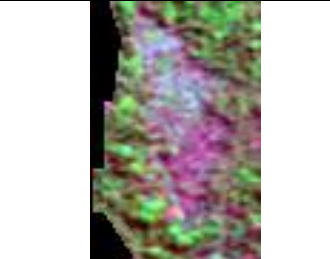
Land cover type	Field illustration	CHM	Radiometry Spot 6/7
1- Agroforests		High : 55,605 Low : 0	
2- Cropland			
3- Old-growth secondary forest			
4- Swampy forest			
5 – *Raphia* spp. stand			

Table IV : Continuation
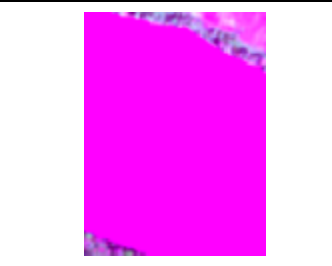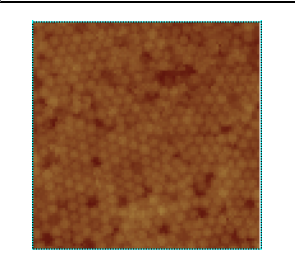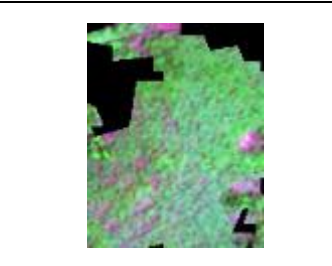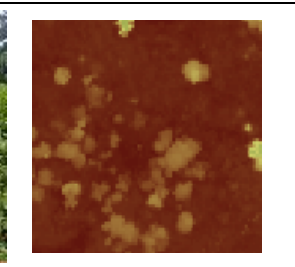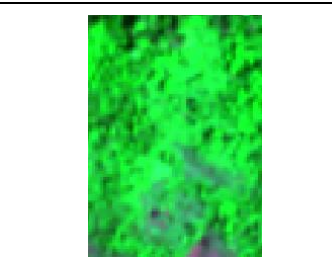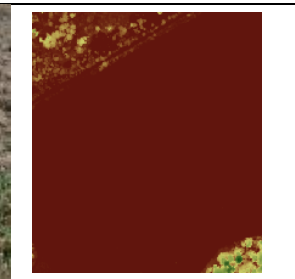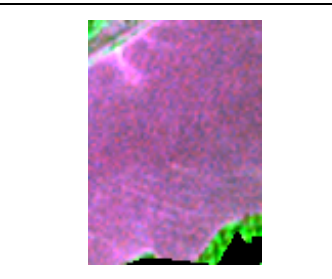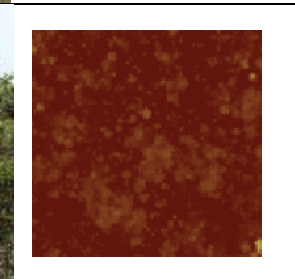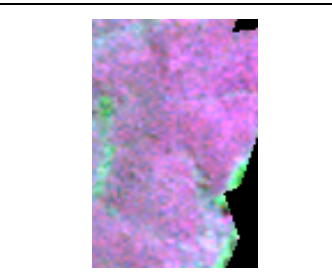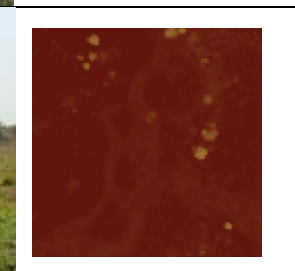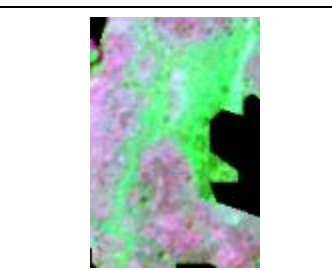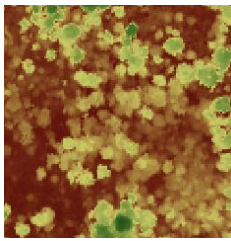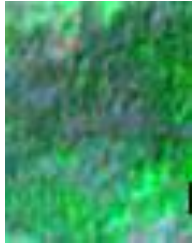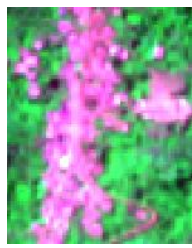
Land cover type	Field illustration	CHM	Radiometry Spot 6/7
6 – River			
7 – *Elaeis guineensis* form			
8 – Degraded secondary forests			
9- Bareground			
10 – Shrubby savanna			
11 – Grassy hydromorphic savanna			

Table V : Continuation

Land cover type	Field illustration	CHM	Radiometry Spot 6/7
12 – Woody savanna			
13 – Urban areas			

Cameroon has proposed categories of land cover types in order to improve its capacities to report on their forest carbon stocks changes following the recommendation of the Intergovernmental Panel on Climate Change (IPCC). Correlations between the land cover categories proposed in this study were established with what was expected at the national level as described by the national unit in charge of REDD + (UN-REDD+). Table VI summarizes the correspondence between the land cover classes proposed by the UN-REDD+ and the classes obtained from this study.

Table VI : Land cover types proposed by the national unit in charge of REDD + (UN-REDD +) and correspondence to the land cover types proposed from this study

Ecological zone	Classes from the UN-REDD +	Classes from this study
Moist humid forest	1- Young secondary moist forests	1- Agroforests
		2- Degraded secondary forest / Fallow
	2- Old-growth secondary moist forests	3- Old-growth secondary forest
Vegetation with a dominant grass layer	3- Woody savanna	4- Woody savanna
	4- Shrubby savanna	5- Shrubby savanna
	5- Grassy savanna	6- Grassy hydromorphic savanna
Vegetation free areas	6- Continental waters	7- Water

Table VII : Continuation

Ecological zone	Classes from the UN-REDD +	Classes from this study
	7- Buildings	8- Bareground
		9- Urban areas
Crop lands	8- Multi annual crops	10- *Elaeis guineensis* form
	9- Annual crops	11- Cropland
Flooded forests and wetlands	10- Swamp forests	12- Swamp forest
	11- Raphia palm swamp forests	13- *Raphia sp*. stand

II.2.2.2.2. Accuracy assessment

The accuracy of the different classifications was obtained from a confusion matrix. In a confusion matrix, the classification results are contrasted with reference ground truth pixels. The quality of a confusion matrix is that it distinguishes the nature of the classification errors, and also their quantities. Several measurements such as Producer's, User's the Overall accuracy and Kappa index of agreement were derived for each class. The producer's accuracy is the fraction of correctly classified pixels with regard to all pixels of that ground truth class (Olofsson *et al.*, 2014). For each class of ground truth pixels (row), the number of correctly classified pixels is divided by the total number of ground truth or test pixels of that class. The User's accuracy is the fraction of correctly classified pixels with regard to all pixels classified as this class in the classified image. For each class in the classified image (column), the number of correctly classified pixels is divided by the total number of pixels which were classified as this class (Zhang, 2014). The overall accuracy is the percentage of all correctly classified pixels (from all the classes) against the total number of pixels being checked (Deng *et al.*, 2014). The Cohen's Kappa (a.k.a Kappa) coefficient is a measure of agreement between two sets of datasets. Kappa coefficient measures the percentage of data values in the main diagonal of the table and then adjusts these values for the amount of agreement that could be expected due to chance alone.

II.2.2.2. Mapping functional attributes of the vegetation

II.2.2.2.1. Aboveground biomass

a) AGB estimation from ALS data

To predict vegetation AGB density from the LiDAR canopy height model, we focused on data collected over the Nachtigal area and used the savanna plot size (40 * 40 m) as our minimum mapping unit (Fig. 24).
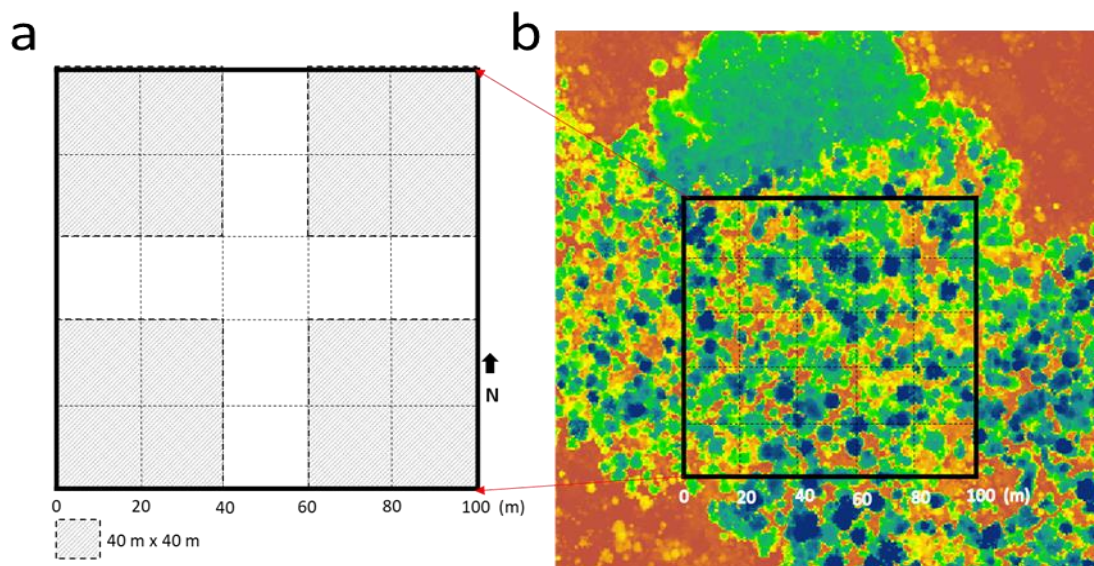
Fig. 24: Canopy height data extraction within 40 m x 40 m subplots (grey hatched squares, a) for each 1 ha forest plots (solid black square). The image represent canopy height variation obtained from airborne LiDAR (b).

We extracted the median canopy height (MCH) of the vegetation for each 40 x 40 m plot (Fig. 24) based on the CHM and fitted a linear model (Equation 3) based on the MCH as in Réjou-Méchain *et al*. (2015). The predictive power of the model was evaluated using a leave-one-out cross-validation (LOO-CV) procedure (Fig. 25).

Equation 3
$$AGB_{FIELD} = 6.27 + 8.52 * MCH$$

Réjou-Méchain *et al.*, 2015

where AGB_{FIELD} is the plot AGB density (Mg.ha^{-1}) derived from field data, MCH is the vegetation median height (m) over the plot on the 2-m CHM obtained above.
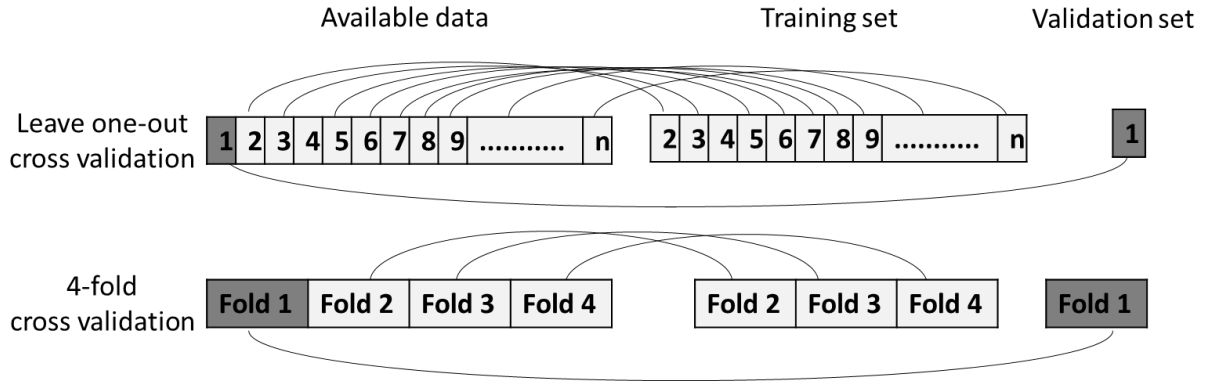
Fig. 25: The principles of the applied cross validation methods used in this study: leave one-out and 4-fold cross-validation.

LOO-CV consists of iteratively training the model on *N*-1 plots (with *N* the total number of plots), each time withholding a different plot for testing. To account for potential autocorrelation between 0.16-ha forest subplots extracted from the same 1-ha plot (which would violate the independence hypothesis between training and test sets of the CV procedure and result in overly optimistic CV statistics), we discarded 0.16-ha forest subplots of the same 1-ha plot from the training set each time a forest subplot was tested. The vector of independent AGB predictions was then used to compute CV statistics, namely the squared correlation between AGB predictions and AGB$_{FIELD}$ (henceforth R²; Equation 4) and the root mean squared prediction error (RMSPE), with:

Equation 4
$$RMSPE = \sqrt{\sum_{i=1}^{n} \frac{(y_i - \hat{y}_i)^2}{n}}$$

Baccini and Asner, 2013

Where *n* is the number of plots, y_i is the AGB$_{FIELD}$ estimate for plot *i*, and $\hat{y}_i$ is its AGB prediction.

b) AGB estimation from satellite data
- **Design-based AGB estimates**

As a reference AGB prediction method, we followed the recommendation of the IPCC (Calvo Buendia *et al.*; Särndal *et al.*, 1978) by averaging AGB density values (either AGB$_{ALS}$ or AGB$_{FIELD}$) per (woody vegetation) land cover class; see section I.2.4.1 for details. In the case of ALS, the area was fully characterized, and hence not sampled *stricto sensu*.

- **Model-based AGB estimates**

Three multispectral sensors were considered, namely Spot 6-7, Landsat 8, and Sentinel 2. Among cloud-free images in sensors archives, we looked for dry-season images acquired: (i) at

(approximately) the same date (to mitigate cross-sensor differences associated to change in land cover or vegetation phenology); and (ii) as close as possible to the ALS acquisition date. The year 2015 matched these criteria and we collected Level-1C images for Spot 6/7 (acquired on January 9th, Row/Column 4912/3514), Landsat 8 (acquired on December 1st; Path/Row 185/057) and Sentinel 2B (acquired on December 19th mosaic of T32NQK and T32NRL).

Spaceborne optical data were processed using the Overland algorithms (Poilvé and Lacase, 2014). Overland is a satellite image processing chain developed by AIRBUS DS Geo which aims to produce cloud and shadow masks and perform image atmospheric corrections, especially for areas with a high degree of cloudiness like western Central Africa. It is primarily coded in the IDL language (Harris) for image processing algorithms, with a core scene model and model inversion engine that has been developed in Matlab (MatWorks) Overland uses look-up tables from LOWTRAN and performs an inversion of a coupled atmospheric scene model (Kneizys *et al.*, 1980) to estimate atmospheric parameters and discard influences from sky, aerosols, and clouds on the surface reflectance. Another feature of Overland is the ability to partition the reflectance of individual pixels into respective contributions of soil, photosynthetic vegetation (green matter), and the non-photosynthetic matter (dead wood), and characterize the self-cast shadows of the rough vegetation canopies. For this, it implements a vegetation model by combining PROSPECT (Jacquemoud and Baret, 1990), SAIL (Verhoef, 1984), and a soil model. By inverting this vegetation model, it is possible to notably derive the fractional cover of green vegetation (fCover), the canopy shade factor (CSF), and the leaf area index (LAI).

To predict vegetation AGB, the three variables provided by Overland were considered, as well as images spectral bands and vegetation indices from corrected images summarized in Table VIII. The dataset of spaceborne optical variables thus consisted of 11 variables for Spot 6/7, 13 variables for Landsat 8 and 24 variables for Sentinel 2.

Table VIII : Band names and vegetation indices used to generate different aboveground biomass predictive models based on satellite data: Spot 6/7 (S. 6/7), Landsat 8 (L. 8), and Sentinel 2 (S. 2).

Designation	Spectral band			Candidate predictors		
	S. 6/7	*L. 8*	*S. 2*	*S. 6/7*	*L. 8*	*S. 2*
Blue	-	B2	B2			
Green	B2	B3	B3	x	x	x
Red	B3	B4	B4	x	x	x
Red1	-	-	B5			x

Red2	-	-	B6			x
Red3	-	-	B7			x
NIR	B4	B5	B8	x	x	x
Red4	-	-	B8$_a$			x
SWIR1	-	B6	B11		x	x
SWIR2	-	B7	B12		x	x

Vegetation indices		
Equations		**References**
RGR	(Red/Green)	(Sims A. and Gamon, 2002)	x	x	x
NIRGR	(NIR/Green)		x	x	x
NDVI	(NIR - Red)/(NIR + Red)	(Tuchker, 1979)	x	x	x
EVI	2.5*[(NIR - Red)/(1 + NIR + 6*Red -7.5*Blue)]	(Huete *et al.*, 2002)	x	x	x
SR	(NIR/RED)	(Jordan, 1969)	x	x	x
SAVI	(NIR - Red)/(NIR + Red + L)*1.5 with L = 0.5	(Huete *et al.*, 2002)			x
IRECI	(NIR - Red)/(Red1/Red2)	(Frampton *et al.*, 2013)			x
S2REP	[705 + 35*(0.5*(Red3 + Red)/2) - NIR)/(Red2 - NIR)]	(Frampton *et al.*, 2013)			x
NDVI1	(NIR - Red1)/(NIR + Red1)	(Kross *et al.*, 2013)			x
NDVI2	(NIR - Red2)/(NIR + Red2)	(Kross *et al.*, 2013)			x
NDVI3	(NIR - Red3)/(NIR + Red3)	(Kross *et al.*, 2013)			x
NDVI4	(NIR - Red4)/(NIR + Red4)	(Sharma *et al.*, 2015)			x

Checked spectral bands and vegetation indices are candidate predictors retained for each model. NIR = near infra-red; Red 1, 2, 3 = red-Edge 1, 2, 3; Red 4 = NIR narrow; SWIR 1, 2 = short-wave infra-red 1, 2; RGR = red green ratio; NIRGR = near infra-red green ratio; NDVI = normalized difference vegetation index; EVI = enhanced vegetation index; SR = simple ratio; SAVI = soil-adjusted vegetation index; IRECI = inverted red-edge chlorophyll index; S2REP = Sentinel 2 red-edge position.

Imagery products from the different satellite sensors were co-aligned to the AGB$_{ALS}$ raster and aggregated to 40 m resolution. The Random Forest (RF) algorithm (Breiman, 2001) was implemented in the randomForest R package (Andy and Matthew, 2002) to model vegetation AGB density from spaceborne optical variables. RF is a popular machine learning technique in remote sensing studies due to its ability to handle high-dimensional datasets, to account for non-linear relationships between response and predictor variables, and to its relative robustness to multicollinearity, model overparameterization and overfitting (Mariana and Lucian, 2016). Here, we built several RF models, considering each time a different set of spaceborne optical variables (i.e. from Spot 6/7, Landsat 8 or Sentinel 2) and using either field-based AGB estimations (strategy 1, henceforth RF$_{FIELD}$) or the LiDAR-based AGB$_{ALS}$ map (strategy 2, henceforth RF$_{ALS}$) for model specification and training. The predictive power of the RF models

was then evaluated by comparing RF models' predictions to independent reference AGB estimations.

Since RF have shown to overfit training data when predictors are correlated (e.g. Mariana and Lucian, 2016; Meyer *et al.*, 2019) or spatially auto-correlated (Meyer *et al.*, 2019), both properties being expected in our sets of optical variables, a spatial forward variable selection procedure (see III.1.1.3) was performed. This procedure starts with no variable in the model, computes the decrease in model's relative RMSPE (calculated by dividing the RMSPE by the mean of "observed" AGB values) that the addition of each candidate explanatory variable would lead to, and adds to the model the variable leading to the largest relative RMSPE decrease. The procedure is iterated as long as adding a supplementary variable in the model leads to relative RMSPE decrease larger than 1%. In the case of RF_{FIELD}, the RMSPE at each iteration of the procedure was computed using a LOO-CV over all the AGB_{FIELD} estimates. In the case of RF_{ALS}, the number of AGB_{ALS} estimates (i.e. 117415 pixels) makes the LOO-CV computationally prohibitive. A four-fold block CV was thus used for variable selection.

The ability of design- and model-based approaches was evaluated to predict vegetation AGB outside training areas using a four-fold cross-validation procedure (Fig. 25) with the LiDAR-based AGB_{ALS} map as reference AGB density values.

For design-based approaches, average AGB densities per vegetation class were assessed in the three training folds (Fig. 25), either using ALS or field data from these folds. In the remaining fold, the mean fold AGB density was computed by multiplying the AGB density of each land cover class by its respective area, relative to the total woody vegetated area of the fold. Validation could only be performed (qualitatively) at the scale of each land cover class or the whole fold.

For model-based approaches, in the case of RF_{ALS}, AGB density predictions were generated outside training areas using the four-fold block CV. In the case of RF_{FIELD}, to circumvent the relatively small plot number, all AGB_{FIELD} estimates were used to train the model and generate AGB density predictions in each of the four folds. The vector of independent AGB predictions was used to compute the CV statistics (i.e., R^2 and RMSPE). The mean signed deviation (MSD; Equation 5) was also computed as an indicator of model bias:

Equation 5
$$MSD = \frac{1}{n} \sum_{i=1}^{n} (\hat{y}_i - y_i)$$

(Ploton *et al.*, 2017)

where n is the number of pixels, $\hat{y}_i$ is the AGB prediction of pixel i by RF_{FIELD} or RF_{ALS} and y_i is its AGB_{ALS} value.

II.2.2.2.2. Spectral floristic assemblages

The progressive increase in spatial and spectral resolutions of open-access spaceborne images offers interesting prospects for the monitoring of biodiversity from space. Species turn-over in the geographical space (β-diversity) for instance, which is a central criterion to identify areas of high biodiversity in conservation programs, has been successfully assessed in tropical forest ecosystems using airborne high spatial and spectral resolution imaging spectroscopy (Féret and Asner, 2014; Féret and Asner, 2012). The method relies on the assumption that species (or groups of species) should be separable based on their spectral signatures, so that the variance in spectral data is lower within than among groups of species. It provided coherent and promising preliminary results when implemented on high resolution multispectral Sentinel 2 data (Féret and Boissieu, 2020). Here the method implemented in the BiodivMapR R package (Féret and Boissieu, 2020) was used to assess and map β-diversity on a cloud free Sentinel 2 image of the dry season (27-01-2020). Forest and savanna pixels were processed separately, using a forest - savanna mask. Within a given landcover subset (i.e., forest or savanna) an unsupervised k-means clustering was used to assign individual pixels to specific classes considered as "spectral species" based on their spectral signatures. Féret *et al*. (2020) suggested using 40 – 50 spectral species to accommodate for the high diversity of tropical forests. However using a large number of spectral species did not change the overall pattern of β-diversity in the study area, therefore the number of spectral species was set to 10. The image was then gridded into 100 x 100 m windows and the dissimilarity between each pair of windows was computed using the Bray-Curtis dissimilarity metric. The resulting dissimilarity matrix was then submitted to a Principal Coordinate Analysis (PCoA, Legendre and Legendre, 1998) and the first axis was retained to reflect changes in (spectral) species composition, for either savanna or forest ecosystems.

II.2.3. Monitoring vegetation dynamics in Google Earth Engine

II.2.3.1. Aggregating temporal images for landcover change analysis

There are three common approaches to deal with archive imagery collections for land cover monitoring. The simplest one consists in using individual, high quality cloud free scenes. In tropical, frequently cloudy conditions, this approach can prove difficult. Alternatively, where sufficient archive is available, temporal aggregates can be produced around pivot dates,

allowing the use of information contained in partially cloudy images, at the expense of a reduced precision on the timing of detected changes. Finally, for dense temporal series, time series analysis on pixels can be performed (Hermosilla *et al.*, 2015), to optimize the use of the available data and the temporal precision of event detection. In this study, the temporal hindsight was prioritized, and therefore had to deal with very sparse series prior to the launch of Landsat 7. The third approach was thus excluded. Moreover, a major difficulty lies in inter-image heterogeneity induced by directional and atmospheric effects. Correction models are now routinely applied to recover bottom-of-atmosphere reflectance (such as the LEDAPS algorithm for Landsat 5 to 8 TM, ETM and OLI data collections produced by USGS, 2020).

To work around the spectral stability issue, different approaches can be taken for image classification, mirroring of the temporal aggregation choices summarized above: (i) re-train a classifier for each image, either manually, or automatically, if the land cover classes are sufficiently distinct. (ii) use the time redundancy to stabilize the signal at the scene level by time-aggregating a sufficient number of images, (iii) use the time redundancy to stabilize the signal at pixel level, to classify stable land cover classes between major breakpoint events.

II.2.3.2. Mapping forest and savanna using supervised methods

A supervised classification approach was first adopted to generate the set of landcover maps used for the landcover change analysis in order to generate a reference product. In this approach, individual or aggregate Landsat images were retrieved from GEE and processed on a desktop computer using supervised, pixel-based classification. Supervised classification usually warrants higher quality of the final mapping product (Khatami *et al.*, 2016), but it comes at the cost of time-consuming human inputs.
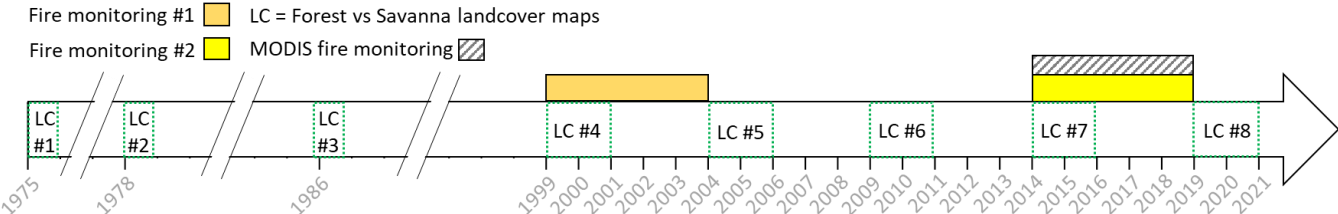
Fig. 26: Temporal domains covered by spaceborne data for vegetation and fire monitoring. Orange and yellow bands represent the years of fire monitoring with Landsat sensors and the hatched band represent the fire monitoring interval from MODIS sensor. The green dotted boxes represent the intervals within which images were selected for landcover monitoring.

Before the year 1999, only three high quality images could be retrieved from GEE: two Landsat 2 images acquired in dec-1975 (LC #1; Fig. 26) and nov-1978 (LC #2) and one Landsat 5 image acquired in dec-1986 (LC #3). Generating temporal aggregate mosaics was also feasible, but

required long (e.g. 2 years or more) aggregation periods, at the cost of a reduced temporal precision for each land cover map. From 1999 onward, 2-years median aggregate images of the dry season reflectance values were generated every 5 years from the Nov. 1999 - Mar. 2000 dry season up to the Nov. 2019 - Mar. 2020 dry season (LC #4 to LC #8 respectively). In total, we thus generated 8 images (3 and 5 images respectively before and after 1999). Forest-savanna classifications were performed with a maximum likelihood algorithm implemented in the Envi 5.0 image processing software, using all spectral bands except the blue (Landsat 7 and 8) and the coastal/aerosol (Landsat 8) bands as predictors. Two vegetation indices: the Normalized Difference Vegetation Index (NDVI, Tucker, 1979) and the Enhanced Vegetation Index (EVI, Huete *et al.*, 2002) were also added to the set of predictors. Classification models were trained using visually-delineated polygons of each land cover class (i.e., forest and savanna) distributed throughout each image. Thus eight binary forest (value of 1) and savanna (value of 0) maps were obtained.

II.2.3.3. Mapping forest and savanna using automated-unsupervised method

An automated and unsupervised landcover mapping pipeline in GEE was developed. Performing landcover classification directly in the GEE is appealing in that it alleviates data transfer between the GEE platform and the operator. Besides, the use of unsupervised classification - which does not require human inputs for the processing of each single image - together with the massive computational capabilities of GEE, offers prospects for large-scale land cover mapping, provided that the unsupervised algorithm can accurately predict the land cover classes of interest.

In the very convenient case of forest-savanna mosaics, the spectral contrast between the two classes is so important, with highly bi-modal radiometric distribution in most spectral bands (Fig. 27), that land-cover classification can easily be performed automatically at the individual image level. This is true as long as cloud, cloud shadows and strong haze can be masked, as well as very distinct land cover classes such as water bodies. Preliminary testing suggested that a simple K-means algorithm with two clusters successfully separated the two classes. On each image passing through the pipeline, we thus randomly drew 10,000 pixels to train a K-means algorithm and predicted the class of each image pixel (using the mean EVI of each cluster to determine which one was forest or savanna). This processing step was applied to the three images available before the year 1999, and to every individual image comprised within the 2-years monitoring periods after 1999.

Unfortunately, the quality of cloud, cloud shadows and haze filters contained in image quality flags are variable across collections. In subsequent analyses, the option to perform automated classifications at the individual image level was thus followed, and then keep the modal class over a series of successive images, to account for possible remaining noise caused by imperfect masking. Similarly to the manual approach, the automated landcover mapping pipeline resulted in eight binary forest (value of 1) and savanna (value of 0) maps.
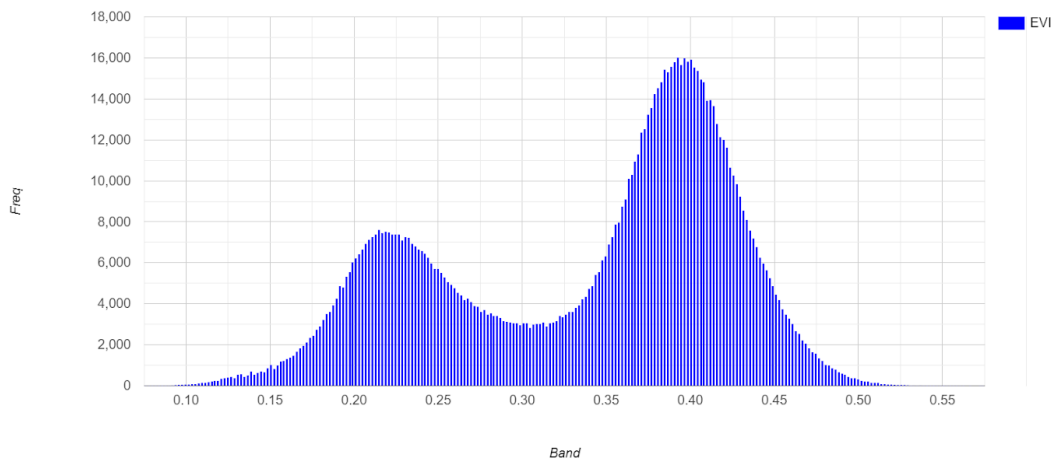
Fig. 27: EVI distribution displaying the bimodality of the forest-savanna landscape from a Landsat level 2 (BOA reflectance) median images of the dry season (Nov. - Mar.) from 2008 to 2010.

II.2.3.4.   Generating transition maps

Landcover maps from the manual and automated classification approaches were processed separately. In each case, the eight landcover maps were stacked to generate a transition map representing landcover change (or vegetation dynamics) between the years 1975 and 2000. Forest existing since 1975 were older than 45 years old (> 45). Pixels that witnessed a permanent change from savanna (0) to forest (1) or the opposite were classified as "forest gain" or "forest loss" respectively and the year of transit detection was recorded. Pixels that underwent more than one transition throughout the monitoring period (i.e., 4% of the cases) were classified as "unstable dynamics" and discarded from the analysis.

II.2.3.5.   Mapping fire frequencies

II.2.2.2.1.   Mapping fires scars

Amongst the numerous vegetation indices used to characterize fire occurrence, the Normalized Burn Ratio (NBR, Kane *et al.*, 2014; Fig. 28) has gained consideration for detecting burn scars left after a fire (Miller and Thode, 2007; Escuin *et al.*, 2008; Sunderman and Weisberg, 2011; Kane *et al.*, 2014).
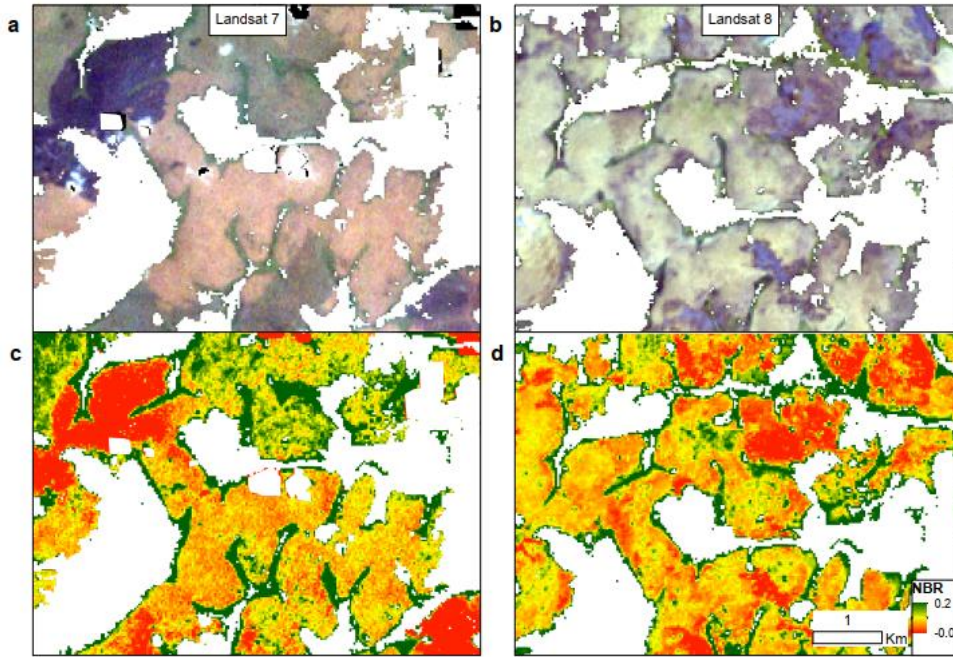
Fig. 28: Example of fire scar discrimination from the Normalized burn ratio (NBR). (a and b) RGB true colour composite of two forest-savanna landscapes from Landsat 7 (LE07_185056_20000315) and Landsat 8 (LC08_185056_20180205) with burn scars appearing in violet. (c and d) NBR of the same areas highlighting burn scars in red, dry savanna grasses in yellow and photosynthetically active savanna vegetation in green. Forest vegetation is masked out (white).

The NBR index (Equation 6) is calculated using reflectance data from passive optical sensors, especially the near infrared (NIR) and Shortwave infrared (SWIR) bands:

Equation 6 $$NBR = (NIR\text{-}SWIR)/(NIR\text{+}SWIR)$$

Key and Benson, 2003

The scarcity in the data acquired before 1999 with Landsat 5 (Tyukavina *et al.*, 2018) limited the fire frequency analysis to the period between 1999 and 2019 (Landsat 7 and 8). Landsat 7 images collected after the 31 may 2003 were discarded due to the failure that occurred on the Scan Line Corrector (SLC) which led to data gaps in images. As the availability of Landsat 8 products started in 2013, three fire monitoring intervals were considered: from 1999 to 2003 (5 years of Landsat 7, before SLC off), from 2015 to 2019 (5 years of Landsat 8) and the entire period of data availability (12 years; 99-03//13-19; see Fig. 26). NBR was computed for each pixel and each observation in their respective time series in GEE. A semi-automated approach was then adopted to map fire scars from NBR time series. First, at least two images in Landsat 7 and Landsat 8 collections with apparent fire scars were selected and polygons on burnt and unburnt areas was visually delineated in each image. Based on a visual interpretation of NBR distribution in burnt and unburnt polygons (Fig. 29), an NBR threshold of 0.1 was fixed below

which pixels were classified as burned and above which pixels were classified as unburned in the entire image collection. This threshold of 0.1 was later comforted when observing the NBR variation with time for frequently and rarely burned pixels (Fig. 30), which showed the progressive fading of fire scars' influence on pixel spectral properties.
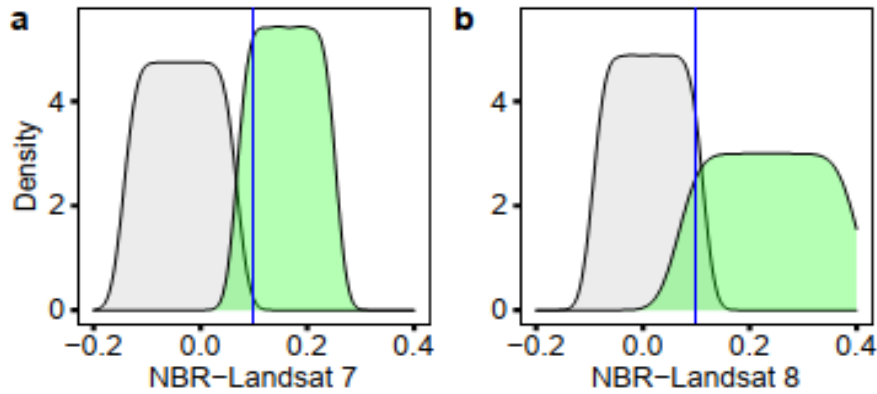
Fig. 29: Density plot of the Normalised Burned Ratio from savanna pixels with fire scars (grey colour) and savanna pixels without fire scars (green colour). The blue vertical line represents the NBR threshold of 0.1 which separates burned from unburned pixels.

For each pixel, the result of this classification process was thus a time series with observations classified as burned or unburned and featuring, for each observation, the associated image acquisition date.
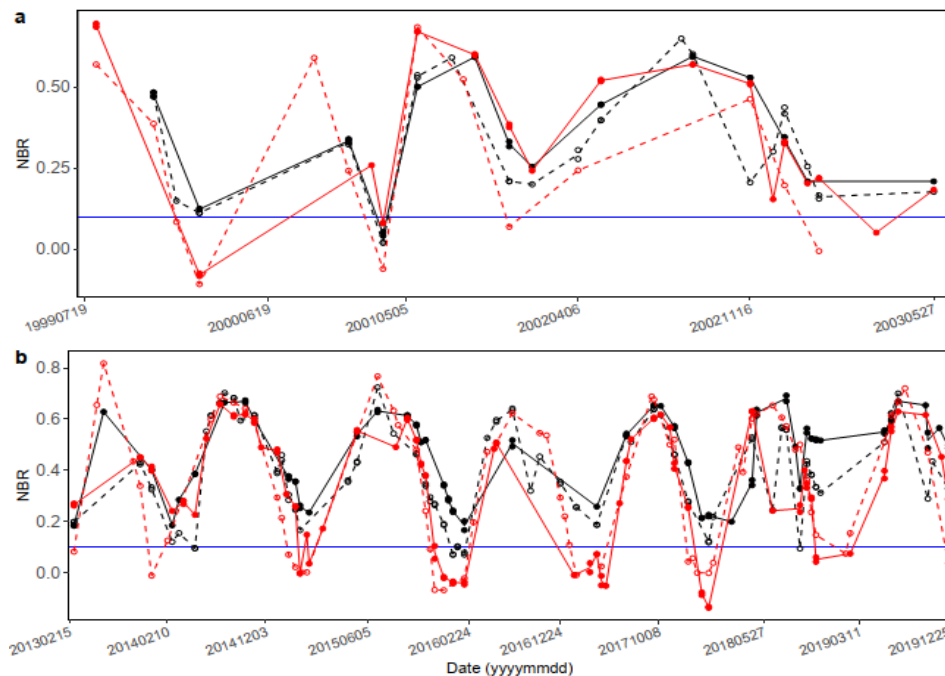
Fig. 30: Normalized Burned Ratio (NBR) variation with time. Dotted and solid lines represent the values of two pixels sampled at different locations with the same fire regimes i.e. frequently burned (red color) and rarely burned pixels (black color). (a) NBR time series from Landsat 7 (before SLC failure 31/05/2003) and (b) NBR time series from Landsat 8 sensor.

II.2.2.2.2.   Quantifying fire frequency

The fire frequency was quantified per fire monitoring period (i.e., 1999 - 2003 and 2014 – 2018; 5 years) by computing a Burn Area Index (BAI). To account for the irregular distribution of spaceborne observations within and among years resulting from the filtering of cloudy or shadowed observations, the information contained in pixels' fire scars time series was first aggregated into yearly observations. For the period between 1999 and 2003, a year was considered as a "burned" year (in which the focal pixel was burned) when at least one fire scar was detected within that year. For the period after 2013 the smaller revisit time of L8 over L7 allowed fixing a more stringent threshold, with at least two consecutive fire scar detections necessary for a year to be considered as "burned". The BAI for a pixel was then computed as the ratio between the numbers of burned years over the total number of years in a given fire

II.2.2.2.3. Comparing Landsat- and MODIS-derived fire frequencies

The MODIS burned area monthly product (MCD64A1.006 Collection 6) at 500 m resolution (Giglio *et al.*, 2015) is a very popular data source that was used for the sake of comparison for the same monitoring interval as our Landsat dataset (2014-2018). Comparison aimed at assessing the interest of increased resolution in the context of our forest-savanna mosaic landscape (30 vs. 500 m pixels).

II.2.2.2.4. Relating land cover change to vegetation structure and floristic composition

Multivariate analysis was made use of to identify the main gradient of floristic composition between forest and savanna plots. Multivariate analysis (or multivariate ordination) has become a well-established framework that facilitates the arrangement of objects that are characterized by multiple variables so that similar objects are closer each other and dissimilar objects are farther from each other (Gauch and Gauch Jr, 1982; Ter Braak and Prentice, 1988; Dray *et al.*, 2012). Major floristic groups were identified by the means of a non-symmetric correspondence (NSCA) analysis. NSCA is a correspondence analysis developed to integrate species diversity indices in a multispecies (plot-by-species floristic table) framework with the aim to capture the prominent features of the species composition of a community (Pélissier *et al.*, 2003; Couteron and Pélissier, 2004). NSCA was suited for this study as it emphasizes abundant species from the plot profile limiting the influence of unknown and not correctly identified species. Species scores from the NSCA was extracted and groups of species were generated based on a k-means clustering. All the statistical analysis was performed in R statistical software (R Core Team, 2018)

CHAPTER III

RESULTS AND DISCUSSION

CHAPTER III. RESULTS AND DISCUSSION

III.1.   RESULTS

III.1.1.   Distribution of the vegetation types and structure within the study area

III.1.1.1. Spatial distribution of the vegetation types from satellite data

The landcover map obtained over the Nachtigal study area (Fig. 31) had an accuracy of 96.5% with a kappa index of 0.95. Shrubby savanna and woody savanna were vegetation with the highest omission errors (8.14 and 8.29% respectively; Table IX) whereas the highest confusion between classes was observed for Woody savanna and Cropland. The highest confusions were made between Woody savanna and Cropland (31 pixels as omission errors a 24 pixels as commission errors)

Table IX : Confusion matrix obtained from the landcover classification using Spot 6/7 multispectral image with 2640 training pixels. AF = Agroforests; BR = Bareground; CL = Croplan; DF = Degraded secondary forests / Fallows; EG = *Elaeis guineensis* form; OF = Old-growth secondary forests; RA = *Raphia* spp. form; SS = Shrubby savanna; SF = Swampy forest; WS = Woody savanna.

Landcover types	SS	BG	CL	AF	OF	EG	RA	WS	SF	DF	Total	Omission (%)
Shrubby savanna	**79**	0	0	0	0	0	0	0	0	0	79	8.14
Bareground	0	**63**	0	0	0	0	0	0	0	0	63	0
Cropland	4	0	**802**	0	0	0	0	31	0	0	837	5.83
Agroforests	0	0	15	**410**	1	0	0	0	0	0	425	2.83
Old-growth secondary forests	0	0	0	2	**255**	0	5	0	0	0	262	0.39
Elaeis guineensis	0	0	0	0	0	**141**	0	0	0	0	141	0
Raphia spp. form	0	0	0	0	0	0	**87**	0	0	0	87	5.43
Woody savanna	0	0	24	1	0	0	0	**343**	0	0	368	8.29
Swampy forest	0	0	0	0	0	0	0	0	**199**	0	199	0
Degraded secondary forests/ Fallow	3	0	3	0	0	0	0	0	0	**172**	178	0
Total	86	63	844	413	256	141	92	374	199	172	2640	
Commission (%)	0	0	4.9	7.7	2.67	0	0	6.79	0	3.37		

The Nachtigal area was dominated by Agroforests (25%) followed by Woody savanna and Shrubby savanna (~22%; Table IX and Fig. 31). Old-growth secondary forests has a low proportion occupying only 11% of the entire landscape.

Table X : Proportion of the different landcover types located in the study area

Land cover types	Area (km²)	Proportion (%)
Agroforests	130.9	25.2
Woody savanna	114.9	22.1
Shrubby savanna	112.0	21.6
Old-growth secondary forests	58.5	11.3
Degraded secondary forests / Fallow	37.8	7.3
River	29.1	5.6
Bareground	13.1	2.5
Elaeis *guineensis* plantation	8.1	1.6
Swampy forest	7.8	1.5
Grassy hydromorphic savanna	6.3	1.2
Cropland	0.9	0.2
Raphia sp. stand	0.2	0.0
Urban areas	0.2	0.0
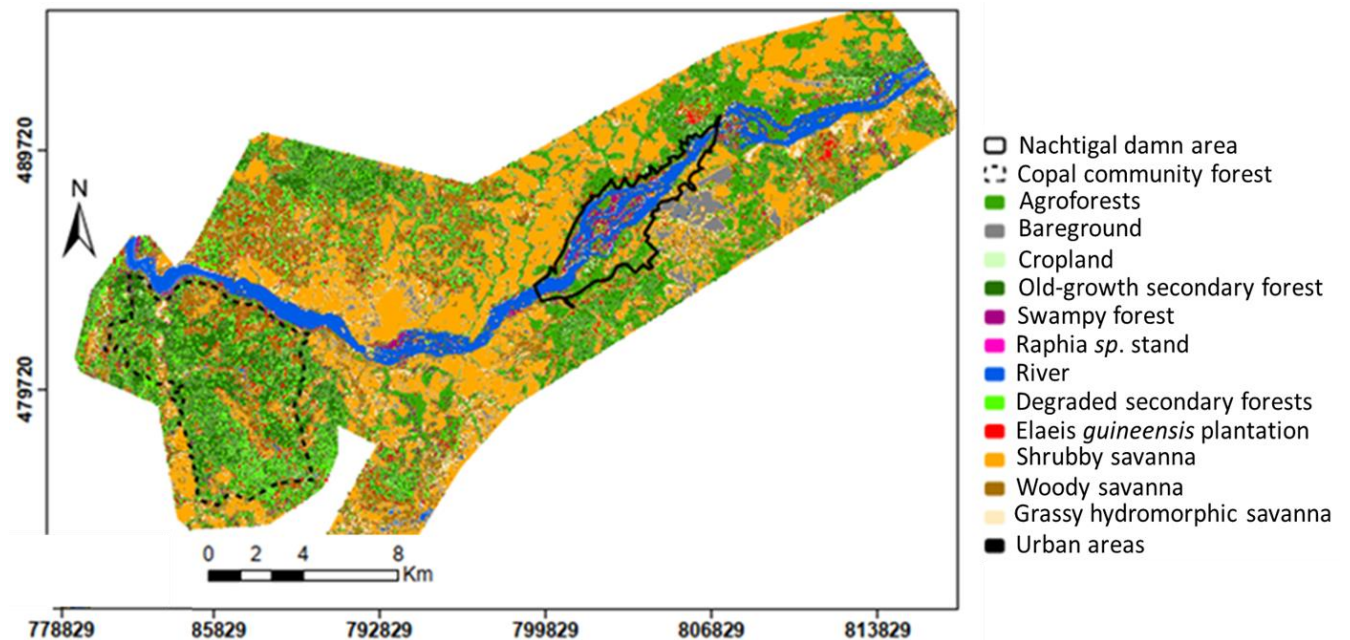
Fig. 31: Spatial distribution of the landcover types within the Nachtigal area.

III.1.1.2. AGB estimation from ALS data

Each 1-ha (100 m x 100 m) forest plots were split into 0.16-ha subplots (40 m x 40 m) to homogenize the size of the sampling plots between forest, savanna and the spatial resolution of the canopy height model derived from ALS data (40 m x 40 m). Field dataset therefore consisted in 62 plots of 0.16-ha distributed as 18 in savanna and 44 in forest. Summary statistics of the field data are detailed in Table XI.

Table XI : Summary statistics of field plot data used in predicting AGB from the canopy height model: mean (min-max). The sites consisted in closed canopy (forest) and open canopy (savanna) vegetation as observed in the field.

Sites	No. Stem (ind.ha^{-1})	Lorey's height (m)	Basal area (m²·ha^{-1})	Woody biomass (Mg·ha^{-1})
Forest	392 (216 - 538)	27 (24 - 33)	28 (19 - 35)	234 (80 - 422)
Savanna	239 (50 - 550)	7 (5 - 10)	18 (12 - 28)	21 (1 - 133)

The LiDAR-based model used to predict vegetation AGB (AGB$_{ALS}$ map; res = 40 m) over the Nachtigal area from the vegetation median canopy height (MCH) yielded a good result with an R² of 0.81 and a RMSPE of 52.7 Mg·ha^{-1} after a leave-one-out cross validation (Fig. 32). AGB$_{ALS}$ map (Fig. 33); constituted our intermediary scale for the calibration and validation of spaceborne-based and design based AGB models (see next section).
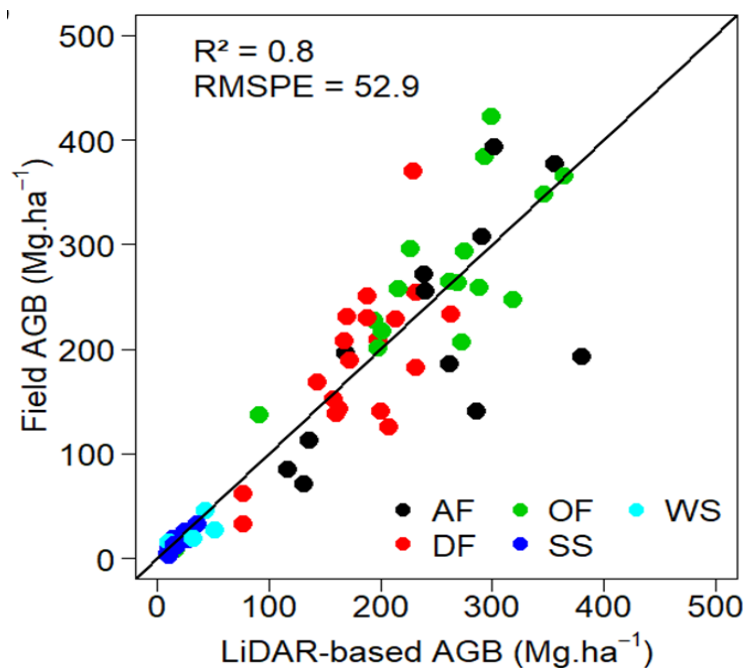
Fig. 32: Scatterplot of field-derived biomass (AGB$_{FIELD}$, Mg·ha^{-1}) *vs* biomass predicted from the ALS model (AGB$_{ALS}$, Mg·ha^{-1}) in the leave-one-out cross-validation.
Solid black line represents the 1:1 line. AF = Agroforest; DF = Degraded secondary forest; OF = Old-growth secondary forest; SS = Shrubby savanna; WS = Woody savanna plots.

When observing the AGB variation for the main vegetation types mapped within the study area (Fig. 33), Old-growth secondary forests store the highest amount of AGB (≈ 200 Mg·ha^{-1}) while Shrubby Savannas store the lowest (≈ 40 Mg·ha^{-1}).
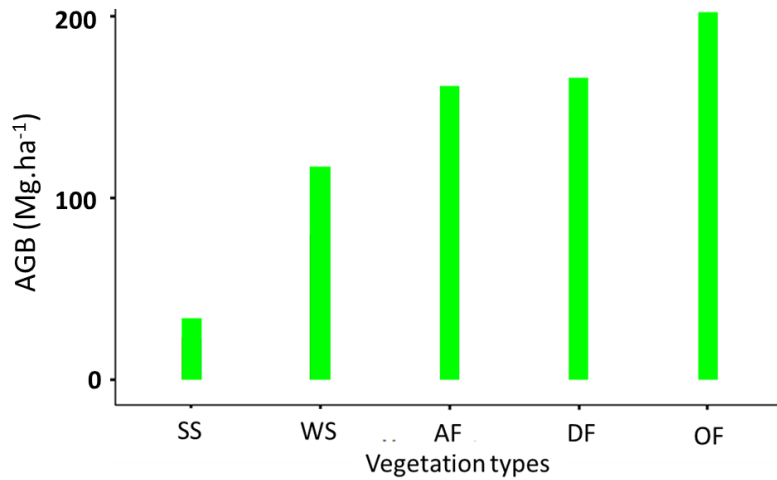
Fig. 33: Histogram of the LiDAR-based AGB variation for the main vegetation types LiDAR footprint at the Nachtigal study area. AF = Agroforests; DF = Degraded secondary forests / Fallows; OF = Old-growth secondary forests; SS = Shrubby savanna; WS = Woody savanna.

III.1.1.3. AGB estimation from optical satellite data

In model-based approaches, the variables selected varied depending on the training data (calibration on field AGB; RF_{FIELD} or calibration on the intermediate AGB_{ALS} map; RF_{ALS}; Fig. 34) and satellite sensor used for model calibration.

Table XII shows the variables selected (RF_{FIELD} and RF_{ALS}) and the model performances in cross-validation for the different models. Independently of the satellite sensor, RF_{FIELD} models gave the poorest performances, with R^2 values around 0.6, and RMSPE of up to 65 Mg.ha^{-1} (i.e. 90%), whereas RF_{ALS} models greatly improved the prediction accuracy (drop of ~30% in RMSPE and relative RMSPE). RF_{ALS} models based on Landsat 8 or Sentinel 2 predictors lead to a decrease of 10% both in RMSPE and relative RMSPE (R^2 = 0.7; RMSPE of c. 43 Mg.ha^{-1} and relative RMSPE of c. 60%) compared to RF_{ALS} models based on Spot 6/7 predictors (R^2 = 0.6; RMSPE = 48 Mg.ha^{-1} and Relative RMSPE = 66.5%)

Table XII : Structure and performances (squared correlation: R^2, root mean squared prediction error: RMSPE in Mg.ha^{-1} and the relative RMSPE in %) of the different models selected for each spaceborne optical sensor. Performance metrics are based on 4-fold cross validation. Spot 6/7 (*S. 6/7*); Landsat 8 (*L. 8*) and Sentinel 2 (*S. 2*). Candidate spectral bands and vegetation indices retained for each models: EVI = enhanced vegetation index; IRECI = inverted red-edge chlorophyll index; NDVI = normalized difference vegetation index; SAVI = soil-adjusted vegetation index; S2REP = Sentinel 2 red-edge position; SWIR 2 = short-wave infra-red 2.

Sensor	RF$_{FIELD}$ models	R^2	RMSPE	Relative RMSPE	RF$_{ALS}$ models	R^2	RMSPE	Relative RMSPE
S. 6/7	Green + CSF + EVI	0.58	65	90	Red + CSF + LAI	0.62	48.3	66.5
L. 8	Red + SWIR 2 + SAVI	0.61	64.8	88	Red + SWIR 2 + Green + fCover + EVI	0.7	43.1	60
S. 2	S2REP + SWIR 2 + NDVI 2	0.58	63.2	85	NDVI 2 + SWIR 2 + IRECI + NDVI 4 + Red + NDVI 3	0.7	42.8	58
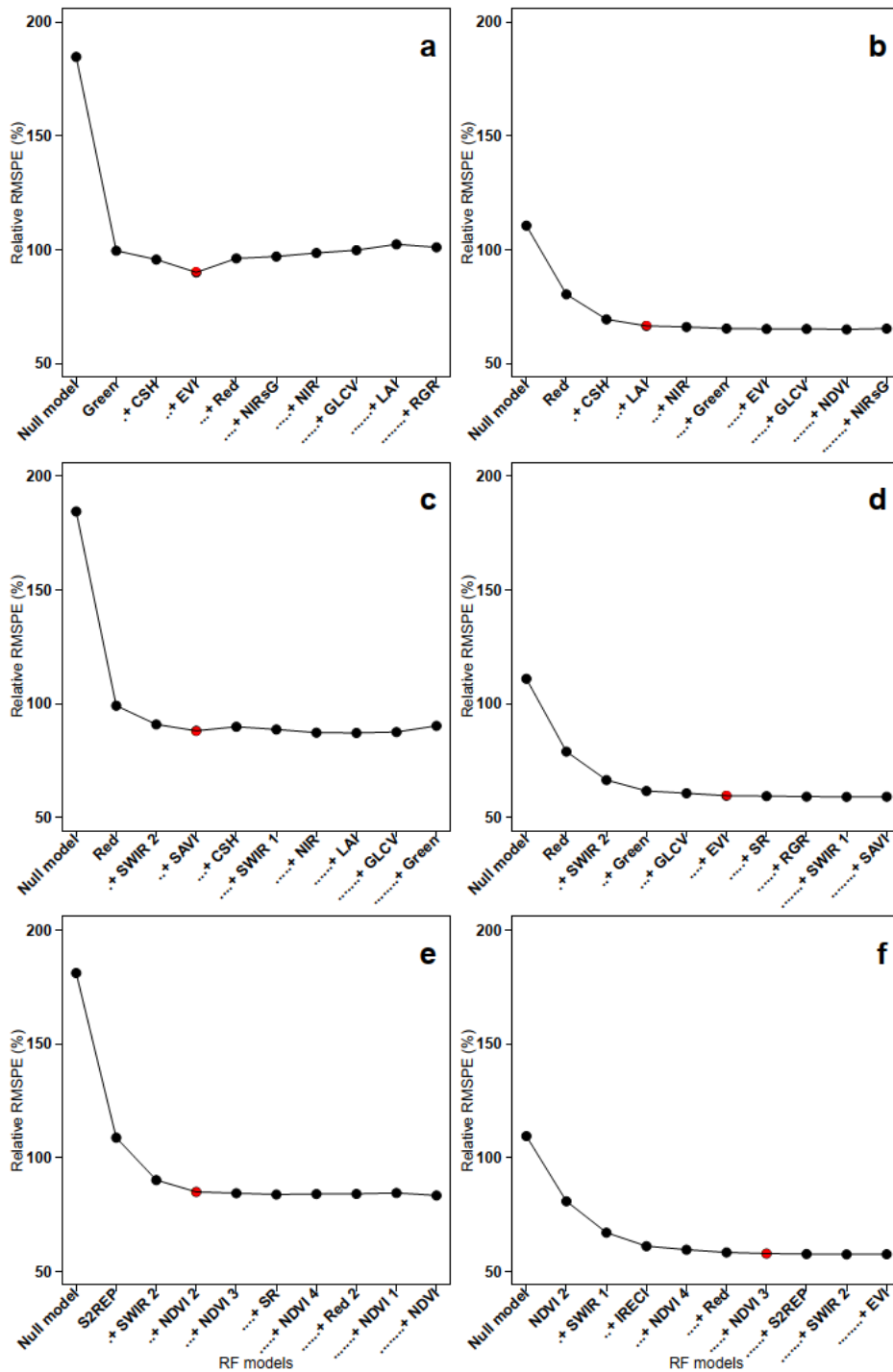
Fig. 34: Results of the spatial forward variable selection procedure for RF$_{FIELD}$ model (left column) and RF$_{ALS}$ Models (right column). (a,b) models based on Spot 6/7; (c,d) models based on Landsat 8 predictors; (e,f) models based Sentinel 2 predictors. The red dot marks the last variable leading to a decrease larger than 1% in model RMSPE.

As model-based approaches provide pixel-wise predictions, we can have a detailed look at the scatterplots of observed vs. predicted AGB density values in Fig. 35 for the Sentinel 2 sensor (sensor with the best performances), and Fig. 36 and Fig. 37 for Spot 6-7 and Landsat 8 respectively. Concordance between predictions and observations was greatly improved, i.e.

closer to the 1:1 line, for models calibrated on ALS data relative to those calibrated with field data, whereas the spaceborne sensor used seemed to make little difference. Predictions were capped around 250 Mg.ha^{-1} for all RF$_{ALS}$ models. At first sight, RF$_{FIELD}$ models seemed capable of predictions over slightly higher AGB ranges than RF$_{ALS}$ (point cloud extending beyond predicted AGB values > 250 Mg.ha^{-1} in Fig. 35 a), but predictions were in fact much less accurate overall and strongly biased in this upper range.
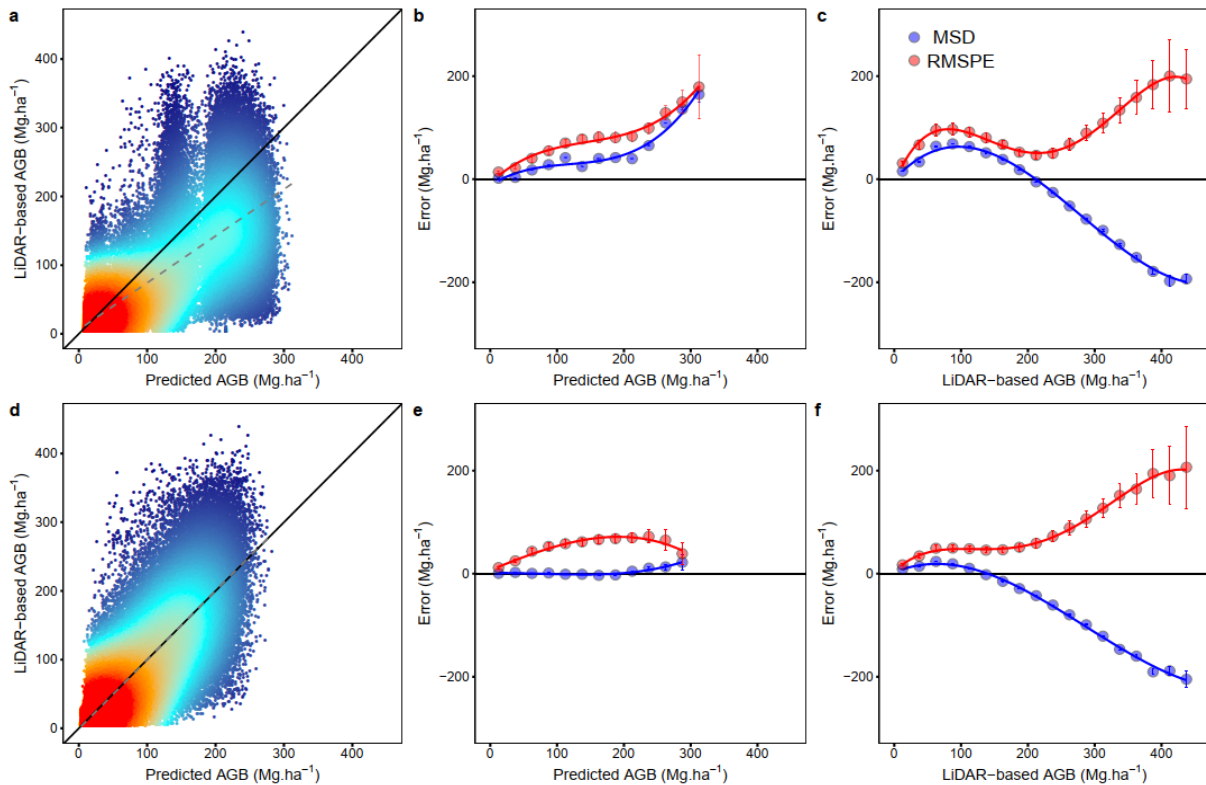
Fig. 35: Performance of RF AGB prediction models (RF$_{FIELD}$: top row; RF$_{ALS}$: bottom row) based on Sentinel 2 optical data. (a, d) Heat plots showing the relationships between Lidar-based AGB estimates vs predictions from RF$_{FIELD}$ (panel a) and RF$_{ALS}$ (panel d) models. Solid black lines represent the 1:1 line. Dashed grey lines represent the fit of simple linear models between observed and predicted AGBs. (b, c, e, f) Plots showing the relationships between statistics of models prediction error (namely the root mean squared prediction error, RMSPE, in red and the mean signed deviation, MSD, in blue) along the ranges of predicted AGB (panels b and e) and "observed" LiDAR-based AGB (panels c and f)

To better characterize the uncertainties of RF models estimates and possible dependence to AGB, we grouped the mean values of the RMSPE and the mean signed deviation (MSD, all in Mg.ha^{-1}) into equally sized bins of 25 Mg.ha^{-1}. We decomposed error and bias along the axes of both predicted and observed AGB. From a prediction perspective, RF$_{FIELD}$ models lead to a systematic overestimation of AGB$_{ALS}$ (MSD > 0, hence predictions are higher than observations) across the whole predicted AGB range, with both increasing bias and error towards large AGB values (Fig. 35 a, b and c). This means that in any predicted AGB bin,

average predictions were both largely inaccurate and imprecise when calibrating extrapolation models with field data, and all the more so at high AGB values. When binning errors along the observed AGB axis, the story was a little different, with a hinge point around 200 Mg.ha^{-1} below which predictions overestimated observed AGBs (MSD > 0) and above which predictions increasingly underestimated observed AGBs. RF$_{ALS}$ models allowed a near complete bias reduction in predicted AGB values with a MSD close to zero (Fig. 35 d and e) along the whole range of predicted AGB values except for the highest values. In other words, despite considerable scatter, predictions were on average unbiased at the landscape level across all AGB bins up to about 200 Mg.ha^{-1}. Along the observed AGB axis, error and bias were distributed similarly to RF$_{FIELD}$, with a slightly lower hinge point.
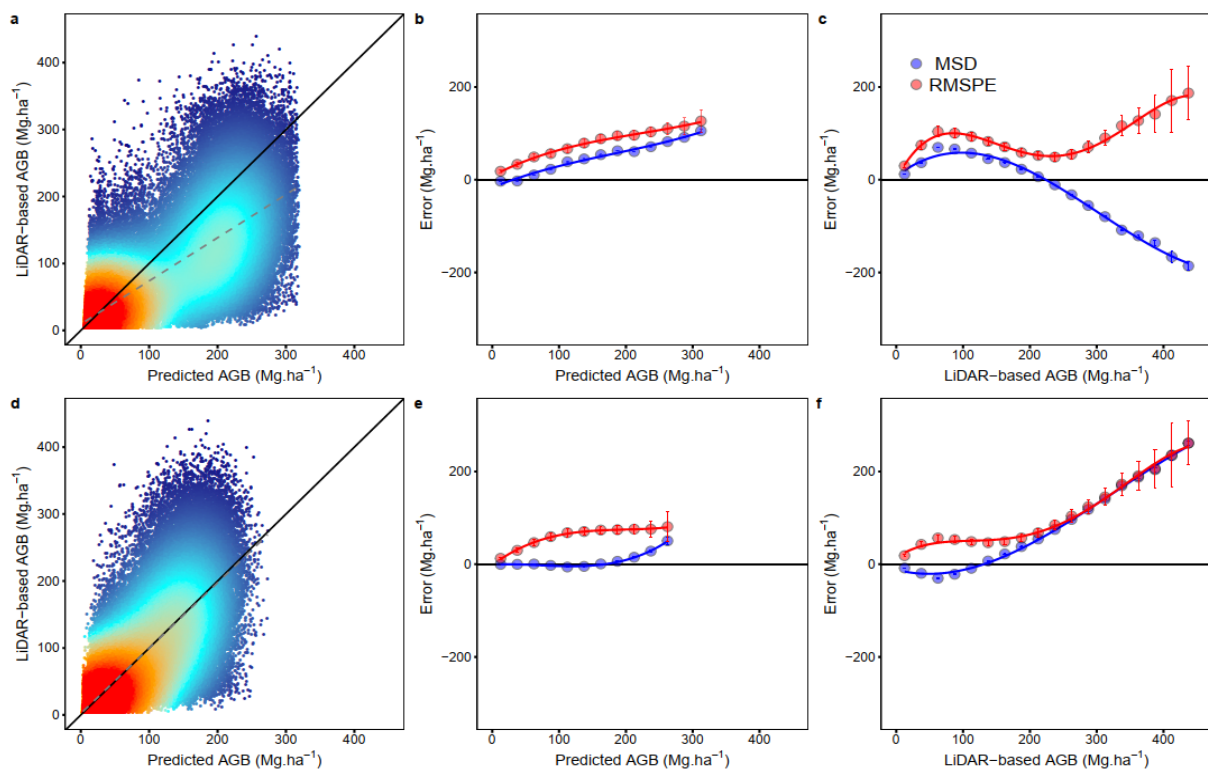
Fig. 36: Performance of RF AGB prediction models (RF$_{FIELD}$: top row; RF$_{FIELD}$: bottom row) based on Spot 6/7 optical data. (a, d) Heat plots showing the relationships between Lidar-based AGB estimates vs RF$_{FIELD}$ (panel a) and RF$_{ALS}$ (panel d) predictions. Solid black lines represent the 1:1 line. Dashed grey lines represent the fit of simple linear models between observed and predicted AGBs. (b, c, e, f) Scatterplots showing the relationships between statistics of models prediction error (namely the root mean squared prediction error, RMSPE, in red and the mean signed deviation, MSD, in blue) along the ranges of predicted AGB (panels b and e) and LiDAR-based AGB (panels c and f)
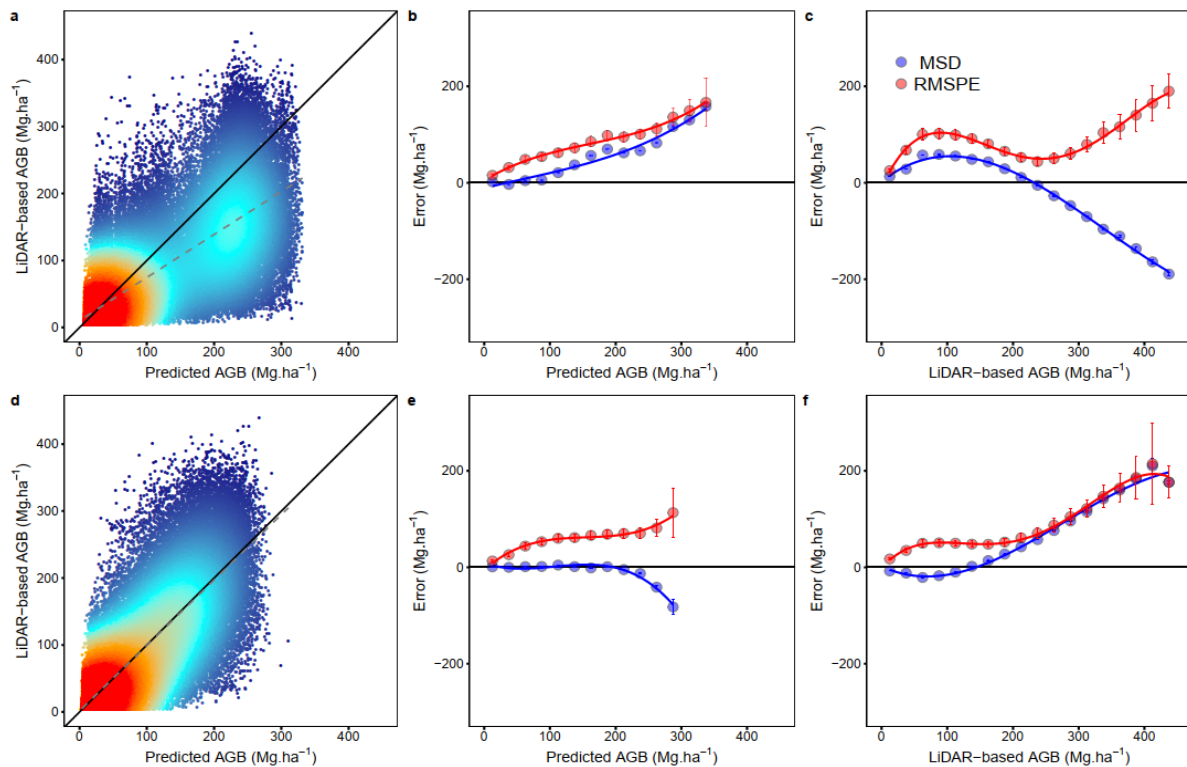
Fig. 37: Performance of RF AGB prediction models (RF$_{FIELD}$: top row; RF$_{FIELD}$: bottom row) based on Landsat 8 optical data. (a, d) Heat plots showing the relationships between Lidar-based AGB estimates vs RF$_{FIELD}$ (panel a) and RF$_{ALS}$ (panel d) predictions. Solid black lines represent the 1:1 line. Dashed grey lines represent the fit of simple linear models between observed and predicted AGBs. (b, c, e, f) Scatterplots showing the relationships between statistics of models prediction error (namely the root mean squared prediction error, RMSPE, in red and the mean signed deviation, MSD, in blue) along the ranges of predicted AGB (panels b and e) and LiDAR-based AGB (panels c and f)

To have a better understanding of the implication of the different AGB prediction approaches outside of training areas, we had a closer look at the distribution of predicted AGB density in the four blocks used in the 4-fold CV (Fig. 38 b). We first investigated the case of ALS-trained approaches (Fig. 39). Using RF$_{ALS}$, (model-based approach, based on Sentinel 2 imagery data), we could use the continuous distribution of biomass predictions. In all folds, but more markedly in the 3rd and 4th folds, the shape of the density curve diverged from the reference (ALS) curve over the higher range of AGB density values, with the expected drop around 250 Mg.ha^{-1}. Folds 3 and 4 comprise a much higher proportion of forest vegetation than the two others (Fig. 38 b), which explains the difficulty of the model-based approach to faithfully reproduce de AGB density distribution. At the fold scale however (coloured arrows beneath density plots), the mean predicted AGB density was close (below +/-10%) to the reference ALS value, except for the 4th fold (+13% difference). This illustrates that a well-trained statistical model, even with poor per-pixel predictive power, can provide unbiased prediction at the landscape level, at least as long as the landscape matrix is not too different from the training conditions. The design-

based approach, which makes the economy of a biomass prediction model and 'blindly' apply an average LiDAR-based AGB density value to each land cover class, appeared to perform equally well, with mean AGB densities between -7.2% and +12% of the ALS reference value.
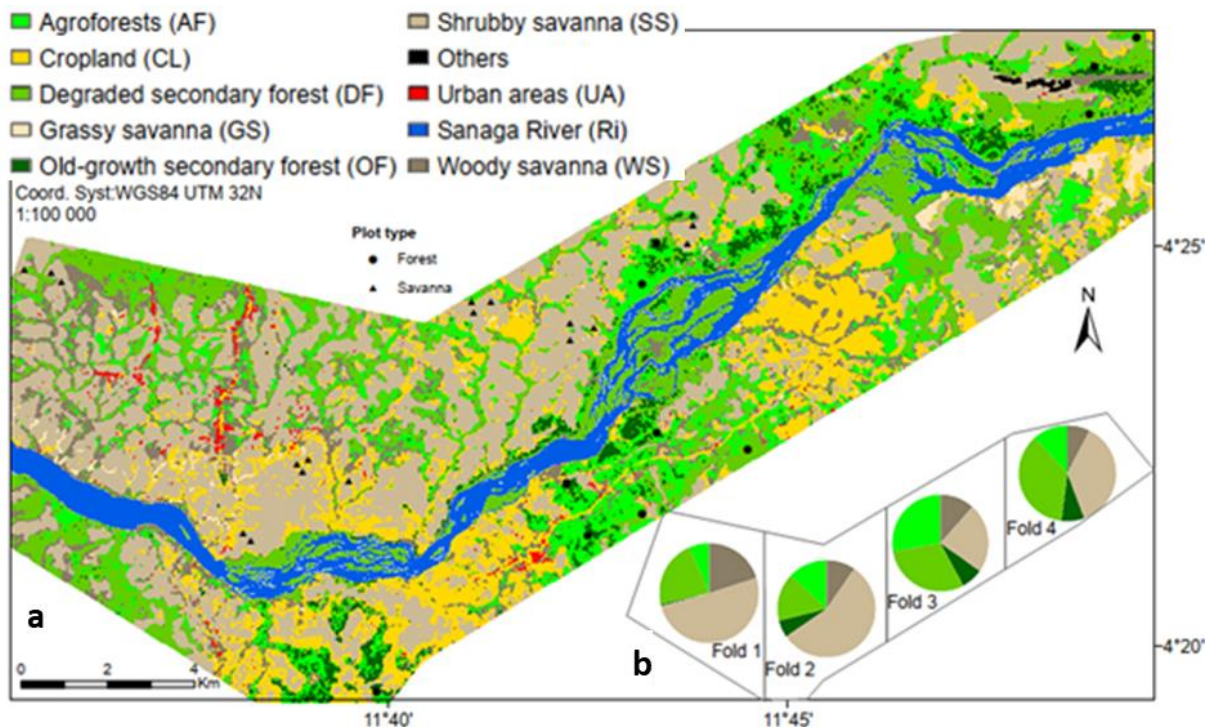
Fig. 38: Subset of the study area. (a) The most dominant vegetation classes and distribution of the field plots. (b) Folding of the study area in four spatial folds for cross-validation of the aboveground biomass prediction models. Proportion of the different vegetation types (with a significant woody component) located within each fold.

When focusing on specific land cover classes (histogram insets in Fig. 39) the model-based approach, as could be expected, systematically underestimated AGB density relative to LiDAR-based estimates in the old-growth secondary forest land cover type. The expected opposite trend (overestimation) at the other end of the biomass gradient, was more subtle in low biomass vegetation's such as woody savanna, with higher overestimations on the 4th fold. Design-based predictors did not present a systematic bias tendency in any vegetation type. A similar analysis with models calibrated with AGB$_{FIELD}$ is presented in Fig. 40. Here model-based predictions showed clearly aberrant density curves, and produced fold-level mean AGB density predictions comprised between +36.6% and +35.4% of the ALS reference. The design-based approach performed better in three folds with mean overall AGB density below 12%, but showed a 30.9% bias in fold 3. These variations can be explained by the poor sampling rate (and design) in the training folds due to the small number of available plots, which results in some large errors in the estimation of the AGB density of some of the land cover classes (up to 100%).
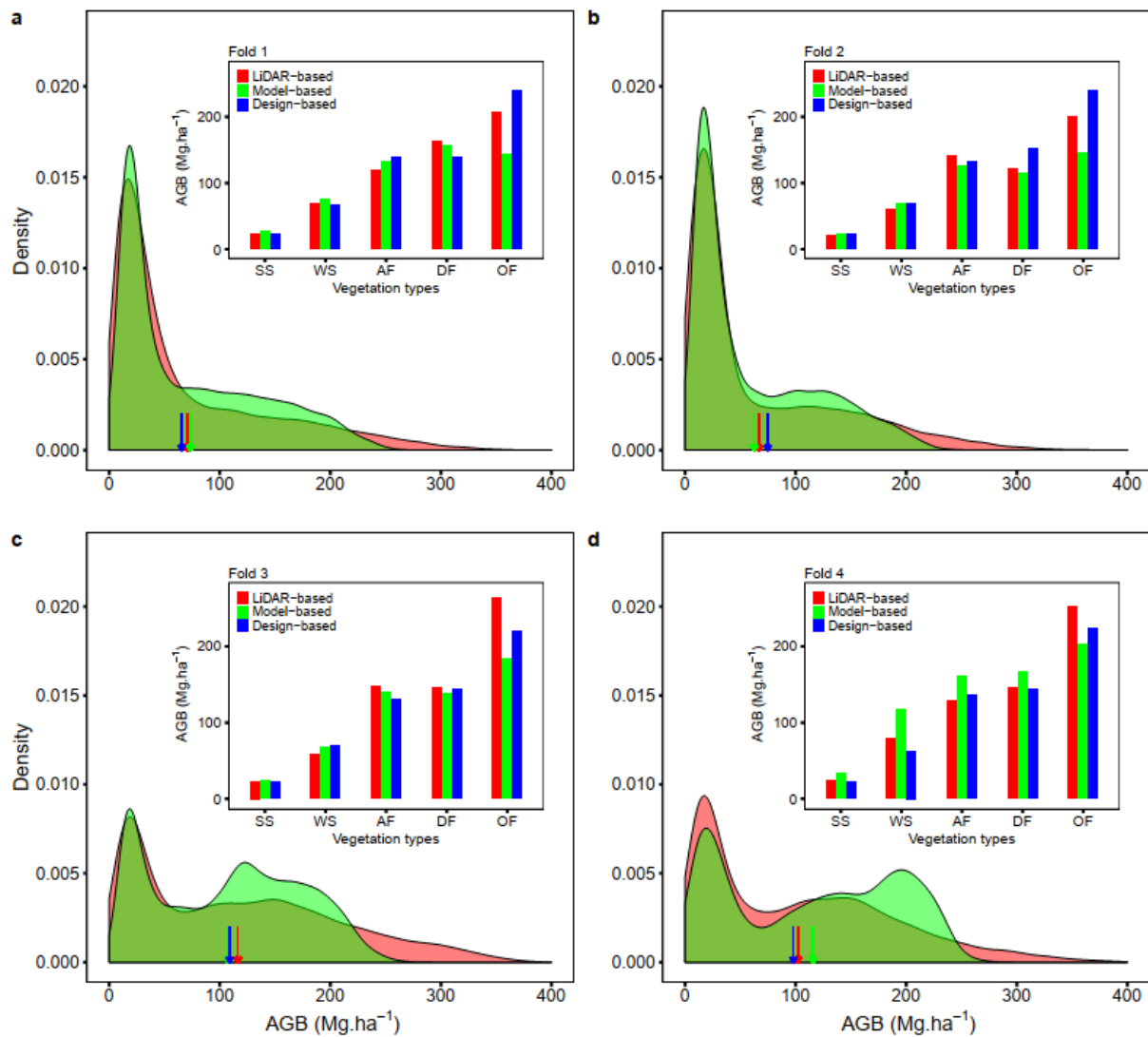
Fig. 39: Detailed analysis of model-based (Sentinel 2 sensor) and design-based AGB predictions in each fold and land-cover class, in the case of ALS trained approaches.

Density curves show the distribution of Lidar-based AGB (red) and model-based predicted AGB values (green). The arrows represent the mean AGB density values obtained by the different approaches. Inset barplots represent mean AGB density estimates for each vegetation class. AF = Agroforest; DF = Degraded secondary forest; OF = Old-growth secondary forest; SS = Shrubby savanna; WS = Woody savanna; GS = Grassy savanna.
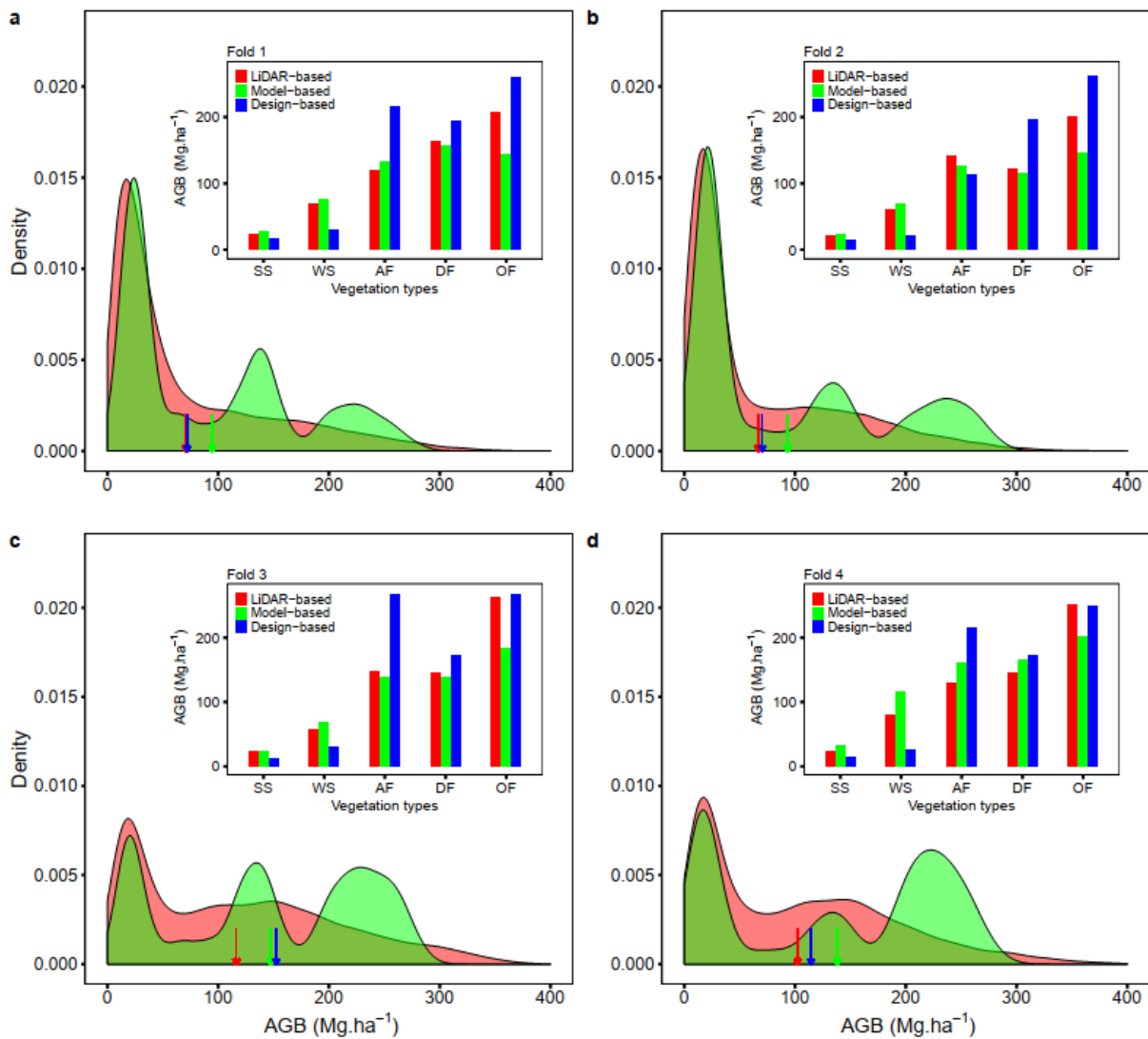
Fig. 40: Detailed analysis of model-based (Sentinel 2 sensor) and design-based AGB predictions in each fold and land-cover class, in the case of AGB$_{FIELD}$ trained approaches. Density curves show the distribution of Lidar-based AGB (red) and model-based predicted AGB values (green). The arrows represent the mean AGB density values obtained by the different approaches. Inset barplots represent mean AGB density estimates for each vegetation class. AF = Agroforest; DF = Degraded secondary forest; OF = Old-growth secondary forest; SS = Shrubby savanna; WS = Woody savanna; GS = Grassy savanna.

III.1.1.4. Differences in the structure and floristic composition within vegetation types

The averaged value (and the standard deviation) of the variables characterising the structure and diversity of the vegetation are shown in Table XIII for the Nachtigal area and the Mpem et Djim National Park (MDNP). When comparing similar vegetation types the MDNP is more diverse (number of species and rarity index) and has higher AGB values compared to Nachtigal.

Table XIII : Structure and diversity of the main vegetation types derived from plot data within the Nachtigal and the Mpem et Djim National Park (MDNP). N ind.: number of individuals

within 1-ha; N sp.: number of species within 1-ha; Rarity: average number of species for N individuals (N= 200 in forests; 16 in woody savanna and 8 in shrubby savanna). Lorey's H = averaged height of trees weighted by the basal area; G: basal area and AGB = aboveground biomass.

Types	Locality	N ind.	N sp.	Rarity	Lorey's H (m)	G (m²/ha)	AGB (Mg/ha)
Agroforests / Degraded secondary forest	Nachtigal	355(±71)	54(±9)	40(±14)	26(±3)	25(±2)	200(±64)
	MDNP	-	-	-	-	-	-
Old-growth secondary forests	Nachtigal	403(±55)	66(±4)	52(±3)	28(±1)	30(±0)	271(±34)
	MDNP	410(±93)	61(±11)	52 (±2)	27(±4)	30(±8)	339(±123)
Woody savanna	Nachtigal	43(±15)	8(±2)	5.1(±0)	8(±1)	6(±1)	19(±6)
	MDNP	49(±18)	6(±2)	5.3 (±1)	9(±2)	10(±5)	40(±33)
Shrubby savanna	Nachtigal	34(±19)	5(±1)	3.4(±1)	6(±1)	4(±2)	10(±6)
	MDNP	23(±4)	5(±1)	3.9(±1)	7(±1)	4(±1)	10(±8)

III.1.2. Variation in the vegetation structure after four decades of monitoring

III.1.2.1. Vegetation cover change

The Landsat 2 acquisition of dec. 1975 (Fig. 41) shows that the Mpem et Djim National Park (MDNP) was at that time dominated by savannas (c. 65% of the park area, following the supervised landcover classification). After four decades of vegetation dynamics (see illustrative panels b and c in Fig. 41), the MDNP was, in 2020, dominated by forest (c. 69% of the park area). Land cover change analyses captured a consistent and regular pattern of forest progression into savanna and thus allowed to deduce current forest age (Fig. 41 d and e) and average rate of forest progression (i.e., c. 1 %.year[-1], or equivalently c. 6 km².year[-1]; Fig. 42). While the opposite transition (i.e., forest loss) was also casually observed in the transition map, it only applied to 0.2 % of the pixels. Since 1975, the MDNP has thus lost about 50% of its initial savanna area, and linear extrapolation of the progression rate suggests that savannas will completely disappear from the park within the next 30 years.
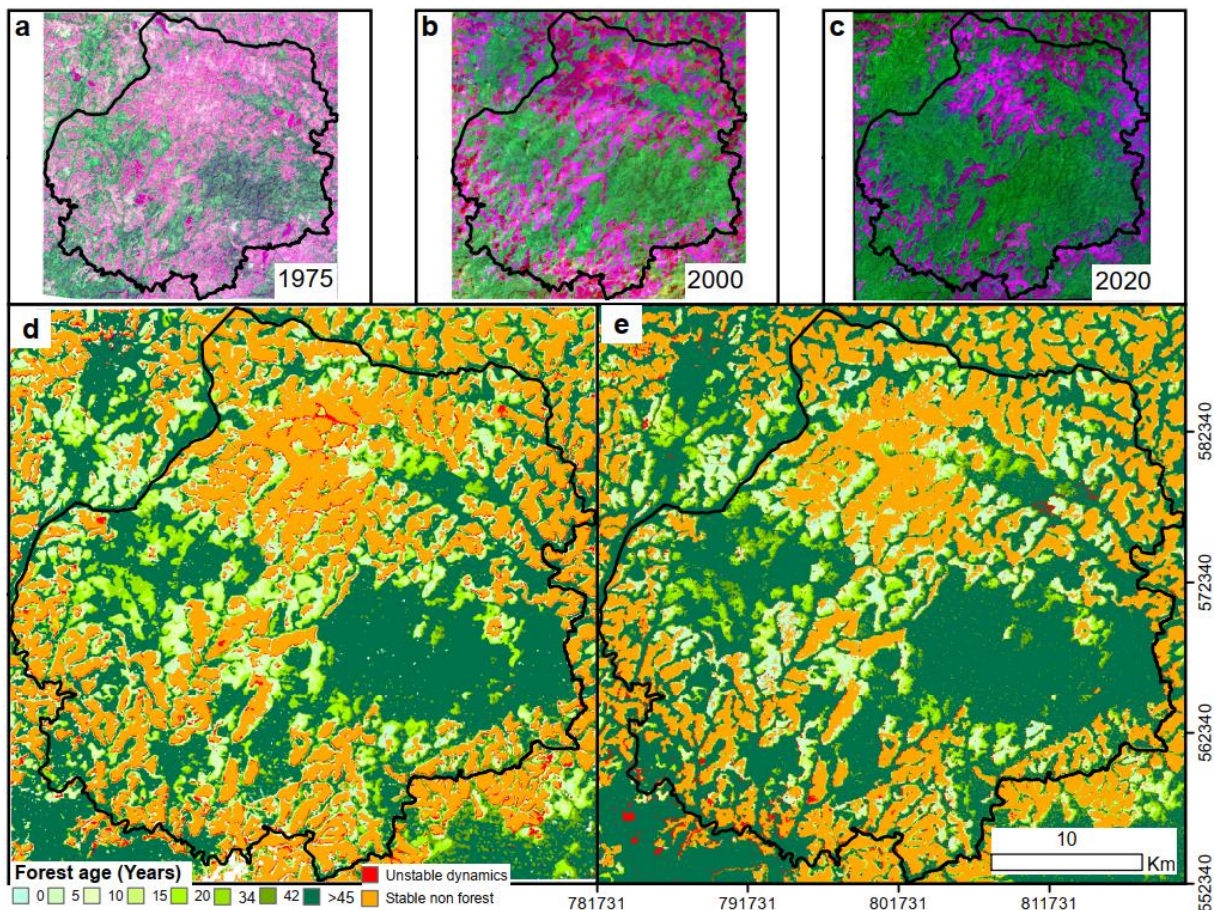
Fig. 41: Vegetation transition map of the Mpem et Djim National Park from 1975 to 2020. (a, b, c) Illustrative Landsat images (RGB colour composites, bands 3, 4, 2) of the MDNP for the years 1975, 2000 and 2020 respectively. Forests appear in green and savannas in violet. Transition map for the 1975-2020 study period using manual (d; ENVI) and automated (e; GEE) land cover classification approaches. Existing forests from 1975's landcover classification are more than 45 years old (>45). From 1975 onward, a gradient of green nuances represents the estimated establishment's year (forest age) of forest patches. Perpetuating savannas are displayed in orange, and pixels with inconsistent dynamics (i.e., more than one transition during the study period) in red.

The automated-unsupervised land cover classification implemented in GEE provided similar results than the supervised approach in terms of vegetation dynamics, capturing the steady increase of forest cover through time and leading to an average rate of forest encroachment virtually equal (i.e., c. 1 %.year^{-1}; Fig. 42). There was, however, a systematic difference in terms of absolute forest cover between the two classification approaches. The automated approach classified a higher proportion of the park area as forests when the forest cover was low (i.e., at the beginning of the study period), and this difference progressively decreased with the increase of forest cover (i.e., toward the end of the study period) which was also concomitant with the increase in density in the image series.
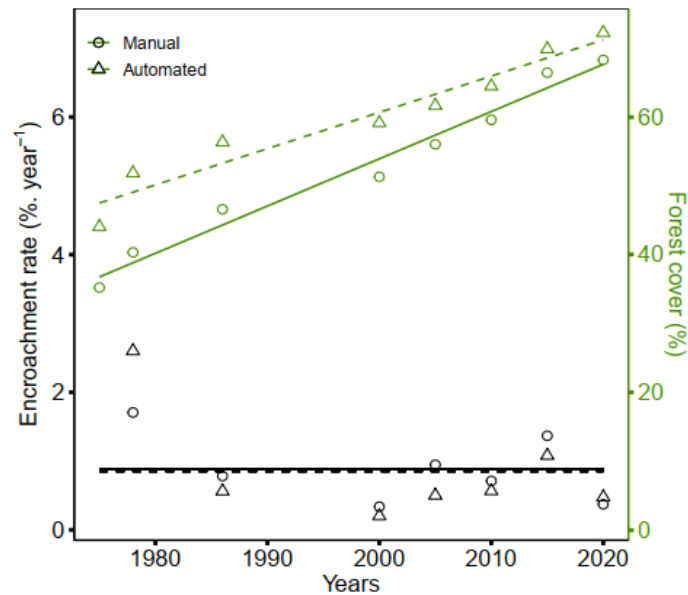
Fig. 42: Change in forest encroachment rate (in %.year^{-1}, black) and forest cover (in % of total park area, dark green) throughout the study period (1975-2020) for the supervised (ENVI; circles and full lines) and unsupervised (GEE; triangles and dashed lines) classification approaches. Green lines represent the fit of simple linear models between forest cover and years, while black lines represent the average forest progression rate, which fluctuated around ca. 1%.

III.1.2.2. Functional change

An assessment was made on the relationships between forest age and its functional attributes characterized by (1) forest composition, indirectly characterized through β-diversity analysis of 100 x 100 m windows spectral response and (2) forest structure, quantified by AGB estimates. The first axis of the Principal coordinate ordination analysis (PCoA) on the dissimilarity matrix of windows "spectral species" composition depicted a gradual change in forest composition from the forest-savanna edges (positive scores on PCoA 1, red tone in Fig. 43 a and b) to the forest interior (negative scores on PCoA 1, blue tone in Fig. 43-b).
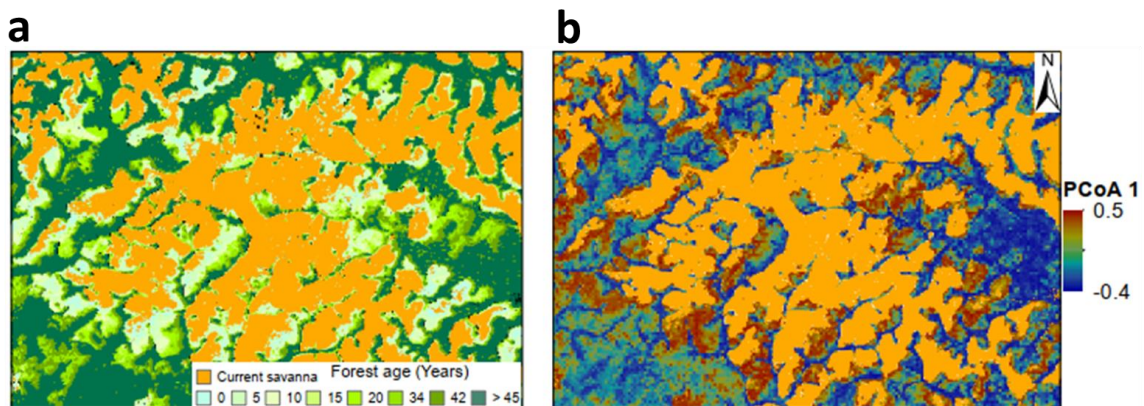
Fig. 43: Relationship between vegetation history and spectral species composition of the forest on an illustrative subset of the study area. (a) Age of the forest transition and associated (b) spectral β-diversity index, derived from the first axis of the Principal coordinate ordination analysis.

68

The spatial structure of forest spectral diversity matched the pattern of forest encroachment, with younger and older stands found on the positive and negative sides of PCoA 1 (Fig. 44-a), respectively. We also observed consistent changes in forest structure (Fig. 44-b), with an increase in forest AGB from 63 ± 47 Mg.ha^{-1} for younger forests up to 210 ± 90 Mg.ha^{-1} for the oldest forests. The transition map thus suggested an average linear increase of about 3.3 Mg.ha^{-1}.year^{-1} in MDNP forests (Fig. 44-b). However young regenerating forests (≤ 20 years) seemed to show a higher AGB accumulation rate of 4.3 Mg.ha^{-1}.year^{-1} whereas older forest successions (>20 years) have a lower AGB accumulation rate of 3.2 Mg.ha^{-1}.year^{-1}.
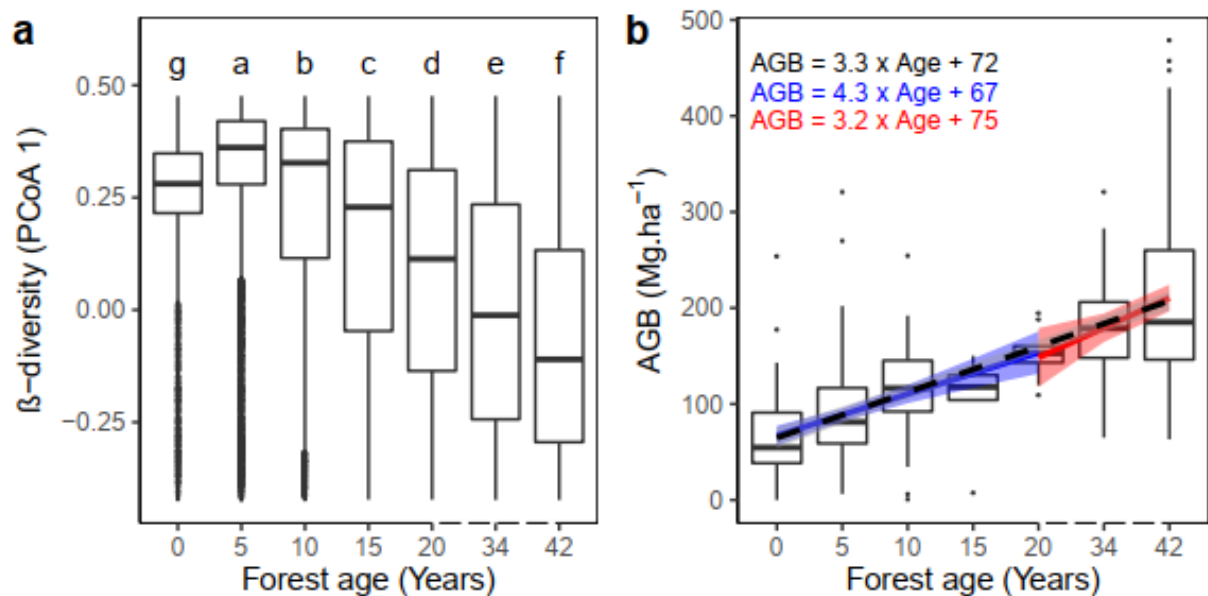
Fig. 44: Relationships between forest age, spectral diversity and structure. (a) Boxplot of pixels spectral β-diversity index, derived from the first axis of the Principal coordinate ordination analysis (PCoA 1), by forest age bins. Labelled letters represent the results of a Tukey honest significant difference (HSD) test, with different letters for boxes having different means at the probability cut-off value of p < 0.05. (b) Boxplot of pixels' aboveground biomass (AGB) by forest age bins. Lines represent the fit of simple linear models between forest age and AGB for young secondary forests (≤ 20years, solid blue line), old secondary forests (> 20 years; solid red line) and all successional stages (dotted black line) with their respective 95% confidence interval ribbons included. Note that in panels a and b, x axes after year 20 are represented with broken lines to mark a change in the interval between age bins.

III.1.3.   Fire influence on land cover dynamics

III.1.3.1. Influence of fire frequency on forest transition

Based on a visual interpretation we noticed that savannas surrounding the park principally in the northern part underwent high fire frequencies for both monitoring periods (1999-2003 and 2014-2018; Fig. 45 a and b). Savannas located at the centre of the park showed decreasing fire frequencies through time (from 1999-2003 to 2014-2018; Fig. 45 c and d). Most of the savanna

that transited to forest between two consecutive dates had an average BAI of 0 in the 5 previous years, meaning that no fire was detected. Persisting savanna that did not undergo any forest transition had a BAI presenting a broad range of values for all the monitoring periods. The proportion of pixels in the highest BAI class (BAI = 1, corresponding to an annual fire frequency) increased from 1999-2003 to 2014-2018.
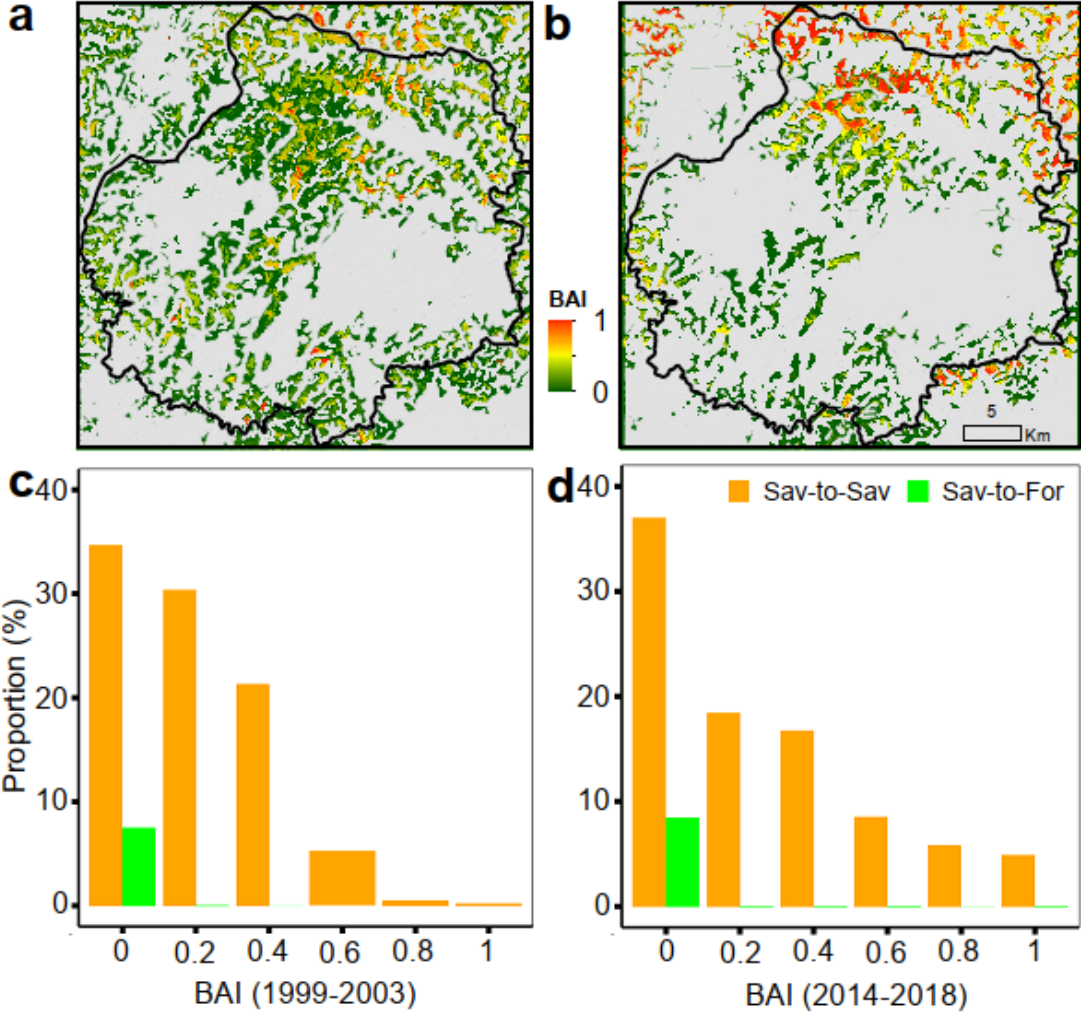
Fig. 45: Maps of the Burn Area Index (BAI) derived from Landsat for the monitoring periods 1999-2003 (a), 2014-2018 (b) and associated barplots (c, d) showing the distribution of BAI classes for savanna pixels that did not transit to forest (Sav-to-Sav; orange) and savanna pixels having transitioned to forest (Sav-to-For; green) in consecutive land cover classifications. Existing forests at the beginning of both fire monitoring periods (a and b) are masked out in grey.

The burned areas detected by the 500 m spatial resolution burn area MODIS product proved higher for low fire frequencies (BAI ≤ 0.2; Fig. 46 a) with an overestimation of up to 98% (Fig. 46 b) compared to the 30 m Landsat estimates. A reverse trend was observed for higher fire frequencies (BAI ≥ 0.4), where Landsat captured higher proportions of burned pixels with the

MODIS product even failing to detect yearly fire frequencies (BAI = 1). Overall the BAIs quantified using Landsat were on average 28% higher than the ones detected from MODIS.
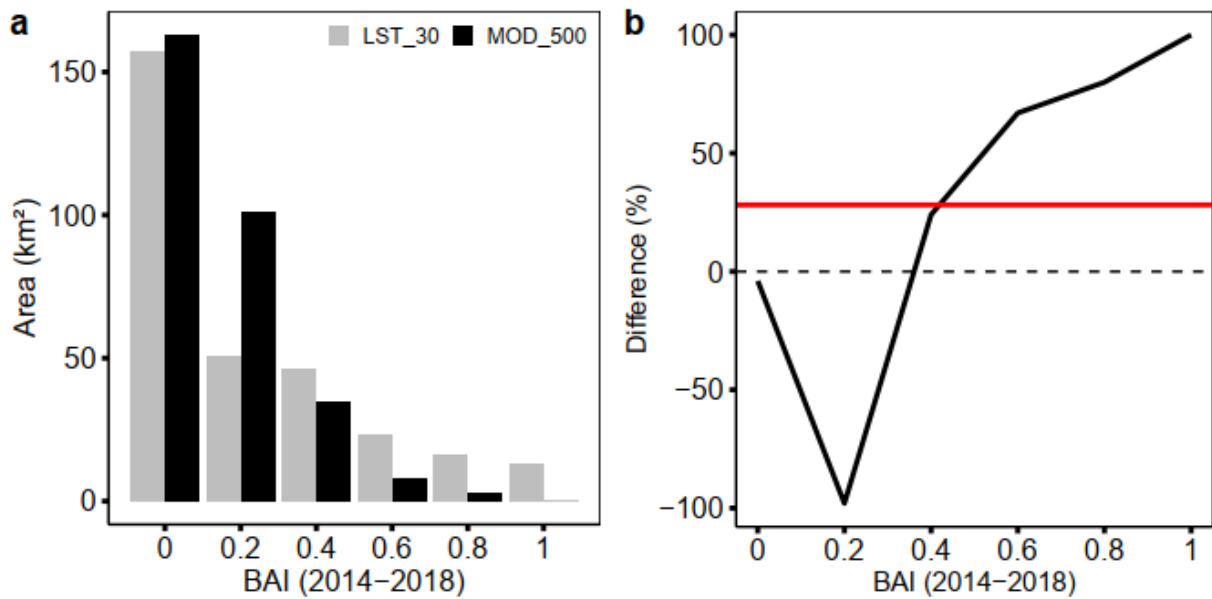
Fig. 46: Burn Area Index (BAI) derived from Landsat at 30 m (LST_30; grey) and the MODIS burn area product at 500 m (MOD_500; black) for the 2014-2018 period over areas classified as savannas in 2020. (a) Burned area (in km²) disaggregated by BAI classes. (b) Difference between the burned area estimated by Landsat and MODIS relative to the Landsat estimate (solid black line). The red line represents the average overall difference.

III.1.3.2. Influence of fire frequency on savanna structure

The relationships between the recent fire frequency (2014-2018) and the composition and structure of current savannas (2020) was investigated. The spatial distribution of savanna's Burn Area Index (BAI) was congruent with distribution patterns of spectral species composition (Fig. 47).
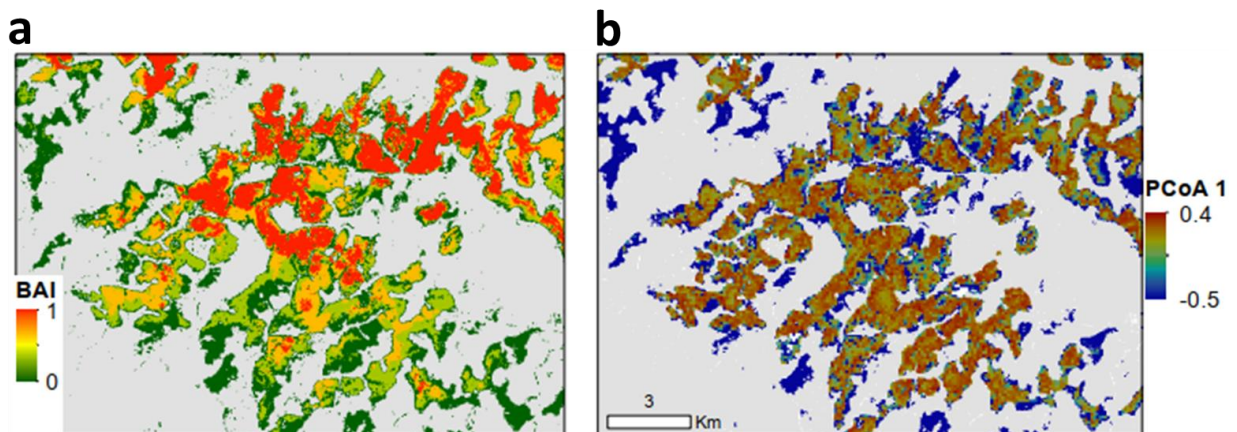
Fig. 47: Relationship between fire history and spectral species composition of the savanna on an illustrative subset of the study area. (a) Spatial distribution of the Burn Area Index (BAI) for the fire monitoring period 2015-2019 and associated (b) spectral β-diversity index, derived from the first axis of the PCoA 1. Only stable savanna pixels from 1975 to 2020 are displayed and pixels classified as "Forest" in 2020 are masked out (white) in b and c.

71

The first axis of the PCoA on the dissimilarity matrix of windows spectral species composition depicted a gradual change in savanna composition from woody savanna (negative scores on PCoA 1, blue tone in Fig. 47) to grassy savanna (positive scores on PCoA 1, red tone in Fig. 47). Savanna's spectral β-diversity indices (PCoA 1) showed a marked bimodality (Fig. 48), with a first mode around ca. -0.5 of PCoA 1 which corresponds to unfrequently burnt savannas (BAI close to 0) and a second mode around ca. 0.4 corresponding to frequently burned savannas (BAI close to 0.4; Fig. 48-a). The two modes in savanna's composition are consistent with distinct gradients in biomass accumulation (Fig. 48-b), with higher AGB values found on unfrequently burnt savannas (c. 49 ± 40 Mg.ha^{-1} for leftmost box in Fig. 48-b) than on frequently burnt savannas (21 ± 18 Mg.ha^{-1} for the rightmost box).
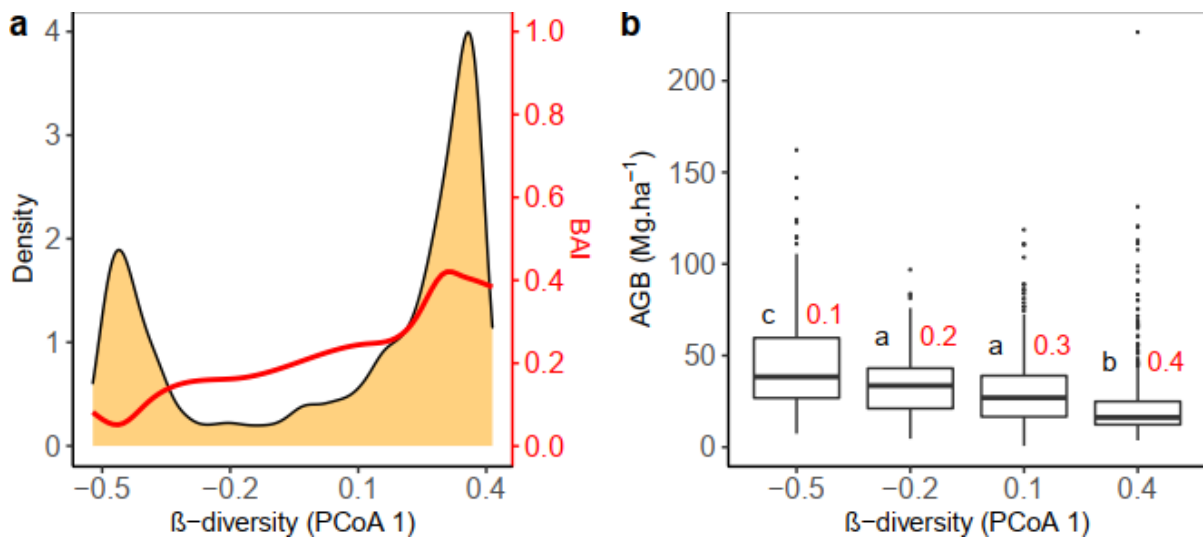
Fig. 48: Relationships between savanna spectral diversity, fire frequency and savanna structure. (a) Density plot of pixels spectral β-diversity score on the first axis of the Principal coordinate analysis (PCoA 1) and associated recent (2015-2019) fire frequency, represented by a smooth average of pixels Burn Area Index (BAI, red line). (b) Boxplot of AGB variation by PCoA 1 bins. The labelled letters represent the results of a Tukey honest significant difference (HSD) test, with different letters for boxes having different means at the probability cut-off value of p < 0.05. Red numbers above the plots represent the average BAI for each PCoA 1 bin.

III.1.4. Species succession dynamics

The dataset used for floristic and structural gradient analysis were collected from 137 plots of 40 m x 40 m size (90 in forest and 47 in savanna; Fig. 49). The dataset consisted in 7425 trees (5857 in forest and 1568 in savanna) belonging to 249 species belonging to 163 genus and 48 families. Summary statistics of the field data are detailed in Table XIV.

Table XIV : Summary statistics of 40 m x 40 m field plot data used in depicting compositional shifts or trends in the floristic composition: mean (min-max).
N ind = Number of individuals; H = Lorey's height in m; BA = basal area in (m².ha^{-1}), Richness = relative species richness in %; AGB$_{wood}$ = Aboveground biomass of the woody layer in (Mg.ha^{-1}); AGB$_{grass}$ = Aboveground biomass of the grass layer in (g.m^{-2}).

Sites	N ind	H	BA	Richness	AGB$_{wood}$	AGB$_{grass}$
Forest	66 (25 - 151)	25 (8 - 34)	28 (6 - 65)	42 (14 - 66)	234 (80 - 422)	-
Savanna	31 (2 - 77)	7 (4 - 9)	5 (1 - 11)	25 (6 - 100)	12 (1 - 41)	116 (9 - 361)
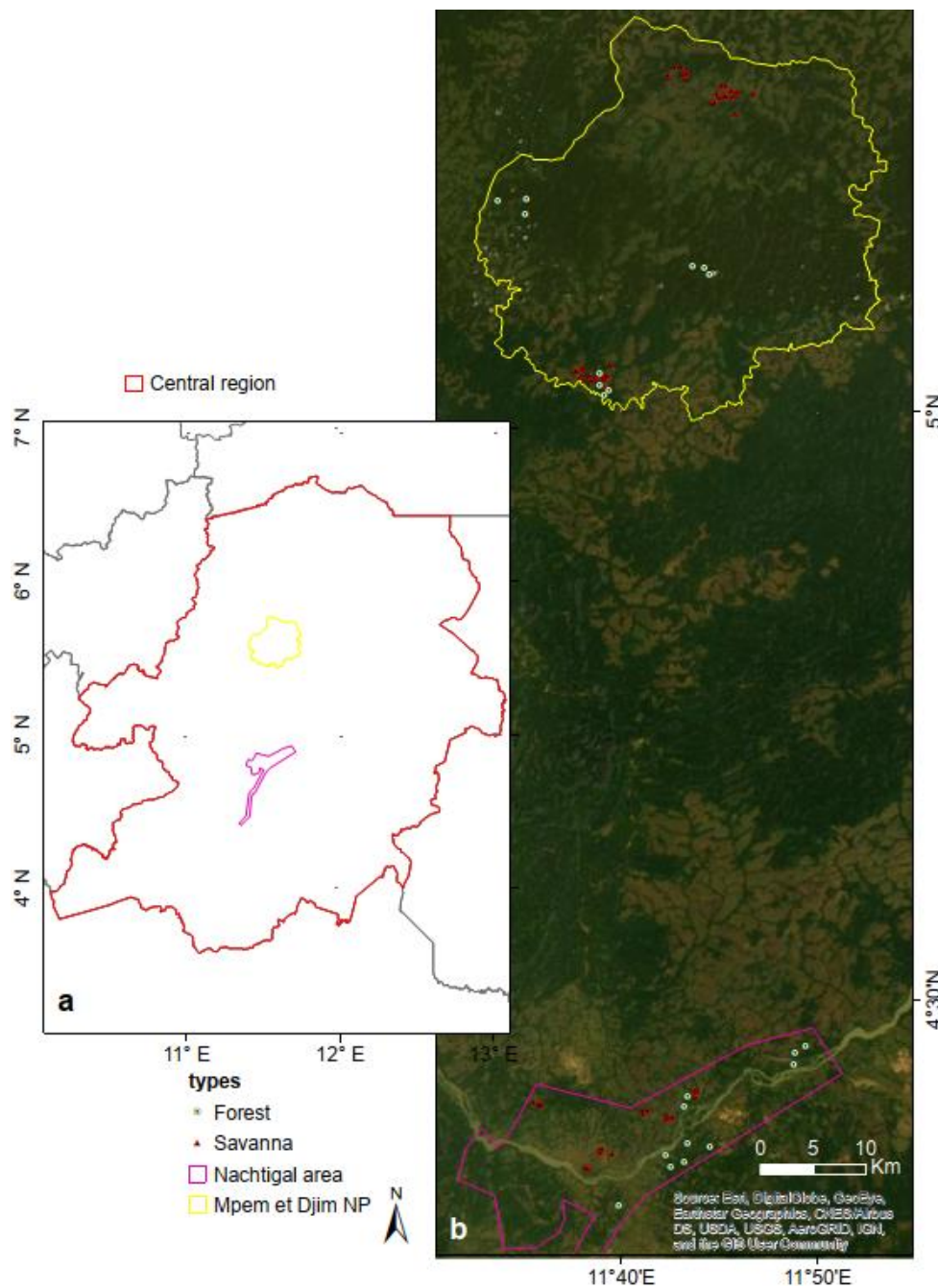
Fig. 49: Spatial distribution of plots within the study area.

III.1.4.1. Gradients in floristic composition

Non-symmetric correspondence analysis on the floristic table revealed two patterns of floristic distribution (Fig. 50). The gradient revealed by the first axis of the NSCA (explains 21% of total variance) separated plots dominated with savanna species (red and orange Fig. 50) from plots dominated by forest species (green). The second axis (explains 10% of total variance) separated between plots sampled in the Nachtigal area (circles) and the ones in Mpem et Djim national park (MDNP).
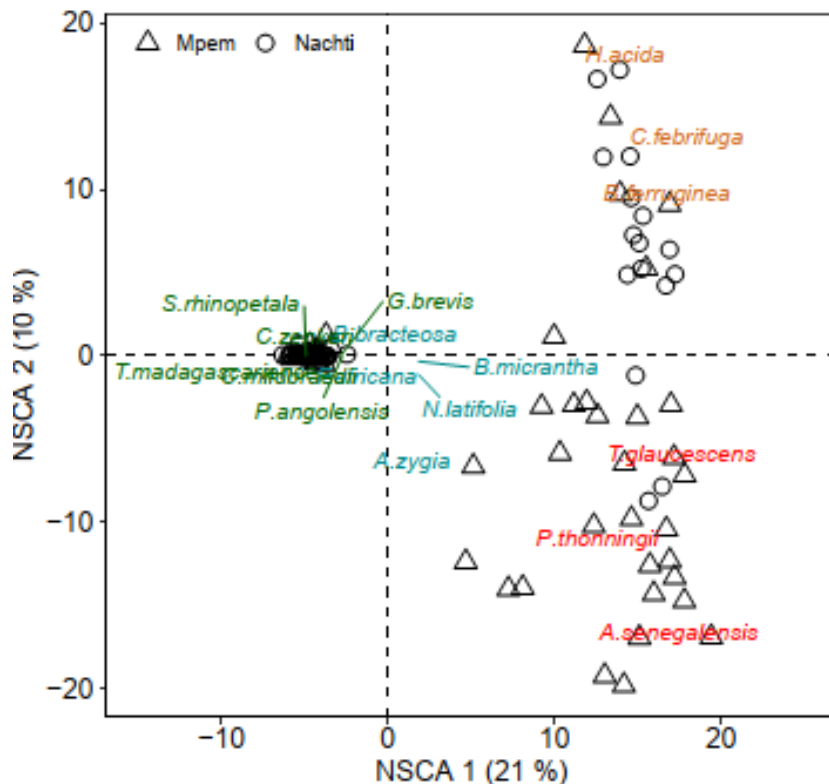
Fig. 50: Floristic pattern depicted by first two axes of a Non-Symmetric correspondence Analysis (NSCA) of the floristic table derived from the 40 x 40 m plots distributed in forest and savanna in the Mpem et Djim National Park (triangle) and Nachtigal (circled). Species colours represent groups from k-means clustering (savanna group 1 = red, savanna group 2 = orange; ecotone species = cyan; and forest species = green). Only species with high contributions on the NSCA 1 and 2 axes are displayed for visualization purposes. See Appendix 4 for the entire list of species belonging to each floristic group.

The species distribution from the NSCA axis revealed four groups of floristic assemblages as depicted by the k-means clustering (Fig. 50) with the first axes separating savanna species (red and orange) from the ecotone species (cyan; dominated with *Albizia zygia, Bridelia micranta, Nauclea latifolia, Oncoba glauca,* and *Treculia obovoidea*) and forest species (green; dominated with *Celtis mildbraedii, Celtis zenkeri, Glyphaea brevis, Sterculia rhinopetala* and *Trilepisium madagascariense*). This axis is therefore an indicator of the succession trend within

the area. The second axis from the NSCA separates the two groups of savanna; the first group (orange) with *Hymenocardia acida*, *Crossopteryx febrifuga* and *Bridelia ferruginea* which dominates Nachtigal and the second group (red) with *Terminalia glaucescens*, *Piliostigma thonningii* and *Annona senegalensis* which dominate the (MDNP). This second axis is therefore an indicator of savavanna structure.

III.1.4.2. Species succession

The relative species abundance within plots for the savanna floristic groups (orange and red for savannas in Nachtigal and Mpem et Djim respectively) is higher in plots with low woody AGB (AGB_{Wood}) and gradually decreases towards plots with higher AGB_{Wood} values up till 40 Mg.ha^{-1} from which they become scarce (Fig. 51-a). Unlike the savanna floristic groups the relative abundance of species characterizing ecotone (cyan) is low in plots with low AGB_{Wood} ($\leq$ 40 Mg.ha^{-1}) and increases towards higher AGB_{Wood} values.
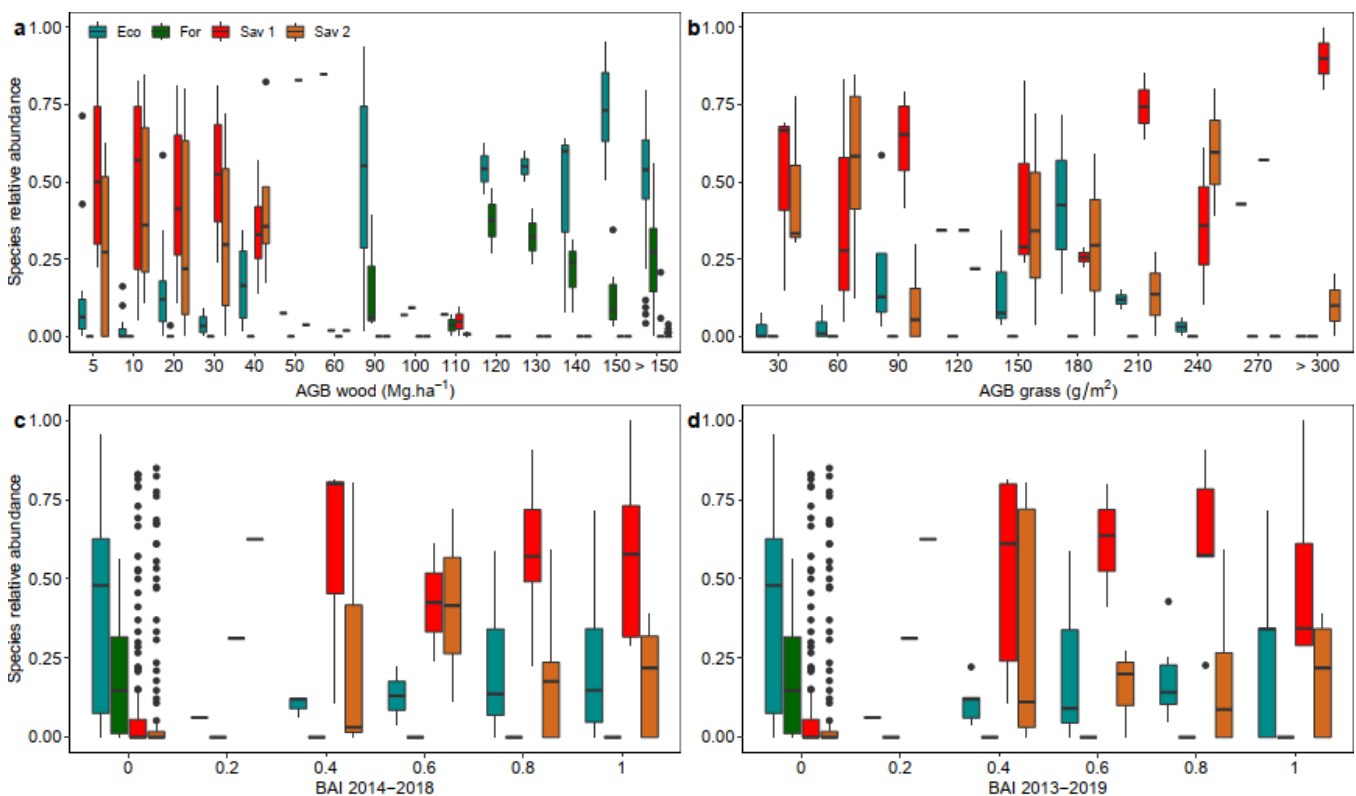
Fig. 51: Relationship between the relative abundance of the different group of species distinguished from the NSCA analysis; the aboveground biomass from the woody (a) and grassy (b) layers and the fire frequencies for (c) 5-year monitoring and (d) 7 years monitoring. Ecotone species (Eco; cyan); forest species (For; green); savanna species from Mpem et Djim national park (Sav 1, orange) and savanna species from Nachtigal (Sav 2, red).

However the relative abundance of forest species (green) becomes significant in plots with $AGB_{Wood} \geq 90$ Mg.ha^{-1}. The savanna floristic groups display no clear pattern with the AGB of

the grass layer (AGB$_{Grass}$) whereas the relative abundance of forest species decreases towards higher AGB$_{Grass}$. The presence of forest species is low in plots with high fire frequency (Fig. 51-c and d) where savanna species dominated with *T. glaucescens*, *P. thonningii* and *A. senegalensis* are more abundant as compared to savanna species dominated with *H. acida*, *C. febrifuga* and *B. ferruginea* (Fig. 51-c and d). Ecotone species are however present in all plots irrespective of the fire frequencies.

The basal area (BA) of savanna species increases towards higher AGB$_{Wood}$ values up till 40 Mg.ha^{-1} where it decreases (Fig. 52-a). The BA of savanna species is higher than the one from forest species for plot's AGB$_{Wood}$ < 40 Mg.ha^{-1} from which the tendency reverses. Forest species display an increase in their BA towards higher AGB$_{Wood}$ values. The basal area for all woody species decreases with the increase in AGB$_{Grass}$ (Fig. 52-b). The basal area for forest species is high for plots with no fire occurrence (BAI =0) and drastically decreases as BAI increases. Savanna species dominated with *T. glaucescens*, *P. thonningii* and *A. senegalensis* have the highest basal area toward higher fire frequencies (Fig. 52-c and d).
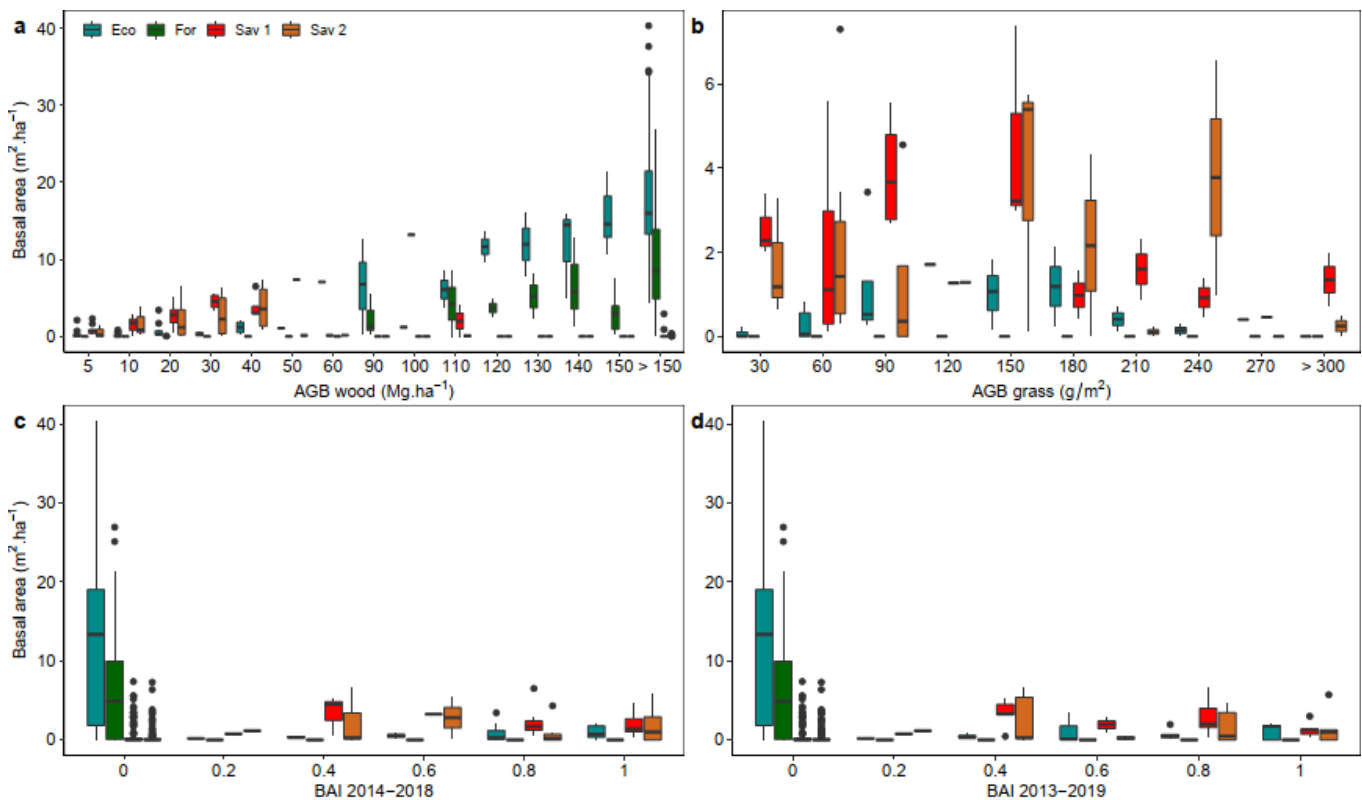
Fig. 52: Relationship between the basal area of the different group of species distinguished from the NSCA analysis and the aboveground biomass (a) woody and (b) grassy layers and fire frequency (c) 5-year monitoring and (d) 7 years monitoring. Ecotone species (Eco; cyan); forest species (For; green); savanna species from Mpem et Djim national park (Sav 1, orange) and savanna species from Nachtigal (Sav 2, red).

III.2. DISCUSSION

III.2.1. Variation in the vegetation types and structure across the study area

III.2.1.1. Spatial distribution of the vegetation types in the Nachtigal area

Detailed information on land cover and land cover change remains a top priority for land managers and decision-makers (Anderson *et al.*, 1976). But this information still remains a challenge especially in heterogeneous landscapes such as forest-savanna transitions. In parallel with technological and computational developments, Spot 6/7 satellite data have proven its potentiality in land cover classification to produce data with high accuracy (96.5%) in this study. The level of details achieved in the land cover types proposed was thanks to both the fine spatial resolution of the Spot 6/7 image (3 m) and the contribution of the canopy structure of the different vegetation obtained from the canopy height model (CHM) derived from LiDAR. Exploiting those two source of information helped in defining training samples ensuring a good spectral separability between classes. The methodology used to obtain this degree of details in land cover classes constitute a reliable reference to implement national scale land cover mapping in Cameroon. This is even more significant in the context of ongoing climate mitigation efforts to Reduce Emissions from Deforestation and Forest Degradation (REDD+) where Measuring, Reporting and Verification (MRV) of carbon stocks and pools are expected for different vegetation types. Achieving unbiased estimation of carbon stocks and fluxes in these highly dynamic environments, characterized by mosaics of very different land uses and covers, is a critical challenge.

III.2.1.2. Landscape-scale AGB estimation

Despite known limitations, multispectral spaceborne data remain broadly used for AGB estimations over the landscape. A widely held assumption is that Airborne LiDAR scanning (ALS) data ensure better model calibration, and hence partly compensates signal limitations (Asner, 2009; Réjou-Méchain *et al.*, 2015; Timothy *et al.*, 2016; Asner and Ordway, 2020). These results indeed show that model fit and error can be drastically improved, with an R² of 0.7 and a RMSE decrease of 30%, when using a Random Forest model calibrated with AGB_{ALS} reference data (RF_{ALS}) instead of field plots (RF_{FIELD}). Predictions of the latter moreover proved highly biased (inaccurate) and imprecise along the whole range of AGB densities. Looking closely at the AGB predictions of RF_{ALS}, we can however see that the signal of multispectral data, whatever the sensor, does not in fact allow accurate AGB predictions in low and high ranges of actual vegetation biomass (i.e., AGB_{ALS}). Indeed, low biomass ranges are

systematically overestimated, and high biomass ranges are underestimated. This behaviour has been already evidenced across the tropics (Zhang *et al.*, 2017; Csillik *et al.*, 2019) in similar studies, highlighting the fact that errors in AGB estimations when using optical signal is unfortunately still both unavoidable and crippling for large scale wall to wall AGB mapping (Réjou-méchain *et al.*, 2019). It is thus important to better benchmark value and limitations of optical signals in varying contexts through landscape-scale studies integrating highly informative ALS data. Here we showed that improved calibration of spaceborne models by ALS data did ensure unbiased estimation of AGB overall. In other words, although the signal does not allow accurate predictions of AGB in a given forest or savanna location, RF_{ALS} models still provide accurate prediction of average AGB levels across the landscape. This is only true, as long as the balance between land cover types in the predicted landscape is comparable to that of the training area. Notably, the underestimation of total AGB will plummet with the share of land harbouring high AGB forests, above the hinge point of saturation of about 225-250 Mg.ha^{-1}. This threshold ought to be kept in mind in any further application.

Regarding possible effects of the compromise between spatial and spectral resolution allowed by different spaceborne sensors, RF_{ALS} models based on lower spatial resolution and narrow-wavelength spaceborne images (i.e. Landsat 8 and Sentinel 2) seemed to perform slightly better than models based on higher spatial resolution broad-wavelength imagery (Spot 6/7) with a minor decrease of 10% in RMSPE. Similarly, the variability in the spectral predictors selected by our forward model selection procedure does not allow being conclusive regarding the relative interest of any given spectral index over others.

The well-accepted design-based approach, on the other end, provided a simple and accurate alternative for landscape-level AGB estimation, when trained with a dense sample of ALS data. As a single AGB value is attributed to each land cover class, this approach does not provide a detailed intra-class variation map. But if the model-based approach does provide such a map, it is unreliable anyways, as it has been shown, as long as the available predictors remain poorly correlated to AGB. It might be better not to lure the user with the pretence of a high-resolution product, when the estimates are only valid at large scale.

III.2.1.3. Differences in the structure and floristic composition between the Nachtigal area and the Mpem et Djim NP

Anthropogenic influence is lower in the Mpem et Djim NP compared to the Nachtigal area and the former displays a vegetation which is more diverse (species richness) and structurally stable

compared to the latter. However the vegetation in the Nachtigal area still supply some ecological and ecosystem services thanks to its less disturbed vegetation that is still maintaining. The Nachtigal area is dominated by Agroforest which covers 25.2% of the surface area while relatively undisturbed Old-growth forests cover only 11%. This ratio is expected to shift towards man-influenced forest types (Agroforest and degraded secondary forest) as forest are the most susceptible to experience profound changes in their structure due to land-use changes in Central Africa (Aleman, 2017). In fact the local population directly rely on forest and savanna for their livelihoods in Africa (FAO, 2007). The expansion and intensification of agriculture, timber and biofuel monocultures to feed and supply the material aspirations of growing and more affluent human populations, the unsustainable harvesting of timber and non-timber forest products (including widespread over- hunting of game vertebrates) and urbanization processes will lead to drastic changes in vegetation structure (Gardner *et al.*, 2010). The hydroelectric dam construction in the area over the Sanaga River will favour a massive flow of people towards the area with a big interest in small and large scale agriculture activities such as artisanal cocoa farms, palm plantations and cropland. Increasing cropland will reduce woody cover in savanna vegetation (Nacoulma *et al.*, 2011). Land-use changes are expected to have the largest effect on changes in land cover distributions and biodiversity (Sala *et al.*, 2000; Aleman *et al.*, 2017).

III.2.2.   Vegetation change patterns

III.2.2.1. Long-term (1975-2020) forest expansion

Forest-savanna ecotones (FSE) of northern hemisphere tropical Africa are currently experiencing forest encroachment over savannas. Several studies, scattered from Guinea to the Central African Republic (and even central Gabon) have illustrated this trend, while referring to time windows of variable lengths within the last six decades. However, in all documented sites, no consistent picture over more than 30 years was available. The conclusion of progressive forest encroachment qualitatively agrees with previous studies in nearby areas of the Guineo-Congolian region in Central Africa that stretched over either an early time window (50s – 80s, Youta, 1998) or a more recent one (1986 – 2006, Mitchard *et al.* 2009). Youta (1998) measured an encroachment rate of 3%.year^{-1} after 39 years (1950-1989) of monitoring in a nearby area in Cameroon (Mbam *et* Kim confluent). Mitchard *et al.* (2009) expressed forest encroachment qualitatively as increases in canopy area index (CAI) and observed a shrinking of low CAI areas (0.2 m²/m² area, interpreted as "grasslands") by 43% over 20 years (0.9% y^{-1} for 1986-2000 and 1.29% for 2000-2006). This highly benefited to intermediate CAI classes

(interpretable as both dense savanna and young forest) with a marginal increase of upper CAI class (>1 m²/m² which unequivocally relates to close canopy forest) (Mitchard *et al*. 2009).

III.2.2.2. Performance of automated cloud computing and Landsat image archives in modelling land cover dynamics

It was shown in the present study that simple principles for distinguishing contrasted vegetation types allow benefitting from massive high spatial resolution image series and cloud computing to consistently document the dynamics of forest-savanna boundaries with unsupervised methods. An integrated picture of vegetation changes was indeed achieved in a protected area in Central Cameroon (MDNP, ca. 100,000 ha) from 1975 to 2020, that is all over the timeframe covered by the Landsat (*sensu lato*) series. The automated, unsupervised landcover classification implemented in GEE provided similar results in terms of vegetation dynamics, capturing the steady increase of forest cover through time and leading to an average rate of forest encroachment virtually equal (i.e., c. 1%.$year^{-1}$) to that obtained with supervised approach. However the performance of automated approaches was dependent upon the number of images available within the timeframe of the analysis and the best performances were achieved after year 1999 from when Landsat sensors had smaller revisit time.

III.2.2.3. Spectral composition structuring along a forest succession

As forest encroaches over savanna, differences in the functional composition of plant communities are apparent in the spectral reflectance of forest canopies captured by Sentinel 2 satellite data. Spectral species diversity appeared structured along a forest-age gradient. This reflects the successional gradient of floristic assemblages where fast growing pioneers species with low aboveground biomass yet strong photosynthetic activity dominate recent transitions and are then gradually replaced by long-lived species in old regenerating forests (Fairhead and Leach, 1994; Youta *et al.*, 2003; Ibanez *et al.*, 2013; Cuni-Sanchez *et al.*, 2016; Deklerck *et al.*, 2019).

III.2.2.4. AGB recovery along a forest succession

Thanks to the integration between spaceborne image series and local UAV-borne LiDAR data, it was able to quantify the pace of AGB increment from recent forest transitions to older forests. AGB was found to steadily increase with a hint of levelling-off after 20 years. The rates of AGB recovery found in this study of 4.3 Mg.ha^{-1}.yr^{-1} found for young secondary forests ($\leq$ 20 years

as defined by the Intergovernmental Panel on Climate Change; IPCC) is 57% lower than the IPCC 2006 default AGB accumulation rates for young tropical rainforest in Africa (~ 10 Mg.ha^{-1}.year^{-1}; Suarez *et al.*, 2019). Refined IPCC 2006 default AGB accumulation rates proposed by Suarez *et al.* (2019) are still above our own estimates by 43.4% (7.6 ± 5.9 Mg.ha^{-1}.yr^{-1}). This would reflect a contrasted scenario of AGB uptake depending on whether the forest recovers after disturbances (reforestation) or encroaches over savanna and woodland (afforestation). The former regeneration process would imply an average AGB uptake 2-fold greater than in the latter scenario. The type of previous land cover or disturbance significantly influences the carbon accumulation rate (Moran *et al.*, 2000; Cook-Patton *et al.*, 2020). Reforestation actually occurs on previously forested soils (Janzen, 2016) keeping characteristics (soil fertility and structural properties) favourable to forest seedlings establishment and growth (Viani *et al.*, 2011). Afforestation on the other hand generally occurs on nutrient-poor savanna soils leading to a slower forest recovery (Moran *et al.*, 2000). As expected, older forest successions (> 20 years) had a lower AGB recovery rate of 3.2 Mg.ha^{-1}.year^{-1} compared to younger forest successions. This is similar to what was found by Suarez *et al.* (2019; 3.5 ± 3.3 Mg.ha^{-1}.yr^{-1}) and close to the IPCC 2006 default rates (~ 3 Mg.ha^{-1}.yr^{-1}) for older secondary tropical rainforests in Africa.

III.2.3.   Influence of fire on vegetation dynamics

III.2.3.1. Performance of Landsat data in characterising fire frequency

The Burn Area Index (BAI) obtained in this study using 30 m Landsat was shown to better retrieve the variability of fire frequencies than the 500 m MODIS fire product. The latter indeed estimated fire frequencies (BAI) 28% lower than the former on average, and totally failed to detect areas with the highest frequency (yearly) of fire regime. This finding accords with Chuvieco *et al.* (2019) and Ramo *et al.* (2021) who found that recent BA products covering Africa with Sentinel-2 images (at 20 m spatial resolution) over a single year reached estimates 1.8 and 3.2 times higher, respectively, than the estimates from MODIS products. This strong discrepancy is mostly caused by insufficient spatial resolution leading to the omission of small fires (< 100 ha) (Roteta *et al.*, 2019) as the study area is likely dominated by small low-intensity fires (Mitchard *et al.*, 2009), in accordance with the fire biomes typology (Archibald *et al.*, 2013). This raises a caveat considering that several studies (Staver *et al.*, 2011a; Diouf *et al.*, 2012; Axelsson and Hanan, 2018; Venter *et al.*, 2018) fully relied on MODIS to assess fire frequency influence on the vegetation structure.

III.2.3.2. Fire influence on savanna structure and dynamics

Under sufficient rainfall, savannas are considered as unstable systems (Langevelde *et al.*, 2003; Sankaran *et al.*, 2005) where regular disturbances such as fire are absolutely required to maintain tree-grass coexistence in the system by buffering against transition to a closed-canopy state (Veenendaal *et al.*, 2018; Venter *et al.*, 2018). Under very high rainfall comparable to the MDNP situation, even fires may not be sufficient to ensure savanna stability (Jeffery *et al.*, 2014; Djeumen *et al.*, 2021). On average, no fire occurrence was recorded for savanna pixels that transited to forest between two consecutive monitoring periods. Fire-free intervals facilitate tree recruitment and allow trees to approach canopy closure which suppress fire by excluding grasses (Bond and Midgley, 2000; Veenendaal *et al.*, 2015, 2018). In the Lopé National Park in Gabon (Jeffery *et al*., 2014) savannas newly protected from fire can sufficiently thicken up over a 15 year period to reach a structure comparable to a colonising forest. In the absence of fire, the system switches from a state of co-occurrence of fire-adapted trees and heliophytic grasses to a state with fire resistant, shade-bearing giant herbs (*Aframomum* spp.) and forbs (*Chromolaena odorata*, a well-known invasive woody grass; Youta, 1996; Olivieras *et al*., 2016) along with saplings of light-demanding forest tree species such as *Albizia* spp., *Macaranga* spp. (Youta and Bonvallot, 1996; Youta, 1998; Youta *et al.*, 2003; Ibanez *et al.*, 2013). Cardoso *et al*. (2020) evidenced the presence of an ecotone community in the Loppé National Park that occupies a narrow belt between savanna and forest and stabilises the forest-savanna mosaic even when the savanna is burned regularly. Such a belt accelerates woody encroachment of the savanna if fire were to be suppressed.

The spectral diversity of savannas still observable in 2020 evidenced two contrasting dominant classes either related to low (1 fire every 5 years) or high (about yearly fire) fire frequencies. Interestingly, we observed a decreasing relationship between AGB and the fire frequency that led from high AGB (median of ca. 40 Mg.ha^{-1}) with low fire frequencies to low AGB (ca. 20 Mg.ha^{-1}) with high fire frequencies situations. This suggests that savanna with low fire frequency accumulates ~ 50% more AGB than with high fire frequency. We may here note that we observed a few savannas displaying intermediate fire frequencies (BAI of 0.2-0.3 year^{-1}) and intermediate AGB (~ 30 Mg.ha^{-1}). Analogously, Mitchard *et al*. (2009) already found that savannas of intermediate CAI were relatively scarce in the nearby Mbam-Djerem region. Our data suggest the relative instability of savanna physiognomies in presence of intermediate fire frequencies (BAI < 0.4 year^{-1}) which do not seem sufficient to prevent biomass build-up and

stand thickening of savanna species under the current conditions experienced by humid savannas. Reciprocally, increased woody biomass and cover is known to depress grass production (Hoffmann *et al.*, 2012; Veenendaal *et al.*, 2018) that fuels fires after drying-up thereby indirectly limiting fire intensity and propagation (Lehmann *et al.*, 2011). The shift towards wooded savannas and associated ineffective fire regimes seems here to occur for AGB values around 30 Mg.ha^{-1}. Once this threshold is overpassed, the AGB build-up towards 40 to 60 Mg.ha^{-1} (i.e. towards a savanna woodland) seems inexorable and prefigures the floristic shift towards stands dominated by forest pioneer species that displayed AGB values in the range 50 - 100 Mg.ha^{-1}. Field prospection allowed us to frequently observe dense woodlands characterized by tall savanna trees (mainly *Terminalia glaucescens*) frequently fringing young forests dominated by species such as *Albizia adianthifolia* and *Macaranga* sp. that overtopped surviving *T. glaucescens* engulfed in dense thickets of *C. odorata*. All this strongly suggests recent afforestation.

It was noticed that some persistent savannas (i.e. which did not witness any forest transition) that still displayed low fire frequencies (BAI < 0.2 i.e. one fire occurrence in five years) over a 5-years of monitoring period (1999-2003 and 2014-2018). Such class of BAI relates to the largest variability in AGB. This suggests that at a local scale other factors like topo-edaphic controls (Colgan *et al.*, 2012a), and herbivory (Langevelde *et al.*, 2003; Sankaran *et al.*, 2008; Venter *et al.*, 2018) may also have influenced forest transition. In addition, fire characteristics also matter, since fires occurring early in the dry season are known to have less impact on woody vegetation than fires taking place after several dry months (Walters, 2010; Jeffery *et al.*, 2014). Yet all those factors were not documented in this study.

III.2.4. Species succession dynamics

A compositionally and structurally distinct tree community existed in the forest-savanna transition sampled in the Central region of Cameroon. The species composition of this transitional landscape characterize transitions between semi-deciduous forests in the south and the soudano-guinean savannas in of the Adamaoua region as described by Letouzey (1985, 1968) and Youta (1998). The floristic transition is gradual as species composition changes to suit the changing environment (Huston, 1994b). As the woody layer within savanna thickens (increase in woody AGB; AGB$_{Wood}$) savanna species (*Hymenocardia acida*, *Crossopteryx febrifuga*, *Bridelia ferruginea, Terminalia glaucescens*, *Piliostigma thonningii* and *Annona senegalensis*) are gradually replaced by fast growing pioneer forest species (*Albizia zygia*,

Bridelia micranta, *Nauclea latifolia*, *Oncoba glauca*, and *Treculia obovoidea*) and old-growth forest species (*Celtis mildbraedii*, *Celtis zenkeri*, *Glyphaea brevis, Sterculia rhinopetala* and *Trilepisium madagascariense*) in the later forest succession. The presence of pioneer forest saplings (low basal area) in more open savannas ($AGB_{Wood} \leq 40$ Mg.ha^{-1}) and their occurrence in grassy savanna would suggest that forest is gradually taking advantage over savanna by secondary succession. During forest expansion, the establishment and the growth of pioneer forest species are likely to shade savanna specialists which are shade-intolerant species. This explains the decrease in the abundance of savanna specialist with the increase in pioneer forest species and their scarcity in forest stands ($AGB_{Wood} > 50$ Mg.ha^{-1}). However the presence of fire-sensitive pioneer forest species in all scenarios of fire frequencies (from low to high fire frequencies) would suggest that the limiting effect of fire on woody vegetation is not sufficient to hinder woody encroachment in the area bringing therefore sufficient humidity required for the establishment of pioneer forest saplings within open savannas. Unlike distinct ecotonal communities found between forest and savanna in the Lopé National Park (Cardoso *et al*., 2020), the forest savanna ecotone in the area is a mixture of forest pioneers and savanna trees which likely accelerate forest encroachment over savanna even in contexts of frequent fires.

III.2.5.   Implication for conservation and management

Woody encroachment is a major conservation challenge across tropical Africa and likely to only become worse in the future with increasing global atmospheric carbon dioxide and increasing rainfall in many parts of central Africa expected to favour the growth of trees over grasses (Bond and Midgley, 2012; Higgins and Scheiter, 2012; Stevens *et al.*, 2016, 2017). The potential ability of the ecotone to transform into the frontier of woody encroachment emphasizes how close forest-savanna mosaics may be to a sudden and practically irreversible state shift, and how important regular burning is for preventing this. The creation of the Mpem *et* Djim National Park (MDNP) in 2004 may have hindered anthropogenic activities principally at its less accessible savanna core where we observed intense forest expansion. A lower proportion of encroaching forests is observed in peripheral savannas, which are more accessible especially in the northern part of the MDNP where natural boundaries constituted by the Mpem et Djim rivers are absent. From the various observations made during field campaigns conducted between 2019 and 2020; we noticed that those savannas were subject to substantial livestock transhumance during the dry season (nov. - mar.). During that period shepherds regularly burn the savanna to favour grass flush (Youta and Bonval, 1996; Mitchard *et al*., 2009). Poachers also set fire to flush small grasses (as described by Walters *et al*. 2010).

Frequent fires limits the growth of pyrophilous woody species and woody build-up in savannas which makes the establishment of forest species unlikely (Jeltsch *et al.*, 2000; Dantas *et al.*, 2013; Venter *et al.*, 2018) delaying thus forest expansion. On the other hand cattle grazing and trampling limit the accumulation of grass fuel and is liable to depress both fire frequency and intensity. Our results suggest the existence of a fire frequency threshold of 0.4 (interpreted as biennials fires) is a necessary condition to limit savanna woody encroachment and maintain the co-occurrence of grassy and woody layers. But considering the dramatic forest expansion that was evidenced, the current, unplanned fire regimes seem unable to preserve the mosaic landscape.

Our findings have important management implications as they provide insight into the ecological paradox associated with woody encroachment, which is a pervasive phenomenon and a growing concern for managers of African savannas (Stevens *et al.*, 2017; Venter *et al.*, 2018). Fire frequency in the MDNP is generally the product of non-managed fires as the park still lacks an effective fire management program. Therefore managers in the MDNP have little influence on how much of the park burns on an annual basis, and that area burnt is largely dictated by uncontrolled actions from transhumant shepherds and poachers. It is very likely that fire frequencies below a 2-year cycle would allow bush encroachment and at longer run afforestation. Even annual, early fires also would. Forest expansion appeared indeed as a continuous and steady process in the MDNP and if we extrapolate the observed fairly constant rate of forest gain into savanna, the area will lose all its savanna in less than 30 years. This is even more certain when we consider the rise in CO_2 concentration and climate change predictions for tropical Africa that expect a rise in precipitations over the next decades (Pachauri and Meyer, 2014) favouring forest expansion (Higgins and Scheiter, 2012; Ma *et al.*, 2013; Stevens *et al.*, 2016, 2017). Local factors including fire management, soil fertility and herbivory pressure are expected to mediate this general prediction. Although carbon mitigation programs such as REDD+ scheme tend to encourage forest expansion, the loss of savanna ecosystems in the area will drastically modify landscape-level diversity (Veldman *et al.*, 2015; Bond, 2016) and ecosystem services, including hydrology (Jackson *et al.*, 2005; Acharya *et al.*, 2018) and soil nutrient cycles (Berthrong *et al.*, 2009), and it would markedly alter community assemblages (Bremer and Farley, 2010; Veldman *et al.*, 2014; Abreu *et al.*, 2017) especially those of savanna plant and animal specialists, including iconic large mammals and big cats.

CHAPTER IV

CONCLUSION AND PERSPECTIVES

CHAPTER IV. CONCLUSION AND PERSPECTIVES

IV.1. CONCLUSION

This study intended to track long-term dynamics of forest-savanna ecotone in the Guineo-Congolian transition area of the Central Region of Cameroon and characterise induced changes in the vegetation structure and composition with the compensation needs for a hydroelectric dam construction. The study area displayed two contrasted scenarios of anthropogenic influences: 1) the Nachtigal area which is subject to intense agricultural activities and targeted for the construction of a hydroelectric dam and 2) the Mpem et Djim National Park which had no management plan since its creation in 2004. The conceptual framework consisted in a nested design to fill in the gap between localised field data and large scale satellite data with intermediate airborne laser (ALS) data. Ground truth data together with canopy structure of the vegetation derived from ALS data helped to discriminate vegetation types with high accuracy (96.5%) within the Nachtigal area using high spatial resolution satellite imagery i.e. Spot 6/7 (3m). The landscape is dominated with Agroforests (25.2%) while undisturbed forests only covered 11% of the total area. Achieving unbiased landscape-scale aboveground biomass (AGB) estimations from spaceborne multispectral data, was significantly improved when integrating intermediate ALS-based AGB data in prediction models with an error reduction of ~30% compared to a field-based AGB calibration. It is however crucial to acknowledge that, due to signal limitations, irrespective of the multispectral sensor and mix of spectral indices used, predictions are only unbiased at the landscape or regional level, and for land cover conditions similar to the training area. Data from upcoming new radar-based (BIOMASS, NISAR) and LiDAR-based space missions (GEDI, ICESat-2, MOLI) are expected to improve our extrapolation capacities by providing both global coverage and signals with better relationships to vegetation structure (Réjou-Méchain *et al*., 2019; Quegan *et al*., 2019). However, some of those valuable data will need spatial interpolation (GEDI or Ice) from optical data or will not be available for long-term monitoring. Therefore improving the use of optical data will remain an issue. Attributing average AGB density values to broad land-cover classes (referred to as design-based sampling here) will continue to remain a valid alternative to obtain regional unbiased AGB estimations. Anthropogenic influence is lower in the Mpem et Djim NP compared to the Nachtigal area and the former displays a vegetation which is more diverse (species richness) and structurally stable compared to the latter. However the vegetation in the Nachtigal area still supply some ecological and ecosystem services thanks to its less disturbed vegetation that is still maintaining. We demonstrated the potential of automated unsupervised

approaches based on open source cloud-based platforms such as Google Earth Engine for long-term (45 years) land cover change monitoring. A distinct functional (β-diversity) structure of the vegetation was described along a forest transitional gradient. AGB recovery rate of regenerating forests was higher (4.3 Mg.ha^{-1}.year^{-1}) in young forest stands (< 20 years old) compared to older forest successions (≥ 20 years old) where AGB recovery is lower (3.2 Mg.ha^{-1}.year^{-1}). This gives way to a new approach which guarantees an improved measurements of national level carbon stocks (Sagang *et al.*, 2020) and carbon stock changes in forest-savanna transitional landscapes (in relation to Tier 2 and Tier 3 accuracy levels), in compliance with the United Nations Framework Convention on Climate Change (UNFCCC) and IPCC requirements for countries still reporting at Tier 1 level especially in Central Africa (Romijn *et al.*, 2015). The burn area product derived from this study using Landsat (spatial resolution of 30 m) is more appropriate in capturing frequent fires compared to 500 m MODIS products and showed good correlation with the vegetation structure with savanna displaying two dominant states of woody cover mediated by the frequency of fire. Two fire occurrences in five years was found to be the threshold below which savanna stability becomes highly unlikely. The relative abundance of savanna specialist species gradually decreases in favour of forest specialist species as succession occurs. The presence of forest pioneers was evidenced within savanna stands with high fire frequency. Fire therefore fails to ensure savanna stability within the landscape. The forest-savanna ecotone in the area appears to encourage an active forest encroachment over savanna.

IV.2. PERSPECTIVES

A useful step forward would be standardization of such methodologies in different forest-savanna transition areas to enable cross-site comparisons. Localized ALS data distributed within different vegetation types are recommended to improve the characterization of the structure of the vegetation over large areas. Integrating multispectral satellite images with smaller revisit time and higher spatial accuracy (i.e. Sentinel 2; Planet) into lancover change analysis can improve the monitoring of forest-savanna transition and drivers of change (i.e. fire) at fine spatial (< 10 m) and temporal (bi-monthly) resolution. Nevertheless fire monitoring was restricted to yearly fire statistics ignoring the seasonality of fire within the year (early or late fires) which have significant influence on the fate of the savanna structure (Bucini *et al*., 2002; Diouf *et al*., 2012). Subsequent efforts are therefore needed to temporally disaggregate annual BAI products. A useful step forward would be standardization of such methodologies in different forest-savanna transition areas to enable cross-site comparisons.

REFERENCES

REFERENCES

Abreu, R.C.R., Hoffmann, W.A., Vasconcelos, H.L., Pilon, N.A., Rossatto, D.R. & Durigan, G. (2017) The biodiversity cost of carbon sequestration in tropical savanna. *Science Advances*, **3**, 1–8.

Accatino, F., Wiegand, K., Ward, D. & De Michele, C. (2016) Trees, grass, and fire in humid savannas—The importance of life history traits and spatial processes. *Ecological Modelling*, **320**, 135–144.

Acharya, B.S., Kharel, G., Zou, C.B., Wilcox, B.P. & Halihan, T. (2018) Woody plant encroachment impacts on groundwater recharge: A review. *Water*, **10**, 26.

Achoundong, G., Youta-Happi, J., Guillet, B., Bonvallot, J. & Beyala, K.V. (1996) *Formation et évolution des recrûs sur savanes. Dynamique à long terme des écosystèmes forestiers intertropicaux*, pp. 115–119.

Adhikari, H., Heiskanen, J., Siljander, M., Maeda, E., Heikinheimo, V. & Pellikka, P.K.E. (2017) Determinants of aboveground biomass across an afromontane landscape Mosaic in Kenya. *Remote Sensing*, **9**, 1–19.

Agenor, P.-R. & Moreno-Dodson, B. (2006) *Public Infrastructure And Growth : New Channels And Policy Implications*, The World Bank.

Alder, D. & Synnott, T.J. (1992) *Permanent sample plot techniques for mixed tropical forest*, Oxford Forestry Institute, University of Oxford.

Aleman, J.C., Jarzyna, M.A. & Staver, A.C. (2017) Forest extent and deforestation in tropical Africa since 1900. *Nature Ecology & Evolution*, **2**, 26–33.

Alexandre, C. (2013) Analyse de l'usage du sol de la région de Bokito (Mbam et Inoubou, Cameroun) à partir de données de télédétection et implications sur les systèmes de culture agroforestiers. MSc. Thesis. Université Montpellier III Paul-Valéry. 40pp.

Anderson, J.R., Hardy, E.E., Roach, J.T. & Witmer, R.E. (1976) A Land Use and Land Cover Classification System for Use with Remote Sensor Data. *USGS Professional Paper 964*.

Andy, L. & Matthew, W. (2002) Classification and Regression by randomForest. *R News*, **2**, 18–22.

Anonyme (2016) *Annuaire Statistique du Cameroun*, Institut National de la Statistique,

Yaoundé.

Archer, S.R. (1997) Tree-Grass Interactions In Savannas. *Annual Review of Ecology and Systematics*, **28**, 44pp.

Archibald, S., Lehmann, C.E.R., Gomez-Dans, J.L. & Bradstock, R. a (2013) Defining pyromes and global syndromes of fire regimes. *Proceedings of the National Academy of Sciences*, **110**, 6442–6447.

Arellano, G., Cala, V., Fuentes, A., Cayola, L., Jørgensen, P. & Macía, M. (2016) A Standard Protocol For Woody Plant Inventories And Soil Characterisation Using Temporary 0.1-Ha Plots In Tropical Forests on JSTOR. *Journal of Tropical Forest Science*, **28**, 508–516.

Asner, G.P. (2009) Tropical forest carbon assessment: integrating satellite and airborne mapping approaches. *Environmental Research Letters*, **4**, 11pp.

Asner, G.P., Brodrick, P.G., Philipson, C., Vaughn, N.R., Martin, R.E., Knapp, D.E., Heckler, J., Evans, L.J., Jucker, T., Goossens, B., Stark, D.J., Reynolds, G., Ong, R., Renneboog, N., Kugan, F. & Coomes, D.A. (2018) Mapped aboveground carbon stocks to advance forest conservation and recovery in Malaysian Borneo. *Biological Conservation*, **217**, 289–310.

Asner, G.P. & Mascaro, J. (2014) Mapping tropical forest carbon: Calibrating plot estimates to a simple LiDAR metric. *Remote Sensing of Environment*, **140**, 614–624.

Asner, G.P., Mascaro, J., Anderson, C., Knapp, D.E., Martin, R.E., Kennedy-Bowdoin, T., van Breugel, M., Davies, S., Hall, J.S., Muller-Landau, H.C., Potvin, C., Sousa, W., Wright, J. & Bermingham, E. (2013) High-fidelity national carbon mapping for resource management and REDD+. *Carbon Balance and Management*, **8**, 14pp.

Asner, G.P. & Ordway, E.M. (2020) Carbon declines along tropical forest edges correspond to heterogeneous effects on canopy structure and function. *Proceedings of the National Academy of Sciences of the United States of America*, **14**, 7863–7870.

Augustine, D.J. & Mcnaughton, S.J. (2004) Regulation of shrub dynamics by native browsing ungulates on East African rangeland. *Journal of Applied Ecology*, **41**, 45–58.

Augustine, D.J. & McNaughton, S.J. (1998) Ungulate effects on the functional species composition of plant communities: herbivore selectivity and plant tolerance. *The Journal of wildlife management*, **4**, 1165–1183.

Avitabile, V. & Camia, A. (2018) An assessment of forest biomass maps in Europe using harmonized national statistics and inventory plots. *Forest Ecology and Management*, **409**, 489–498.

Axelsson, C.R. & Hanan, N.P. (2018) Rates of woody encroachment in African savannas reflect water constraints and fire disturbance. *Journal of Biogeography*, **45**, 1209–1218.

Baccini, A. & Asner, G.P. (2013) Improving pantropical forest carbon maps with airborne LiDAR sampling. *Carbon Management*, **4**, 591–600.

Baccini, A., Goetz, S.J., Walker, W.S., Laporte, N.T., Sun, M., Sulla-Menashe, D., Hackler, J., Beck, P.S.A., Dubayah, R., Friedl, M.A., Samanta, S. & Houghton, R.A. (2012) Estimated carbon dioxide emissions from tropical deforestation improved by carbon-density maps. *Nature Climate Change*, **2**, 182–185.

Baillie, I. (1987) M. M. Cole 1986. The savannas: biogeography and geobotany. *Journal of Tropical Ecology*, **3**, 370–371.

Balch, J.K., Nepstad, D.C., Curran, L.M., Brando, P.M., Portela, O., Guilherme, P., Reuning-Scherer, J.D. & de Carvalho Jr, O. (2011) Size, species, and fire behavior predict tree and liana mortality from experimental burns in the Brazilian Amazon. *Forest Ecology and Management*, **261**, 68–77.

Barlow, J. & Peres, C.A. (2008) Fire-mediated dieback and composi- tional cascade in an Amazonian forest. *Philosophical Transactions of the Royal Society B: Biological Sciences*, **363**, 1787–1794.

Bastarrika, A., Alvarado, M., Artano, K., Martinez, M.P., Mesanza, A., Torre, L., Ramo, R. & Chuvieco, E. (2014) BAMS: A tool for supervised burned area mapping using Landsat data. *Remote Sensing*, **6**, 12360–12380.

Bastin, J.-F., Barbier, N., Couteron, P., Adams, B., Shapiro, A., Bogaert, J. & Cannière, C. De (2014) Aboveground biomass mapping of African forest mosaics using canopy texture analysis : Toward a regional approach Aboveground biomass mapping of African forest mosaics using canopy texture analysis : toward a regional approach. *Ecological Applications*, **24**, 1984–2001.

Bastin, J.F., Finegold, Y., Garcia, C., Mollicone, D., Rezende, M., Routh, D., Zohner, C.M. & Crowther, T.W. (2019) The global tree restoration potential. *Science*, **364**, 76–79.

Beer, C., Reichstein, M., Tomelleri, E., Ciais, P., Jung, M., Carvalhais, N., Rödenbeck, C., Arain, M.A., Baldocchi, D., Bonan, G.B., Bondeau, A., Cescatti, A., Lasslop, G., Lindroth, A., Lomas, M., Luyssaert, S., Margolis, H., Oleson, K.W., Roupsard, O., Veenendaal, E., Viovy, N., Williams, C., Woodward, F.I. & Papale, D. (2010) Terrestrial gross carbon dioxide uptake: Global distribution and covariation with climate. *Science*, **329**, 834–838.

Bergen, K., Goetz, S., Dubayah, R., Henebry, G., Hunsaker, C., Imhoff, M., Nelson, R. & Parker, G. (2009) Remote sensing of vegetation 3-D structure for biodiversity and habitat: review and implications for lidar and radar spaceborne missions. *J Geophys Res Biogeosciences*, **114**.

Berthrong, S.T., Jobbágy, E.G. & Jackson, R.B. (2009) A global meta-analysis of soil exchangeable cations, pH, carbon, and nitrogen with afforestation. *Ecological Applications*, **19**, 2228–2241.

Binet, J. (1956) Condition des femmes dans la région cacaoyère du Cameroun. *Cahiers internationaux de sociologie*, **20**, 109–123.

Bond, W.J. (2016) Ancient grasslands at risk. *Science*, **351**, 120–122.

Bond, W.J. (2008) What limits trees in C4 grasslands and savannas? *Annual review of ecology, evolution, and systematics*, **39**, 641–659.

Bond, W.J. & Keeley, J.E. (2005) Fire as a global ' herbivore ': the ecology and evolution of flammable ecosystems. *Trends in Ecology and Evolution*, **20**, 8pp.

Bond, W.J. & Midgley, G.F. (2000) A proposed CO2-controlled mechanism of woody plant invasion in grasslands and savannas. *Global Change Biology*, **6**, 865–869.

Bond, W.J. & Midgley, G.F. (2012) Carbon dioxide and the uneasy interactions of trees and savannah grasses. *Philosophical Transactions of the Royal Society B: Biological Sciences*, **367**, 601–612.

Bond, W.J. & Parr, C.L. (2010) Beyond the forest edge: Ecology, diversity and conservation of the grassy biomes. *Biological Conservation*, **143**, 2395–2404.

Bond, W.J., Woodward, F.I. & Midgley, G.F. (2005) The global distribution of ecosystems in a world without fire. *New Phytologist*, **165**, 525–538.

Boulvert, Y. (1990) *Avancée ou recul de la forêt centrafricaine : changements climatiques,*

influence de l'homme et notamment des feux. Paysages quaternaires de l'Afrique centrale atlantique, pp. 353–366. Paris.

Boutrais & Jean (1990) *La géographie rurale à l'ORSTOM. Affiches de la géographie* (ed. by 1990/12/12-13 La Géographie : Situer, Evaluer, Modéliser, Paris (FRA)), p. 130. Paris.

Bouvet, A., Mermoz, S., Le Toan, T., Villard, L., Mathieu, R., Naidoo, L. & Asner, G.P. (2018) An above-ground biomass map of African savannahs and woodlands at 25 m resolution derived from ALOS PALSAR. *Remote Sensing of Environment*, **206**, 156–173.

Ter Braak, C.J.F. & Prentice, I.C. (1988) A theory of gradient analysis. *Advances in ecological research*, **18**, 271–317.

Breiman, L. (2001) Random forests. *Machine learning*, **45**, 5–32.

Bremer, L.L. & Farley, K.A. (2010) Does plantation forestry restore biodiversity or create green deserts? A synthesis of the effects of land-use transitions on plant species richness. *Biodiversity and Conservation*, **19**, 3893–3915.

Broadbent, E.N., Asner, G.P., Peña-Claros, M., Palace, M. & Soriano, M. (2008) Spatial partitioning of biomass and diversity in a lowland Bolivian forest: Linking field and remote sensing measurements. *Forest Ecology and Management*, **255**, 2602–2616.

Buitenwerf, R., Bond, W.J., Stevens, N. & Trollope, W.S.W. (2012) Increased tree densities in South African savannas: >50 years of data suggests CO 2 as a driver. *Global Change Biology*, **18**, 675–684.

Buzon, V. (1990) .Les savanes du Nord de la Côte d'Ivoire. Mésologie et dynamique : l'herbe, le feu et le pâturage. PhD Thesis. Université de Paris 7. 301pp.

Calvo Buendia, E., Tanabe, K., Kranjc, A., Baasansuren, J., Fukuda, M., Ngarize, S., Osako, A., Pyrozhenko, Y. Shermanau, P. & Federici, S. *2019 Refinement To the 2006 Ipcc Guidelines for National Greenhouse Gas Inventoriess*,.

Cardoso, A.W., Oliveras, I., Abernethy, K.A., Jeffery, K.J., Glover, S., Lehmann, D., Edzang Ndong, J., White, L.J.T., Bond, W.J. & Malhi, Y. (2020) A distinct ecotonal tree community exists at central African forest–savanna transitions. *Journal of Ecology*, **00**, 1–14.

Caughlin, T.T., Rifai, S.W., Graves, S.J., Asner, G.P. & Bohlman, S.A. (2016) Integrating

LiDAR-derived tree height and Landsat satellite reflectance to estimate forest regrowth in a tropical agricultural landscape. *Remote Sensing in Ecology and Conservation*, **2**, 190–203.

Ceccherini, G., Duveiller, G., Grassi, G., Lemoine, G., Avitabile, V., Pilli, R. & Cescatti, A. (2020) Abrupt increase in harvested forest area over Europe after 2015. *Nature*, **583**, 72–77.

Chauhan, H.B. & Nayak, S. (2005) Land use/land cover changes near Hazira Region, Gujarat using remote sensing satellite data. *Journal of the Indian society of Remote Sensing*, **33**, 413–420.

Chave, J., Coomes, D., Jansen, S., Lewis, S.L., Swenson, N.G. & Amy, E. (2009) Towards a worldwide wood economics spectrum. *Ecology Letters*, **12**, 351–366.

Chave, J., Réjou-Méchain, M., Búrquez, A., Chidumayo, E., Colgan, M.S., Delitti, W.B.C., Duque, A., Eid, T., Fearnside, P.M., Goodman, R.C., Henry, M., Martínez-Yrízar, A., Mugasha, W.A., Muller-Landau, H.C., Mencuccini, M., Nelson, B.W., Ngomanda, A., Nogueira, E.M., Ortiz-Malavassi, E., Pélissier, R., Ploton, P., Ryan, C.M., Saldarriaga, J.G. & Vieilledent, G. (2014) Improved allometric models to estimate the aboveground biomass of tropical trees. *Global Change Biology*, **20**, 3177–3190.

Chen, D., Pereira, J.M.C., Masiero, A. & Pirotti, F. (2017) Mapping fire regimes in China using MODIS active fire and burned area data. *Applied Geography*, **85**, 14–26.

Chuvieco, E., Mouillot, F., van der Werf, G.R., San Miguel, J., Tanasse, M., Koutsias, N., García, M., Yebra, M., Padilla, M., Gitas, I., Heil, A., Hawbaker, T.J. & Giglio, L. (2019) Historical background and current developments for mapping burned area from satellite Earth observation. *Remote Sensing of Environment*, **225**, 45–64.

Ciais, P., Bombelli, A., Williams, M., Piao, S.L., Chave, J., Ryan, C.M., Henry, M., Brender, P. & Valentini, R. (2011) The carbon balance of Africa: synthesis of recent research studies. *Philosophical Transactions of the Royal Society A: Mathematical, Physical and Engineering Sciences*, **369**, 2038–2057.

Clark, D.B., Castro, C.S., Alvarado, L.D.A. & Read, J.M. (2004) Quantifying mortality of tropical rain forest trees using high-spatial-resolution satellite data. *Ecology Letters*, **7**, 52–59.

Clark, D.B. & Louis, S. (2012) *Quantifying spatial and temporal dynamics of tropical forest structure using high resolution airborne lidar*. *IEEE International Geoscience and Remote Sensing Symposium*, pp. 1664–1667. Munich, Germany.

Clark, M.L., Roberts, D.A. & Clark, D.B. (2005) Hyperspectral discrimination of tropical rain forest tree species at leaf to crown scales. *Remote Sensing of Environment*, **96**, 375–398.

CloudCompare (2020) CloudCompare [GPL software].

Cochrane, M.A. & Schulze, M.D. (1999) Fire as a recurrent event in tropical forests of the eastern Amazon: Effects on forest structure, biomass, and species composition. *Biotropica*, **31**, 2–16.

Colgan, M.S., Asner, G.P., Levick, S.R. & Martin, R.E. (2012a) Topo-edaphic controls over woody plant biomass in South African savannas. *Biogeosciences*, **9**, 1809–1821.

Colgan, M.S., Asner, G.P. & Swemmer, T. (2013) Harvesting tree biomass at the stand level to assess the accuracy of field and airborne biomass estimation in savannas. *Ecological Applications*, **23**, 1170–1184.

Colgan, M.S., Baldeck, C.A., Féret, J. baptiste & Asner, G.P. (2012b) Mapping savanna tree species at ecosystem scales using support vector machine classification and BRDF correction on airborne hyperspectral and LiDAR data. *Remote Sensing*, **4**, 3462–3480.

Cook-Patton, S.C., Leavitt, S.M., Gibbs, D., Harris, N.L., Lister, K., Anderson-Teixeira, K.J., Briggs, R.D., Chazdon, R.L., Crowther, T.W., Ellis, P.W., Griscom, H.P., Herrmann, V., Holl, K.D., Houghton, R.A., Larrosa, C., Lomax, G., Lucas, R., Madsen, P., Malhi, Y., Paquette, A., Parker, J.D., Paul, K., Routh, D., Roxburgh, S., Saatchi, S., van den Hoogen, J., Walker, W.S., Wheeler, C.E., Wood, S.A., Xu, L. & Griscom, B.W. (2020) Mapping carbon accumulation potential from global natural forest regrowth. *Nature*, **585**, 545–550.

Corona, P. & Fattorini, L. (2008) Area-based lidar-assisted estimation of forest standing volume. *Canadian Journal of Forest Research*, **38**, 2911–2916.

Couteron, P. & Pélissier, R. (2004) Additive apportioning of species diversity: towards more sophisticated models and analyses. *Oikos*, **107**, 215–221.

Csillik, O., Kumar, P., Mascaro, J., Shea, T.O. & Asner, G.P. (2019) Monitoring tropical forest carbon stocks and emissions using Planet satellite data. *Scientific Reports*, **9**, 1–12.

Cuni-Sanchez, A., White, L.J.T., Calders, K., Jeffery, K.J., Abernethy, K., Burt, A., Disney, M., Gilpin, M., Gomez-Dans, J.L. & Lewis, S.L. (2016) African savanna-forest boundary dynamics: A 20-year study. *PLoS ONE*, **11**, 1–23.

Curran, P.J. (1989) Remote sensing of foliar chemistry. *Remote Sensing of Environment*, **30**, 271–278.

Daldegan, G.A., de Carvalho Júnior, O.A., Guimarães, R.F., Gomes, R.A.T., Ribeiro, F. de F. & McManus, C. (2014) Spatial patterns of fire recurrence using remote sensing and GIS in the Brazilian savanna: Serra do Tombador Nature Reserve, Brazil. *Remote Sensing*, **6**, 9873–9894.

Daldegan, G.A., Roberts, D.A. & Ribeiro, F. de F. (2019) Spectral mixture analysis in Google Earth Engine to model and delineate fire scars over a large extent and a long time-series in a rainforest-savanna transition zone. *Remote Sensing of Environment*, **232**, 15pp.

Dantas, V. de L., Batalha, M.A. & Pausas, J. (2013) Fire drives functional thresholds on the savanna – forest transition. *Ecology*, **94**, 2454–2463.

Deklerck, V., De Mil, T., Ilondea, B.A., Nsenga, L., De Caluwé, C., Van den Bulcke, J., Van Acker, J., Beeckman, H. & Hubau, W. (2019) Rate of forest recovery after fire exclusion on anthropogenic savannas in the Democratic Republic of Congo. *Biological Conservation*, **233**, 118–130.

Deng, X., Zhang, L., Lei, P., Xiang, W., Yan, W., Deng, X., Zhang, L., Lei, P., Xiang, W. & Yan, W. (2014) Variations of wood basic density with tree age and social classes in the axial direction within Pinus massoniana stems in Southern China To cite this version : Variations of wood basic density with tree age and social classes in the axial direction within. *Annals of Forest Science*, **71**, 505–516.

Devine, A.P., McDonald, R.A., Quaife, T. & Maclean, I.M.D. (2017) Determinants of woody encroachment and cover in African savannas. *Oecologia*, **183**, 939–951.

Devine, A.P., Stott, I., Mcdonald, R.A. & Maclean, I.M.D. (2015) Woody cover in wet and dry African savannas after six decades of experimental fires. *Journal of Ecology*, **103**, 473–478.

DeVries, B., Verbesselt, J., Kooistra, L. & Herold, M. (2015) Robust monitoring of small-scale forest disturbances in a tropical montane forest using Landsat time series. *Remote Sensing*

of Environment, **161**, 107–121.

Dinerstein, E., Joshi, A.R., Vynne, C., Lee, A.T.L., Pharand-Deschênes, F., França, M., Fernando, S., Birch, T., Burkart, K., Asner, G.P. & Olson, D. (2020) A "global safety net" to reverse biodiversity loss and stabilize earth's climate. *Science Advances*, **6**, 13pp.

Diouf, A., Barbier, N., Lykke, A.M., Couteron, P., Deblauwe, V., Mahamane, A., Saadou, M. & Bogaert, J. (2012) Relationships between fire history , edaphic factors and woody vegetation structure and composition in a semi-arid savanna landscape (Niger , West Africa). *Applied Vegetation Science*, **15**, 488–500.

Djeumen, I.V.Y., Dumont, Y., Doizy, A. & Couteron, P. (2021) A minimalistic model of vegetation physiognomies in the savanna biome. *Ecological Modelling*, **440**, 24pp.

Djoufack, M.V. (2011) Étude multi-échelles des précipitations et du couvert végétal au Cameroun : Analyses spatiales, tendances temporelles, facteurs climatiques et anthropiques de variabilité du NDVI. PhD Thesis. Université de Bourgogne et Université de Yaoundé I. 321pp.

Donaldson, D. (2018) Railroads of the Raj: Estimating the Impact of Transportation Infrastructure. *American Economic Review*, **108**, 899–934.

Drake, J.B., Dubayah, R.O., Knox, R.G., Clark, D.B. & Blair, J.B. (2002) Sensitivity of large-footprint lidar to canopy structure and biomass in a neotropical rainforest. *Remote Sensing of Environment*, **81**, 378–392.

Dray, S., Pélissier, R., Couteron, P., Fortin, M.-J., Legendre, P., Peres-Neto, P.R., Bellier, E., Bivand, R., Blanchet, F.G., De Cáceres, M. & others (2012) Community ecology in the age of multivariate multiscale spatial analysis. *Ecological Monographs*, **82**, 257–275.

Duncanson, E.L., Disney, M., Armston, J., Nickeson, J. & Minor, D. (2021) Committee on Earth Observation Satellites Working Group on Calibration and Validation Land Product Validation Subgroup Aboveground Woody Biomass Product Validation Good Practices Protocol. 0–236.

Dutrieux, L.P., Verbesselt, J., Kooistra, L. & Herold, M. (2015) Monitoring forest cover loss using multiple data streams, a case study of a tropical dry forest in Bolivia. *ISPRS Journal of Photogrammetry and Remote Sensing*, **107**, 112–125.

Eckhardt, H.C., van Wilgen, B.W. & Biggs, H.C. (2000) Trends in woody vegetation cover in

the Kruger National Park, South Africa, between 1940 and 1998. *African Journal of Ecology*, **38**, 108–115.

Eden, M.J., McGregor, D.F.M. & Vieira, N.A.Q. (1990) Pasture development on cleared forest land in northern Amazonia. *Geographical Journal*, 283–296.

Eldridge, D.J., Bowker, M.A., Maestre, F.T., Roger, E., Reynolds, J.F. & Whitford, W.G. (2011) Impacts of shrub encroachment on ecosystem structure and functioning: towards a global synthesis. *Ecology Letters*, **14**, 709–722.

Ene, L.T., Næsset, E., Gobakken, T., Gregoire, T.G., Ståhl, G. & Nelson, R. (2012) Assessing the accuracy of regional LiDAR-based biomass estimation using a simulation approach. *Remote Sensing of Environment*, **123**, 579–592.

Ermgassen, S.O.S.E. zu, Utamiputri, P., Bennun, L., Edwards, S. & Bull, J.W. (2019) The Role of "No Net Loss" Policies in Conserving Biodiversity Threatened by the Global Infrastructure Boom. *One Earth*, **1**, 305–315.

Escuin, S., Navarro, R. & Fernández, P. (2008) Fire severity assessment by using NBR (Normalized Burn Ratio) and NDVI (Normalized Difference Vegetation Index) derived from LANDSAT TM/ETM images. *International Journal of Remote Sensing*, **29**, 1053–1073.

Estes, L., Elsen, P.R., Treuer, T. & Ahmed, L. (2018) The spatial and temporal domains of modern ecology. *Nature Ecology & Evolution ·*, **2**, 819–826.

Fahey, T.J., Woodbury, P.B., Battles, J.J., Goodale, C.L., Hamburg, S.P., Ollinger, S. V & Woodall, C.W. (2010) Forest carbon storage: ecology, management, and policy. *Frontiers in Ecology and the Environment*, **8**, 245–252.

Fairhead, J. & Leach, M. (1994) Contested forests: Modern conservation and historical land use in guinea's ziama reserve. *African Affairs*, **93**, 481–512.

FAO (2007) *State of the world's forest*, Rome.

Favier, C., Aleman, J., Bremond, L., Dubois, M.A., Freycon, V. & Yangakola, J. (2012) Abrupt shifts in African savanna tree cover along a climatic gradient. *Global Ecology and Biogeography*, **21**, 787–797.

Favier, C., Chave, J., Fabing, A., Schwartz, D. & Dubois, M.A. (2004a) Modelling forest-

savanna mosaic dynamics in man-influenced environments: Effects of fire, climate and soil heterogeneity. *Ecological Modelling*, **171**, 85–102.

Favier, C., Namur, C. De & Dubois, M. (2004b) Forest progression modes in littoral Congo , Central Atlantic Africa. *Journal of Biogeography*, **31**, 1445–1461.

February, E.C., Higgins, S.I., Bond, W.J. & Swemmer, L. (2013) Influence of competition and rainfall manipulation on the growth responses of savanna trees and grasses. *Ecology*, **94**, 1155–1164.

Fensham, R.J. & Fairfax, R.J. (2003) Assessing woody vegetation cover change in north-west Australian savanna using aerial photography. *International Journal of Wildland Fire*, **12**, 359–367.

Fensham, R.J., Fairfax, R.J. & Ward, D.P. (2009) Drought-induced tree death in savanna. *Global Change Biology*, **15**, 380–387.

Féret, J.-B. & Asner, G.P. (2014) Mapping tropical forest canopy diversity using high-fidelity imaging spectroscopy. *Ecological Applications*, **24**, 1289–1296.

Féret, J. & Boissieu, F. de (2020) biodivMapR: An r package for α- and β-diversity mapping using remotely sensed images. *Methods in Ecology and Evolution*, **11**, 64–70.

Foody, G.M., Boyd, D.S. & Cutler, M.E.J. (2003) Predictive relations of tropical forest biomass from Landsat TM data and their transferability between regions. *Remote Sensing of Environment*, **85**, 463–474.

Forkuor, G., Zoungrana, J.-B.B., Dimobe, K., Ouattara, B., Prasad, K.V. & Tondoh, J.E. (2019) Above Ground Biomass Mapping in West African Dryland Forest Using Sentinel-1 and 2 Datasets - A Case Study. *Remote Sensing of Environment*, **236**, 15pp.

Frampton, W.J., Dash, J., Watmough, G. & Milton, J.E. (2013) Evaluating the capabilities of Sentinel-2 for quantitative estimation of biophysical variables in vegetation. *ISPRS Journal of Photogrammetry and Remote Sensing*, **82**, 83–92.

Ganivet, E. & Bloomberg, M. (2019) Towards rapid assessments of tree species diversity and structure in fragmented tropical forests: A review of perspectives offered by remotely-sensed and field-based data. *Forest Ecology and Management*, **432**, 40–53.

Gardner, T.A., Barlow, J., Sodhi, N.S. & Peres, C.A. (2010) A multi-region assessment of

tropical forest biodiversity in a human-modified world. *Biological Conservation*, **143**, 2293–2300.

Gauch, H.G. & Gauch Jr, H.G. (1982) *Multivariate analysis in community ecology*, Cambridge University Press.

Gautier, D., Ankogui-Mpoko, G.-F., Réounodji, F., Njoya, A. & Seignobos, C. (2005) Agriculteurs et éleveurs des savanes d'Afrique centrale : de la coexistence à l'intégration territoriale. *Espace géographique*, **34**, 223pp.

Giglio, L., Justice, C., Boschetti, L. & Roy., D. (2015) MCD64A1 MODIS/Terra+Aqua Burned Area Monthly L3 Global 500m SIN Grid V006.

Goetz, S., Steinberg, D., Dubayah, R. & Blair, B. (2007) Laser remote sensing of canopy habitat heterogeneity as a predictor of bird species richness in an eastern temperate forest, USA. *Remote Sensing of Environment*, **108**, 254–263.

Gomes, L., Miranda, H.S., Soares-Filho, B., Rodrigues, L., Oliveira, U. & Bustamante, M.M.C. (2020) Responses of Plant Biomass in the Brazilian Savanna to Frequent Fires. *Frontiers in Forests and Global Change*, **3**, 11pp.

Good, S.P. & Caylor, K.K. (2011) Climatological determinants of woody cover in Africa. *Proceedings of the National Academy of Sciences*, **108**, 4902–4907.

Gorelick, N., Hancher, M., Dixon, M., Ilyushchenko, S., Thau, D. & Moore, R. (2017) Google Earth Engine: Planetary-scale geospatial analysis for everyone. *Remote Sensing of Environment*, **202**, 18–27.

Hamunyela, E., Verbesselt, J., Bruin, S. de & Herold, M. (2016) Monitoring deforestation at sub-annual scales as extreme events in landsat data cubes. *Remote Sensing*, **8**, 16pp.

Hansen, M.C., Potapov, P. V, Moore, R., Hancher, M., Turubanova, S.A. & Tyukavina, A. (2013) High-Resolution Global Maps of 21st-Century Forest Cover Change. *Science*, **342**, 850–854.

Hély, C., Bremond, L., Alleaume, S., Smith, B., Sykes, M.T. & Guiot, J. (2006) Sensitivity of African biomes to changes in the precipitation regime. *Global Ecology and Biogeography*, **15**, 258–270.

Hermosilla, T., Wulder, M.A., White, J.C., Coops, N.C. & Hobart, G.W. (2015) An integrated

Landsat time series protocol for change detection and generation of annual gap-free surface reflectance composites. *Remote Sensing of Environment*, **158**, 220–234.

Heurich, Nm. & Thoma, F. (2008) Estimation of Forestry Stand Parameters Using Laser Scanning Data in Temperate, Structurally Rich Natural European Beech (Fagus Sylvatica) and Norway Spruce (Picea Abies) Forests. *Forestry*, **81**, 645–661.

Higgins, S.I., Bond, W.J. & Trollope, W.S.W. (2000) Fire, resprouting and variability: A recipe for grass-tree coexistence in savanna. *Journal of Ecology*, **88**, 213–229.

Higgins, S.I., Cheiter, S.I.S., Owry, R.I.S., Rollope, L.Y.N.N.T. & Rollope, W.I.S.W.T. (2007) Effects of four decades of fire manipulation on woody vegetation structure in savanna. *Ecology*, **88**, 1119–1125.

Higgins, S.I. & Scheiter, S. (2012) Atmospheric CO2 forces abrupt vegetation shifts locally, but not globally. *Nature*, **488**, 209–212.

Hijmans, R.J. (2016) raster: Geographic data analysis and modeling.

Hill, M.J. (2013) Vegetation index suites as indicators of vegetation state in grassland and savanna: An analysis with simulated SENTINEL 2 data for a North American transect. *Remote Sensing of Environment*, **137**, 94–111.

Hirata, Y., Furuya, N., Saito, H., Pak, C., Leng, C., Sokh, H., Ma, V., Kajisa, T., Ota, T. & Mizoue, N. (2018) Object-based mapping of aboveground biomass in tropical forests using LiDAR and very-high-spatial-resolution satellite data. *Remote Sensing*, **10**, 21pp.

Hirota, M., Nobre, C., Oyama, M.D. & Bustamante, M.M.C. (2010) The climatic sensitivity of the forest, savanna and forest--savanna transition in tropical South America. *New Phytologist*, **187**, 707–719.

Hoffmann, W.A., Adasme, R., Haridasan, M., De Carvalho, M.T., Geiger, E.L., Pereira, M.A.B., Gotsch, S.G. & Franco, A.C. (2009) Tree topkill, not mortality, governs the dynamics of savanna-forest boundaries under frequent fire in central Brazil. *Ecology*, **90**, 1326–1337.

Hoffmann, W.A., Geiger, E.L., Gotsch, S.G., Rossatto, D.R., Silva, L.C.R., Lau, O.L., Haridasan, M. & Franco, A.C. (2012) Ecological thresholds at the savanna-forest boundary: How plant traits, resources and fire govern the distribution of tropical biomes. *Ecology Letters*, **15**, 759–768.

Hoffmann, W.A., Orthen, B. & Nascimento, P.K.V. do (2003) Comparative fire ecology of tropical savanna and forest trees. *Functional Ecology*, **17**, 720–726.

Hopkins, B. (1992) Ecological processes at the forest-savanna boundary. *Nature and dynamics of forest-savanna boundaries.*, 21–33.

Huang, Q., Swatantran, A., Dubayah, R. & Goetz, S.J. (2014) The influence of vegetation height heterogeneity on forest and woodland bird species richness across the United States. *PLoS One*, **9**, e103236.

Huete, A., Didana, K., Miuraa, T., Rodriguez, E.P., Gao, X. & Ferreira, L.G. (2002) Overview of the radiometric and biophysical performance of the MODIS vegetation indices. *Remote Sensing of Environment*, **83**, 195–213.

Huggett, R. (2002) *Geoecology: an evolutionary approach*, Routledge.

Hurault, J. (1975) *Surpaturage et transformation du milieu physique; formations vegetales, hydrologie de surface, geomorphologie, l'exemple des hauts plateaux de l'Adamaoua (Cameroun)*, Paris. Vol.2. 149-151.

Ibanez, T., Munzinger, J., Gaucherel, C., Curt, T. & Hély, C. (2013) Inferring savannah-rainforest boundary dynamics from vegetation structure and composition: A case study in New Caledonia. *Australian Journal of Botany*, **61**, 128–138.

Jackson, R.B., Jobbágy, E.G., Avissar, R., Roy, S.B., Barrett, D.J., Cook, C.W., Farley, K.A., Le Maitre, D.C., McCarl, B.A. & Murray, B.C. (2005) Atmospheric science: Trading water for carbon with biological carbon sequestration. *Science*, **310**, 1944–1947.

Jacquemoud, S. & Baret, F. (1990) PROSPECT: A model of leaf optical properties spectra. *Remote Sensing of Environment*, **34**, 75–91.

Jagoret, P., Michel-Dounias, I., Snoeck, D., Ngnogué, H.T. & Malézieux, E. (2012) Afforestation of savannah with cocoa agroforestry systems: A small-farmer innovation in central Cameroon. *Agroforestry Systems*, **86**, 493–504.

Janzen, H.H. (2016) The Soil Remembers. *Soil Science Society of America Journal*, **80**, 1429–1432.

Jayakumar, S., Kim, S.S. & Heo, J. (2011) Floristic inventory and diversity assessment-a critical review Vegetation analysis and Remote sensing View project Climate Change

View project Floristic inventory and diversity assessment-a critical review. *Proceedings of the International Academy of Ecology and Environmental Sciences*, **1**, 151–168.

Jean-Romain, R., David, A., Florian, D.B. & Anderw, S.M. (2019) Airborne LiDAR Data Manipulation and Visualization for Forestry Applications [R package]. *Package 'lidR.'*

Jeffery, K.J., Korte, L., Palla, F., Walters, G., White, L.J.T. & Abernethy, K.A. (2014) Fire management in a changing landscape: A case study from Lopé national park, Gabon. *Parks*, **20**, 39–52.

Jeltsch, F., Weber, G.E. & Grimm, V. (2000) Ecological buffering mechanisms in savannas: A unifying theory of long-term tree-grass coexistence. *Plant Ecology*, **161**, 161–171.

Jha, N., Tripathi, N.K., Chanthorn, W., Brockelman, W., Nathalang, A., Pélissier, R., Pimmasarn, S., Ploton, P., Sasaki, N., Virdis, S.G.P. & Réjou-Méchain, M. (2020) Forest aboveground biomass stock and resilience in a tropical landscape of Thailand. *Biogeosciences*, **17**, 121–134.

Jones, I.L. & Bull, J.W. (2020) Major dams and the challenge of achieving "No Net Loss" of biodiversity in the tropics. *Sustainable Development*, **28**, 435–443.

Jordan, C.F. (1969) Derivation of Leaf-Area Index from Quality of Light on the Forest Floor. *Ecology*, **50**, 663–666.

Joseph, S., Herold, M., Sunderlin, W.D. & Verchot, L. V. (2013) REDD+ readiness: Early insights on monitoring, reporting and verification systems of project developers. *Environmental Research Letters*, **8**, 15pp.

Kane, V.R., North, M.P., Lutz, J.A., Churchill, D.J., Roberts, S.L., Smith, D.F., McGaughey, R.J., Kane, J.T. & Brooks, M.L. (2014) Assessing fire effects on forest spatial structure using a fusion of Landsat and airborne LiDAR data in Yosemite National Park. *Remote Sensing of Environment*, **151**, 89–101.

Kangas, A. & Maltamo, M. (2006) *Forest inventory: methodology and applications*, Springer Science \& Business Media.

Key, C.H. & Benson, N.C. (2003) The Normalized Burn Ratio (NBR): A Landsat TM radiometric measure of burn severity. *US Geological Survey Northern Rocky Mountain Science Center. U.S. Department of the Interior, U.S. Geological Survey, Northern Rocky Mountain Science Center.*

Khatami, R., Mountrakis, G. & Stehman, S. V. (2016) A meta-analysis of remote sensing research on supervised pixel-based land-cover image classification processes: General guidelines for practitioners and future research. *Remote Sensing of Environment*, **177**, 89–100.

King, M.D. & Platnick, S. (2005) Spatial and temporal distribution of tropospheric clouds observed by MODIS onboard the terra and aqua satellites. *IEEE Transactions On Geoscience And Remote Sensing*, **51**, 3826–3852.

Klauberg, C. (2018) LiDAR Analysis in R and rLiDAR for Forestry Applications.

Kneizys, F.X., Shettle, E.P., Gallery, W.O., Chetwynd, J H, J. & Abreu, L.W. (1980) Atmospheric Transmittance/Radiance: Computer Code LOWTRAN 5.

Kottek, M., Grieser, J., Beck, C., Rudolf, B. & Rubel, F. (2006) World map of the Köppen-Geiger climate classification updated. *Meteorologische Zeitschrift*, **15**, 259–263.

Kross, A., Seaquist, W.J., Roulet, T.N., Fernandes, R. & Sonnentag, O. (2013) Estimating carbon dioxide exchange rates at contrasting northern peatlands using MODIS satellite data. *Remote Sensing of Environment*, **137**, 234–243.

Kumar, L., Sinha, P., Taylor, S. & Alqurashi, A.F. (2015) Review of the use of remote sensing for biomass estimation to support renewable energy generation. *Journal of Applied Remote Sensing*, **9**, 28pp.

Kuzucu, A.K., Balcik, F.B. & Faculty, C.E. (2017) Testing the potential of vegetation indices for land use/cover classification using high resolution data. *Photogrammetry, Remote Sensing and Spatial Information Sciences*, **IV**, 14–15.

Langevelde, V.F., Van De Vijver, C.A.D.M., Kumar, L., Van De Koppel, J., De Ridder, N., Van Andel, J., Skidmore, A.K., Hearne, J.W., Stroosnijder, L., Bond, W.J., Prins, H.H.T. & Rietkerk, M. (2003) Effects of fire and herbivory on the stability of savanna ecosystems. *Ecology*, **84**, 337–350.

Langner, A., Miettinen, J., Kukkonen, M., Vancutsem, C., Simonetti, D., Vieilledent, G., Verhegghen, A., Gallego, J. & Stibig, H.-J. (2018) Towards operational monitoring of forest canopy disturbance in evergreen rain forests: A test case in continental Southeast Asia. *Remote Sensing*, **10**, 544.

Legendre, P. & Legendre, L.F.J. (1998) *Numerical ecology*, Elsevier.

Lehmann, C.E.R., Archibald, S.A., Hoffmann, W.A. & Bond, W.J. (2011) Deciphering the distribution of the savanna biome. *New Phytologist*, **191**, 197–209.

Letouzey, R. (1985) *Carte phytogéographique du Cameroun, 1:500 000, 8 feuillets + 5 notices*, Institut de la Carte Internationale de la Végétation, Toulouse, France.

Letouzey, R. (1968) *Etude phytogéographique du Cameroun. Encyclopédie Biologique 69*, p. 511.

Levick, S.R. & Rogers, K.H. (2011) Context-dependent vegetation dynamics in an African savanna. *Landscape Ecology*, **26**, 515–528.

Lewis, S.L. (2006) Tropical forests and the changing earth system. *Philosophical Transactions of the Royal Society Biological Sciences*, **361**, 195–210.

Lewis, S.L., Edwards, D.P. & Galbraith, D. (2005) Increasing human dominance of tropical forests. *Scandinavian Journal of Statistics*, **349**, 827–832.

Lewis, S.L., Sonke, B., Sunderland, T., Begne, S.K., Lopez-Gonzalez, G., van der Heijden, G.M.F., Phillips, O.L., Affum-Baffoe, K., Baker, T.R., Banin, L., Bastin, J.-F., Beeckman, H., Boeckx, P., Bogaert, J., De Canniere, C., Chezeaux, E., Clark, C.J., Collins, M., Djagbletey, G., Djuikouo, M.N.K., Droissart, V., Doucet, J.-L., Ewango, C.E.N., Fauset, S., Feldpausch, T.R., Foli, E.G., Gillet, J.-F., Hamilton, A.C., Harris, D.J., Hart, T.B., de Haulleville, T., Hladik, A., Hufkens, K., Huygens, D., Jeanmart, P., Jeffery, K.J., Kearsley, E., Leal, M.E., Lloyd, J., Lovett, J.C., Makana, J.-R., Malhi, Y., Marshall, A.R., Ojo, L., Peh, K.S.-H., Pickavance, G., Poulsen, J.R., Reitsma, J.M., Sheil, D., Simo, M., Steppe, K., Taedoumg, H.E., Talbot, J., Taplin, J.R.D., Taylor, D., Thomas, S.C., Toirambe, B., Verbeeck, H., Vleminckx, J., White, L.J.T., Willcock, S., Woell, H. & Zemagho, L. (2013) Above-ground biomass and structure of 260 African tropical forests. *Philosophical Transactions of the Royal Society B: Biological Sciences*, **368**, 20120295–20120295.

Libalah, M.B. (2018) The Role of Environmental Drivers in Tree Community Structure of Central African Lowland Forests. Thesis. Department of Plant Biology. University of Yaounde 1.

Lin, Y.-P., Wu, P.-J. & Hong, N.-M. (2008) The effects of changing the resolution of land-use modeling on simulations of land-use patterns and hydrology for a watershed land-use planning assessment in Wu-Tu, Taiwan. *Landscape and Urban Planning*, **87**, 54–66.

Liu, J., Heiskanen, J., Maeda, E.E. & Pellikka, P.K.E. (2018) Burned area detection based on Landsat time series in savannas of southern Burkina Faso. *International Journal of Applied Earth Observation and Geoinformation*, **64**, 210–220.

Lu, D. (2006) The potential and challenge of remote sensing-based biomass estimation. *International Journal of Remote Sensing*, **27**, 1297–1328.

Ma, X., Huete, A., Yu, Q., Coupe, N.R., Davies, K., Broich, M., Ratana, P., Beringer, J., Hutley, L.B., Cleverly, J., Boulain, N. & Eamus, D. (2013) Spatial patterns and temporal dynamics in savanna vegetation phenology across the north australian tropical transect. *Remote Sensing of Environment*, **139**, 97–115.

Malhi, Y. & Wright, J. (2004) Spatial patterns and recent trends in the climate of tropical rainforest regions. *Philosophical Transactions of the Royal Society B: Biological Sciences*, **359**, 311–329.

Maniatis, D., Saint André, L., Temmerman, M., Malhi, Y. & Beeckman, H. (2011) The potential of using xylarium wood samples for wood density calculations: A comparison of approaches for volume measurement. *IForest*, **4**, 150–159.

Marchant, R. (2010) Understanding complexity in savannas : climate , biodiversity and people. *Current Opinion in Environmental Sustainability*, **2**, 101–108.

Mariana, B. & Lucian, D. (2016) Random forest in remote sensing: A review of applications and future directions. *ISPRS Journal of Photogrammetry and Remote Sensing*, **114**, 24–31.

Marselis, S.M., Tang, H., Armston, J.D., Calders, K., Labrière, N. & Dubayah, R. (2018) Distinguishing vegetation types with airborne waveform lidar data in a tropical forest-savanna mosaic: A case study in Lopé National Park, Gabon. *Remote Sensing of Environment*, **216**, 626–634.

Marticou, H. (1962) *Les structures agricoles dans le Centre Cameroun*, Direction. (ed. by Secretariat d'Etat au Developpement Rural) Chambre d'Agriculture, de l'Elevage et des Forets du Cameroun, Yaoundé-Cameroun. 67pp.

Martin, M.E. & Aber, J.D. (1997) High spectral resolution remote sensing of forest canopy lignin, nitrogen, and ecosystem processes. *Ecological Applications*, **7**, 431–443.

Masek, J.G., Vermote, E.F., Saleous, N.E., Wolfe, R., Hall, F.G., Huemmrich, K.F., Gao, F.,

Kutler, J. & Lim, T.-K. (2006) A Landsat surface reflectance dataset for North America, 1990-2000. *IEEE Geoscience and Remote Sensing Letters*, **3**, 68–72.

Mbobda, R., Zapfack, L., Noumi, V., Funwi, P., Zekeng, J., Ngoma, L., Banoho, L., Tagnang, N., Yonkeu, A., Votio, M., Nyeck, B. & Chimi, C. (2018) Diversity, structure and carbon storage potential of the Dja Wildlife Reserve vegetation cover. *Journal of Biodiversity and Environmental Sciences*, **180**, 180–199.

McRoberts, R.E., Næsset, E., Liknes, G.C., Chen, Q., Walters, B.F., Saatchi, S. & Herold, M. (2019) Using a Finer Resolution Biomass Map to Assess the Accuracy of a Regional, Map-Based Estimate of Forest Biomass. *Surveys in Geophysics*, **40**, 1001–1015.

Mcroberts, R.E., Næsset, E., Saatchi, S., Liknes, G.C., Walters, B.F., Chen, Q., Service, U.S.F. & Paul, S. (2019) Int J Appl Earth Obs Geoinformation Local validation of global biomass maps. *Int J Appl Earth Obs Geoinformation*, **83**, 101931.

Melissa, L. & Ian, S. (2015) *Carbon Conflicts and Forest Landscapes in Africa.*, (ed. by L. Melissa) and S. Ian) Routledge, Oxon. 250pp.

Mermoz, S., Le Toan, T., Villard, L., Réjou-Méchain, M. & Seifert-Granzin, J. (2014) Biomass assessment in the Cameroon savanna using ALOS PALSAR data. *Remote Sensing of Environment*, **155**, 109–119.

Meyer, H., Reudenbach, C., Wöllauer, S. & Nauss, T. (2019) Importance of spatial predictor variable selection in machine learning applications – Moving from data reproduction to spatial prediction. *Ecological Modelling*, **411**, 34pp.

Miller, J.D. & Thode, A.E. (2007) Quantifying burn severity in a heterogeneous landscape with a relative version of the delta Normalized Burn Ratio (dNBR). *Remote Sensing of Environment*, **109**, 66–80.

Mills, A.J., Milewski, A. V., Fey, M. V., Gröngröft, A., Petersen, A. & Sirami, C. (2013) Constraint on woody cover in relation to nutrient content of soils in western southern Africa. *Oikos*, **122**, 136–148.

Mitchard, E.T.A. & Flintrop, C.M. (2013) Woody encroachment and forest degradation in sub-Saharan Africa ' s woodlands and savannas 1982 – 2006. *Philosophical Transactions of the Royal Society B: Biological Sciences*, **368**, 1–7.

Mitchard, E.T.A., Saatchi, S.S., Baccini, A., Asner, G.P., Goetz, S.J., Harris, N.L. & Brown, S.

(2013) Uncertainty in the spatial distribution of tropical forest biomass : a comparison of pan-tropical maps. *Carbon Balance and Management*, **8**, 13pp.

Mitchard, E.T.A., Saatchi, S.S., Gerard, F.F., Lewis, S.L. & Meir, P. (2009) Measuring woody encroachment along a forest-savanna boundary in Central Africa. *Earth Interactions*, **13**, 29pp.

Mitchard, E.T.A., Saatchi, S.S., Lewis, S.L., Feldpausch, T.R., Woodhouse, I.H., Sonké, B., Rowland, C. & Meir, P. (2011) Measuring biomass changes due to woody encroachment and deforestation / degradation in a forest – savanna boundary region of central Africa using multi-temporal L-band radar backscatter. *Remote Sensing of Environment*, **115**, 2861–2873.

Moran, E.F., Brondizio, E.S., Tucker, J.M., da Silva-Forsberg, M.C., McCracken, S. & Falesi, I. (2000) Effects of soil fertility and land-use on forest succession in Amazônia. *Forest Ecology and Management*, **139**, 93–108.

Moreira, A.G. (2000) Effects of fire protection on savanna structure in Central Brazil. *Journal of biogeography*, **27**, 1021–1029.

Morton, D.C., Nagol, J., Carabajal, C.C., Rosette, J., Palace, M., Cook, B.D., Vermote, E.F., Harding, D.J. & North, P.R.J. (2014) Amazon forests maintain consistent canopy structure and greenness during the dry season. *Nature*, **506**, 221–224.

Murphy, B.P. & Bowman, D.M.J.S. (2012) What controls the distribution of tropical forest and savanna? *Ecology Letters*, **15**, 748–758.

Nacoulma, B.M.I., Schumann, K., Traoré, S., Bernhardt-Römermann, M., Hahn, K., Wittig, R. & Thiombiano, A. (2011) Impacts of land-use on West African savanna vegetation: a comparison between protected and communal area in Burkina Faso. *Biodiversity and Conservation*, **20**, 3341–3362.

Næsset, E., Gobakken, T., Solberg, S., Gregoire, T.G., Nelson, R., Ståhl, G. & Weydahl, D. (2011) Model-assisted regional forest biomass estimation using LiDAR and InSAR as auxiliary data: A case study from a boreal forest area. *Remote Sensing of Environment*, **115**, 3599–3614.

Nangendo, G., Steege, H.T.E.R. & Bongers, F. (2006) Composition of woody species in a dynamic forest – woodland – savannah mosaic in Uganda : implications for conservation

and management. *Biodiversity and Conservation*, **15**, 1467–1468.

Neba, B., Kaam, R., Tchamba, M., Zapfack, L., Chimi, C. & Tanougong, A. (2020) Assessing the spatial distribution of bamboo species using remote sensing in Cameroon. *Journal of Ecology and the Natural Environment*, **12**, 172–183.

O'Connor, T.G., Puttick, J.R. & Hoffman, M.T. (2014) Bush encroachment in southern Africa: Changes and causes. *African Journal of Range and Forage Science*, **31**, 67–88.

Oliveras, I. & Malhi, Y. (2016) Many shades of green: the dynamic tropical forest–savannah transition zones. *Philosophical Transactions of the Royal Society Biological Sciences*, **371**, 15pp.

Olofsson, P., Foody, G.M., Herold, M., Stehman, S. V., Woodcock, C.E. & Wulder, M.A. (2014) Good practices for estimating area and assessing accuracy of land change. *Remote Sensing of Environment*, **148**, 42–57.

Olson, D.M., Dinerstein, E., Wikramanayake, E.D., Burgess, N.D., Powell, G.V.N., Underwood, E.C., Amico, J.A.D., Itoua, I., Strand, H.E., Morrison, J.C., Loucks, J., Allnutt, T.F., Ricketts, T.H., Kura, Y., Lamoreux, J.F., Wesley, W., Hedao, P. & Kassem, K.R. (2001) Terrestrial Ecoregions of the World : A New Map of Life on Earth. *BioScience*, **51**, 933–938.

Owen-Smith, N., Page, B., Teren, G. & Druce, D.J. (2019) *Megabrowser impacts on woody vegetation in savannas*. *Savanna woody plants and large herbivores* (ed. by Wiley), pp. 585–611.

Pachauri, R.. & Meyer, L.A. (2014) *Climate Change 2014: Synthesis Report. Contribution of Working Groups I, II and III to the Fifth Assessment Report of the Intergovernmental Panel on Climate Change*, Geneva, Switzerland.

Palmer, M.W., Earls, P.G., Hoagland, B.W., White, P.S. & Wohlgemuth, T. (2002) *Quantitative tools for perfecting species lists*. *Environmetrics*, pp. 121–137. John Wiley & Sons, Ltd.

Pandit, S., Tsuyuki, S. & Dube, T. (2018) Estimating Above-Ground Biomass in Sub-Tropical Buffer Zone Community Forests, Nepal, Using Sentinel 2 Data. *Remote Sensing*, **10**, 18pp.

Papastergiadou, E.S., Retalis, A., Kalliris, P. & Georgiadis, T. (2007) *Land use changes and associated environmental impacts on the Mediterranean shallow Lake Stymfalia, Greece*.

Shallow Lakes in a changing world, pp. 361–372. Springer.

Parr, C.L., Lehmann, C.E.R., Bond, W.J., Hoffmann, W.A. & Andersen, A.N. (2014) Tropical grassy biomes: misunderstood, neglected, and under threat. *Trends in Ecology & Evolution*, **29**, 205–213.

Pélissier, R., Couteron, P., Dray, S. & Sabatier, D. (2003) Consistency between ordination techniques and diversity measurements: two strategies for species occurrence data ¨. *Ecology*, **84**, 242–251.

Ploton, P. (2017) Improving tropical forest aboveground biomass estimations: insights from canopy trees structure and spatial organization. PhD Thesis. AgroParisTech. Université de Montpellier. 144pp.

Ploton, P., Barbier, N., Couteron, P., Antin, C.M., Ayyappan, N., Balachandran, N., Barathan, N., Bastin, J.-F., Chuyong, G., Dauby, G., Droissart, V., Gastellu-Etchegorry, J.-P., Kamdem, N.G., Kenfack, D., Libalah, M., Mofack, G., Momo, S.T., Pargal, S., Petronelli, P., Proisy, C., Réjou-Méchain, M., Sonké, B., Texier, N., Thomas, D., Verley, P., Zebaze Dongmo, D., Berger, U. & Pélissier, R. (2017) Toward a general tropical forest biomass prediction model from very high resolution optical satellite images. *Remote Sensing of Environment*, **200**, 140–153.

Poilvé, H. & Lacase, R. (2014) *geoland2 - BioPar Methods Compendium of MERIS FR Biophysical Products. Technical report,*.

Poulter, B., Frank, D., Ciais, P., Myneni, R.B., Andela, N., Bi, J., Broquet, G., Canadell, J.G., Chevallier, F., Liu, Y.Y., Running, S.W., Sitch, S. & Van Der Werf, G.R. (2014) Contribution of semi-arid ecosystems to interannual variability of the global carbon cycle. *Nature*, **509**, 600–603.

Poursanidis, D., Chrysoulakis, N. & Mitraka, Z. (2015) Landsat 8 vs. Landsat 5: A comparison based on urban and peri-urban land cover mapping. *International Journal of Applied Earth Observation and Geoinformation*, **35**, 259–269.

Quintano, C., Fernandez-Manso, A. & Roberts, D.A. (2017) Burn severity mapping from Landsat MESMA fraction images and Land Surface Temperature. *Remote Sensing of Environment*, **190**, 83–95.

R Core Team (2018) R: A language and environment for statistical computing. R Foundation

for Statistical Computing.

Ramo, R., Roteta, E., Bistinas, I., van Wees, D., Bastarrika, A., Chuvieco, E. & van der Werf, G.R. (2021) African burned area and fire carbon emissions are strongly impacted by small fires undetected by coarse resolution satellite data. *Proceedings of the National Academy of Sciences*, **118**, e2011160118.

Ranger, N., Reeder, T. & Lowe, J. (2013) Addressing 'deep' uncertainty over long-term climate in major infrastructure projects: four innovations of the Thames Estuary 2100 Project. *EURO Journal on Decision Processes*, **1**, 233–262.

Ratnam, J., Bond, W.J., Fensham, R.J., Hoffmann, W.A., Archibald, S., Lehmann, C.E.R., Anderson, M.T., Higgins, S.I. & Sankaran, M. (2011) When is a "forest" a savanna, and why does it matter? *Global Ecology and Biogeography*, **20**, 653–660.

Reiche, J., Lucas, R., Mitchell, A.L., Verbesselt, J., Hoekman, D.H., Haarpaintner, J., Kellndorfer, J.M., Rosenqvist, A., Lehmann, E.A., Woodcock, C.E., Seifert, F.M. & Herold, M. (2016) Combining satellite data for better tropical forest monitoring. *Nature Climate Change*, **6**, 120–122.

Réjou-méchain, M., Barbier, N., Couteron, P., Ploton, P., Vincent, G., Herold, M., Mermoz, S., Saatchi, S., Chave, J., Boissieu, F. De, Féret, J., Takoudjou, S.M. & Pélissier, R. (2019) Upscaling Forest Biomass from Field to Satellite Measurements : Sources of Errors and Ways to Reduce Them. *Surveys in Geophysics*, **40**, 31pp.

Réjou-Méchain, M., Tanguy, A., Piponiot, C., Chave, J. & Hérault, B. (2017) biomass: An r package for estimating above-ground biomass and its uncertainty in tropical forests. *Methods in Ecology and Evolution*, **8**, 5pp.

Réjou-Méchain, M., Tymen, B., Blanc, L., Fauset, S., Feldpausch, T.R., Monteagudo, A., Phillips, O.L., Richard, H. & Chave, J. (2015) Using repeated small-footprint LiDAR acquisitions to infer spatial and temporal variations of a high-biomass Neotropical forest. *Remote Sensing of Environment*, **169**, 93–101.

Rocchini, D., Boyd, D.S., Féret, J.B., Foody, G.M., He, K.S., Lausch, A., Nagendra, H., Wegmann, M. & Pettorelli, N. (2016) Satellite remote sensing to monitor species diversity: potential and pitfalls. *Remote Sensing in Ecology and Conservation*, **2**, 25–36.

Romijn, E., Lantican, C.B., Herold, M., Lindquist, E., Ochieng, R., Wijaya, A., Murdiyarso, D.

& Verchot, L. (2015) Assessing change in national forest monitoring capacities of 99 tropical countries. *Forest Ecology and Management*, **352**, 109–123.

Roteta, E., Bastarrika, A., Padilla, M., Storm, T. & Chuvieco, E. (2019) Development of a Sentinel-2 burned area algorithm: Generation of a small fire database for sub-Saharan Africa. *Remote Sensing of Environment*, **222**, 1–17.

Ruggiero, P.G.C., Batalha, M.A., Pivello, V.R. & Meirelles, S.T. (2002) Soil-vegetation relationships in cerrado (Brazilian savanna) and semideciduous forest, Southeastern Brazil. *Plant Ecology*, **160**, 1–16.

Russell-Smith, J., Whitehead, P.J., Cook, G.D. & Hoare, J.L. (2003) Response of Eucalyptus-dominated savanna to frequent fires: lessons from Munmarlary, 1973--1996. *Ecological Monographs*, **73**, 349–375.

Ryan, C.M. & Williams, M. (2011) How does fire intensity and frequency affect miombo woodland tree populations and biomass? *Ecological Applications*, **21**, 48–60.

Saatchi, S.S., Harris, N.L., Brown, S., Lefsky, M., Mitchard, E.T.A., Salas, W., Zutta, B.R., Buermann, W., Lewis, S.L., Hagen, S., Petrova, S., White, L., Silman, M. & Morel, A. (2011) Benchmark map of forest carbon stocks in tropical regions across three continents. *Proceedings of the National Academy of Sciences of the United States of America*, **108**, 9899–904.

Sagang, L.B.T., Ploton, P., Sonké, B., Poilvé, H., Couteron, P. & Barbier, N. (2020) Airborne Lidar Sampling Pivotal for Accurate Regional AGB Predictions from Multispectral Images in Forest-Savanna Landscapes. *Remote Sensing*, **12**, 20pp.

Sala, O.E., Chapin, F.S., Armesto, J.J., Berlow, E., Bloomfield, J., Dirzo, R., Huber-Sanwald, E., Huenneke, L.F., Jackson, R.B., Kinzig, A., Leemans, R., Lodge, D.M., Mooney, H.A., Oesterheld, M., Poff, N.L.R., Sykes, M.T., Walker, B.H., Walker, M. & Wall, D.H. (2000) Global biodiversity scenarios for the year 2100. *Science*, **287**, 1770–1774.

Sankaran, M., Hanan, N.P., Scholes, R.J., Ratnam, J., Augustine, D.J., Cade, B.S., Gignoux, J., Higgins, S.I., Le Roux, X., Ludwig, F., Ardo, J., Banyikwa, F., Bronn, A., Bucini, G., Caylor, K.K., Coughenour, M.B., Diouf, A., Ekaya, W., Feral, C.J., February, E.C., Frost, P.G.H., Hiernaux, P., Hrabar, H., Metzger, K.L., Prins, H.H.T., Ringrose, S., Sea, W., Tews, J., Worden, J. & Zambatis, N. (2005) Determinants of woody cover in African savannas. *Nature*, **438**, 846–849.

Sankaran, M., Ratnam, J. & Hanan, N.P. (2008) Woody cover in African savannas : The role of resources , fire and herbivory. *Global Ecology and Biogeography*, **17**, 236–245.

Santoir, C. & Bopda, A. (1995) Atlas régional Sud-Cameroun. 53.

Särndal, C.-E., Thomsen, I., Hoem, J.M., Lindley, D. V, Barndorff-Nielsen, O. & Dalenius, T. (1978) Design-Based and Model-Based Inference in Survey Sampling [with Discussion and Reply]. *Scandinavian Journal of Statistics*, **5**, 27–52.

Schwartz, D., Foresta, H. De, Mariotti, A., Balesdent, J., Cyril, G. & P, M.J. (1996) Present dynamics of the savanna-forest boundary in the Congolese Mayombe : A pedological , botanical and isotopic (13C and 14C) study. *Oecologia*, **106**, 516–524.

Sexton, J.O., Urban, D.L., Donohue, M.J. & Song, C. (2013) Remote Sensing of Environment Long-term land cover dynamics by multi-temporal classi fi cation across the Landsat-5 record. *Remote Sensing of Environment*, **128**, 246–258.

Sharma, R., Chakraborty, A. & Joshi, K.P. (2015) Geospatial quantification and analysis of environmental changes in urbanizing city of Kolkata (India). *Environmental Monitoring and Assessment*, **187**, 12pp.

Sims A., D. & Gamon, A.J. (2002) Relationships between leaf pigment content and spectral reflectance across a wide range of species, leaf structures and developmental stages. *Remote Sensing of Environment*, **81**, 337–354.

Sirami, C., Seymour, C., Midgley, G. & Barnard, P. (2009) The impact of shrub encroachment on savanna bird diversity from local to regional scale. *Diversity and Distributions*, **15**, 948–957.

Smith, T.B., Kark, S., Schneider, C.J., Wayne, R.K. & Moritz, C. (2001) Biodiversity hotspots and beyond: the need for preserving environmental transitions. *Trends in Ecology & Evolution*, **16**, 431–431.

Solbrig, O.T. (1996) The diversity of the savanna ecosystem. *Biodiversity and savanna ecosystem processes*, 1–27.

Song, C., Woodcock, C.E., Seto, K.C., Lenney, M.P. & Macomber, S.A. (2001) Classification and change detection using Landsat TM data: When and how to correct atmospheric effects? *Remote Sensing of Environment*, **75**, 230–244.

St-Onge, B.A. & Cavayas, F. (1997) Automated forest structure mapping from high resolution imagery based on directional semivariogram estimates. *Remote Sensing of Environment*, **61**, 82–95.

Staver, A.C., Archibald, S. & Levin, S. (2011a) Tree cover in sub-Saharan Africa : Rainfall and fire constrain forest and savanna as alternative stable states. *Ecological studies*, **92**, 1063–1072.

Staver, A.C., Archibald, S. & Levin, S.A. (2011b) The Global Extent and Determinants of Savanna and Forest as Alternative Biome States. *Science*, **334**, 230–232.

Steinmann, K., Mandallaz, D., Ginzler, C. & Lanz, A. (2013) Small area estimations of proportion of forest and timber volume combining Lidar data and stereo aerial images with terrestrial data. *Scandinavian Journal of Forest Research*, **28**, 373–385.

Stevens, N., Erasmus, B.F.N., Archibald, S. & Bond, W.J. (2016) Woody encroachment over 70 years in South African savannahs: Overgrazing, global change or extinction aftershock? *Philosophical Transactions of the Royal Society Biological Sciences*, **371**, 9pp.

Stevens, N., Lehmann, C.E.R., Murphy, B.P. & Durigan, G. (2017) Savanna woody encroachment is widespread across three continents. *Global Change Biology*, **23**, 235–244.

Suarez, D.R., Phillips, O.L., Rozendaal, D.M.A., Sy, V. De, Dávila, E.A., Teixeira, K.A., Araujo, A., Luzmila, M., Timothy, A., Frans, R.B., Griscom, B.W., Carter, S., Cook, S.C., Ted, P., Harris, N., Hérault, B., Leavitt, S.M., Lewis, S.L., N, J.K., Guessan, A.E.N., Sist, P., Mendoza, A.M., Sonké, B., Sullivan, M.J.P., Wang, M.M.H., Martius, C., Vilanova, E. & Herold, M. (2019) Estimating aboveground net biomass change for tropical and subtropical forests : Refinement of IPCC default rates using forest plot data. *Global Change Biology*, 3609–3624.

Sunderman, S.O. & Weisberg, P.J. (2011) Remote sensing approaches for reconstructing fire perimeters and burn severity mosaics in desert spring ecosystems. *Remote Sensing of Environment*, **115**, 2384–2389.

Swaine, M.D., Hawthorne, W.D. & Orgle, T.K. (1992) The effects of fire exclusion on savanna vegetation at Kpong, Ghana. *Biotropica*, **24**, 166–172.

Thiers et al., B. (2020) (continuously updated). Index Herbariorum: A global directory of public

herbaria and associated staff. New York Botanical Garden's Virtual Herbarium. [continuously updated].

Thomas, C.D., Anderson, B.J., Moilanen, A., Eigenbrod, F., Heinemeyer, A., Quaife, T., Roy, D.B., Gillings, S., Armsworth, P.R. & Gaston, K.J. (2013) Reconciling biodiversity and carbon conservation. *Ecology Letters*, **16**, 39–47.

Timothy, D., Onisimo, M., Cletah, S., Adelabu, S. & Tsitsi, B. (2016) Remote sensing of aboveground forest biomass: A review. *Tropical Ecology*, **57**, 125–132.

Tinley, K.L. (1982) The influence of soil moisture balance on ecosystem patterns in southern Africa. *Huntley B.J., Walker B.H. (eds) Ecology of Tropical Savannas. Ecological Studies (Analysis and Synthesis)*, **42**, 175–192.

Torres, A., Jaeger, J.A.G. & Alonso, J.C. (2016) Assessing large-scale wildlife responses to human infrastructure development. *Proceedings of the National Academy of Sciences*, **113**, 8472–8477.

Townsend, A.R., Asner, G.P. & Cleveland, C.C. (2008) The biogeochemical heterogeneity of tropical forests. *Trends in Ecology and Evolution*, **23**.

Tuchker, C.J. (1979) Red and photographic infrared linear combinations for monitoring vegetation. *Remote Sensing of Environment*, **8**, 127–150.

Tyukavina, A., Hansen, M.C., Potapov, P., Parker, D., Okpa, C., Stehman, S. V., Kommareddy, I. & Turubanova, S. (2018) Congo Basin forest loss dominated by increasing smallholder clearing. *Science Advances*, **4**.

Uhl, C. & Kauffman, J.B. (1990) Deforestation, fire susceptibility, and potential tree responses to fire in the eastern Amazon. *Ecology*, **71**, 437–449.

USGS (2020) United States Geological Survey. Science for a changing world.

Ustin, S.L. & Gamon, J.A. (2010) Remote sensing of plant functional types. *New Phytologist*, **186**, 795–816.

Ustuner, M., Sanli, F.B. & Dixon, B. (2015) Application of support vector machines for landuse classification using high-resolution rapideye images: A sensitivity analysis. *European Journal of Remote Sensing*, **48**, 403–422.

Veenendaal, E.M., Feldpausch, T.R., Domingues, T.F., Gerard, F., Schrodt, F., Saiz, G.,

Quesada, C.A., Djagbletey, G., Ford, A., Kemp, J., Marimon, B.S., Lenza, E., Ratter, J.A., Maracahipes, L., Sasaki, D., Zapfack, L., Villarroel, D., Schwarz, M., Ishida, F.Y., Gilpin, M., Nardoto, G.B., Arroyo, L., Bloomfield, K., Ceca, G., Compaore, H., Davies, K., Diallo, A., Fyllas, N.M., Gignoux, J., Hien, F., Johnson, M., Mougin, E., Hiernaux, P., Killeen, T., Metcalfe, D., Miranda, H.S., Steininger, M., Sykora, K., Bird, M.I., Grace, J., Lewis, S., Phillips, O.L. & Lloyd, J. (2015) Structural , physiognomic and above-ground biomass variation in savanna – forest transition zones on three continents – how different are co-occurring savanna and forest formations ? *Biogeosciences*, **12**, 2927–2951.

Veenendaal, E.M., Torello-Raventos, M., Miranda, H.S., Sato, N.M., Oliveras, I., Langevelde, F., Asner, G.P. & Lloyd, J. (2018) On the relationship between fire regime and vegetation structure in the tropics. *New Phytologist*, **218**, 153–166.

Veldman, J.W., GE, O., D, N., G, M., S, L.S., GW, F., G, D., E, B., FE, P. & WJ, B. (2014) Tyranny of trees in grassy biomes. *Science*, **347**, 484–485.

Veldman, J.W., Overbeck, G.E., Negreiros, D., Mahy, G., Le Stradic, S., Fernandes, G.W., Durigan, G., Buisson, E., Putz, F.E. & Bond, W.J. (2015) Where Tree Planting and Forest Expansion are Bad for Biodiversity and Ecosystem Services. *BioScience*, **65**, 1011–1018.

Venter, Z.S., Cramer, M.D. & Hawkins, H.J. (2018) Drivers of woody plant encroachment over Africa. *Nature Communications*, **9**, 1–7.

Verhoef, W. (1984) Light scattering by leaf layers with application to canopy reflectance modeling: The SAIL model. *Remote Sensing of Environment*, **16**, 125–141.

Vermote, E.F., El Saleous, N., Justice, C.O., Kaufman, Y.J., Privette, J.L., Remer, L., Roger, J.C. & Tanre, D. (1997) Atmospheric correction of visible to middle-infrared EOS-MODIS data over land surfaces: Background, operational algorithm and validation. *Journal of Geophysical Research: Atmospheres*, **102**, 17131–17141.

Viani, R.A.G., Rodrigues, R.R., Dawson, T.E. & Oliveira, R.S. (2011) Savanna soil fertility limits growth but not survival of tropical forest tree seedlings. *Plant Soil*, **349**, 341–353.

Vieilledent, G., Gardi, O., Grinand, C., Burren, C., Andriamanjato, M., Camara, C., Gardner, C.J., Glass, L., Rasolohery, A., Rakoto Ratsimba, H., Gond, V. & Rakotoarijaona, J.R. (2016) Bioclimatic envelope models predict a decrease in tropical forest carbon stocks with climate change in Madagascar. *Journal of Ecology*, **104**, 703–715.

Vincent, G., Weissenbacher, E., Blanc, L., Proisy, C. & Couteron, P. (2010) Détection des variations de structure de peuplements en forêt dense tropicale humide par Lidar aéroporté. *Revue Francaise de Photogrammetrie et de Teledetection*, **191**, 42–51.

Walters, G.M. (2010) The Land Chief's embers: ethnobotany of Batéké fire regimes, savanna vegetation and resource use in Gabon.

Wang, D., Wan, B., Liu, J., Su, Y., Guo, Q., Qiu, P. & Wu, X. (2020) Estimating aboveground biomass of the mangrove forests on northeast Hainan Island in China using an upscaling method from field plots, UAV-LiDAR data and Sentinel-2 imagery. *International Journal of Applied Earth Observation and Geoinformation*, **85**, 16pp.

Ward, D., Hoffman, M.T. & Collocott, S.J. (2014) A century of woody plant encroachment in the dry Kimberley savanna of South Africa. *African Journal of Range and Forage Science*, **31**, 107–121.

Western, D., Mose, V.N., Worden, J. & Maitumo, D. (2015) Predicting extreme droughts in savannah Africa: A comparison of proxy and direct measures in detecting biomass fluctuations, trends and their causes. *PLoS ONE*, **10**, 1–18.

White, F.J.C. (1986) La végétation de l'Afrique. Mémoire accompagnant la carte de végétation de l'Afrique. UNESCO/AETFAT/UNSO. *Recherche sur les ressources naturelles, ORTSOM/ UNESCO*, 384 p.

Whittaker, R.H. (1970) Communities and ecosystems. 158 pp.

Whittaker, R.H. & Levin, S. (1977) The role of mosaic phenomena in natural communities. *Theoretical population biology*, **12**, 117–139.

Williams, R.J., Myers, B.A., Eamus, D. & Duff, G.A. (1999) Reproductive Phenology of Woody Species in a North Australian Tropical Savanna1. *Biotropica*, **31**, 626–636.

Wilson, S.D. (2000) Heterogeneity, diversity and scale in plant communities. *The ecological consequences of environmental heterogeneity*.

Woodward, F.I. & Lomas, M.R. (2004) Vegetation dynamics - Simulating responses to climatic change. *Biological Reviews of the Cambridge Philosophical Society*, **79**, 643–670.

Wulder, M.A., Coops, N.C., Roy, D.P., White, J.C. & Hermosilla, T. (2018) Land cover 2.0. *International Journal of Remote Sensing*, **39**, 4254–4284.

Wulder, M.A., White, J.C., Loveland, T.R., Woodcock, C.E., Belward, A.S., Cohen, W.B., Fosnight, E.A., Shaw, J., Masek, J.G. & Roy, D.P. (2016) The global Landsat archive: Status, consolidation, and direction. *Remote Sensing of Environment*, **185**, 271–283.

Xu, L., Saatchi, S.S., Shapiro, A., Meyer, V., Ferraz, A., Yang, Y., Bastin, J.F., Banks, N., Boeckx, P., Verbeeck, H., Lewis, S.L., Muanza, E.T., Bongwele, E., Kayembe, F., Mbenza, D., Kalau, L., Mukendi, F., Ilunga, F. & Ebuta, D. (2017) Spatial Distribution of Carbon Stored in Forests of the Democratic Republic of Congo. *Scientific Reports*, **7**, 1–12.

Young, S.M. (2017) Land Change Monitoring, Assessment, and Projection (LCMAP) revolutionizes land cover and land change research. *U.S. Geological Survey General Information Product 172*, 4.

Youta-Happi, J. (1998) Arbres contre graminées : la lente invasion de la savane par la forêt au Centre-Cameroun. PhD Thesis. Université De Paris-Sorbone (PARIS IV). 241 p.

Youta-Happi, J. & Bonvallot, J. (1996) *La disparition des savanes au Centre Cameroun entre 1950 et 1990. Dynamique à long terme des écosystèmes forestiers intertropicaux* (ed. by CNRS-ORSTOM), p. 3. Paris, France.

Youta-Happi, J., Bonvallot, J., Hotyat, M., Guillet, B., Peltre, P., Schwartz, D., Servant, M. & Simonneaux, V. (2003) *Bilan de la dynamique du contact forêt-savane en quarante ans (1950-1990) Dans la région du confluent du Mbam et du Kim, Centre-Cameroun. Peuplements anciens et actuels des forêts tropicales* (ed. by É. IRD), p. 380 p.

Zanne, A.E., Lopez-Gonzalez, G., Coomes, D.A., Ilic, J., Jansen, S., Lewis, S.L., Miller, R.B., Swenson, N.G., Wiemann, M.C., Chave, J., Zanne, A.E., Lopez-Gonzalez, G., Coomes, D.A., Ilic, J., Jansen, S., Lewis, S.L., Miller, R.B., Swenson, N.G., Wiemann, M.C. & Chave, J. (2009) Global Wood Density Database.

Zelazowski, P., Malhi, Y., Huntingford, C., Sitch, S. & Fisher, J.B. (2011) Changes in the potential distribution of humid tropical forests on a warmer planet. *Philosophical Transactions of the Royal Society A: Mathematical, Physical and Engineering Sciences*, **369**, 137–160.

Zeng, Z., Piao, S., Chen, A., Lin, X., Nan, H., Li, J. & Ciais, P. (2013) Committed changes in tropical tree cover under the projected 21st century climate change. *Scientific Reports*, **3**, 1951.

Zhang, L., Xu, M., Qiu, S., Li, R., Zhao, H., Shang, H., Lai, C. & Zhang, W. (2017) Improving the estimate of forest biomass carbon storage by combining two forest inventory systems. *Scandinavian Journal of Forest Research*, **32**, 297–305.

Zhu, Z. & Woodcock, C.E. (2014) Continuous change detection and classification of land cover using all available Landsat data. *Remote Sensing of Environment*, **144**, 152–171.

Zolkos, S.G., Goetz, S.J. & Dubayah, R. (2013) A meta-analysis of terrestrial aboveground biomass estimation using lidar remote sensing. *Remote Sensing of Environment*, **128**, 289–298.

APPENDICES

APPENDICES

Appendix 1. Detailed materials and usages in field data collection.

Materials	Quantity	Use
Plot establishment		
Trimble (Geo7X 50cm)	1	This is a mini-computer for encoding data. It contains a very precise GSP allowing to geo-reference the plot
GPS (Gamin 62s)	1	Used for prospecting and locating geographic coordinates of parcels
TruPulse 360	1	Measure the slope of the ground and the heights of the trees
Digital camera	1	Digital camera 1 Photographing plants, botanical collections and landscapes
Compass	2	To orientate and give the azimuth of the transects
Machetes	4	To clear transects and harvest grass layer
Decametres	3	Measure the length/width of the transects
Toposignals	5	To serve as a topographic signal
DBH meter 3m	3	Measure the diameter of the trees
DBH meter 5m	2	Measure the diameter of the trees
Telescopic ladder 6-8m	1	Measure diameter of trees with buttresses or stilt roots and collect botanical specimens
Non corrosives nails (≥ 7 cm)	3 kg*	Fix tags on trees
Hammer	2	Hammer nails on trees
Metal tags	Set of 600	Bearing a unique number to identify the different individuals trees within each plot
1.60 m pole	25	Wooden pole to mark the intersections between transects and quadrats
PVC pipes of 60 cm	4*	Mark the four corners of the plot
5 kg paint	1*	Red oil paint to mark the measurement height on the tree
Brush 1 cm	3*	Paint the heights of measurement
Forestry chalk	3*	Mark the heights of diameter measurements and the location of the label
Rope (> 100 m)	3	Materialize the boundaries of the plots
Grassy layer sampling		
15 kg Kern mechanic scale	1	Weight grass samples
100 g mechanic Pesola scale	1	
1000 g Kern electronic scale	1	
Oven	1	Dry grass samples
Plastic bags	Set of 100	Store grass samples
Botanical collections		
Pruning shears	1	Cut leaf and small branches of botanical samples
Collection pole	1	Collect botanical samples for tall trees
News papers	10 kg	Presser/conserve botanical specimens
Paper tags	100*	Tagged specimens

Plant press		2	Press vouchers					
Alcohol 70-95°		5 L	Conserve specimens					
Envelopes and silica gel		100	To dry the samples for genetic analysis, if desire					
Markers, ordinary pencils, eraser		2	To mark and take notes					
Notebook with hard cover		1	Take notes in the field					

* Average quantity for each plot

Appendix 2. Coordinates and structure of the 74 plots sampled within the study area.

N ind.: number of individuals within 1-ha; N sp.: number of species within 1-ha; Lorey's H = averaged height of trees weighted by the basal area; G: basal area and AGB = aboveground biomass; N Sp.: Number of species.

ID	Plot name	Size (ha)	lon	lat	N ind	Lorey's H (m)	G (m²/ha)	AGB (Mg/ha)	N Sp.
1	Mpem001	1	11.6558	5.0181	371	33	37	377	70
2	Mpem002	1	11.6479	5.0324	313	33	39	511	68
3	Mpem003	1	11.6479	5.0223	278	25	24	208	33
4	Mpem004	1	11.6520	5.0143	354	30	24	250	59
5	Mpem005	1	11.5615	5.1790	568	23	28	239	58
6	Mpem006	1	11.5848	5.1683	353	21	17	122	46
7	Mpem007	1	11.5860	5.1806	397	29	36	361	75
8	Mpem008	1	11.7411	5.1172	590	28	44	494	79
9	Mpem009	1	11.7368	5.1229	535	25	28	233	67
10	Mpem010	1	11.7272	5.1237	342	22	17	118	53
11	nachtigal001	1	11.7229	4.3782	356	28	30	247	65
12	nachtigal002	1	11.7084	4.3570	429	33	26	237	33
13	nachtigal003	1	11.7418	4.3747	330	25	23	180	62
14	nachtigal004	1	11.7040	4.3678	538	24	35	240	28
15	nachtigal005	1	11.7198	4.3612	216	29	28	220	60
16	nachtigal006	1	11.6642	4.3246	353	28	26	250	53
17	nachtigal007	1	11.7229	4.4177	368	27	29	268	60
18	nachtigal008	1	11.7200	4.4093	337	29	19	102	16
19	nachtigal009	1	11.8143	4.4540	485	28	30	272	72
20	nachtigal010	1	11.8232	4.4601	509	24	28	225	74
21	nachtigal011	1	11.8133	4.4440	386	23	24	161	60
22	sav_Mpem001	0.16	11.6529	5.0213	26	8	5	14	5
23	sav_Mpem002	0.16	11.6452	5.0270	40	8	7	23	5
24	sav_Mpem003	0.16	11.6521	5.0277	46	8	22	72	5
25	sav_Mpem004	0.16	11.6527	5.0306	18	6	3	7	6
26	sav_Mpem005	0.16	11.6545	5.0302	77	21	24	203	12
27	sav_Mpem006	0.16	11.6457	5.0307	29	9	8	25	4
28	sav_Mpem007	0.16	11.6413	5.0267	19	6	3	6	4
29	sav_Mpem008	0.16	11.6394	5.0311	27	8	6	20	5

30	sav_Mpem009	0.16	11.6325	5.0293	17	7	3	7	4
31	sav_Mpem010	0.16	11.6288	5.0349	37	6	4	8	6
32	sav_Mpem011	0.16	11.6269	5.0356	41	6	3	7	4
33	sav_Mpem012	0.16	11.6337	5.0364	53	9	11	42	6
34	sav_Mpem013	0.16	11.6339	5.0308	40	6	6	13	4
35	sav_Mpem014	0.16	11.6569	5.0395	73	15	19	101	4
36	sav_Mpem015	0.16	11.7199	5.2837	51	8	9	31	7
37	sav_Mpem016	0.16	11.7178	5.2928	18	9	4	15	5
38	sav_Mpem017	0.16	11.7116	5.2938	21	4	2	2	3
39	sav_Mpem018	0.16	11.7201	5.2882	32	9	6	19	7
40	sav_Mpem019	0.16	11.7212	5.2878	25	9	5	18	4
41	sav_Mpem020	0.16	11.7062	5.2853	29	6	3	7	4
42	sav_Mpem021	0.16	11.7060	5.2860	126	6	15	28	5
43	sav_Mpem022	0.16	11.7557	5.2682	64	6	10	22	7
44	sav_Mpem023	0.16	11.7635	5.2695	10	7	2	7	4
45	sav_Mpem024	0.16	11.7601	5.2671	27	5	3	4	4
46	sav_Mpem025	0.16	11.7602	5.2727	18	5	2	5	4
47	sav_Mpem026	0.16	11.7550	5.2777	14	5	3	4	3
48	sav_Mpem027	0.16	11.7519	5.2772	46	5	6	11	3
49	sav_Mpem028	0.16	11.7538	5.2697	38	8	11	30	6
50	sav_Mpem029	0.16	11.7437	5.2624	7	5	1	1	4
51	sav_Mpem030	0.16	11.7452	5.2639	50	7	9	24	6
52	sav_Mpem031	0.16	11.7649	5.2714	11	5	1	2	5
53	sav_Mpem032	0.16	11.7476	5.2706	22	7	6	17	5
54	sav_Mpem033	0.16	11.7634	5.2532	2	7	1	2	2
55	sav_Mpem034	0.16	11.7492	5.2679	32	7	4	10	7
56	sav_Mpem035	0.16	11.7789	5.2706	66	6	8	13	5
57	sav_nachtigal001	0.16	11.6884	4.4056	51	5	4	6	4
58	sav_nachtigal002	0.16	11.6847	4.4034	57	8	11	31	6
59	sav_nachtigal003	0.16	11.7049	4.3978	55	5	5	9	6
60	sav_nachtigal004	0.16	11.7049	4.4011	77	6	11	23	8
61	sav_nachtigal005	0.16	11.7099	4.4002	17	7	2	4	3
62	sav_nachtigal006	0.16	11.6501	4.3729	8	5	1	1	4
63	sav_nachtigal007	0.16	11.6490	4.3702	16	6	2	4	5
64	sav_nachtigal008	0.16	11.6479	4.3721	20	6	3	7	5
65	sav_nachtigal009	0.16	11.6586	4.3685	15	6	2	4	5
66	sav_nachtigal010	0.16	11.6366	4.3577	18	6	4	9	3
67	sav_nachtigal011	0.16	11.6382	4.3559	18	5	2	2	5
68	sav_nachtigal012	0.16	11.5967	4.4120	57	8	7	25	9
69	sav_nachtigal013	0.16	11.5988	4.4102	28	7	5	13	6
70	sav_nachtigal014	0.16	11.5911	4.4127	51	24	17	150	7
71	sav_nachtigal015	0.16	11.7293	4.4177	40	7	6	16	6
72	sav_nachtigal016	0.16	11.7306	4.4214	46	6	5	9	7
73	sav_nachtigal017	0.16	11.7306	4.4238	88	24	35	300	20
74	sav_nachtigal018	0.16	11.6843	4.4058	27	13	6	38	4

Appendix 3 : Species list and total number of inviduals (N) sampled from the 10 1-ha forest plots and 35 0.16-ha savanna plots installed in the forest-savanna transition area of Cameroon

Index	Species	Familly	N	Index	Species	Familly	N
244	Theobroma cacao	Malvaceae	706	172	Myrianthus arboreus	Urticaceae	72
255	Trilepisium madagascariense	Moraceae	528	46	Bridelia micrantha	Phyllanthaceae	67
238	Terminalia glaucescens	Combretaceae	271	180	Oncoba glauca	Salicaceae	67
226	Sterculia rhinopetala	Malvaceae	254	207	Rauvolfia macrophylla	Apocynaceae	65
17	Annona senegalensis	Annonaceae	247	253	Trichilia welwitschii	Meliaceae	64
78	Crossopteryx febrifuga	Rubiaceae	212	71	Cola cordifolia	Malvaceae	62
239	Terminalia ivorensis	Combretaceae	203	229	Strombosia pustulata	Olacaceae	60
45	Bridelia ferruginea	Phyllanthaceae	194	246	Treculia obovoidea	Moraceae	60
196	Piliostigma thonningii	Fabaceae	186	3	Albizia adianthifolia	Fabaceae	54
136	Hymenocardia acida	Phyllanthaceae	182	53	Ceiba pentandra	Malvaceae	53
56	Celtis mildbraedii	Cannabaceae	179	153	Macaranga spinosa	Euphorbiaceae	53
59	Celtis zenkeri	Cannabaceae	175	163	Milicia excelsa	Moraceae	53
209	Ricinodendron heudelotii	Euphorbiaceae	170	171	Musanga cecropioides	Urticaceae	51
236	Syzygium guineense	Myrtaceae	150	61	Chrysophyllum boukokoense	Sapotaceae	50
206	Pycnanthus angolensis	Myristicaceae	146	176	Newbouldia laevis	Bignoniaceae	50
127	Glyphaea brevis	Malvaceae	139	129	Grewia coriacea	Malvaceae	48
21	Anthonotha macrophylla	Fabaceae	122	135	Hylodendron gabunense	Fabaceae	48
55	Celtis africana	Cannabaceae	115	222	Sorindeia juglandifolia	Anacardiaceae	48
260	Uapaca paludosa	Phyllanthaceae	111	86	Desplatsia dewevrei	Malvaceae	46
73	Cola lateritia	Malvaceae	108	213	Rothmannia longiflora	Rubiaceae	46
24	Antidesma membranaceum	Phyllanthaceae	106	170	Morus mesozygia	Moraceae	45
36	Berlinia bracteosa	Fabaceae	106	147	Lannea welwitschii	Anacardiaceae	44
268	Xylopia aethiopica	Annonaceae	101	68	Cola acuminata	Malvaceae	43
121	Funtumia africana	Apocynaceae	99	110	Eribroma oblongum	Malvaceae	43
256	Triplochiton scleroxylon	Malvaceae	98	116	Fernandoa adolfi-friderici	Bignoniaceae	43
58	Celtis tessmannii	Cannabaceae	84	117	Ficus exasperata	Moraceae	42
158	Mansonia altissima	Malvaceae	84	118	Ficus mucuso	Moraceae	40
241	Terminalia superba	Combretaceae	84	259	Uapaca guineensis	Phyllanthaceae	40
6	Albizia zygia	Fabaceae	81	27	Antrocaryon klaineanum	Anacardiaceae	39
160	Mareyopsis longifolia	Euphorbiaceae	79	70	Cola chlamydantha	Malvaceae	39
128	Greenwayodendron suaveolens	Annonaceae	77	197	Piptadeniastrum africanum	Fabaceae	39
250	Trichilia prieuriana	Meliaceae	76	41	Bombax brevicuspe	Malvaceae	37

Index	Species	Familly	N
156	*Mallotus oppositifolius*	Euphorbiaceae	37
167	*Millettia sanagana*	Fabaceae	36
227	*Sterculia tragacantha*	Malvaceae	36
57	*Celtis philippensis*	Cannabaceae	35
12	*Angylocalyx pynaertii*	Fabaceae	34
242	*Tetrapleura tetraptera*	Fabaceae	34
251	*Trichilia rubescens*	Meliaceae	33
2	*Afzelia bipindensis*	Fabaceae	32
103	*Elaeis guineensis*	Arecaceae	31
122	*Funtumia elastica*	Apocynaceae	30
144	*Klaineanthus gaboniae*	Euphorbiaceae	30
161	*Margaritaria discoidea*	Phyllanthaceae	30
201	*Pseudospondias microcarpa*	Anacardiaceae	30
252	*Trichilia tessmannii*	Meliaceae	29
134	*Homalium letestui*	Salicaceae	28
186	*Pancovia laurentii*	Sapindaceae	28
10	*Amphimas pterocarpoides*	Fabaceae	27
111	*Eriocoelum macrocarpum*	Sapindaceae	27
174	*Nauclea latifolia*	Rubiaceae	27
164	*Millettia barteri*	Fabaceae	26
179	*Olax subscorpioidea*	Olacaceae	25
205	*Pterygota bequaertii*	Malvaceae	25
175	*Nesogordonia papaverifera*	Malvaceae	24
231	*Strombosiopsis tetrandra*	Olacaceae	24
257	*Turraeanthus africanus*	Meliaceae	24
264	*Vitex doniana*	Lamiaceae	24
40	*Blighia welwitschii*	Sapindaceae	23
183	*Ongokea gore*	Olacaceae	23
62	*Chrysophyllum lacourtianum*	Sapotaceae	22
91	*Diospyros canaliculata*	Ebenaceae	22
270	*Xylopia quintasii*	Annonaceae	22
245	*Treculia africana*	Moraceae	19
265	*Vitex grandifolia*	Lamiaceae	19
101	*Duboscia macrocarpa*	Malvaceae	18
148	*Lasiodiscus mannii*	Rhamnaceae	18

Index	Species	Familly	N
198	*Plagiostyles africana*	Euphorbiaceae	18
266	*Vitex rivularis*	Lamiaceae	18
69	*Cola altissima*	Malvaceae	17
76	*Cordia platythyrsa*	Boraginaceae	17
145	*Klainedoxa gabonensis*	Irvingiaceae	17
214	*Rothmannia talbotii*	Rubiaceae	17
34	*Barteria fistulosa*	Passifloraceae	16
168	*Monodora myristica*	Annonaceae	16
204	*Pterocarpus soyauxii*	Fabaceae	16
228	*Strombosia grandifolia*	Olacaceae	16
8	*Alstonia boonei*	Apocynaceae	15
150	*Lophira alata*	Ochnaceae	15
199	*Pouteria alnifolia*	Sapotaceae	15
225	*Staudtia kamerunensis*	Myristicaceae	15
94	*Diospyros suaveolens*	Ebenaceae	14
181	*Oncoba mannii*	Salicaceae	14
263	*Vitex cienkowskii*	Lamiaceae	14
18	*Anonidium mannii*	Annonaceae	13
192	*Pericopsis laxiflora*	Fabaceae	13
89	*Dialium guineense*	Fabaceae	12
90	*Diospyros bipindensis*	Ebenaceae	12
130	*Guarea cedrata*	Meliaceae	12
178	*Ochtocosmus africanus*		12
50	*Canarium schweinfurthii*	Burseraceae	11
84	*Desbordesia insignis*	Irvingiaceae	11
88	*Dialium bipindense*	Fabaceae	11
95	*Discoglypremna caloneura*	Euphorbiaceae	11
113	*Erythrophleum suaveolens*	Fabaceae	11
138	*Irvingia gabonensis*	Irvingiaceae	11
77	*Corynanthe pachyceras*	Rubiaceae	10
210	*Rinorea dentata*	Violaceae	10
247	*Trema orientalis*	Cannabaceae	10
269	*Xylopia hypolampra*	Annonaceae	10
15	*Annickia affinis*	Annonaceae	9
31	*Aulacocalyx jasminiflora*	Rubiaceae	9

Index	Species	Familly	N
39	Blighia sapida	Sapindaceae	9
133	Holoptelea grandis	Ulmaceae	9
139	Irvingia grandifolia	Irvingiaceae	9
157	Mangifera indica	Anacardiaceae	9
274	Zanthoxylum macrophyllum	Rutaceae	9
4	Albizia ferruginea	Fabaceae	8
20	Anthonotha cladantha	Fabaceae	8
81	Dacryodes klaineana	Burseraceae	8
114	Erythroxylum mannii	Erythroxylaceae	8
208	Rauvolfia vomitoria	Apocynaceae	8
254	Tridesmostemon omphalocarpoides	Sapotaceae	8
5	Albizia glaberrima	Fabaceae	7
19	Anthocleista nobilis	Gentianaceae	7
74	Cola lepidota	Malvaceae	7
87	Detarium macrocarpum	Fabaceae	7
92	Diospyros crassiflora	Ebenaceae	7
96	Dovyalis zenkeri	Salicaceae	7
108	Entandrophragma cylindricum	Meliaceae	7
125	Gambeya lacourtiana	Sapotaceae	7
155	Maesopsis eminii	Rhamnaceae	7
193	Persea americana	Lauraceae	7
233	Symphonia globulifera	Clusiaceae	7
262	Uvariastrum pierreanum	Annonaceae	7
271	Xylopia rubescens	Annonaceae	7
13	Aningeria altissima	Sapotaceae	6
54	Celtis adolfi-friderici	Cannabaceae	6
66	Cleistopholis patens	Annonaceae	6
75	Cola verticillata	Malvaceae	6
83	Daniellia oliveri	Fabaceae	6
106	Entandrophragma angolense	Meliaceae	6
202	Pteleopsis hylodendron	Combretaceae	6
223	Spathodea campanulata	Bignoniaceae	6
230	Strombosia zenkeri	Olacaceae	6
237	Tabernaemontana crassa	Apocynaceae	6
272	Zanthoxylum gilletii	Rutaceae	6

Index	Species	Family	N
7	Alchornea cordifolia	Euphorbiaceae	5
16	Annickia chlorantha	Annonaceae	5
33	Balanites wilsoniana	Zygophyllaceae	5
109	Entandrophragma utile	Meliaceae	5
132	Harungana madagascariensis	Hypericaceae	5
190	Pentaclethra macrophylla	Fabaceae	5
217	Sapium ellipticum	Euphorbiaceae	5
240	Terminalia macroptera	Combretaceae	5
275	Zanthoxylum tessmannii	Rutaceae	5
26	Antidesma vogelianum	Phyllanthaceae	4
42	Bombax buonopozense	Malvaceae	4
52	Casearia aculeata	Salicaceae	4
63	Chrysophyllum pruniforme	Sapotaceae	4
72	Cola flavovelutina	Malvaceae	4
97	Drypetes capillipes	Putranjivaceae	4
126	Garcinia ovalifolia	Clusiaceae	4
162	Markhamia lutea	Bignoniaceae	4
173	Nauclea diderrichii	Rubiaceae	4
187	Panda oleosa	Pandaceae	4
195	Picralima nitida	Apocynaceae	4
220	Scottellia klaineana	Achariaceae	4
235	Synsepalum stipulatum	Sapotaceae	4
273	Zanthoxylum heitzii	Rutaceae	4
30	Aulacocalyx caudata	Rubiaceae	3
35	Beilschmiedia congolana	Lauraceae	3
43	Borassus aethiopum	Arecaceae	3
60	Centroplacus glaucinus	Centroplacaceae	3
67	Coelocaryon preussii	Myristicaceae	3
93	Diospyros mannii	Ebenaceae	3
102	Duguetia staudtii	Annonaceae	3
137	Hymenostegia afzelii	Fabaceae	3
143	Kigelia africana	Bignoniaceae	3
149	Leptactina involucrata	Rubiaceae	3
177	Ochna calodendron	Ochnaceae	3

Index	Species	Familly	N
182	*Oncoba welwitschii*	Salicaceae	3
249	*Tricalysia pangolina*	Rubiaceae	3
258	*Uapaca acuminata*	Phyllanthaceae	3
9	*Amphimas ferrugineus*	Fabaceae	2
22	*Antiaris toxicaria*	Moraceae	2
25	*Antidesma venosum*	Phyllanthaceae	2
32	*Baikiaea insignis*	Fabaceae	2
80	*Dacryodes edulis*	Burseraceae	2
82	*Dacryodes macrophylla*	Burseraceae	2
99	*Drypetes klainei*	Putranjivaceae	2
100	*Drypetes leonensis*	Putranjivaceae	2
104	*Elaeophorbia drupifera*	Euphorbiaceae	2
112	*Erythrophleum ivorense*	Fabaceae	2
115	*Euphorbia drupifera*	Euphorbiaceae	2
119	*Ficus sycomorus*	Moraceae	2
123	*Gambeya africana*	Sapotaceae	2
124	*Gambeya boukokoensis*	Sapotaceae	2
141	*Keayodendron bridelioides*	Phyllanthaceae	2
142	*Khaya anthotheca*	Meliaceae	2
159	*Maranthes glabra*	Chrysobalanaceae	2
166	*Millettia macrophylla*	Fabaceae	2
188	*Pauridiantha floribunda*	Rubiaceae	2
200	*Pseudospondias longifolia*	Anacardiaceae	2
211	*Rinorea oblongifolia*	Violaceae	2
215	*Rothmannia whitfieldii*	Rubiaceae	2
216	*Santiria trimera*	Burseraceae	2
232	*Swartzia fistuloides*	Leguminosae	2
234	*Synsepalum dulcificum*	Sapotaceae	2
243	*Tetrorchidium didymostemon*	Euphorbiaceae	2
267	*Voacanga africana*	Apocynaceae	2
1	*Afrostyrax kamerunensis*	Huaceae	1
11	*Angylocalyx oligophyllus*	Fabaceae	1
14	*Aningeria robusta*	Sapotaceae	1
23	*Antidesma laciniatum*	Phyllanthaceae	1

Index	Species	Familly	N
28	*Antrocaryon micraster*	Anacardiaceae	1
29	*Aoranthe cladantha*	Rubiaceae	1
37	*Berlinia hollandii*	Fabaceae	1
38	*Bersama abyssinica*	Greyiaceae	1
44	*Brenania brieyi*	Rubiaceae	1
47	*Burkea africana*	Fabaceae	1
48	*Calpocalyx dinklagei*	Fabaceae	1
49	*Campylospermum mannii*	Ochnaceae	1
51	*Canarium schweinfurtii*	Burseraceae	1
64	*Citrus sinensis*	Rutaceae	1
65	*Cleistopholis glauca*	Annonaceae	1
79	*Cylicodiscus gabunensis*	Fabaceae	1
85	*Desplatsia chrysochlamys*	Malvaceae	1
98	*Drypetes gossweileri*	Putranjivaceae	1
105	*Entada africana*	Fabaceae	1
107	*Entandrophragma candollei*	Meliaceae	1
120	*Ficus vogeliana*	Moraceae	1
131	*Guarea thompsonii*	Meliaceae	1
140	*Irvingia robur*	Irvingiaceae	1
146	*Klainedoxa microphylla*	Irvingiaceae	1
151	*Lophira lanceolata*	Ochnaceae	1
152	*Lovoa trichilioides*	Meliaceae	1
154	*Maesobotrya klaineana*	Phyllanthaceae	1
165	*Millettia laurentii*	Fabaceae	1
169	*Morinda lucida*	Rubiaceae	1
184	*Oxyanthus oliganthus*	Rubiaceae	1
185	*Pachypodanthium staudtii*	Annonaceae	1
189	*Pausinystalia macroceras*	Rubiaceae	1
191	*Pentadesma butyracea*	Clusiaceae	1
194	*Petersianthus macrocarpus*	Lecythidaceae	1
203	*Pterocarpus mildbraedii*	Fabaceae	1
212	*Rothmannia lateriflora*	Rubiaceae	1
218	*Schumanniophyton magnificum*	Rubiaceae	1
219	*Scottellia coriacea*	Achariaceae	1

Index	Species	Familly	N	Index	Species	Familly	N
221	*Sorindeia grandifolia*	Anacardiaceae	1	248	*Tricalysia achoundongiana*	Rubiaceae	1
224	*Spondias cytherea*	Anacardiaceae	1	261	*Uapaca vanhouttei*	Phyllanthaceae	1

Appendix 4. List species sampled within the 137 plots of 40 m x 40 m size both in forest and savanna to study the dynamics of floristic succession (see section III.1.4).

Species are classified according to their successional groups (Grp) with Eco = Ecotone species; For = forest species; Sav1 = fire-prone savanna species; Sav-2 = fire-sensitive savanna species. co1 and co2 = scores of the different species for the first and second axis from an NSCA. Freq (%) = relative abundance of the species within the successional group they belong to.

Species	Grp	co1	co2	Freq	Species	Grp	co1	co2	Freq
Forest pioneer species					*Anthocleista nobilis*	Eco	-0.1	0.0	0.2
Afrostyrax kamerunensis	Eco	0.0	0.0	0.0	*Antiaris toxicaria*	Eco	0.0	0.0	0.0
					Antidesma venosum	Eco	0.0	0.0	0.1
Afzelia bipindensis	Eco	-0.2	0.0	0.9	*Antidesma vogelianum*	Eco	0.0	0.0	0.1
Albizia adianthifolia	Eco	-0.2	-0.1	1.4					
					Aulacocalyx caudata	Eco	0.0	0.0	0.1
Albizia ferruginea	Eco	0.0	-0.1	0.3					
Albizia glaberrima	Eco	0.0	0.0	0.3	*Aulacocalyx jasminiflora*	Eco	-0.1	0.0	0.3
Albizia zygia	Eco	0.9	-2.7	3.3					
Alchornea cordifolia	Eco	0.1	-0.1	0.2	*Baikiaea insignis*	Eco	0.0	0.0	0.0
					Balanites wilsoniana	Eco	-0.1	0.0	0.2
Alstonia boonei	Eco	-0.1	0.0	0.4					
Amphimas ferrugineus	Eco	0.0	0.0	0.1	*Barteria fistulosa*	Eco	-0.1	0.0	0.4
					Beilschmiedia congolana	Eco	0.0	0.0	0.0
Amphimas pterocarpoides	Eco	-0.2	0.0	0.7					
					Bersama abyssinica	Eco	0.0	0.0	0.0
Angylocalyx pynaertii	Eco	-0.2	0.0	0.8					
					Blighia sapida	Eco	0.0	0.0	0.2
Annickia affinis	Eco	0.0	0.0	0.1	*Blighia welwitschii*	Eco	-0.2	0.0	0.6
Annickia chlorantha	Eco	0.0	0.0	0.1	*Bombax brevicuspe*	Eco	-0.2	0.0	0.9
Anonidium mannii	Eco	-0.1	0.0	0.3	*Bombax buonopozense*	Eco	0.0	0.0	0.0
Anthonotha cladantha	Eco	-0.1	0.0	0.3	*Borassus aethiopum*	Eco	0.0	0.0	0.1
Antrocaryon klaineanum	Eco	-0.3	0.0	1.2	*Brenania brieyi*	Eco	0.0	0.0	0.0
					Bridelia micrantha	Eco	0.6	-0.2	2.6
Antidesma laciniatum	Eco	0.0	0.0	0.0	*Burkea africana*	Eco	0.0	0.1	0.0
Antrocaryon micraster	Eco	0.0	0.0	0.0	*Campylospermum mannii*	Eco	0.0	0.0	0.0

Species	Grp	co1	co2	Freq	Species	Grp	co1	co2	Freq
Canarium schweinfurthii	*Eco*	-0.1	0.0	0.3	*Desbordesia insignis*	*Eco*	-0.1	0.0	0.4
Casearia aculeata	*Eco*	0.0	0.0	0.1	*Detarium macrocarpum*	*Eco*	0.0	0.0	0.1
Ceiba pentandra	*Eco*	-0.3	0.0	1.1					
Celtis adolfi-fridericii	*Eco*	0.0	0.0	0.2	*Dialium bipindense*	*Eco*	-0.1	0.0	0.3
					Dialium guineense	*Eco*	-0.1	0.0	0.4
Celtis philippensis	*Eco*	-0.3	0.0	1.2	*Diospyros bipindensis*	*Eco*	-0.1	0.0	0.3
Centroplacus glaucinus	*Eco*	0.0	0.0	0.0	*Diospyros crassiflora*	*Eco*	0.0	0.0	0.1
Chlamydocola chlamydantha	*Eco*	-0.3	0.0	1.4	*Diospyros mannii*	*Eco*	0.0	0.0	0.1
Chrysophyllum africanum	*Eco*	0.0	0.0	0.0	*Diospyros physocalycina*	*Eco*	-0.2	0.0	0.7
Chrysophyllum boukokoense	*Eco*	-0.3	0.0	1.4	*Diospyros suaveolens*	*Eco*	-0.1	0.0	0.5
Chrysophyllum lacourtianum	*Eco*	-0.2	0.0	0.7	*Discoglypremna caloneura*	*Eco*	-0.1	0.0	0.3
Chrysophyllum pruniforme	*Eco*	0.0	0.0	0.1	*Dovyalis zenkeri*	*Eco*	-0.1	0.0	0.3
					Drypetes capillipes	*Eco*	0.0	0.0	0.0
Cleistopholis glauca	*Eco*	0.0	0.0	0.0	*Drypetes gossweileri*	*Eco*	0.0	0.0	0.0
Cleistopholis patens	*Eco*	0.0	0.0	0.2	*Drypetes klainei*	*Eco*	0.0	0.0	0.1
					Drypetes leonensis	*Eco*	0.0	0.0	0.1
Coelocaryon preussii	*Eco*	0.0	0.0	0.1	*Duboscia macrocarpa*	*Eco*	-0.1	0.0	0.5
Cola acuminata	*Eco*	-0.3	0.0	1.1	*Duguetia staudtii*	*Eco*	0.0	0.0	0.1
Cola altissima	*Eco*	-0.1	0.0	0.6	*Elaeophorbia drupifera*	*Eco*	0.0	0.0	0.0
Cola cordifolia	*Eco*	-0.4	0.0	1.8					
Cola flavovelutina	*Eco*	0.0	0.0	0.1	*Elaeis guineensis*	*Eco*	-0.2	0.0	0.8
Cola lepidota	*Eco*	0.0	0.0	0.1	*Entada africana*	*Eco*	0.0	0.0	0.0
Cola verticillata	*Eco*	0.0	0.0	0.2	*Entandrophragma angolense*	*Eco*	-0.1	0.0	0.2
Corynanthe pachyceras	*Eco*	0.0	0.0	0.2	*Entandrophragma candollei*	*Eco*	0.0	0.0	0.0
Cordia platythyrsa	*Eco*	-0.1	0.0	0.5	*Entandrophragma cylindricum*	*Eco*	0.0	0.0	0.2
Cylicodiscus gabunensis	*Eco*	0.0	0.0	0.0					
Dacryodes edulis	*Eco*	0.0	0.0	0.0	*Entandrophragma utile*	*Eco*	-0.1	0.0	0.2
Dacryodes klaineana	*Eco*	-0.1	0.0	0.2	*Eriocoelum macrocarpum*	*Eco*	-0.2	0.0	0.8
Dacryodes macrophylla	*Eco*	0.0	0.0	0.0	*Eribroma oblonga*	*Eco*	-0.2	0.0	0.8
Daniellia oliveri	*Eco*	0.2	0.2	0.3	*Erythrophleum ivorense*	*Eco*	0.0	-0.1	0.1
Desplatsia chrysochlamys	*Eco*	0.0	0.0	0.0	*Erythroxylum mannii*	*Eco*	0.0	0.0	0.1
Desplatsia dewevrei	*Eco*	-0.3	0.0	1.1	*Erythrophleum suaveolens*	*Eco*	-0.1	0.0	0.3

Species	Grp	co1	co2	Freq	Species	Grp	co1	co2	Freq
Fernandoa adolfi-friderici	*Eco*	-0.2	0.0	0.9	*Millettia barteri*	*Eco*	-0.2	0.0	0.7
					Milicia excelsa	*Eco*	-0.3	0.0	1.1
Ficus exasperata	*Eco*	-0.2	0.0	0.8	*Millettia laurentii*	*Eco*	0.0	0.0	0.0
Ficus mucuso	*Eco*	-0.2	0.0	0.7	*Millettia macrophylla*	*Eco*	0.0	0.0	0.1
Ficus sycomorus	*Eco*	0.0	0.0	0.1					
Ficus vogeliana	*Eco*	0.0	0.0	0.0	*Millettia sanagana*	*Eco*	-0.2	0.0	1.0
Funtumia elastica	*Eco*	-0.3	0.0	1.1	*Monodora myristica*	*Eco*	-0.1	0.0	0.5
Garcinia ovalifolia	*Eco*	0.0	0.0	0.1					
Grewia coriacea	*Eco*	-0.4	0.0	1.5	*Morus mesozygia*	*Eco*	-0.2	0.0	1.1
Harungana madagascariensis	*Eco*	0.1	-0.1	0.2	*Musanga cecropioides*	*Eco*	-0.4	0.0	1.5
Holoptelea grandis	*Eco*	-0.1	0.0	0.3	*Nauclea diderrichii*	*Eco*	0.0	0.0	0.0
Homalium le-testui	*Eco*	-0.2	0.0	0.8	*Nauclea latifolia*	*Eco*	0.6	-0.6	1.2
Hylodendron gabunense	*Eco*	-0.2	0.0	1.1	*Nesogordonia kabingaensis*	*Eco*	-0.2	0.0	0.8
Hymenostegia afzelii	*Eco*	0.0	0.0	0.0	*Newbouldia laevis*	*Eco*	-0.2	0.0	1.1
Irvingia gabonensis	*Eco*	-0.1	0.0	0.3	*Olax subscorpioidea*	*Eco*	-0.2	0.0	0.7
Irvingia grandifolia	*Eco*	-0.1	0.0	0.3	*Oncoba glauca*	*Eco*	-0.4	0.0	1.8
Keayodendron bridelioides	*Eco*	0.0	0.0	0.1	*Oncoba mannii*	*Eco*	-0.1	0.0	0.5
					Oncoba welwitschii	*Eco*	0.0	0.0	0.1
Khaya anthotheca	*Eco*	0.0	0.0	0.0	*Ongokea gore*	*Eco*	-0.2	0.0	0.8
Kigelia africana	*Eco*	0.0	0.0	0.1	*Oxyanthus oliganthus*	*Eco*	0.0	0.0	0.0
Klainedoxa gabonensis	*Eco*	-0.2	0.0	0.6					
					Pancovia laurentii	*Eco*	-0.2	0.0	0.6
Klaineanthus gabonii	*Eco*	-0.1	0.0	0.6	*Panda oleosa*	*Eco*	0.0	0.0	0.2
Lannea welwitschii	*Eco*	-0.2	0.1	1.4	*Pentadesma butyracea*	*Eco*	0.0	0.0	0.0
Lasiodiscus mannii	*Eco*	-0.1	0.0	0.6	*Pentaclethra macrophylla*	*Eco*	0.0	0.0	0.2
Leplaea cedrata	*Eco*	-0.1	0.0	0.3					
Leptactina involucrata	*Eco*	0.0	0.0	0.1	*Pericopsis laxiflora*	*Eco*	0.1	-0.3	0.6
Leplaea thompsonii	*Eco*	0.0	0.0	0.0	*Petersianthus macrocarpus*	*Eco*	0.0	0.0	0.0
Lophira alata	*Eco*	-0.1	0.0	0.3	*Phyllocosmus africanus*	*Eco*	-0.1	0.0	0.3
Lophira lanceolata	*Eco*	0.0	0.0	0.0					
Macaranga spinosa	*Eco*	-0.3	0.0	1.6	*Picralima nitida*	*Eco*	0.0	0.0	0.2
Maesopsis eminii	*Eco*	0.0	0.0	0.1	*Piptadeniastrum africanum*	*Eco*	-0.2	0.0	1.0
Maesobotrya klaineana	*Eco*	0.0	0.0	0.0	*Plagiostyles africana*	*Eco*	-0.1	0.0	0.6
Mallotus oppositifolius	*Eco*	-0.2	0.0	1.1	*Pouteria alnifolia*	*Eco*	-0.1	0.0	0.2
Mangifera indica	*Eco*	0.0	0.0	0.2	*Pouteria altissima*	*Eco*	-0.1	0.0	0.2
Margaritaria discoidea	*Eco*	-0.2	0.0	0.8	*Pouteria pierrei*	*Eco*	0.0	0.0	0.0
					Pseudospondias microcarpa	*Eco*	-0.1	0.0	0.6
Maranthes glabra	*Eco*	0.0	0.0	0.1					
Markhamia lutea	*Eco*	0.0	0.0	0.1					

Species	Grp	co1	co2	Freq	Species	Grp	co1	co2	Freq
Pterygota bequaertii	*Eco*	-0.1	0.0	0.5	*Synsepalum dulcificum*	*Eco*	0.0	0.0	0.1
Pteleopsis hylodendron	*Eco*	0.0	0.0	0.2	*Synsepalum stipulatum*	*Eco*	0.0	0.0	0.1
Pterocarpus mildbraedii	*Eco*	0.0	0.0	0.0	*Tabernaemontana crassa*	*Eco*	-0.1	0.0	0.2
Pterocarpus soyauxii	*Eco*	-0.1	0.0	0.4	*Terminalia macroptera*	*Eco*	0.0	0.0	0.1
Rauvolfia caffra	*Eco*	-0.3	0.0	1.5	*Terminalia superba*	*Eco*	-0.4	0.0	1.6
Rauvolfia vomitoria	*Eco*	0.0	0.0	0.2	*Tetrorchidium didymostemon*	*Eco*	0.0	0.0	0.1
Rinorea dentata	*Eco*	0.0	0.0	0.1	*Tetrapleura tetraptera*	*Eco*	-0.2	0.0	1.0
Rinorea oblongifolia	*Eco*	0.0	0.0	0.1	*Treculia africana*	*Eco*	-0.1	0.0	0.5
Rothmannia lateriflora	*Eco*	0.0	0.0	0.0	*Treculia obovoidea*	*Eco*	-0.4	0.0	1.8
					Trema orientalis	*Eco*	0.0	0.0	0.2
Rothmannia longiflora	*Eco*	-0.2	0.0	1.0	*Tricalysia achoundongiana*	*Eco*	0.0	0.0	0.0
Rothmannia talbotii	*Eco*	-0.1	0.0	0.2	*Tridesmostemon omphalocarpoides*	*Eco*	0.0	0.0	0.2
Rothmannia whitfieldii	*Eco*	0.0	0.0	0.0	*Tricalysia pangolina*	*Eco*	0.0	0.0	0.1
Santiria trimera	*Eco*	0.0	0.0	0.1	*Trichilia prieuriana*	*Eco*	-0.3	0.0	1.1
Schumanniophyton magnificum	*Eco*	0.0	0.0	0.0	*Trichilia rubescens*	*Eco*	-0.3	0.0	1.1
Scottellia klaineana	*Eco*	0.0	0.0	0.1	*Tricalysia sp.nov.1*	*Eco*	0.0	0.0	0.1
Shirakiopsis elliptica	*Eco*	0.0	0.0	0.2	*Trichilia tessmannii*	*Eco*	-0.2	0.0	0.9
Sorindeia grandifolia	*Eco*	0.0	0.0	0.0	*Trichilia welwitschii*	*Eco*	-0.4	0.0	1.7
Sorindeia juglandifolia	*Eco*	-0.3	0.0	1.1	*Turraeanthus africanus*	*Eco*	-0.2	0.0	0.7
Spathodea campanulata	*Eco*	0.0	0.0	0.1	*Uapaca acuminata*	*Eco*	0.0	0.0	0.1
					Uapaca guineensis	*Eco*	-0.3	0.0	1.2
Staudtia kamerunensis	*Eco*	-0.1	0.0	0.4	*Uvariastrum pierreanum*	*Eco*	0.0	0.0	0.2
Sterculia tragacantha	*Eco*	-0.3	0.0	1.1	*Vitex doniana*	*Eco*	-0.1	-0.1	1.0
Strombosia grandifolia	*Eco*	-0.1	0.0	0.4	*Vitex grandifolia*	*Eco*	-0.1	0.0	0.4
					Vitex rivularis	*Eco*	-0.1	0.0	0.3
Strombosia pustulata	*Eco*	-0.4	0.0	1.7	*Xylopia hypolampra*	*Eco*	-0.1	0.0	0.2
Strombosiopsis tetrandra	*Eco*	-0.2	0.0	0.7	*Xylopia quintasii*	*Eco*	-0.1	0.0	0.6
					Xylopia rubescens	*Eco*	0.0	0.0	0.2
Strombosia zenkeri	*Eco*	0.0	0.0	0.2	*Zanthoxylum gilletii*	*Eco*	-0.2	0.0	0.7
Swartzia fistuloides	*Eco*	0.0	0.0	0.1					
Symphonia globulifera	*Eco*	0.0	0.0	0.2	*Zanthoxylum heitzii*	*Eco*	0.0	0.0	0.1
					Old-growth forest species				

Species	Grp	co1	co2	Freq	Species	Grp	co1	co2	Freq
Anthonotha macrophylla	*For*	-0.8	0.0	4.7	*Ricinodendron heudelotii*	*For*	-0.7	0.0	4.2
Antidesma membranaceum	*For*	-0.8	0.0	4.3	*Sterculia rhinopetala*	*For*	-1.8	0.0	9.5
Berlinia bracteosa	*For*	-0.6	0.2	3.7	*Trilepisium madagascariense*	*For*	-2.4	0.1	13.0
Celtis africana	*For*	-0.9	0.0	4.9
Celtis mildbraedii	*For*	-1.1	0.0	6.0	*Triplochiton scleroxylon*	*For*	-0.5	0.0	2.8
Celtis tessmannii	*For*	-0.5	0.0	2.8
Celtis zenkeri	*For*	-1.1	0.0	5.9	*Uapaca mole*	*For*	-0.8	-0.1	5.2
Cola lateritia	*For*	-0.6	0.0	3.3	*Xylopia aethiopica*	*For*	-0.6	0.0	3.6
Funtumia africana	*For*	-0.6	0.0	3.5	**Fire-prone savanna species**				
Glyphaea brevis	*For*	-1.1	0.0	5.7	*Annona senegalensis*	Sav 1	6.6	-8.0	34.5
Greenwayodendron suaveolens	*For*	-0.5	0.0	2.9	*Piliostigma thonningii*	Sav 1	4.9	-5.1	26.3
Mansonia altissima	*For*	-0.5	0.0	3.0
Mareyopsis longifolia	*For*	-0.5	0.0	3.0	*Terminalia glaucescens*	Sav 1	8.1	-3.0	39.2
Myrianthus arboreus	*For*	-0.5	0.0	2.8	**Fire-sensitive savanna species**				
					Bridelia ferruginea	Sav 2	5.6	4.5	32.3
Pycnanthus angolensis	*For*	-0.9	0.0	5.1	*Crossopteryx febrifuga*	Sav 2	6.0	6.3	36.0
					Hymenocardia acida	Sav 2	4.7	8.9	31.7

Appendix 5. Publications

Sagang, L.B.T., Ploton, P., Sonké, B., Poilvé, H., Couteron, P., Barbier, N., 2020. Airborne Lidar Sampling Pivotal for Accurate Regional AGB Predictions from Multispectral Images in Forest-Savanna Landscapes. *Remote Sensing*. **12**, 20p. https://doi.org/doi:10.3390/rs12101637

Sagang, L.B.T., Ploton, P., Viennois G., Féret JB., Sonké, B., Couteron, P., Barbier, N.,. Monitoring vegetation dynamics with open earth observation tools: the case of fire-modulated savanna to forest transitions in Central Africa. *International Journal of Applied Earth Observation and Geoinformation*. Under review.